Musculoskeletal and spinal cord imaging in bilateral spastic cerebral palsy

Noble, Jonathan James

Awarding institution:
King's College London

Musculoskeletal and spinal cord imaging in bilateral spastic cerebral palsy

Jonathan James Noble

2014

Department of Imaging Sciences and Biomedical Engineering
School of Medicine
King's College London

Submitted in fulfilment of the requirements for the degree of Doctor of Philosophy

Abstract

Periventricular leucomalacia (PVL) is the most common brain injury in bilateral spastic cerebral palsy (BSCP). Cerebral palsy is a group of conditions that affect the development of the motor system, that are attributed to non-progressive lesions in the developing brain. In PVL, damage is caused by a primary arterial ischemic injury to the white matter in the posterior limb of the internal capsule, although other regions of the brain can also be affected including the spinal cord. Alterations in spinal cord development may lead to many of the clinical problems observed in BSCP, including altered motor control, co-contraction of agonist and antagonist muscle groups, progressive musculoskeletal deformities and weakness. Further to this, a heightened fracture risk of the long bones of the skeleton may be related to poor muscle development subsequent to the original brain injury.

In the work contributing to this thesis, the fat content of five muscles and the volume of nine major muscles of the lower limbs of ambulant adolescents and young adults with and without BSCP are investigated using MRI. The relationship between bony geometry and muscle volume are also studied. Studies of spinal cord white matter organisation are also performed using diffusion tensor imaging (DTI) MRI techniques to investigate whether there are associations between spinal cord organisation and gross functional development in BSCP.

Lower limb muscle volumes in BSCP were found to be smaller with increased intramuscular fat compared to their typically developing peers. Bone strength estimated from bony geometry was found to be significantly dependent on muscle volume independent of diagnosis. No differences were observed in spinal cord white matter microstructure between the subject groups, although a reduced white matter cross-sectional area was observed in the BSCP group. The clinical implications of this work are discussed in detail.

Acknowledgements

This thesis would not have been possible without the help, guidance, and encouragement of a number of people during the course of the project.

I would like to thank my supervisors for their time and support: Dr Adam Shortland for his insight, assistance, and enthusiasm throughout the PhD, and for providing a fountain of knowledge together with Mr Martin Gough on the clinical landscape for individuals with cerebral palsy and their assistance with subject identification and recruitment; and to Dr Geoff Charles-Edwards for his guidance and practical help with MRI sequence development and manuscript preparation.

Thank you to Andrew Lewis for his collaboration and willingness to volunteer for countless MRI scans during the early stages of the PhD; Susie Turner for her time and assistance with data collection and subject identification; Dr Nicola Fry and Dr Stephen Keevil for their support throughout the project and their assistance with manuscript preparation; and to the research radiographers at the Rayne Institute for their assistance with MRI data collection throughout the PhD.

I would also like to thank my family and friends for their unwavering support and for providing a welcome distraction when required, with a special mention to my sister Sarah for her assistance with recruitment of volunteers.

To all of the staff at the One Small Step Gait Laboratory, thank you for your support and for providing an interesting, motivating and enjoyable atmosphere to work in during the course of this project.

Finally, I would like to say a big thank you to all of the volunteers who took part in the studies without whom none of this would have been possible.

Contents

List of Figures

Published figures in Chapter 5

Published figures in Chapter 7

List of Tables

Published tables in Chapter 5

Nomenclature

2PD	Two-point Dixon
3PD	Three-point Dixon
4PD	Four-point Dixon
ACh	Acetylcholine
ADC	Apparent diffusion coefficient
ADP	Adenosine diphosphate
AFO	Ankle-foot orthoses
ATP	Adenosine triphosphate
AMP	Adenosine monophosphate
BMD	Bone mineral density
BMI	Body mass index
BSCP	Bilateral spastic cerebral palsy
BTX	Botulinum toxin
Br	Buckling ratio
cAMP	Cyclic adenosine monophosphate
CoA	Co-enzyme A
COV	Coefficient of variation
CP	Cerebral palsy
CSA	Cross sectional area
CT	Cortical bone thickness
DTI	Diffusion tensor imaging
DXA	Dual-energy X-ray absorption
EMCL	Extramyocellular lipid
EPI	Echo planar imaging
FA	Fractional anisotropy
FAD	Flavin adenine dinuclide
FDRO	Femoral derotation osteotomy
FG	Fast glycolytic
FOG	Fast oxidative-glycolytic
FOV	Field of view
GMax	Gluteus maximus

GMFCS	Gross motor function classification system
GMFM	Gross motor function measure
GMH-IVH	Germal matrix haemorrhage – intraventricular haemorrhage
GTP	Guanosine triphosphate
GTPT	Greater trochanter prominence test
GZLM	Generalized linear model
HDL-C	High-density lipoprotein cholesterol
ICC	Intra-class correlation
IDEAL	Iterative decomposition of water and fat with echo asymmetry and least squares approach
IMAT	Intermuscular adipose tissue
IMCL	Intramyocellular lipid
IntraMF	Intramuscular fat
IRS	Insulin receptor substrate
J	Polar moment of inertia
LG	Lateral gastrocnemius
MEP	Motor evoked potential
MG	Medial gastrocnemius
MRI	Magnetic resonance imaging
MRS	Magnetic resonance spectroscopy
MTS	Modified Tardieu scale
MTU	Musculo-tendinous unit
NAD	Nicotinamide adenine dinuclide
NSA	Number of signals averaged
OVS	Outer volume suppression
PCr	Phosphocreatine
PCSA	Physiological cross-sectional area
PCW	Post-conception weeks
P_i	Inorganic phosphate
PLIC	Posterior limb of the internal capsule
pQCT	Peripheral quantitative computed tomography
PRESS	Point resolved spectroscopy
PVHI	Periventricular haemorrhage infarction
PVL	Periventricular leucomalacia

RF	Rectus femoris
ROI	Region of interest
ROM	Range of movement
SCALE	Selective control assessment of the lower extremity
SCI	Spinal cord injury
SCP	Spastic cerebral palsy
SDD	Smallest detectable difference
SDR	Selective dorsal rhizotomy
SE	Spin echo
SEM	Standard error of measurement
SF/M	Subcutaneous fat to muscle volume ratio
SM	Semimembranosus
SNR	Signal-to-noise ratio
SO	Slow oxidative
SOL	Soleus
SS-EPI	Single-shot echo planar imaging
SSFP	Steady state free procession sequence
ST	Semtiendinosus
STEAM	Stimulated echo acquisition mode
TA	Tibialis anterior
TD	Typically developing
TE	Echo time
TMS	Transcranial magnetic stimulation
TP	Tibialis posterior
TR	Repetition time
TSRT	Tonic stretch threshold
VIF	Variance inflation factor
VL+VI	Vastus lateralis and vastus intermedius complex
WHO	Word Health Organisation
ZOOM-EPI	Zonally magnified oblique multi-slice echo planar imaging
Zp	Polar section modulus

1. Introduction

Cerebral palsy affects approximately 1 in 500 live births in the UK and is the most prevalent cause of motor disability in children[1]. Cerebral palsy recently has been defined as *a group of disorders of the development of movement and posture, causing activity limitation, that are attributed to non-progressive disturbances that occurred in the developing fetal or infant brain. The motor disorders of cerebral palsy are often accompanied by disturbances of sensation, perception, cognition, communication, and, behaviour, by epilepsy, and by secondary musculoskeletal problems*[2].. Periventricular leucomalacia (PVL) is the most common brain injury in bilateral spastic cerebral palsy. The location of these lesions, in the posterior limb of the internal capsule, results in damage to the corticospinal tract with the destruction of a number of axons. Many other areas of the brain may also be affected by the injury, either directly or by mal-development subsequent to the injury[3]. Currently there is no cure for cerebral palsy and the primary aim of clinical interventions, including physiotherapy, orthoses and orthopaedic surgery, are to improve a patient's functional capabilities and quality of life.

Although cerebral palsy is considered neurologically non-progressive, cerebral palsy may affect the neurology of the developing child including the spinal cord and motor systems. As these children grow, many develop bony and muscular deformities, which are progressive, and may interfere with their mobility and function. Acquisition of early motor skills in children with cerebral palsy is variably delayed, and in more affected individuals, these motor skills may not be acquired, such as independent walking.

Children with cerebral palsy are often categorised by the severity of their condition into one of five levels on the Gross Motor Function Classification System (GMFCS)[4]. This system categorises children into five levels based in their functional ability scored using

the Gross Motor Function Measure (GMFM)[5]. The GMFM is a clinical tool designed to evaluate change in gross motor function in children with cerebral palsy. Items on the GMFM span the spectrum from activities in lying and rolling up to walking, running and jumping skills. If a child is classified onto one of the levels at an early age, the trajectory of the functional development is predictable up to 21 years of age[6]. High functioning individuals with cerebral palsy (GMFCS levels I and II) typically remain stable into early adulthood[6]; however, lower functional individuals typically have a decline in functional ability from 8 years of age[6]. Into adulthood, individuals with cerebral palsy (GMFCS levels II-V) typically show a decline in their functional ability with increasing age[7], culminating in the early loss of mobility[7,8], with deterioration in motor ability associated with the level of neurological impairment and the timing of the acquisition of early motor mile-stones[9].

Adults with cerebral palsy have a life expectancy close to that of the general population[8,10,11], with life expectancy related to the severity of condition[10-12]. The most common cause of death in older adults with cerebral palsy is disease of the circulatory system[11]. These individuals may have a two to three times greater risk of dying from ischemic heart disease compared to the general population[13]. Considering the relative long life expectancy of adults with cerebral palsy and its apparent relationship with mobility[8,10,12], maximising an individual's potential mobility is important. An individual's mobility can be limited by muscle function, including reduced muscle volume and altered muscle composition. If present in this group, targeted interventions to improve muscle volume and composition may enable an individual to maximise their mobility, to improve both their quality of life and life expectancy.

This programme of work utilises magnetic resonance imaging techniques to first examine muscle volume and composition in bilateral spastic cerebral palsy, and their impact on skeletal strength, compared to their typically developing peers, and secondly to investigate whether white matter organisation in the spinal cord is altered in subjects with bilateral spastic cerebral palsy compared to their typically developing peers. Relationships between any altered spinal cord white matter organisation and gross motor function, and selective motor control are also explored. Chapter 1 and Chapter 2 provide an introduction to the neurological and musculoskeletal pathology associated

with cerebral palsy to enable an understanding of the condition to be developed before discussing the specific details of each study performed in this programme of work.

1.1 Thesis Aims

The aims of this programme of work are:

- To compare lower limb muscle volumes of subjects with bilateral spastic cerebral palsy (BSCP) to their typically developing (TD) peers using MRI.
- To investigate if there is a relationship between muscle volume and bone strength in the lower limb.
- To compare intramuscular fat in the distal muscles of subjects with BSCP and compare with their TD peers.
- To investigate white matter organisation in the cervical and thoracic spines of adolescents and young adults with BSCP and compare with their TD peers using diffusion tensor imaging (DTI) MRI.
- To investigate any relationships between white matter organisation in the thoracic spine and gross motor function, selective motor control.

1.2 The adult motor system

The human motor system comprises three main components: the nervous system, the skeletal musculature, and the skeletal system. The nervous system is subdivided into the central nervous system (CNS), the brain and spinal cord, and the peripheral nervous system (PNS), the nerves that transmit signals to and from the CNS. Descending tracts of the spinal cord are grouped into two major pathways, the pyramidal and extra-pyramidal tracts. The pyramidal tract, including the corticospinal tract, consists of motor neurons that conduct ionic signals from the motor region of the brain to the spinal cord where they form connections with the lower motor neurons either directly or through inter connecting neurons (interneurons) of the spinal cord, which in turn innervate skeletal muscles resulting in a muscular contraction. The extra-pyramidal tract controls posture and muscle tone via the brainstem. Ascending tracts of the spinal cord

transmit sensory signals from the peripheral receptors to the brain. Integration of sensory and motor systems enables the development of fine motor control.

1.2.1 Neurons

Nervous tissue is comprised of two types of cells: neurons and neuroglia. Neuroglia support, nourish and protect neurons and maintain homeostasis of the fluid surrounding the neurons. Neurons are formed of three parts as shown in Figure 1.1: cell body, dendrites, and axon. The cell body contains the nucleus surrounded by cytoplasm and typical cell organelles. The majority of the molecules required for the neuron's operation are synthesised in the cell body. From the cell body two types of extensions are present: multiple dendrites that receive inputs and generally a single axon, glands and muscle fibres. The axon end divides into axon collaterals, which end by dividing into many fine axon terminals.

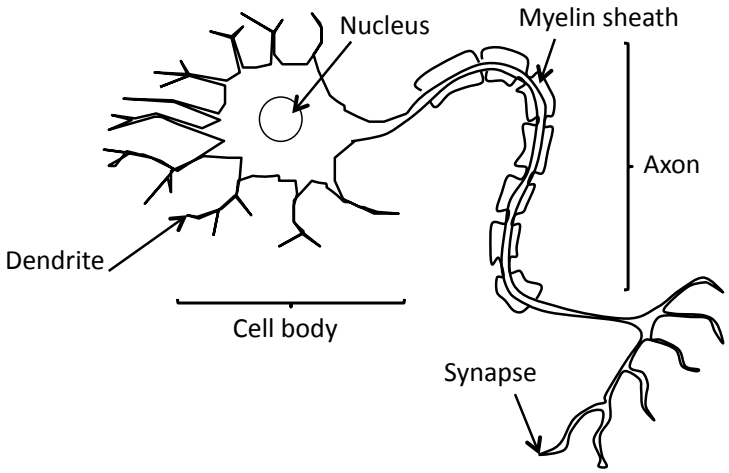

Figure 1.1 Basic components of a neuron

Neurons transmit information in the form of an electrical impulse along the axon – the action potential. The nerve action potential is a unidirectional, self-propagating reversal of the plasma membrane polarity. Initially there is an influx of sodium ions through voltage gated channels in the plasma membrane causing the membrane polarity to rise to +40 mV, follows by a rapid return to the resting membrane potential of -80 mV as potassium ions leave the axon. Action impulses are transmitted in only one direction, down the axon away from the original stimulation point. The axons of many neurons

are surrounded by a myelin sheath: a covering formed of lipid and protein. Myelin sheaths insulate the axon and increase the nerve impulse conduction velocity.

Communication between a neuron and other neurons and effector cells (the muscle, gland or organ cell that responds to a stimulus at the terminal end of an efferent neuron or motor neuron) is possible through synapses. The ends of the axon terminals form synaptic end bulbs through which chemical neurotransmitters pass to enable communication since action potentials themselves cannot pass across the synapses. A neuron may concentrate all of there connections onto a single cell or post-synaptic neuron. However, neurons can also be divergent, where a neuron synapses with many cells, or convergent, where many neurons synapse onto a single target. Convergent connections enable the integration of information from many sources and divergent connections enable a neuron to exert a widespread effect. The junctions between neurones and muscle fibres are called the neuromuscular junction. At a neuromuscular junction the nerve action potential is passed from the axon synapse, across a synaptic cleft into the muscle fibre to set up a muscle action potential via neurotransmitters.

Postsynaptic potentials can be excitatory or inhibitory. Postsynaptic excitation results in the depolarisation of the postsynaptic neuron at the cell body or dendrites, leading to an increase in the probability of initiating an action potential at the base of the second neuron's axon resulting in an action impulse along the axon. Postsynaptic inhibition is the hyperpolarisation of the postsynaptic neuron at the cell body, dendrites, or at the base of the axon. This hyperpolarisation stops the formation of the action potential, preventing the transmission of the signal along the axon. In a more complex network of connections, multiple neurons may synapse with these neurons, for example at the pre-synaptic terminal of the first axon to cause inhibition, preventing an excitation of the second neuron. It is through learning synaptic excitation and inhibition that motor and sensory systems interact to facilitate motor control.

1.2.2 The corticospinal system

The corticospinal system connects the motor cortex with the spinal cord grey matter, and is the principal motor system for controlling precise voluntary movements. The corticospinal tract conducts impulses from the brain down the spinal cord. The corticospinal tract is the last motor system to develop; brainstem motor systems are well

developed by birth, the corticospinal system continues to develop over a protracted postnatal period whilst key motor milestones are developed[14].

The corticospinal tract originates at the cerebral cortex, from the primary motor cortex, the supplementary motor area, and the pre-motor cortex. The axonal projections of the neurons in the motor cortex form the corticospinal tract that descends the spinal cord. The corticospinal tract descends at first through the posterior crus of the internal capsule, traverses the cerebral preduncle in the midbrain, the pons, and then form a discrete bundle, known as the pyramid, at the rostral level of the medulla oblongata[15]. About 70-90% of the corticospinal fibres cross the median plane in the pyramidal decussation to form the lateral corticospinal tract; of remaining, 10% continue uncrossed in the lateral corticospinal tract, and 10% continue to descend as the anterior corticospinal tract (Figure 1.2). Since the corticospinal tracts traverse the medullary pyramids, they are often referred to as the *pyramidal tracts*, a term that also includes the corticobulbar tract which diverge at this level to terminate onto the cranial motor nuclei[15].

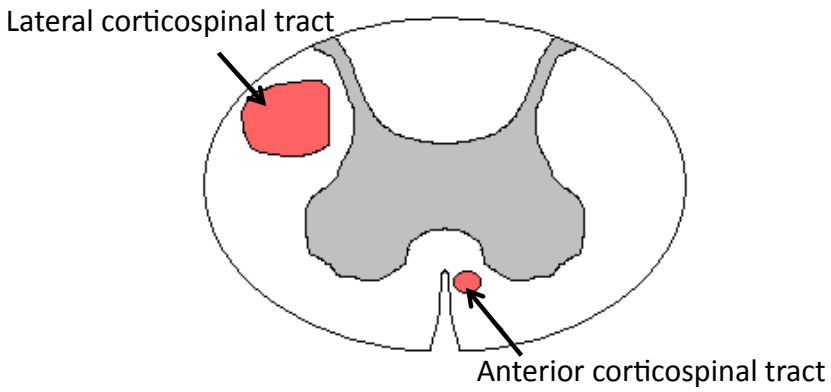

Figure 1.2 Schematic diagram of cervical spinal cord showing the location of the lateral and anterior corticospinal tracts (red) in relation to the grey matter (grey)

The lateral corticospinal tract descends in the lateral funiculus throughout most of the spinal cord, progressively diminishing in size and ending at the S4 spinal segment, as axons terminate onto the motor neurons in the ventral horn grey matter of spinal cord. This completes the connection, via the corticospinal tract, between the neurons in the motor cortex (known as the upper motor neurons) and the motor neurons in the spinal cord grey matter (known as lower motor neurons). The axons from the lower motor

neurons exit the spinal cord via anterior roots of spinal nerves and terminate at the motor end plate within a specific muscle providing motor innervation for voluntary muscles. The anterior corticospinal tract is typically much smaller than the lateral corticospinal tract. The anterior corticospinal tract descends in the anterior funiculus of the spinal cord and diminishes as it descends, ending at the mid-thoracic spine. As the anterior corticospinal tract descends, fibres cross the median plane and terminate with spinal motor neurons in the anterior white commissure[15]. Therefore, axons from the anterior corticospinal tract predominantly synapse with spinal motor neurons on the contralateral side compared to the tract, whereas axons from the lateral corticospinal tract predominantly synapse with the spinal motor neurons on the ipsilateral side.

1.2.3 Muscle tone: The vestibulospinal and reticulospinal tracts

Muscle tone is the resting resistance of a muscle to stretch due to a combination of muscle activity and the visco-elastic properties of muscle and connective tissue. Background muscle activity is controlled by brainstem nuclei, particularly the reticular and vestibular nuclei. The vestibulospinal nuclei produce two tracts, each functionally and topographically distinct: the medial and lateral vestibulospinal tracts. The lateral vestibulospinal tract descends ipsilaterally in the periphery of the antero-lateral funiculus and then shifts into the medial portion of the anterior funiculus at lower spinal cord levels. The medial vestibulospinal tract descends via the medial longitudinal funiculus into the anterior funiculus close to the midline of the spinal cord (see Figure 1.2). Unlike, the lateral vestibulospinal tract, the medial vestibulospinal tract contains crossed and uncrossed axons and does not extend beyond the mid-thoracic spine level. The vestibulospinal nuclei are involved in balance and support with the vestibulospinal tracts exciting the motor neurons in the spinal cord causing contractions of the extensor muscles in the lower limbs.

The reticulospinal tracts originate from the reticular nuclei and form three tracts: the medullary, pontine, and lateral reticulospinal tracts. The medullary axons originate from the gigantocellular reticular nucleus and descend bilaterally in the antero-lateral quadrant of the spinal cord. Pontine reticulospinal axons originate from the oral and caudal pontine nuclei and descend down the spinal cord together with the medullary reticulospinal the brain stem, collectively forming the medial reticulospinal tract. The lateral reticulospinal tract originates from the ventral-lateral tegmental field of the pons

and descends down the spinal cord in the lateral funiculus throughout the length of the spinal cord and synapses with muscle motor neurons in the spinal cord grey matter. The reticulospinal tracts are involved in locomotion and posture control and facilitation and inhibition of voluntary movement affecting muscle tone. The medial reticulospinal tract synapses with interneurons and lower motor neurons stimulating the extensor muscles and inhibiting the flexor muscles of the axial and proximal limb musculature. The lateral reticulospinal tract also synapses with lower motor neurons and interneurons but has the complementary effect to the medial reticulospinal tract: having an inhibitory effect on the extensors muscle and an excitatory effect on the flexor muscles of the axial and proximal limb musculature. Figure 1.3 summarises the location of the reticulospinal, and vestibulospinal tracts at the mid cervical level.

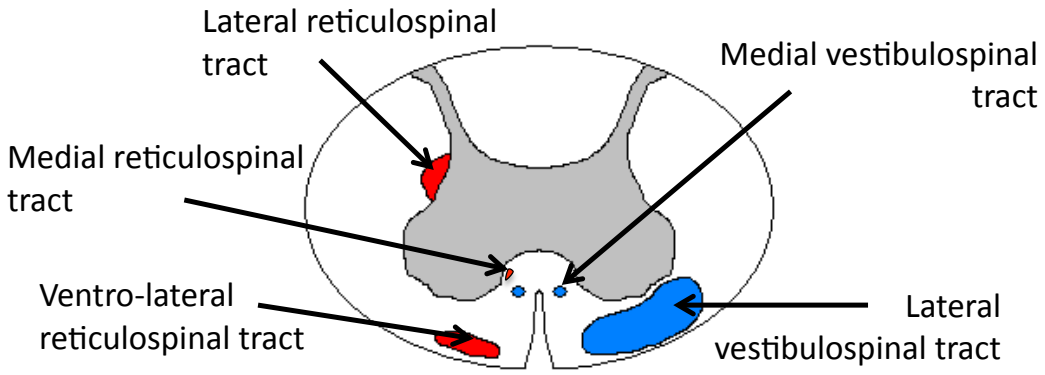

Figure 1.3 Schematic diagram of the cervical spinal cord showing the location of the vestibulospinal tracts (blue) and reticulospinal tracts (red) in relation to the grey matter (grey)

1.3 Corticospinal tract development

Once the corticospinal tract has descended through the internal capsule, traversed the cerebral preduncle in the midbrain, and brain stem, the growing corticospinal axons descend into the spinal white matter. A small number of "pioneer" corticospinal axons first enter the spinal cord between 17 and 29 post-conception weeks (PCW)[16] followed by later waves of axons that further populate the corticospinal tract[17,18], innervating the ventral horn of the spinal cord from 31 to 35 PCW[16]. The pioneer axons are guided by tissue molecular signals that are detected by the pioneer axon[19,20]. Longitudinal growth of the pioneer axon is followed by the formation of collateral branches that extend into the surrounding grey matter towards the spinal motor neurons. The innervation of the

spinal grey matter by these collateral axon branches is mediated by target-specific chemotropic factors from the target cell that induces branching[18]. This process controls each neuron's function by controlling which spinal motor neuron and corticospinal neuron interact.

The targeting of corticospinal axons to spinal motor neurons through diffuse chemical signals only enables the development of a coarse corticospinal network. However, a more refined mechanism is required to determine whether a corticospinal axon forms a functional connection with a particular segment or propriospinal circuit. This refined connectivity ultimately determines the specific functional network required to perform precise voluntary movements[14].

In the immature spinal cord, the transient corticospinal terminations are extensive in both the ipsilateral and contralateral grey matter. During the first year of postnatal life, there is growth of the spinal cord grey matter and elimination of transient terminations onto the cells of the grey matter, with the majority of the corticospinal tracts terminating in the contralateral grey matter to their origin in the motor cortex. Over the first few years of life, an adult pattern of termination emerges and axon myelination is largely complete. These refinements are augmented by stronger post-synaptic facilitation of the motor neurons, where the post-synaptic impulse potential (signal strength) is increased when the impulse closely follows a prior impulse. This results in stronger post-synaptic potentials leading to improved activation of muscle, encouraging muscle development. The refinement process is mediated by neuronal activity, with competition between terminals of the corticospinal tract. The more active the terminals are, the more competitive they are, increasing the probability they will not be eliminated[14]. However, the elimination of transient corticospinal terminations is only one aspect of the refinement process. The other refinement process is the growth of axon terminal branches and synaptic boutons[21]. This process begins during early development along side transient terminations but continues late into the postnatal period, and possibly into maturity[21], resulting in the development of fine axon branches and dense clusters of synaptic boutons[22].

There is also evidence in that suggests there are interactions between the developing corticospinal and muscle systems[23]. The elimination of transient corticospinal terminals

may leave more space in the spinal grey matter reducing the competition and thereby reducing the pruning of muscle afferent fibre branches[24].

1.3.1 Motor control and the developing corticospinal tract

As discussed above, during early postnatal development extensive anatomical changes occur in the morphology and topography of the corticospinal terminals in the grey matter of the spinal cord. This period coincides with a rapid improvement in an individual's motor skills. These improvements in motor skills can be partly attributed to development of the cognitive, sensory, and motor systems, including the corticospinal system. The refinement of the corticospinal terminals and the generation of synaptic connections through synaptic bouton and synaptic vesicle development enables effective synaptic activation of spinal motor circuits and a larger post-synaptic response for a given descending control signal down the corticospinal tract[25]. The signal transition between corticospinal and motor control is also strengthened through temporal facilitation of the control system. If a second activation signal is received at the synapse a short time after an initial control signal, the response in the post-synaptic circuit is increased compared to the size of the response evoked by the first signal. This temporal strengthening of the post-synaptic response results in stronger muscle activation signals, and therefore a greater motor response, encouraging muscle development.

However, it is important to note that the development of motor control is not just dependent on the corticospinal tract, but also on the simultaneous development of the sensory systems, including the proprioceptive, visual, and vestibular systems. Reciprocal inhibition is a key example of this. In reciprocal inhibition, the antagonist muscle stretch reflex is inhibited when the agonist muscle is contracted. This is achieved through synapse inhibition of interneurons on the motor neurons of the antagonist muscle when the motor neuron for the agonist muscle group is selectively activated, thereby reducing the contraction of the antagonist muscle. Motor-sensory development in primates and the development of the corticospinal tract are highly correlated[26]. The rostral-caudal direction of the corticospinal tract growth in the spinal cord and the correlation between corticospinal tract maturation and motor sensory function suggest a particular sequence for the acquisition of motor skills. This is

supported by observations of the order of human motor development with head control, followed by upper limb control, sitting, crawling and finally standing and walking.

1.4 Cerebral Palsy

Recently, cerebral palsy has been defined as a group of permanent disorders of the development of movement and posture, causing activity limitations that are attributed to non-progressive disturbances that occurred in the developing foetal or infant brain. The motor disorders of cerebral palsy are often accompanied by disturbances of sensation, perception, cognition, communication and behaviour, by epilepsy and by secondary musculoskeletal problems[2].

Cerebral palsy is caused by an injury to the brain during the pre-natal or peri-natal periods. The most common injuries in pre-term babies are periventricular leucomalacia (PVL) and periventricular haemorrhagic infarction (PVHI). PVL is the most common brain injury in bilateral spastic CP (BSCP) and is caused by a primary arterial ischemic injury to the white matter. This infarction causes necrosis of all cell types and axonal pathways coursing adjacent to the ventricles in the region. This infarction is typically focal, bilateral, and located dorso-lateral to the external angle of the lateral ventricle[27], in the posterior limb of the internal capsule (PLIC), resulting in damage to the corticospinal tract. Diffuse white matter injuries around the infarction foci may also occur, with many other areas of the brain potentially affected by the injury, either directly or by mal-development subsequent to the injury (for review, see Volpe (2009)[3]). PVHI is caused by germinal matrix haemorrhage through the ependymal lining, resulting in an intraventricular haemorrhage (GMH-IVH). GMH-IVH impairs blood drainage through the terminal vein, causing venous stasis and ischemia through large areas of the hemisphere. PVHI is the most common brain injury in hemiplegia, tending to affect unilaterally more of the corticospinal tract than PVL, affecting one arm and one leg contralateral to the PVHI injury.

In term births, the principal cerebro-vascular lesions result from global hypoxia-hypo-perfusion insults to the entire brain, for example post-asphyxial encephalopathy, and focal infarction following embolic occlusions of a cerebral artery, arterio-occlusive strokes. Post-asphyxial encephalopathy, caused by birth trauma or intrauterine deficit,

results in a range of neuro-pathologies, with the most metabolically active regions of the brain typically affected. The patterns of the brain injuries are associated with different neuro-developmental outcomes[28]. Focal strokes may also further complicate peri-natal asphxia.

1.4.1 Classification of Cerebral Palsy

Cerebral palsy is a heterogeneous condition in aetiology, type, and severity of impairments. Therefore, children and adults with cerebral palsy exhibit a wide range of clinical presentations and functional abilities and are often subcategorised by the nature and severity of the condition. Traditionally, cerebral palsy is subcategorised by the distribution pattern of affected limbs (topographic) and the predominant type of tone or movement abnormality (physiological). A commonly utilised classification system is shown in Table 1.1. Spastic cerebral palsy is the most common type, affecting approximately 85% of all individuals with cerebral palsy[29]. This approach facilitates the comparison of a group of individuals with similar clinical presentation enabling a broad comparison of the natural histories and planning of future service needs. However, this traditional classification system is based upon clinical presentation and does not take into account the severity or location of damage in the brain, limiting the ability of the natural history and treatment efficacy to be investigated effectively. Individuals may have similar clinical presentation but may have different aetiologies, and may have a different natural history and response to a particular intervention. Instead, treatment and identification of individuals based on the specific patho-physiology of the patient and not their clinical presentation is likely to produce more homogenous treatment groups that may result in improved patient outcome.

A group chaired by Goldstein and Bax[2] recently suggested a new classification framework. This framework has been developed to include recent developments in neuro-imaging and to improve the reliability of classification, with the ultimate aim of a standardised classification scheme to enable different clinicians to classify an individual in the same way. Bax *et al.* also recommend the discontinuation of the term 'spastic diplegia' due to the variable definitions currently in use. Currently the term can be used to describe an individual with both legs affected, or one arm and one leg of the individual are affected. Individuals may present with asymmetry, where one side is affected more than the other. In this report, the term 'bilateral' will be used to describe

individuals with both legs affected and minimal arm involvement, and 'hemiplegia' will be used to describe individuals with one arm and one leg involvement.

Topographic Classification	Explanation
Monoplegia	One lower limb involved
Hemiplegia	Unilateral involvement; usually arm more than leg
Diplegia	Bilateral involvement of the legs Minimal involvement of the upper limbs
Quadriplegia	All four limbs involved; lower more than upper
Double Hemiplegia	All four limbs involved; upper more than lower
Physiological Classification	
Ataxic	Exhibit hypotonia – reduced resistance to muscle stretch
Spastic	Exhibit hypertonia - an increased resistance to muscle stretch due to muscle spasticity (see section 1.4.2)
Athetoid	Mixed muscle tone

Table 1.1 Topographic and physiological classification of cerebral palsy

1.4.2 PVL and the developing motor system

PVL is the most common brain injury in bilateral spastic cerebral palsy and is caused by a primary arterial ischemic injury to the white matter. This infarction causes necrosis of all cell types and axonal pathways coursing adjacent to the ventricles in the region, resulting in damage to the corticospinal tract. PVL tends to occur between 24 and 33 PCW, before the transient spinal terminations of the corticospinal tract in the spinal cord grey matter have been eliminated and mature projections onto the cells of the spinal grey matter have formed. As a result of the injury, intrinsic cord networks may not mature and muscle development may be delayed[30]. An injury to the developing corticospinal tract results in the loss of fine selective voluntary muscle control in distal limb muscles. Spinal cord and subsequent muscle development is likely to be affected by the extent, severity and timing of the original brain injury.

An upper motor neuron lesion results in a combination of negative (reduced voluntary motor activity), and positive (increased involuntary muscle activity). Positive effects include increased tendon reflexes, clonus, spasticity, co-contractions, and

flexor/extensor spasms and negative effects include loss of selective motor control, muscle weakness, and fatigability. Spasticity is a common but not inevitable consequence of an upper motor neuron syndrome and is associated with damage to the corticospinal at the level of the cortex or internal capsule, and the reticulospinal and vestibulospinal tracts at the level of the spinal cord. Currently, there is no set definition of spasticity in the literature. The most commonly used definition of spasticity is by Lance (1980): '*spasticity is a motor disorder characterized by a velocity dependent increase in tonic stretch reflexes (muscle tone) with exaggerated tendon jerks, resulting from hyper-excitability of the stretch reflexes, as one component of the upper motorneuron syndrome'*[31]. However, the velocity dependence of a muscle to stretch is dependent on both muscle activity and the visco-elastic properties of the musculotendinous unit. Therefore, a review by Pandyan et al 2005 has suggested a new definition of spasticity: '*disordered sensori-motor control, resulting from an upper motor neurone lesion, presenting as intermittent or sustained activation of muscles*'[32].

Damage to the developing corticospinal tract may lead to spasticity. During normal corticospinal tract development the sensory neural pathways to the spinal cord are reduced and the effect of efferent motor neural pathways are strengthened. Damage to the developing corticospinal tract may alter the development of the intrinsic spinal networks, altering the excitatory and inhibitory connections between the upper motor neurons, interneurons, lower motor neurons and sensory neurons. This potential mal-refinement of afferent connections and reduced development of inhibitory interneurons may explain the clinical findings of spasticity in this group. Furthermore, damage to the corticospinal tract may lead to abnormal development of the spinal reflexes including muscle stretch reflexes and flexion withdrawal, leading to persistence of a low threshold response and persistence of excitatory connections to antagonist muscle groups. Therefore, any structural changes to the spinal cord white matter following PVL may relate to the degree of spasticity in cerebral palsy.

1.5 Summary

Cerebral palsy is caused by an injury to the brain during the pre-natal or peri-natal periods, with PVL the most common brain injury in bilateral spastic cerebral palsy. Children with bilateral spastic cerebral palsy often present with reduced voluntary

selective motor control and muscle spasticity due to damage to the corticospinal tract and the vestibulospinal and reticulospinal tracts of the upper motor neurons. The corticospinal tract plays an important role in spinal cord development and the development of motor control. PVL tends to occur between 24 and 33 PCW, before the transient spinal terminations of the corticospinal tract in the spinal cord grey matter have been eliminated and mature projections onto the cells of the spinal grey matter have formed. As a result of the injury, intrinsic cord networks may not mature and muscle development may be delayed[30]. Spinal cord and subsequent muscle development is likely to be affected by the extent, severity and timing of the original brain injury.

2. Muscle and Bone

The upper and lower motor neurons enable the control of human movement, however, it is the musculoskeletal system that executes the movement. As discussed in Chapter 1, the motor neurones conduct ionic signals from the brain to the muscles to cause a muscular contraction. It is through contraction and relaxation of the muscles that the body can manipulate the relative positioning of the skeleton to produce a movement. Pathology of the motor neurone system can lead to mal-development of the musculoskeletal system. This chapter discusses healthy bone, muscle micro- and macrostructure, and muscle metabolism before introducing musculoskeletal impairment in cerebral palsy, including muscle structure, weakness, volume, and composition.

2.1 Skeletal muscle microstructure

Skeletal, cardiac and smooth muscles are the three types of muscle in the human body. The focus of this programme of work is on skeletal muscle, which is attached to bone and enables the body to move. A schematic representation of skeletal muscle structure is shown in Figure 2.1. Each skeletal muscle is a separate organ comprised of thousands of elongated cylindrical cells known as muscle fibres, which run parallel to each other. Skeletal muscle fibres are highly specialised cells that produce force and movement. Muscle fibres are cylindrical with a diameter of 10-100 μm but are of varying length depending on the muscle's architecture and the number of fibres in series (see section 2.2). A collagen mesh structure, the endomysium, surrounds the muscle fibres. This connective tissue structure supports the muscle fibres and may play a central role in transmission of tension between the muscle fibres and tendon and may influence the passive mechanical properties of the fibres[33].

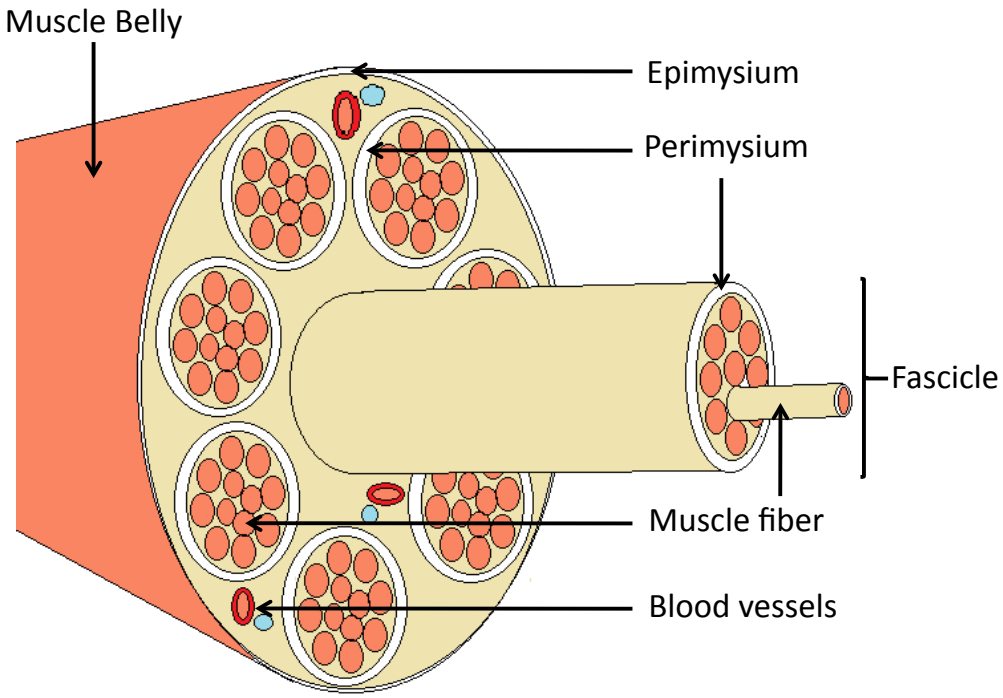

Figure 2.1 Skeletal muscle structure

Each fibre is surrounded by a plasma membrane (sarcolemma). The muscle fibre's cytoplasm (sarcoplasm) contains many mitochondria to enable production of large quantities of adenosine triphosphate (ATP) during a muscle contraction (muscle metabolism is described in section 2.3). The sarcoplasmic reticulum is a fluid filled membrane that extends throughout the sarcoplasm, which stores calcium ions required for muscle contractions. Transverse tubules (T-tubules) tunnel in from the surface to the centre of each muscle fibre along which muscle fibre action potentials travel. Along the entire length of each muscle fibre there is a cylindrical structure known as a myofibril. Each myofibril is composed of two types of protein filaments: *thin filaments* and *thick filaments*. The thin and thick filaments overlap in specific patterns to form compartments called *sarcomeres*, with sarcomeres separated by dense proteinous layers called Z discs.

Thick filaments contain the protein myosin, within myosin tails that are arranged parallel to each other with the myosin heads projecting outward from the filament surface. Thin filaments are primarily formed of the protein actin and are anchored to the Z discs. Each individual actin molecule contains a myosin-binding site that enables the myosin heads of the thick filaments to attach. However, thin filaments also contain

tropomyosin and troponin. Tropomyosin, in a relaxed muscle, blocks the myosin binding sites on the actin preventing binding occurring between the thin and thick filaments. Troponin holds the tropomyosin molecules in place. It is through manipulation of the interactions between thin and thick filaments that muscle contractions can occur through the 'sliding filament contraction mechanism' as summarised below.

1. Muscle action potential travels along transverse tubules opening Ca^{2+} channels in the sarcoplasmic reticulum membrane.
2. Ca^{2+} flows into the sarcoplasm down its concentration gradient.
3. Ca^{2+} binds to troponin on the thin filaments exposing the myosin binding sites.
4. The actin-myosin bridge rapidly dissociates due to binding with ATP.
5. The free myosin bridge moves into position to attach to actin, during which ATP is hydrolyzed.
6. The free myosin bridge and its hydrolyzed products rebind to the actin filament.
7. The-cross bridge generates force and actin replaces the reaction products (ADP and P_i) from the myosin cross-bridge ready for further ATP binding in step 4.
8. Ca^{2+} channels in sarcoplasmic reticulum close and Ca^{2+} active transport pumps use ATP to restore low Ca^{2+} concentration in the sarcoplasmic reticulum.
9. Troponin-tropomyosin complex slides back over actin binding sites blocking the myosin of the thick filaments.
10. Muscle relaxes until another muscle action potential arrives.

2.2 Muscle macrostructure

2.2.1 Muscle fibre types

In addition to the muscle microstructure discussed above, there are different fibre types with different morphological, contractile, and metabolic properties. Classically, muscle fibres are categorised into one of three types; Type 1 (SO), Type 2a (FOG), or Type 2b (FG). The morphological, contractile, and metabolic properties for each category is summarised in Table 2.1. Each fibre type is present in varying proportions within the different muscles in the body. However, this classification system is a simplification of the diverse variability between muscle fibres, with a spectrum of possible morphological, contractile, and metabolic properties.

2.2.2 Skeletal Muscle Architecture

Muscle fibre architecture is the arrangement of muscle fibres with respect to the force generation axis. Muscles have adopted different fibre alignments dependent on their function in the body. The maximum contraction force generated by a muscle is dependent on the muscle architecture. Muscle fibre architectures are broadly categorised into three categories. Muscles with fibres that extend parallel to the muscle force-generating axis and extend along most of the muscle length have a parallel or longitudinal architecture. Muscles with fibres orientated over a narrow range of angles relative to the force-generating axis (the pennation angle) are termed to have uni-pennate architecture. Muscles with fibres orientated at several pennation angles are termed to have a multi-pennate architecture. As well as pennation angle, muscle force is also dependent on muscle fibre length, fibre diameter, sarcomere length and muscle mass. The measurement of architectural parameters enables the calculation of the physiological cross sectional area (PCSA), which is directly proportional to the maximum force, generated by the muscle (Equation 2.1). Equation 2.1 can be further simplified since muscle volume (cm^3) is equivalent to muscle mass divided by density (Equation 2.2).

$$PCSA\,(mm^2) = \frac{M \cdot \cos\theta}{\rho \cdot L} \qquad \textit{Equation 2.1}$$

$$PCSA\,(mm^2) = \frac{V \cdot \cos\theta}{L} \qquad \textit{Equation 2.2}$$

Where M = Muscle mass, θ = Pennation angle, L = fibre length, ρ = muscle density, V = Muscle volume

Type 1 Slow oxidative (SO)	• Small in diameter. Contract slowest of the fibre types • Large amounts of myoglobin and mitochondria enabling ATP generation through aerobic respiration. • Very fatigue resistant: prolonged sustained contractions
Type 2a Fast oxidative-glycolytic (FOG)	• Contain large amounts of myoglobin • Generate ATP through aerobic respiration and glycolysis • Moderately high resistance to fatigue and are faster than SO fibres
Type 2b Fast glycolytic (FG)	• Largest in diameter. Generate the most powerful and fastest contractions • Low myoglobin and mitochondria content • Generate ATP predominately through glycolysis: fatigue quickly

Table 2.1 The three muscle fibre types and their properties[34]

2.3 Skeletal muscle development

Skeletal muscle development can be subdivided into four simultaneous processes: axonal outgrowth; myogenesis; synaptogenesis; and synapse elimination. In this section a brief overview of the four processes of muscle development are outlined, however, the detailed mechanisms within each process are not discussed.

Axonal outgrowth is the process by which axons traverse from the ventral root of the spinal cord to the muscles. There is an approximate correspondence between the location of ventral root of the spinal cord with the muscles they innervate, for example the nerve root of biceps brachii is at the C5-C6 spinal level and the nerve root of the soleus is L5, S1-S2, however, this is variable between individuals.

Myogenesis is the formation of muscle fibres. This process begins in the embryo where somites, the masses of tissue arranged in regular intervals along an embryos length, are differentiated and are destined to become skeletal muscle stem cells (myoblasts). This process of determination is controlled by two proteins, myoD and myf5[33]. Myoblasts are the precursors of muscle fibers, whose development through differentiation and maturation is controlled by myogenic regulatory factors (mrf4 and myogenin)[33]. These regulatory factors cause the myoblasts to cluster and fuse forming multi-nucleated cells called myotubes that are 0.1 – 0.3 mm in length[33]. Myoblasts continue to fuse onto the ends of the myotubes enabling the myotubes to increase in length. These early myotubes are called primary myotubes. Primary myotubes and some less differentiated cells separate from the other primary myotubes to form clusters that are surrounded by a sheath – the basal lamina. Myoblasts then begin to cluster and aggregate beneath the basal lamina of the primary myotubes to form a secondary myotube. Unfused myoblasts also remain present beneath the basal lamina and are known as satellite cells. The primary and secondary myotubes contained within a single membrane then further differentiate towards becoming muscle fibres and become filled with contractile proteins.

Synaptogenesis is the formation of the neuromuscular junction. As the muscle fibres develop acetylcholine (ACh) receptor proteins are integrated into the muscle membrane, the sarcolemma. As the outgrowing nerve from the spinal cord contacts the muscle

fibre, ACh receptors cluster around the site of the nerve, increasing the number of ACh receptors at the nerve junction and decreasing the number of ACh receptors elsewhere in the muscle. Once the ACh receptors are localised, the muscle fibre nuclei near the neuromuscular junction express the genes responsible for normal neuromuscular junction function. Once a neuromuscular junction has formed with a muscle fibre, due to neuromuscular junction activity it can no longer make new neuromuscular connections limiting the number of neuromuscular junctions on each muscle fibre to one[33]. However, once one neuromuscular junction has formed multiple other motor neurons may form a connection with the fibre through this neuromuscular junction. The number of motor neuron connections at the synapse is then subsequently reduced (synapse elimination) through inter-synaptic competition and synaptic withdrawal. In the maturing motor system, the number of motor neurons connecting to neuromuscular junction on a muscle fibre is reduced so that each muscle fibre is connected to only one motor neuron.

2.4 Muscle metabolism

Muscle cells, like all cells in the body, require energy to maintain cellular processes. However, muscle cells also additionally require energy to produce movement and force generation. Adenosine triphosphate (ATP) is the cellular energy molecule: a large amount of chemical energy is stored within each ATP molecule, which can then be transported around the cell to provide energy for example for muscle contraction, ion transport, and protein synthesis. The energy is acquired from ATP molecules by splitting it into adenosine diphosphate (ADP), an inorganic phosphate (P_i) (Equation 2.3).

$$ATP \Longleftrightarrow ADP + P_i + Energy \qquad \textit{Equation 2.3}$$

Where ATP = Adenosine triphosphate, ADP= Adenosine diphosphate, P_i = inorganic phosphate

ATP in muscle is primarily used in the contraction process (see section 2.1), where ATP enables the detaching of the myosin cross-bridges from the actin filaments, and to provide energy for metabolic pumps. The sodium-potassium pump (Na^+-K^+) maintains a resting potential difference across the muscle fibre membrane, and the calcium (Ca^{2+}) pump returns Ca^{2+} to the sarcoplasmic reticulum after muscle activation. Energy is

generated within the muscle fibres through glucose and lipid oxidation, and stored in phosphocreatine, glycogen and lipid droplets within the sarcoplasm of the muscle fibres.

2.4.1 Phosphocreatine energy reserve

To enable muscle fibre activity to be sustained, a renewable supply of ATP is required. This is achieved in the short term through energy stores within the muscle fibres in the form of phosphocreatine (PCr). As ATP is expended, the enzyme creatine kinase replenishes ATP stores from PCr:

$$PCr + ADP \Longleftrightarrow ATP + Cr \qquad \textit{Equation 2.4}$$

Where Cr = Creatine

However, PCr stores are not unlimited and become exhausted after 5-8 seconds of maximal contractions. For muscle activity to continue, the muscle fibres become reliant on glucose and lipid oxidation. The PCr stores are then replenished once the activity has been completed.

2.4.2 Glucose oxidation

Glycolysis is the breakdown of glucose into pyruvate producing a net gain of 2 ATP molecules. A simplified chemical reaction is shown in Equation 2.4. Additional intermediary molecules are produced between the start and end molecules that are not shown in Equation 3.4. This chemical reaction takes place in the muscle fibre cytosol and is anaerobic.

$$Glucose + 2ADP + 2P_i \Rightarrow 2Pyruvate + 2ATP \qquad \textit{Equation 2.4}$$

Once glucose has been broken down to produce pyruvate (pyruvic acid), there are two different pathways for further oxidation depending on the availability of oxygen. In anaerobic conditions, for example during sustained strong contractions when the pressure inside the muscle becomes greater than the systolic blood pressure limiting oxygen perfusion into the muscle, pyruvate is oxidised to lactate (lactic acid) by nicotinamide adenine dinucleotide coenzyme (Equation 2.5). The anaerobic pathway results in a build up of lactate within the muscle. Since lactate is an acid molecule it alters the intracellular pH, which in turn alters subsequent cellular contraction and

metabolic activity. Furthermore, once the muscle activity intensity reduces, energy is required to transport the lactate in the blood to be further metabolised in the liver. Glycolysis is an inefficient process that does not produce enough energy to sustain muscle contractions in purely anaerobic conditions for much longer than 10-30 seconds.

$$\text{Pyruvate} + \text{NADH} \Rightarrow \text{Lactate} + \text{NAD}^+ \qquad \textit{Equation 2.5}$$

The second pathway requires oxygen and is the preferential pathway for energy production as this pathway produces more ATP. When oxygen is present, pyruvate is rapidly taken up into the mitochondria to be oxidised to carbon dioxide and water (Equation 2.6). This pathway produces 15 ATP molecules for each pyruvate molecule oxidised, totalling 30 ATP for each glucose molecule initially broken down by glycolysis and is, therefore, the most efficient method for cells to manufacture ATP molecules from glucose.

$$\text{Pyruvate} + 15\text{ADP} + 15\text{P}_i + 4\text{O}_2 \Rightarrow 3\text{CO}_2 + \text{H}_2\text{O} + 15\text{ATP} \qquad \textit{Equation 2.6}$$

The oxidation of pyruvate begins with decarboxylation and combination with coenzyme A (CoA) to create acetyl CoA. Acetyl CoA then combines with oxaloacetic acid to make citric acid. Through a further series of reactions, two carbon atoms within the citric acid molecule are oxidised and removed to produce CO_2, resulting in the eventual formation of oxaloacetic acid again. Therefore, the metabolism of axaloacetate forms a cycle known as the citric acid cycle (or Krebs cycle). Once Pyruvate has been combined with CoA to produce acetyl CoA, the energy is harnessed into ATP in two ways. One way is the creation of a high-energy phosphate bond within guanosine triphosphate (GTP), which in turn donates its phosphate to ADP forming ATP. The second way is the predominant producer of energy in the citric cycle, the electron transfer chain. Electrons are first received by the hydrogen receptor molecules, nicotinamide adenine dinuclide (NAD) and flavin adenine dinuclide (FAD) and are then passed to cytochromes on the inner mitochondrial membrane. As the electrons are passed along the cytochromes of the electron transfer chain, the electrons drop down their energy levels, with the released energy used to transport protons across the inner mitochondrial membrane against their concentration gradient. The energy generated by this proton gradient is sufficient to drive ATP synthesis, coupling oxidation to phosphorylation. The protons then diffuse back across the inner mitochondrial membrane through ATP

synthase channels into the mitochondrial matrix. Figure 2.2 schematically shows the reactions in the citric acid cycle.

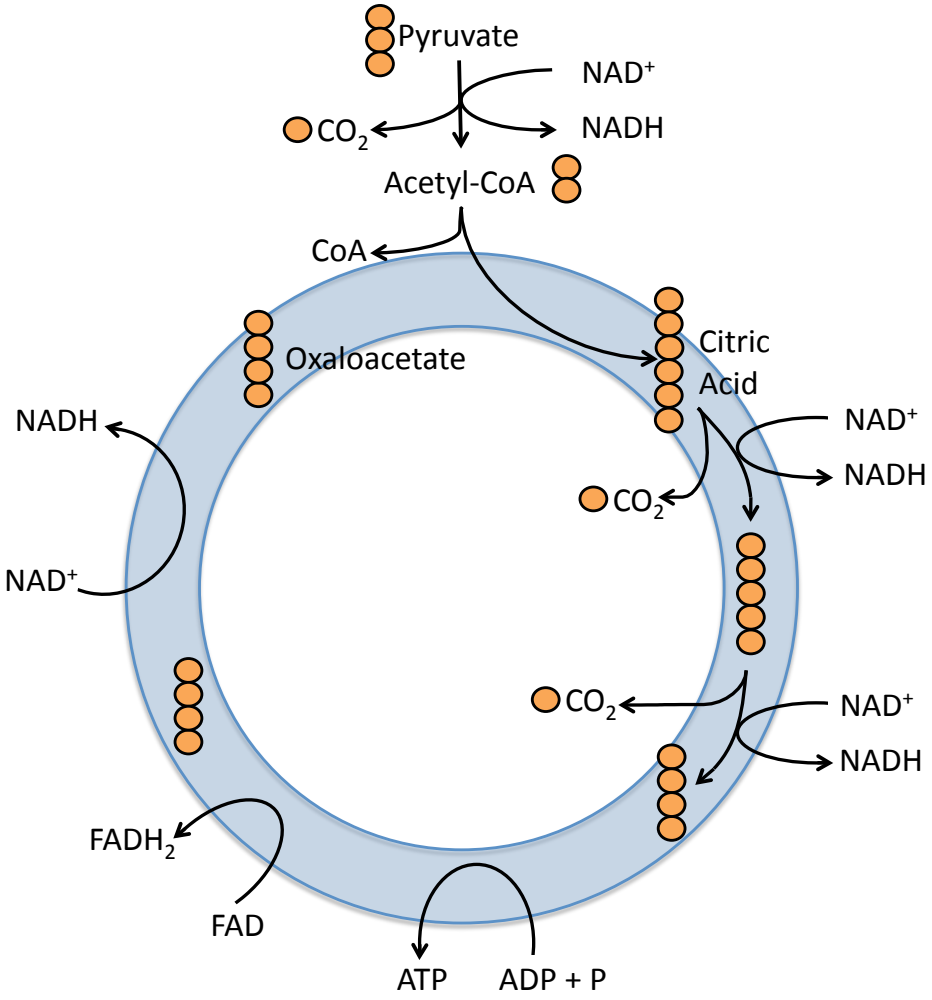

Figure 2.2 Citric acid cycle. The orange circles represent the number of carbon molecules in each intermediate molecule. The carbon atoms are removed as CO_2 and NAD+ and FAD (two carrier molecules in the electron transfer chain) take up the H atoms

2.4.3 Glycogen degradation and synthesis

Muscle fibres can oxidise glucose directly from the blood stream, however, during muscle contractions the majority of the glucose oxidised to produce ATP is provided by the hydrolysis of glycogen stored in the muscle fibre sarcoplasm. Glycogen is synthesised by the enzyme glycogen synthase, which links thousands of glucose molecules together to form glycogen. The glycogen molecules are then broken down by the enzyme glycogen phosphorylase.

However, this is the final stage of the reactions that enable glycogen hydrolysis to occur. First, epinephrine (adrenaline) in the blood stream, released in response to stress, binds with G protein receptors on the muscle fibre sarcoplasm activating the membrane enzyme adenyll cyclise. This enzyme then produces a secondary messenger molecule, cyclic adenosine monophosphate (cAMP), which activates the enzyme protein kinase. Once activated, protein kinase activates the enzyme glycogen phosphorylase through phosphorylation, which can in turn then break down glycogen to produce glucose. Therefore, the amount of glucose available to the muscle fibre to produce ATP is controlled by epinephrine.

2.4.4 Lipid oxidation

As well as glucose, lipids (fatty acids) provide another source of energy to the muscle cells. Lipid metabolism is used to supply the energy for resting muscles and during exercise, particularly during low intensity exercise. However, during prolonged exercise such as long distance running, all the muscle glycogen stores are depleted and continued exercise is predominantly dependent on lipid metabolism[35]. The most abundant dietary lipids are triglycerides, which are composed of a glycerol backbone, to which three fatty acids are esterified. Triglycerides are also the form of lipid stored in lipid droplets within a cell's sarcoplasm.

The first step in lipid metabolism is the breakdown of the triglyceride lipid molecules into a glycerol and three fatty acid molecules. Fatty acid molecules vary in length. Short and medium chain fatty acids pass directly through the inner mitochondrial membrane into the inner matrix space of the mitochondria. Long chain fatty acids, for example palmitic acid (16 carbon atoms) and stearic acid (18 carbon atoms), require transportation into the mitochondria. At the outer mitochondrial membrane, long chain fatty acids are first activated by esterification with CoA and ATP to acyl-CoA by acyl-CoA synthetase enzymes in two steps: first, the fatty acid molecule replaces the diphosphate group in ATP; second, CoA replaces the adenosine monophosphate (AMP) group in ATP to form acyl-CoA (Equation 2.7). Different acyl-CoA synthetase enzymes are present in the mitochondrial outer membrane for fatty acids of different lengths.

$$\text{Fatty acid} + \text{ATP} + \text{CoA} \Rightarrow \text{acylCoA} + \text{AMP} + 2\text{P}_\text{i} \qquad \textit{Equation 2.7}$$

No transport system is present for acyl-CoA to transport it into the inner mitochondrial matrix. Therefore, acyl-CoA enters the mitochondria via a shuttle system facilitated by the ammonium compound carnatine, which is biosynthesised from the amino acids lysine and methionine. The enzyme carnatine palmityl transferase I converts acyl-CoA to acetyl-carnatine at the outer surface of the inner mitochondrial membrane. Acetyl-carnatine is then transported into the mitochondrial matrix by the enzyme acetyl-carnatine translocase in exchange for carnatine molecules from the inner matrix space.

Once in the mitochondrial matrix, acetyl-carnatine is converted back to acyl-CoA by the enzyme carnatine palmityl transferase II. The short and medium chain fatty acids are converted directly into acyl-CoA within the mitochondrial matrix by acyl-CoA synthetase enzymes, in the same process that takes place for the long chain fatty acids at the mitochondrial outer membrane (Equation 2.7). The transfer of fatty acids into the mitochondria is summarised in Figure 2.3. Next, all acyl-CoA molecules are oxidatively phosphorylated in the β-oxidation pathway to produce acetyl-CoA: 1) Activation of acyl-CoA by ATP. 2) Oxidation by FAD. 3) Hydration (adding of a hydroxyl group and a hydrogen cation to the carbon-carbon double bond). 4) Oxidation by nicotinamide adenine dinucleotide (NAD^+). 5) Thiolysis (splitting one molecule in two with an organic sulphur compound) to produce acetyl-CoA.

$$\text{Palmitic acid} + \text{Acetyl CoA} + 7O_2 \Rightarrow 7CO_2 + 4H_2O + 129\text{ATP} \qquad \textit{Equation 2.7}$$

Once the acyl-CoA molecules have been converted into acetyl-CoA, acetyl-CoA then enters the citric acid cycle and is oxidised to CO_2 and H_2O producing ATP (Figure 2.5). This is the same process that pyruvate enters in the aerobic glucose metabolism pathway. Equation 3.8 shows the overall reaction and ATP production for an example fatty acid palmitic acid, which has 16 carbon atoms. The transfer of fatty acids into the mitochondrial matrix is shown in Figure 2.4. A summary of the oxidative reactions in the mitochondria to produce energy is shown in Figure 2.4.

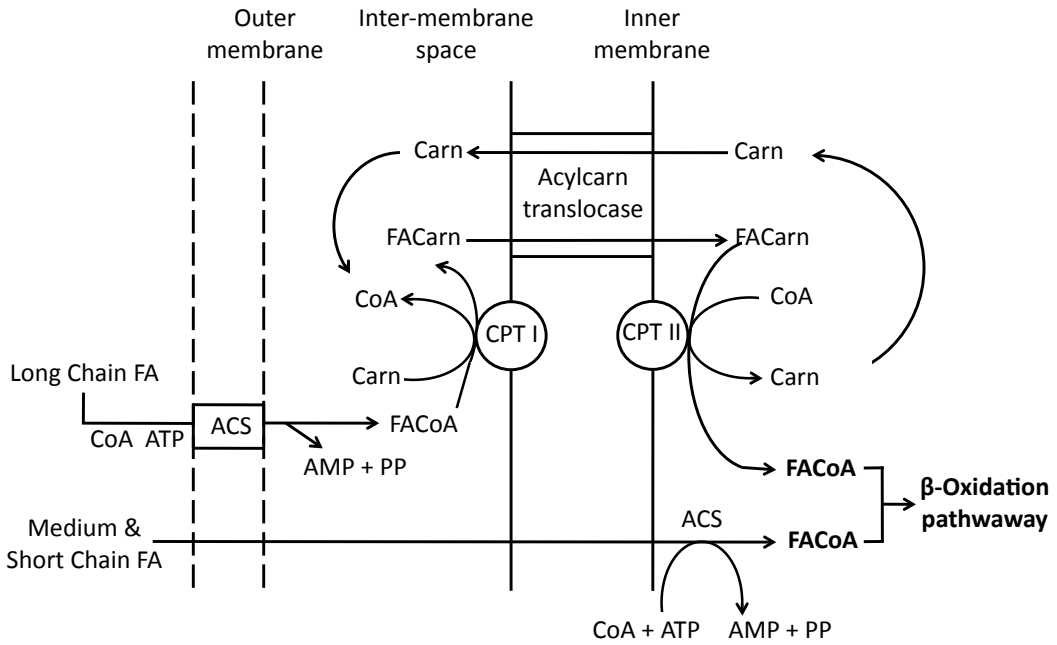

Figure 2.3 Transfer of fatty acids into the mitochondrial matrix. ACS = Acyl-CoA synthase; Carn = Carnatine; CPT = Carnatine plamityltransferase; FA = Fatty acid

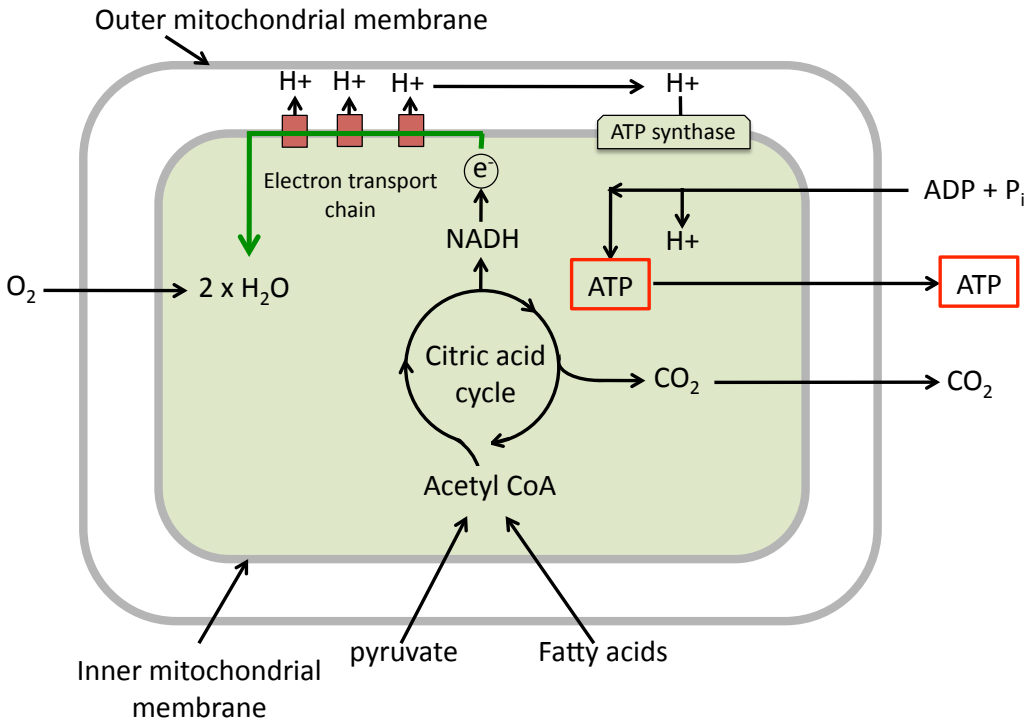

Figure 2.4 Summary of the oxidative reactions in the mitochondria that produce energy in the form of ATP molecules by converting pyruvate and fatty acids to CO_2 and H_20

2.4.5 Insulin, glucagon and skeletal muscle metabolism

Insulin and glucagon are peptide hormones produced by the beta and alpha cells in the pancreas respectively. Insulin and glucagon regulate blood glucose levels. Glucagon causes the liver to convert stored glycogen into glucose, which is released into the blood stream. Insulin reduces blood glucose levels by causing the uptake of glucose from blood in the liver, skeletal muscles, and adipocytes (fat cells) and causes the transition from lipid metabolism to glucose metabolism. Skeletal muscle is the most abundant insulin-sensitive tissue, 40-50% by body mass, is responsible for approximately 20-30% of resting oxygen consumption, and is responsible for 75-95% of all insulin mediated glucose disposal[36-38]. Therefore, skeletal muscle is not only responsible for force generation and movement facilitation, but also plays a significant role in metabolic health.

Humans, and mammals in general, have the ability to switch metabolism between carbohydrates in times of abundance (decreased insulin) and lipids in times of calorific scarcity (decreased insulin), as the primary energy source is termed metabolic flexibility[39,40]. Insulin can also enhance lipid and glucose metabolism in periods of high metabolic demand due to exercise. The skeletal muscle insulin signalling pathways is summarised below.

Insulin binds with α-subunits of insulin receptors on the sarcolemma. This causes increased intracellular β-subunit tyrosine kinase activity, which in turn causes autophosphorylation and phosphorylation of the insulin receptors and insulin receptor substrates (IRS-1, IRS-2), respectively. Tyrosine phosphorylation of IRS-1 and its association to the p85 regulatory subunit of phosphatidylinositol-3-kinase (PI3K) activates the p110 catalytic subunit, which increases phosphoinositides such as phosphatidylinositol 3,4,5-trisphosphate. This leads to the activation of phosphoinositide-dependent protein kinase (PDK) and downstream protein kinase B (Akt) and/or atypical protein kinase C (PKC). Phosphorylation of Akt substrate 160 (AS160), which has a guanosine-5'-triphosphate (GTP)ase-activating domain (Rab4), allows translocation of an insulin sensitive glucose transporter (GLUT4) to the sarcolemma to facilitate glucose entry into the cell. Intracellular glucose is then rapidly

phosphorylated by hexokinase and directed to oxidative or non-oxidative (glycogen synthesis) pathways[41].

As well as the insulin signalling pathway summarised above, which increases glucose metabolism, insulin also suppresses fatty acid oxidation in skeletal muscle[42]. This mechanism is not as well understood. However, one possible mechanism is that at high physiological insulin concentrations there is a decrease in lipoprotein lipase and increased malonyl CoA levels[43].

2.4.6 Intramuscular fat and muscle metabolism

There is a strong relationship between intramuscular fat content, insulin resistance and type-II diabetes[44-46], with raised intramuscular fat levels potentially providing a marker of impaired mitochondrial content and/or function[41]. Within skeletal muscle, fat is stored in two separate compartments: Intramyocellular lipid (IMCL) and extramyocellular lipid (EMCL). EMCL is found within adipose cells adjacent to the muscle fibres, and IMCL is located within the muscle fibres along with enzymes involved in fatty acid esterification, hydrolysis, and transport into the mitochondria[47]. Enhanced storage of IMCL occurs due to the combined effects of high concentration of serum insulin and free fatty acids[48]. In particular, greater IMCL in the soleus correlates with glucose-insulin-lipid metabolism and insulin sensitivity[49-52], with soleus IMCL content being the only differentiating feature in a study of lean insulin-resistant subjects and their TD peers matched for BMI, body fat distribution, percentage body fat and physical fitness[52].

Adults with cerebral palsy have a life expectancy close to that of the general population[8,10,11], with life expectancy related to the severity of condition[10-12]. The most common cause of death in older adults with cerebral palsy are diseases of the circulatory system[11]. These individuals may have a two to three times greater risk of dying from ischemic heart disease than their typically developing peers[13]. Further to the shorter life expectancy, individuals with cerebral palsy tend to show a decline in their functional ability with increasing age[7], culminating in the early loss of mobility[7,8]. Weakness is a prevalent feature of individuals with cerebral palsy[53-55]. Weakness may be manifest in changes to intrinsic properties of the muscle itself, for example reduced muscle volume[53,56-61], reduced non-contractile myofibrillar tissue, an inability to

optimally control the available muscle resources, for example reduced selective activation and co-activation of antagonist muscle groups. Raised intramuscular fat corresponds to reduced contractile tissue content, resulting in a weaker muscle than predicted from muscle mass alone. Furthermore, inflammatory cytokines produced by intramuscular fat may interfere with the action of myofibrillar proteins reducing specific force production[62]. These secondary pathologies may contribute to a deficit in the "functional reserve" of adults with BSCP, and may expose these individuals to a heightened risk of immobility with increasing age[60].

Decreased physical activity is associated with increased intermuscular fat[63-66]. Intramuscular fat has also previously been correlated with deficits in central muscle activation[67], increased risk of future mobility loss[68,69], and insulin resistance[70] in the elderly population. Considering the typically sedentary behaviour observed in cerebral palsy[71,72] and similarities between muscles in the elderly and in cerebral palsy, including reduced muscle volume[73], increased stiffness[74] and reduced voluntary muscle activation[75], individuals with cerebral palsy may have raised levels of intra- and intermuscular fat. However, it is important to note that the comparison of muscle in cerebral palsy with the elderly is limited due to the aetiology of the two groups. Muscle properties in the elderly are related to a degradation of muscle function with age, which is of different aetiology to muscle in cerebral palsy, which is abnormal as a result of altered muscle development including myogenesis and hypertrophy in this group. There are limited studies in the literature that have investigated body or muscle composition in this group. Since individuals with cerebral palsy have reduced muscle mass, even those with body mass index (BMI) in the normal range may have relatively increased levels of adipose tissue. Previous studies in children with cerebral palsy have suggested raised levels of fat[76,77]. In an MRI study of the lower limbs in children with quadriplegic cerebral palsy (GMFCS levels III-V), Johnson *et al*[76] found increased levels of intermuscular and subcutaneous fat[76]. To date, there have been no studies of intramuscular fat in adults or children with cerebral palsy. Therefore, a study investigating intramuscular fat in adults with cerebral palsy is required due to the multi factorial implications intramuscular fat may have on an individuals life, including: cardio-metabolic disease risk, muscle weakness, and the decline in mobility with increasing age reported in this group.

2.5 Bone

The skeletal system provides several functions including support, protection, enabling movements, mineral homeostasis, blood cell production and triglyceride storage. The main focus of this programme of work is on the effect of cerebral palsy on an individual's mobility, therefore, only aspects of bone morphology will be discussed. Bones are broadly classified into four categories based on their shape, long (e.g. femur), short (e.g. wrist and ankle bones), flat (e.g. scapulae, sternum), and irregular bones which do not fit into the other three categories. In this thesis, it is the long bones that are of primary interest as they form the main segments of the limbs on to which the muscles act to produce movement. The typical macroscopic structure of a long bone is shown in Figure 2.5.

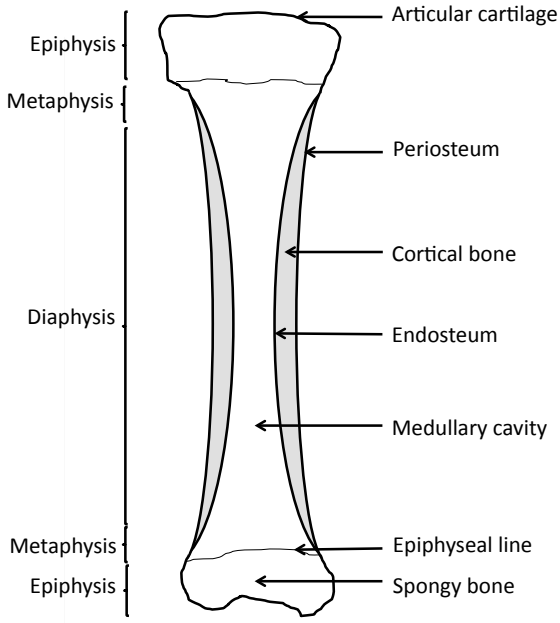

Figure 2.5 Schematic diagram of long bone structure

The *metaphyses* are the regions in a mature bone where the diaphysis joins the epiphysis. However, in a growing bone each metaphyses contains an *epiphyseal plate*, a layer of hyaline cartilage that allows the diaphysis of the bone to grow in length through ossification. Articular cartilage is a thin layer of hyaline cartilage covering the parts of the epiphyses where the bone forms a joint with another bone. The role of articular cartilage is to reduce friction and absorb shock at freely moveable joints. Where the bone surface is not covered by articular cartilage it is covered by the periosteum. This is

a tough sheath of irregular connective tissue containing bone forming cells that enable bone to grow in diameter but not in length.

2.5.1 Bone development

Bone initially begins as a soft tissue model made from aggregated mesenchymal cells, to produce a hyaline cartilage model by bone[78]. The process of replacing this cartilage with bone is called osteogenesis. Osteogensis starts at the centre of the cartilage model, at an ossification centre during embryonic development *in utero*. The majority of bones have multiple ossification centres, the first ossification centre, *or primary ossification centre*, appears in late embryonic to early foetal life (7-16 weeks post-conception[15]) from which the bone diaphysis is formed. Secondary ossification sites form at birth at the ends of the long bones and at the extremities of flat bones where cartilaginous epiphyses ossify. Osteogenesis has a different mechanism depending on bone type: intramembranous (flat bones) and endochondral bones (long bones). The process of endochondral ossification can be divided into seven stages summarised below. Hyaline cartilage is left on the ends of the bones to form articular cartilage, and the epiphyseal plates (growth plates) are also formed to enable later increases in bone length. A brief overview of endochondral bone development is outlined below and in Figure 2.6.

1. *Periosteum formation:* A hyaline cartilage model of the bone grows by a continuous division of chondrocytes accompanied by the secretion of an extracellular matrix, forming a layer of dense irregular connective tissue and undifferentiated stem cells (osteogenic cells) that surrounds the cartilage. The osteogenic cells then differentiate into osteoblasts.

2. *Bone collar formation:* The osteoblasts secrete osteoid, a gelatinous substance consisting of collagen and mucopolysaccharide), onto the outside of the periosteum, resulting in the formation of a bony collar on the outside of the cartilage.

3. Calcification of the matrix: Chondrocytes in the primary centre of ossification undergo hypertrophy and begin to secrete alkaline phosphatase instead of collagen. This enzyme removes the phosphate group from compounds enabling their calcification.

4. Cavity formation: The calcification of the primary centre makes the inner cartilage impermeable to the diffusion of nutrients. As a result the inner cartilage starts to deteriorate and cavities begin to form.

5. Vascular invasion: The vessels that are within the periosteum will pass through the lamellar (compact bone) bony collar and invade the inner cavity of the cartilage model. The remaining cartilage is broken down by osteoclasts and the osteoblasts secrete their osteoid forming trabaculae (spongy bone).

6. Elongation: As blood vessels, osteoclasts, and osteocytes continue to invade the bone, endochondral ossification spreads outwards along the bone diaphysis causing the bone to elongate. At this time, blood vessels also invade the hyaline cartilage at the ends (the epiphyses) of the long bones forming secondary ossification centres.

7. Epiphyseal ossification: This is similar to step 3, except instead of forming compact bone, spongy bone is formed.

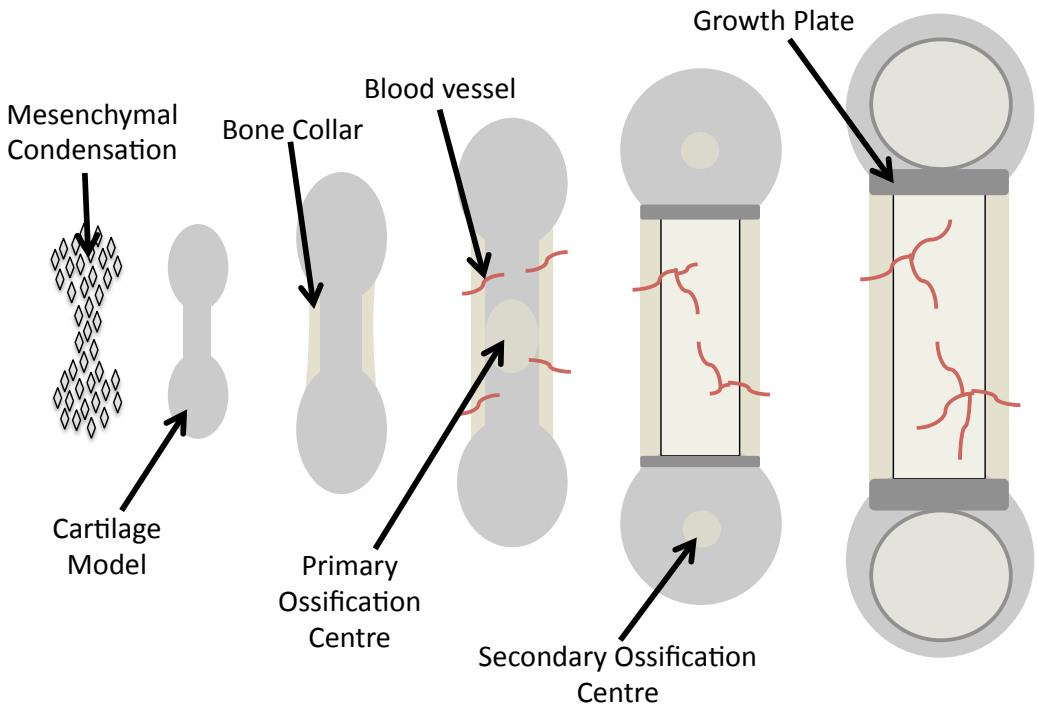

Figure 2.6 Summary of endochondral bone development

Increases in bone length occur at the epiphyseal plate where hyaline cartilage expansion and ossification continues until skeletal maturity when fusion of the diaphysis and epiphysis occurs. In order for bones to increase in a width a new layer of compact bone is deposited into the outside of the bone. The peripheral edge of bone is lined by the periosteum in which osteoblasts secrete osteoid and become trapped in their secreted matrix directly beneath the periosteum, forming osteocytes. The bone cavity then increases in diameter through bone resorption by osteoclasts. This process is known as bone modelling: during growth, the skeleton is sculpted to achieve the desired shape and size by the removal of bone from one site by osteoclasts and deposition at a different site by osteoblasts. Once the skeleton has reached maturity, this process continues in the form of a periodic replacement of old bone with new at the same location, a process known as bone remodelling[79]. Bone remodelling enables micro-fractures to be repaired and calcium homeostasis.

2.5.2 Bone strength

Bone strength is dependent on the ultimate strength of bone tissue, the spatial distribution of bone tissue (density, geometry), and the ability for bones to repair micro-damage. Mechanical forces are a significant factor affecting bone strength and development. During growth, longitudinal growth increases lever arms and bending moments leading to greater forces experienced by the bone[80]. Greater muscle force also applies mechanical forces to the bones during muscle contraction. Body weight alone puts relatively small loads on bones, but the effect of weight is amplified by muscle action[81], with bending and torsional forces being the predominant loading factors in long bone diaphysis[82,83]. There are two possible physiological adaptation processes influencing the relationship between bone and muscle strength; individual and evolutionary[84]. The evolutionary adaptation is evident from genetic factors influencing bone and muscle mass[85]. Bone strength is closely related to an individual's height, as the bending forces experiences by the bones will increase with increasing length. The mechanism by which an individual increases bone strength to muscle strength mediated by strain is termed the Mechanostat Theory[86,87]. In this theory, the muscle-bone relationship, expressed as the "bone-muscle unit," is modelled as a mechanical relationship modulated by the hormonal system.

Bone strength is determined predominantly by bone geometry and bone density,. The ability of a bone to resist torsional and bending forces (the polar section modulus, Zp) is inversely proportional to bone length to the third power and directly related to bone diameter to the third power[88]. Assuming a cylindrical bone shape, with circular cross-section, the polar moment of inertia (J) is calculated using Equation 2.12[89]. The polar section modulus (Zp), which is a measure of torsional and bending strength, is calculated using Equation 2.13[90]. The stability of long bones to compressional forces can be estimated by the buckling ratio (BR), which is a ratio of the bone radius (r) to cortical bone thickness (t) given by Equation 2.14, with compressional bone strength related to the cortical-bone CSA.

$$Polar\ moment\ of\ inertia\ (J) = \frac{\pi}{32}\left(T^4 - M^4\right) \qquad Equation\ 2.12$$

$$Polar\ section\ modulus\ (Z_p) = \frac{J}{(T/2)} \qquad Equation\ 2.13$$

$$Buckling\ ratio\ (BR) = \frac{r}{t} \qquad Equation\ 2.14$$

Where T = *Anterior-posterior periosteal diameter*
M = *Anterior-posterior medullary diameter*
R = *Bone radius*
T = *Cortical bone thickness*

In typically developing children, before puberty, overall bone strength is determined primarily by muscle area[91]. Following puberty, lower limb bone strength appears to be determined by a combination of weight- bearing and lean body mass[91]. With age, bone mass decreases: bending strength is maintained by a gradual increase in bone diameter by periosteal addition of bone, and endosteal resorption leading to a wider bone but a thinner cortex. This maintains bending strength but reduces the ability of the bone to cope with compressive loads. There is evidence in the literature that typically developing adult subjects have a limited potential to increase their bone mass[84,92,93]. However, immature bone in children and adolescents can increase their bone strength in response to increased loading[93-95].

2.6 Musculoskeletal impairment in cerebral Palsy

Individuals with cerebral palsy have musculoskeletal impairments. The most common impairments are muscle contractures[72,73], muscle weakness[53-55,96], altered muscle composition[97-99], spasticity, poor selective motor control[100-104], incomplete activation of the motor pool[53,105,106], and bony deformities.

2.6.1 Muscle contracture

Muscle contractures occur when the musculo-tendinous unit (MTU) becomes short relative to the adjacent long bone resulting in restricted range of movement at a joint. Although this is widely reported in the literature[107,108], the causal mechanism of muscle contractures is not known. Altered muscle tissue stiffness[109] and decreased muscle fibre length have previously been suggested as possible causes of contractures, however, this has not been established in the literature[59,110-113].

2.6.2 Muscle weakness and reduced muscle volume

It is well known that individuals with cerebral palsy present with muscle morphological and structural differences compared to their typically developing peers. In cerebral palsy muscle strength is consistently reduced[53-55,96], contributing to the overall functional deficit in this group[60,114,115]. This reduction in muscle strength has previously been attributed to an inability to optimally control the available muscle resources, for example reduced selective activation and co-activation of antagonist muscle groups[105]. However, these factors do not entirely explain the reduced muscle strength observed. Stackhouse *et al*.[105] compared maximum voluntary and augmented voluntary activation (using electrical stimulation) contraction forces of individuals with cerebral palsy and their typically developing peers. The study found that the comparatively reduced voluntary activation in the cerebral palsy group could not fully explain the differences in muscle strength. A key factor affecting muscle strength is the physiological cross-sectional area (PCSA). PCSA is a relationship between muscle volume, fascicle length, and pennation angle, representing the number of muscle fascicles working in parallel[61]. Therefore, the reduced muscle strength observed must also be due to changes in muscle morphology in addition to the neurological factors.

Lower limb muscles volumes have been shown to be greatly reduced in spastic cerebral palsy compared to typically developing individuals[53,56-60] and compared to the non-paretic limb in hemiplegia[59,53,116], with muscle volumes ranging from 50% to 70% of their typically developing peers[61]. Predominantly, these studies have been investigating the muscle of older children. However, Barber et al[58] showed on average a 22% reduction in medial gastrocnemius muscle volume in children aged 2 to 5 years. As noted by Shortland[117], this is a key finding as it indicates that since there is a large muscle volume reduction at a young age, this volume reduction may not be caused solely by abnormal usage of the muscles during motor skill development. The superposition of the cerebral injury on the developing motor system may have an important role in muscle development. As discussed in Chapter 1, as the corticospinal tract and motor skills develop, afferent sensory neural pathways to the spinal cord are reduced and the efferent motor neural pathways are strengthened. In cerebral palsy the corticospinal tract and intrinsic spinal cord network development may be altered by the cerebral injury, with the spinal cord organisation potentially affected distally from the level corresponding to the timing of the cerebral injury. This may play an important role in muscle size and development. If spinal organisation is more adversely affected distally along the spinal cord, this may explain the greater reduction of muscle volumes observed distally in the lower limb[56,116].

If the superposition of the cerebral injury on the developing motor system is related to muscle development, measuring white matter organisation in the corticospinal tract may provide a fundamental measure of the impact of the cerebral injury on the development of the motor system.

2.6.3 Muscle composition

The mechanical potential of muscle depends on gross morphology (cross sectional area, fibre length[118]), muscle fibre type, and muscle composition (fraction of intramuscular fat and connective tissue). Two recent reviews of the literature have suggested that structural and mechanical properties may be altered in spastic muscle, including evidence for alterations in fibre size and distribution, proliferation of extracellular tissue (connective and adipose tissue infiltration), and altered stiffness of muscle cells[97,98]. In the lower limb, biopsy studies have demonstrated increases in the connective tissue fraction, reduced muscle fibre diameter, and altered muscle fascicle stiffness[119,120], as

well as increased fat content in the most affected muscles[99]. Unlike muscle fibre size and cell stiffness, adipose tissue infiltration can be assessed non-invasively using MRI.

Due to the typically sedentary behaviour observed in this group[71,72], one aspect of muscle composition that may be altered in cerebral palsy is the level of intramuscular fat. Fatty infiltration into muscle results in a reduced proportion of contractile tissue per unit muscle volume and may alter muscle fibre orientation limiting the maximal contraction force of the muscle. Intramuscular fat also may secrete inflammatory cytokines that can reduce the myofibrillar force even in the absence of muscle atrophy[62]. If present in this group, raised intramuscular fat may have important consequences for physical performance, and implications for exercise regimes employed in their physical management.

Adults with cerebral palsy have an increased risk of dying from diseases of their circulatory system than their typically developing peers[11,13], and heightened levels of inter- and intra- muscular fat are associated with cardiovascular risk[44,121]. Therefore, if present in this group, raised levels intramuscular and intermuscular fat may contribute to the cardiovascular risk in this group. Since individuals with cerebral palsy have reduced muscle mass, even those with body mass index (BMI) in the normal range may have relatively increased levels of adipose tissue. Previous studies in children with cerebral palsy have suggested raised levels of fat[76,77]. In an MRI study of the lower limbs in children with quadriplegic cerebral palsy (Gross Motor Function Classification System (GMFCS) levels III-V), Johnson *et al*[76] found increased levels of intermuscular and subcutaneous fat[76]. To date, there have been no studies of intramuscular fat in adults or children with cerebral palsy even though this non-invasively quantified parameter appears to be one of those most associated with cardio-metabolic disease[122].

2.6.4 The effect of intramuscular fat on muscle metabolism

The metabolic syndrome is a combination of medical disorders that, when occurring together, increase the risk of developing cardiovascular disease and type2 diabetes mellitus. The World Health Organisation (WHO) state that individual's have the metabolic syndrome if they have any one of diabetes mellitus, impaired glucose tolerance, impaired fasting glucose or insulin resistance, and any two of the following: Blood pressure: ≥ 140/90 mmHg; Dyslipidemia: triglycerides: ≥ 1.695 mmol/L and

high-density lipoprotein cholesterol (HDL-C) ≤ 0.9 mmol/L (male), ≤ 1.0 mmol/L (female); Central obesity: waist: hip ratio > 0.90 (male); > 0.85 (female), or body mass index > 30 kg/m$^{2;}$ and Microalbuminuria: urinary albumin excretion ratio ≥ 20 μg/min or albumin:creatinine ratio ≥ 30 mg/g. Therefore, the WHO emphasises the role of insulin resistance as a risk factor for declining metabolic health and cardiovascular disease.

The ability for insulin to increase skeletal muscle glucose transport is dependent on the cellular expression of insulin-sensitive glucose transporters, e.g. GLUT4, and the capacity for flux through the insulin signalling pathway[41]. Two of the potential mechanisms contributing to impaired insulin signalling and action is the accumulation of intramuscular lipids and lipid by-products[123] and reduced physical activity. In particular, increased intramyocellular lipid (IMCL) is prevalent with aging, obesity, insulin resistance, diabetes mellitus, and the metabolic syndrome[124-129], with skeletal muscle lipid accumulation associated with increased insulin resistance and loss of metabolic flexibility[39,43,130,131]. Intravenous lipid infusion inhibits the effect of insulin on muscle metabolism, reducing insulin-stimulated glucose transport, phophorylation, oxidation, and glycogen synthesis[132]. This inhibition may be due to the accumulation of intracellular fatty acyl CoA, diacylglycerol and ceramides[133,134], which may impair steps in the insulin-signalling pathway. Alternatively, intramuscular lipid accumulation may not play a direct role in insulin inhibition, but may mark a chronic imbalance between the supply and oxidation of lipids, due to either a chronic dietary imbalance or due to reduced oxidative capacity of fatty acids caused by impaired mitochondrial number/density and/or function[41].

Despite links between skeletal muscle lipids and reductions in mitochondrial size, density and function[135-137] and insulin resistance[39,43,130,131], there are instances where raised IMCL content is concurrent with insulin sensitivity and high oxidative capacity in response to exercise and in endurance athletes[43,138,139]. However, it is likely that there are differences in the subcellular localisation, structure, and proximity to mitochondria between athletes and individuals with low levels of physical activity[140,141]. As noted in a recent review by Petersen *et al.*[142], considering the degree of muscle atrophy and sedentary behaviour among individuals with cerebral palsy, combined with fatigability during physical activity, it may be possible that there are non-cerebral palsy specific

mechanistic defects occurring. Excess intramuscular lipid, decreased mitochondrial function, or chronic inflammation may further exaggerate the functional impairment in this patient group, and may lead to progressive metabolic disease risk[142]. Therefore, understanding any potential secondary mediators of muscle quality or metabolic abnormalities affecting muscle force production and fatigue-ability could have important implications for the life long mobility and physical management of patients with cerebral palsy.

2.6.5 Bony deformity and fracture risk

Bones adapt their mechanical strength to maintain the strain caused by physiological loads as close as possible to a set point[86]. Bone geometry and mineral density adapts to the forces and activity levels they experience[143] and cortical bone cross-sectional area is significantly related to muscle cross-sectional area[91,144,145]. Changes in bone mass lag behind changes in muscle strength by approximately 3 months[146].

Individuals with cerebral palsy can have delayed acquisition of the motor milestones (sitting, crawling, and walking) compared to their typically developing peers. As a result their bones are exposed to different forces and loading patterns resulting in adaptations of the bones to these altered forces. The cortical bone mineral content, thickness and strength have been shown to be reduced in individuals with cerebral palsy[147]. Furthermore, the bone geometries can also be altered causing some individuals with cerebral palsy to develop bony deformities. These deformities include acetabular malformations, increased tibial torsion and femoral anteversion, and equinovarus and planovalgus deformities of the foot.

There is a high prevalence of fractures in individuals with cerebral palsy[148-152], with lower limb fractures most prevalent[149,150], commonly occurring in the distal femur and proximal tibia[150]. In ambulant children with cerebral palsy, high-energy fractures are the most common type, with fractures sustained through significant trauma. As discussed in section 2.5.1, bone strength is dependent on the ultimate strength of bone tissue, the spatial distribution of bone tissue (density, geometry), and the ability for bones to repair micro-damage. In typically developing children and adolescents, factors associated with bone fractures are bone mineral density (BMD), bone geometry, and bone size[153]. Poor

nutrition, lack of weight-bearing physical activity, obesity and high exposure to trauma may also influence fracture risks in the general paediatric population[153].

Although Dual-energy X-ray Absorption (DXA) is the most common method for measuring BMD in cerebral palsy, the technique suffers from systematic errors depend on skeletal site and body size[154]. Since individuals with cerebral palsy often have a smaller body size than their TD peers[155], an apparent low BMD score may be measured when assessed by DXA, thereby underestimating BMD in cerebral palsy. Gold standard assessments using peripheral quantitative computed tomography, pQCT, suggest that children with cerebral palsy do not have a deficit in BMD, but in fact have reduced cortical bone thickness[147]. Bone geometry can also be assessed using MRI, which also has shown reduced cortical bone thickness at the mid-femur of children with quadriplegic cerebral palsy[156].

Bones in non-ambulant children with cerebral palsy have reduced strength due to their reduced cortical thickness[156]. As discussed in section 2.6.2, muscle weakness in individuals with cerebral palsy is well documented, and is attributable to reduced muscle activation[53,105,106], co-activation of agonist and antagonist groups[105,106], and to reduced muscle volume[53,56-61]. Therefore, in individuals with cerebral palsy, the reduced bone strength and hence increased fracture rate may be due to the reduced mechanical loading applied to the bones by the local musculature. Bone geometry and the effects of reduced muscle strength and volume in ambulant individuals with cerebral palsy have not been assessed.

2.6.6 Treatment of musculoskeletal impairments in cerebral palsy

A wide range of interventions are utilised in the treatment of musculoskeletal deformities in cerebral palsy. Exercise interventions are commonly employed with the aim to improve joint ranges of motion (ROM), gait or mobility deficits, and muscle strength. Serial casting is commonly used, where a series of plaster casts are applied to the limb with the muscle of interest held in a stretched position, with the aim to increase joint ROM. Ankle foot orthoses (AFOs) are also commonly used with the aim to provide stability at the ankle during walking and to try and limit the development short plantarflexors by holding the ankle either in dorsiflexion or a neural position.

More invasive treatments are also employed. Botulinum toxin (BTX) injections may be given to patients with tight hamstrings and plantarflexors, although other muscles also can be injected. BTX is a protein exotoxin that binds with high affinity and specificity to the pre-synaptic membranes of cholinergic motor neurones, and is then internalised[157]. Once inside the cell, one of its two subunits specifically cleaves components of the cell's exocytotic machinery so that the discharge of acetylcholine-containing vesicles, and hence neurotransmission at the neuromuscular junction, is prevented[158]. Injection of BTX into selected muscles therefore produces dose-dependent chemical denervation resulting in reduced muscular activity[159]. As well as the injection of BTX, a variety of soft tissue and bony surgeries are often utilised. Intramuscular and tendinous lengthening can be used to lengthen short musculo-tendinous units, and bones can be de-rotated, lengthened, or shortened by bony surgery. All of these interventions treat the secondary and tertiary effects of the initial primary injury to the brain. Although these interventions are performed to improve a patient's clinical presentation, these interventions may in turn have negative consequences on muscle and bone.

2.8 Summary

Muscles play an important role in the execution of a movement initiated through the motor system. However, muscle also has an important role in bone development and metabolic health. In cerebral palsy, the secondary muscle weakness to the initial insult to the motor control system may have further consequences on the individual's metabolic and bone health.

There are limited studies investigating lower limb muscle volume in the literature and no studies have been published to date investigating the relationship between muscle size and bone strength in ambulant individuals with cerebral palsy. Considering the high fracture rate in this group[148-152], muscle size may prove to be a valuable target for intervention to reduce an individual's fracture risk. Muscle strength in cerebral palsy may also be affected by a potentially greater intramuscular fat content compared to their typically developing peers. As well as affecting muscle strength, increased intramuscular fat can also affect an individual's metabolic health[39,43,130,131]. Therefore, investigating intramuscular fat levels in cerebral palsy may not only have implications for muscle function, but also for the life long health in this patient group.

3. Assessment Techniques

In this chapter the techniques employed in the literature for investigating selective motor control, spasticity, functional ability, and spinal cord pathology in this programme of work are reviewed. Magnetic resonance imaging (MRI) provides the best soft tissue detail of all imaging modalities and provides a unique method for investigating tissue structure *in vivo*. In this chapter only the specific techniques relating to the programme of work are discussed. The underlying working principles of MRI are described in Appendix A.

3.1 GMFCS and functional outcome measures

Functional outcome measures are important for the assessment of treatments given to individuals with mobility disabilities and measure the combined effect of the both the musculoskeletal and neurological impairment on an individual's functional ability. For cerebral palsy, various measures have been developed including the Gross Motor Function Measure (GMFM)[5], the Gross Motor Performance Measure (GMPM)[160], the Functional Independence Measure for Children (WeeFIM), the Gillette Functional Assessment Questionnaire (GFAQ)[161] and the Timed Up and Go test (TUG)[162]. It is important to use a functional outcome measure in this study to investigate a potential relationship between measured whiter matter organisation using DTI and the individual's functional capacity. In order to select a functional outcome measure it is important to consider the group it is to be applied to. The range of functional abilities of the group must be accounted for in the scale of the outcome measure, i.e. the measure can successfully differentiate functional ability within the study group. In this section the most widely used outcome measure in the literature, the GMFM, is discussed in detail together with the Gross Motor Function Classification System (GMFCS)[4] that is based on the GMFM.

3.1.1 Gross Motor Function Classification System (GMFCS)

The GMFCS was first developed in 1997 and is a five level classification system that describes the gross motor function of children and youths with cerebral palsy based on their self-initiated movement with particular emphasis on sitting, walking, and wheeled mobility[4].

The aim of the GMFCS is to determine an individual's present abilities and limitations in gross motor function, focusing on their typical performance in home, school, and community settings (i.e., what they do), rather than their full capability. A summary of the five GMFCS levels is given in Table 3.1. For each functional level in the scale descriptions of motor function are given for different age groups in the following ranges: before age 2, 2 to 4 years, 4 to 6 years, and 6 to 12 years of age. Descriptions for youths aged 12 to 18 years have been added in an expanded and revised version of the GMFCS in 2008[163]. GMFCS has good inter-rater reliability[4,163] and has been used for clinical practice and research[164,165 166]. Children who have motor problems similar to those classified in Level I can generally walk without restrictions but tend to be limited in some of the more advanced motor skills. Children whose motor function has been classified at "Level V" are generally very limited in their ability to move themselves around even with the use of assistive technology. Therefore, the scale encompasses the very wide ranges in functional ability observed in cerebral palsy but only differentiates this range into five categories. When investigating relationships with functional ability using GMFCS level, the limited resolution of the system to differentiate between individuals should be accounted for. Therefore, utilising a measure with greater discrimination of functional ability is advisable.

GMFCS Level	Description
I	Walks without limitations
II	Walks with limitations
III	Walks using a hand-held mobility device
IV	Self-mobility with limitations, may use powered mobility
V	Transported in a manual wheelchair

Table 3.1 Summary of the Gross Motor Function Classification System

3.1.2 Gross Motor Function Measure

The Gross Motor Function Measure (GMFM) was developed in the 1980's as a clinical tool for evaluating change in gross motor function of children with cerebral palsy[5]. The initial GMFM consisted of 85 parts as used in a validation performed by Russel *et al*[5]. However, in response to feedback during this initial validation study the authors added three additional measures to form the GMFM-88[167]. The GMFM-88 is separated into four main dimensions: lying and rolling; sitting; crawling and kneeling; standing; and walking, running, and jumping. Scores for each dimension are expressed as a percentage score of the maximum score possible in that dimension, with the total score calculated as an average of the percentage scores across the five dimensions. Administering the GMFM-88 takes approximately 45-60 minutes for an experienced assessor.

The GMFM-88 has been validated in the literature for children aged 5 months to 16 years with cerebral palsy[5,168,169] and has been used as a functional outcome measures in studies investigating various interventions including selective dorsal rhizotomy[170-179], intrathecal baclofen[180], physical therapy[181], strength training[182], and muscle tendon surgery[183]. Despite the extensive use of the GMFM-88 in the literature, it is important to note that there are limitations in design and how the GMFM-88 has been used in the literature. Due to the wide range of functional abilities examined in the GMFM-88 and the time required to perform the measure, some researchers have utilised only the dimensions that are most relevant to their study as restricting the number of dimensions increases the measures sensitivity to changes in the functions of interest. There are two main limitations of the GMFM-88: 1) the potential for two individuals with different functional abilities producing the same total score. Two individuals can achieve the same score despite the individuals having different functional abilities within each dimension as the scores are combined to produce the total score. 2) Children with total scores in the middle range have a greater potential to change their score compare to those with low or high scores.

A shortened version of the GMFM has also been developed, the GMFM-66[184]. The GMFM-66 was developed in response to the limitations of GMFM-88 highlighted in the literature, with the ordering of items according to difficulty, altered interval scale

properties for improved interpretability, and a decrease in administration time. GMFM-66 has been shown to have comparable reliability scores as the GMFM-88. However, many items in the lower dimensions of functional ability have been removed causing the measure to be less descriptive and less sensitive to change in children with low functional abilities. Of the 22 items removed from the GMFM-88 13 were from the lying and rolling dimension, five from the sitting dimension, and four from the kneeling and crawling dimension.

Selective Dorsal Rhizotomy (SDR) is a neurosurgical procedure that can be used in children with cerebral palsy with the aim to relieve the effects of spasticity and improving motor function. SDR involves the incomplete transection of the posterior lumbosacral rootlets in the lumbar spinal cord, reducing the excitatory sensory input from the lower limbs entering the spinal cord. The results of the studies performed in this thesis on white matter organisation in the spinal cord may be applicable for aiding SDR treatment planning and decision-making. The common use of the GMFM as a functional outcome measure in SDR studies in the literature makes the measure appropriate for use in this study; SDR studies have shown that a functional difference can be detected following SDR (i.e. surgically altering the white matter organisation in the spinal cord) using this tool[172,174-179,184-186].

3.2 Assessing selective voluntary motor control

Selective muscle control has been defined as the ability to isolate the activation of muscles in a selected pattern in response to demands of a voluntary movement or posture[187]. Selective voluntary motor control describes the performance of specific isolated joint movements upon request, rather than the activation of selected muscles during functional tasks[188]. Voluntary muscle control is produced through the corticospinal tract, controlling both directionality and force production[189]. An injury to the corticospinal tracts affects the force, speed, timing, and patterns of voluntary movements. In cerebral palsy, damage commonly occurs to the corticospinal tracts in the periventricular area of the brain[190].

In the literature, selective motor voluntary control impairment has been reported indirectly in cerebral palsy through muscle recruitment timing errors during maximum

voluntary contractions[100], simultaneous associated movements at contra-lateral joints, mass patterns of flexion and extension (synergies) during movements[101], and coupled hip, knee and ankle movements during gait and voluntary movements[101-104]. However, in cerebral palsy the patho-physiology of impaired selective voluntary motor control is not well understood with several potential causes including a loss of inhibition, the persistence of low threshold stretch reflexes and primitive flexor/extensor patterns, a loss of connections with the corticospinal tract, or a combination of these factors. Due to the reduced selective voluntary motor control capabilities in cerebral palsy, investigating a potential relationship with selective voluntary motor control is an important factor of a study investigating spinal cord white matter organisation.

Importantly for this study, a relationship has been reported in the literature for spinal white matter organisation (determined by diffusion tensor imaging) in the cervical spine with precision grip force control in 24 healthy volunteers. Fractional Anisotropy (see Chapter 3) was found to be higher in subjects with low error in force tracking tasks[191]. This result infers a higher white matter organisation in subjects with better force control and is indicative that a reduced axon organisation may be observed in individuals with cerebral palsy who have reduced selective voluntary muscle control compared to their typically developing peers.

Clinical assessment of selective voluntary motor control have been described and used as outcome measures in the literature[192-194]. Recently a clinical tool been developed which evaluates the entire lower limb: Selective Control Assessment of the Lower Extremity (SCALE)[188]. SCALE involves the scoring of the hip, knee, ankle, subtalar joints, and toes, and summing to produce an assessment of the entire lower limb. The authors have demonstrated content and construct validity, good reliability between assessors and a strong relationship to gross motor classification. SCALE has been used in the literature to show increased distal motor impairment in spastic cerebral palsy[195], and that the independence of knee and hip joint motion in the swing phase of gait is positively related to selective voluntary motor control [196]. However, SCALE is a qualitative measure that involves subjective scoring selective voluntary motor control from zero to two: normal (2); impaired (1); or unable (0). Quantitative evaluation of selective voluntary motor control requires instrumentation. This could be achieved through electromyography or utilising a device similar to that proposed by Lindberg *et*

al[197] for the lower limb, for example a pedal-force control system. Defining a task that subjects with CP could successfully perform across a range of functional abilities is difficult due to the large variation in joint ranges of movement and selective motor control within this group. Therefore, despite the qualitative nature of SCALE it is currently the only non-instrumented clinical assessment technique that assesses the entire lower limb. Therefore, SCALE will be used in this study to assess selective voluntary motor control due to the number of tests to be performed in this study and the time constraints this imposes on the study.

3.3 Assessing spasticity

Spasticity is a complex phenomenon that currently has no set definition in the literature. As a result a range of measurement techniques have been developed and utilised in the literature that measure different components of spasticity. These techniques range of clinical non-instrumented tests to instrumented isokinetic tests with electromyography and dynamometers.

Non-instrumented techniques commonly used for the clinical assessment of spasticity can be categorised into three main groups; Ashworth-like scales, Tardieu-like scales, and other clinical grading scales[198]. The Ashworth-like scales are based on scoring the resistance encountered in a specific muscle group by passively moving a limb at one non-specified velocity through its range of movement on a 5 point scale initially described by Ashworth[199]. The Tardieu-like scales are based on the description by Tardieu[200] involving the measurement of joint-angle measured at different velocities of muscle stretch. Derived clinical assessments (the Tardieu Scale[201]) involves passive movement of the joints at three specified velocities and the intensity and duration of the muscle reaction to stretch (*X*) is rated on a 5 point scale, with the joint-angle (*Y*) at which this muscle reaction is first felt. A simplified scoring system, the Modified Tardieu Scale (MTS)[193]. The MTS only defines the moment of the 'catch', seen in the ROM at a particular joint angle at a fast passive stretch. In a review by Scholtes *et al*[198] the authors state that only the Tardieu-like scales are suitable instruments for the clinical measurement of spasticity since the Ashworth-like scales only grade muscle tone intensity at one velocity of passive stretch. However, these descriptive clinical measures do not strictly measure spasticity, but are a grading of a joint's resistance to stretch. In

these tests the cause of this stretch resistance cannot be elucidated and can be caused by altered stretch reflexes, persistent muscle activation, altered elasticity of the musculo-tendinous unit, or a combination of these factors.

Instrumented quantitative measures have been developed, including quantifying muscle activity to measure the response to stretching of muscles, tendon tap, or electrical stimulation and can be acquired simultaneously with the clinical non-instrumented techniques including the modified Ashworth scale[202-205]. The resistance to stretch can be quantified at a joint using isokinetic dynamometry, during which the peak passive toque of a joint to passive movements can be measured[206-209]. Muscle reflexes can also be measured in conjunction with isokinetic dynamometry using electromyography. This enables the contribution of an increased muscle reflex on the muscle stretch resistance to be investigated. This enables patients with increased stretch resistance to be categorised by the contribution of muscle reflexes to the stretch resistance depending on EMG activity[210]

Conclusion: Currently there are no non-instrumented clinical tests for grading the degree of muscle spasticity. Although these techniques assess muscle resistance to stretch, they require additional neurophysiological measurements to enable the contribution of muscle reflexes to stretch resistance to be identified. Isokinetic dynamometry combined with electromyography currently enables both the passive stretch resistance and degree of muscle activation to be quantified; however the relative contributions of altered muscle reflexes and muscle tissue structure cannot be elucidated. In this study, due to the limited time scale to perform the spasticity tests, and that the primary outcome measures for altered corticospinal tract development are altered selective motor control and subsequent muscle development only non-instrumented trials have been employed. Therefore, despite having limitations, the modified Ashworth will be performed in this study for grading spasticity due to its short acquisition time and large usage in the literature.

3.4 In vivo methods for assessing intramuscular fat

Ultrasound is a common non-invasive method used to assess adipose tissue infiltration in muscles. Khoury *et al*.[211] assessed the fatty infiltration and pennation pattern in the

supraspinatus shoulder muscle of individuals with rotator cuff disease. The fatty infiltration was evaluated by assessing the echogenicity of the supraspinatus muscle compared to normal trapezius muscles of the same individuals. Khoury *et al*.[211] compared the ultrasound results with MRI images. The MRI images were evaluated subjectively by examining the proportion of fat within the muscle on the sagittal and coronal T_1-weighted images using a grading method by Goutallier et al.[212]. In this method normal muscle with no fatty streak is grade 0; mild fatty muscle has a few streaks is grade 1; moderately fatty muscle is grade 2; and approximately equal amounts of fat and muscle, i.e. severe fatty infiltration, is grade 3. Grading methods, such as the Goutallier technique[212], enable intramuscular fat assessment but are only a qualitative technique.

T_1-weighted image segmentation is commonly used to quantify intermuscular adipose tissue (IMAT) using MRI. IMAT defined as the visible fat within the muscles (intramuscular fat) and between the muscles beneath the fascia (intermuscular fat). This is typically achieved by drawing regions around adipose tissue on T_1-weighted images. The adipose tissue is separated into inter-muscular, subfascial or subcutaneous and the percentage of adipose tissue calculated. Although this method is effective for assessing intermuscular and subcutaneous fat volumes, it is not an accurate method for measuring fat within individual muscles (intramuscular fat) due to the mixed tissue and therefore signal intensities within muscle. Alternative quantitative methods for intramuscular fat are magnetic resonance spectroscopy (MRS) and chemical shift imaging techniques.

3.4.1 Magnetic Resonance Spectroscopy (MRS)

MRS produces a spectrum of signal intensity vs. frequency that shows the chemical shift of 1-H within different molecules. These differences arise due to the differing electron shielding of specific atoms, which creates a difference in magnetic field strength and, therefore, frequency. This means that the spectrum contains the information as to the metabolites present.

Due to the very large quantities of water molecules compared to metabolites in the body water suppression techniques are required to suppress the spectral peak of water so that it does not dominate the spectra. This also enables the analogue to digital converter to have increased dynamic range over the small signals of interest. Water suppression is

achieved by applying a narrow-bandwidth radio frequency pulse that excites only the water molecules. A spoiler gradient is then applied which dephases these excited spins. This is carried out before the main MRS sequence, although the sequence is often run first without water suppression to obtain reference spectra. There are two main sequences for single voxel MRS: PRESS and STEAM. Point Resolved Spectroscopy (PRESS) uses a 90^o excitation pulse followed by two refocusing 180^o pulses, with a slice selection gradient applied during each pulse such that the echo originates only from the required voxel of interest defined by the overlapping region of each slice select gradient (Figure 3.1). STimulated Echo Acquisition Mode (STEAM) uses a stimulated echo rather than a double spin echo to localize the signal from a single voxel, with three spatially selective 90^o pulses, each with a gradient on one of three orthogonal axes (Figure 3.2).

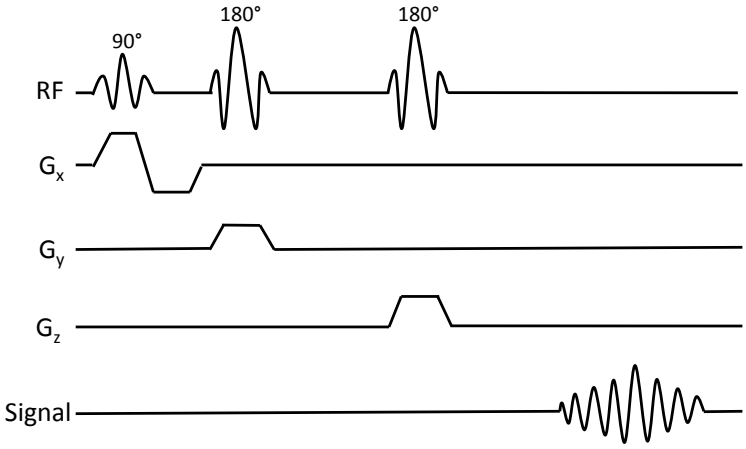

Figure 3.1 Point Resolved Spectroscopy (PRESS) sequence

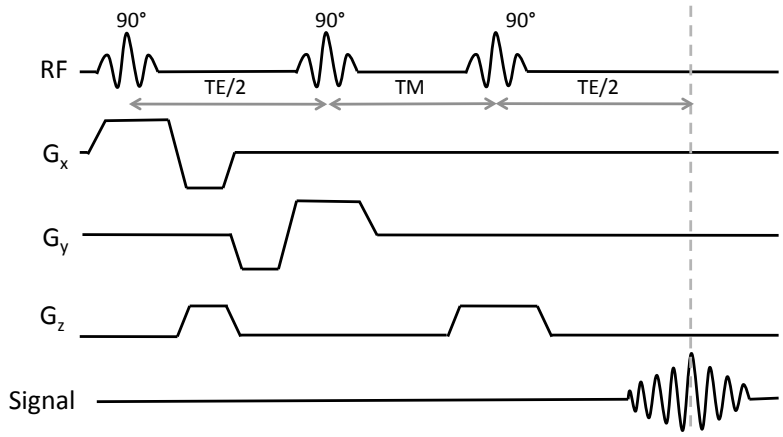

Figure 3.2 STimulated Echo Acquisition Mode (STEAM) sequence. TM denotes the time between the second and third 90° RF pulses, known as the mixing time.

^{1}H Spectroscopy can be used to assess the fat content of muscles and is considered to be the 'Gold Standard' for intramuscular fat quantification. As well as quantifying fat, MRS can be used to measure a wide range of metabolites in tissues using ^{1}H and ^{31}P spectroscopy. In the literature, MRS has been used in the assessment of lipid content of the supraspinatus muscle in asymptomatic volunteers and patients with supraspinatus tendon lesions and compared with qualitative fat infiltration assessment of T_1-weighted images[213]. Comparable results were obtained between the quantitative MRS results and the qualitative grading of the T_1-weighted images. The authors conclude that routine assessment of the apparent lipid content is feasible with proton MR spectroscopy and provides the possibility to quantify fatty atrophy of the supraspinatus muscle. However, MRS has limited spatial resolution and, therefore, is not suitable if the entire muscle cross-section or volume is of interest.

3.4.2 Dixon Imaging

As discussed above, in the literature fat-water fraction measurements are predominantly obtained using localized proton (1-H) MR spectroscopy (MRS)[213-216]. However, MRS has a limited spatial resolution compared to imaging techniques. Consequently MRI techniques for the measurement of fat-water ratios are desirable, particularly in spatially heterogeneous tissue.

Chemical shift imaging methods based on the Dixon technique[217] utilise the predictable phase evolution between water and fat signal constituents due to their chemical shift difference to enable the calculation of separate water and fat images, permitting the calculation of the fat fraction. The fat fraction is the signal intensity attributable to fat, normalised by the total signal from all mobile proton species. Recent advancements in image processing techniques, such as IDEAL (iterative decomposition of water and fat with echo asymmetry and least-squares approach)[218,219], have further helped to separate fat and water signals in inhomogeneous magnetic field regions and Dixon sequences are now becoming more widely available on clinical MRI systems (Philips –mDixon, Siemens – Dixon, Hitachi – FatSep, GE –IDEAL).

These techniques have been widely used in studies quantifying the degree of liver fat in hepatic steatosis (for review see Reeder[220]). Dixon imaging is increasingly being

utilised for clinical intramuscular fat quantification[121,221], including in Duchenne Muscular Dystrophy[222,223]. To date no studies having been published in the literature investigated intramuscular fat in cerebral palsy using Dixon imaging techniques. The increasing use of Dixon techniques for *in vivo* intramuscular fat quantification demonstrates a need for an *in vivo* comparison evaluation of these techniques with MRS that is currently considered the gold standard for in vivo intramuscular fat quantification. However, to effectively test the validity of these imaging techniques a study comparing intramuscular fat measured using Dixon techniques with muscle biopsy is required.

Dixon imaging technique

The Dixon imaging technique[217] discriminates between fat and water spins based on the difference between their resonant frequencies to produce separate fat and water images. The original two-point Dixon (2PD) technique acquired two spin-echo images: one image is acquired with water and fat in phase, and the second image is acquired with the water and fat signals out of phase, with 180^{o} water-fat phase difference (Figure 3.3A-B). These images then undergo complex addition or subtraction to produce water only and fat only images respectively, from which a fat-water ratio image can be calculated. Therefore, a fat-water fraction measurement can be made for a much larger region of interest and with much higher spatial resolution using Dixon techniques compared to MRS.

The three-point Dixon (3PD) technique[224] was developed to reduce sensitivity to magnetic field inhomogeneities, and, therefore, phase errors, that are associated with 2PD[225] by utilising a combination of multipoint acquisition and image processing techniques. Phase errors are different in each voxel and typically result in swapped water and fat assignment for the voxels affected[225]. Figure 3.3 C shows the effect of a phase error on the relative phases of the water and fat signals. Equations 3.1 to 3.4 show how the phase error and water (W) and fat (F) images are calculated from three point acquisitions (S_o, S_1 and S_{-1}). A four-point Dixon (4PD) technique has also been developed[226], in which the extra acquisition enables a more accurate correction of the phase error, increasing the image acquisition time.

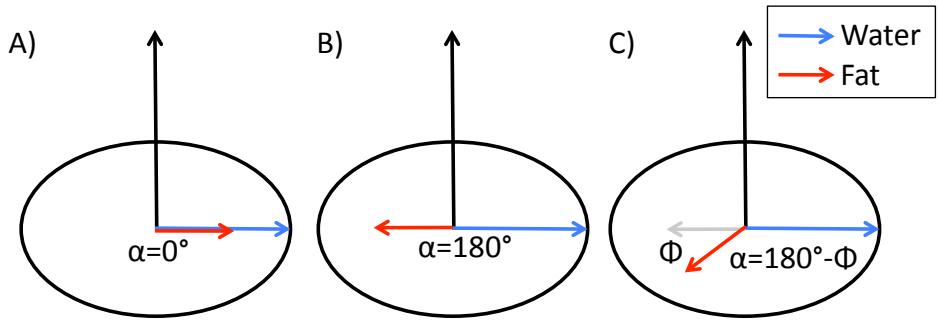

Figure 3.3 Schematic diagram showing the relative phases of water (blue) and fat (red) in Dixon imaging, where α = phase difference between water and fat signals and Φ = phase error

$$S_0 = (W + F) \qquad S_1 = (W - F)\cdot e^{i\phi} \qquad S_{-1} = (W - F)\cdot e^{-i\phi} \qquad \textit{Equation 3.1}$$

$$\phi = 0.5\cdot \arctan(S_1 - S_{-1}^{*}) \qquad \text{Equation 3.2}$$

$$W = 0.5\cdot \left|S_0 + S_1\cdot e^{-i\phi}\right| \qquad \textit{Equation 3.3}$$

$$F = 0.5\cdot \left|S_0 - S_1\cdot e^{-i\phi}\right| \qquad \textit{Equation 3.4}$$

Where S_o, S_1 and S_{-1} are the signals from the three acquisitions

W = Water signal, F = fat signal, Φ = Phase error

3.5 Transcranial magnetic stimulation

Transcranial magnetic stimulation (TMS) is a non-invasive method for depolarising or hyperpolarising neurons in the brain though electromagnetic induction. TMS induces electric currents in the brain, causing either general or location specific activation of the brain, enabling the study of brain functions and the treatment of a range of psychiatric disorders.

TMS of the sensory-motor cortex is often utilised to infer anatomical connections between the cortex and musculature by invoking a motor response. TMS studies have been performed in children to investigate the development of the motor systems, and are considered to be sensitive to corticospinal functional connectivity evoked by stimulation[227,228]. There are four TMS measures that are typically made when investigating the motor system connectivity: *Motor evoked potential (MEP) threshold* is the minimum potential applied to the brain that stimulates the motor cortex, evoking a

motor response*; MEP latency is* the latency of a TMS evoked MEP is an estimate of the central motor conduction time; *Cortical maps:* by stimulating a number of different areas of the scalp, different regions of the motor cortex are stimulated enabling an estimate of the somatotopic representations of muscles within the motor cortex; *Ipsilateral MEP:* Stimulation of the motor cortex may evoke an MEP in the homologous target muscle ipsilateral to the stimulation. This indicates the presence of an ipsilateral corticofugal motor projection.

TMS has been utilised in the literature to investigate the cerebral damage and motor system connectivity in cerebral palsy. TMS has detected enhanced plasticity of the developing brain, altered cortical maps, and transcallosal inhibition in children with cerebral palsy. Enhanced plasticity of the developing brain has been shown in children with hemiplegia, with some children exhibiting prominent mirror movements of the paretic hand when the non-paretic hand is voluntarily controlled. TMS evoked ipsilateral projections that appear to originate from branched corticospinal tract neurons in the primary motor cortex of the contra-lesional hemisphere are associated with prominent mirror movements. Conversely, projections that appear to arise from areas other than the primary motor cortex have been found to not be associated with mirror movements[229-231]. Cortical maps detected using TMS have suggested that the cortical map of the lower extremity muscles are laterally displaced in children with bilateral spastic cerebral palsy caused by PVL[232]. TMS has also detected that children with PVL may have structural deficits in the corpus callosum. The ipsilateral silent period (a marker of transcallosal motor inhibition) is a measure of myelination state of the mid-body of the corpus callosum where axons connecting the motor areas in both hemispheres meet[233]. In children with spastic diplegia, the ipsilateral silent period is absent, suggesting demyelination of the callosal structure[234].

TMS is a valuable tool for assessing connectivity of the motor system to be investigated, however, it does not quantify the underlying neural structure. TMS is also limited by the stimulation method. The stimulating coils placed onto the scalp are of a finite size, and therefore have limitations in the precision of the area of stimulation. This can prevent the electrode from stimulating the area of interest alone without collateral stimulation of the surround neurons. Also, since the technique is transcranial, the area of

the motor cortex that is stimulated is superficial. The region of the motor cortex responsible for lower limb motor control is deep within the motor cortex, limiting the ability of TMS to stimulate the lower limb motor neurons, especially without co-stimulation of other motor areas. Due to the difficulty in selectively stimulating the region of the motor cortex related to lower limb motor control together with the practicalities of utilising TMS including subject recruitment, TMS will not be used in this programme of work.

3.6 Diffusion tensor imaging

Anatomical MRI is routinely used to evaluate a range of neurological conditions. In cerebral palsy, MRI can reveal anatomic abnormalities, for example signal and volume abnormalities or white matter abnormalities. These abnormalities have been shown to correlate well with type and severity of neurologic sequelae[235] and long-term motor outcome measures[236,237]. However, studies have shown that not all patients diagnosed with cerebral palsy exhibit neurological abnormalities in MRI images; a recent European study of 351 patients with CP found that 11.7% had normal MRI results[238]. Therefore, the high sensitivity of diffusion tensor imaging (DTI) to tissue structure may not only complement the clinical assessment of those patients exhibiting neurological abnormalities, but also enable the detection of abnormalities in the white matter microstructure of patients with insignificant findings on anatomical imaging techniques. This section discusses the application of DTI for quantifying spinal cord white matter organisation. For a detailed explanation of the principles of MRI and DTI sequences see Appendix A.

In the literature, DTI has been used successfully in the brain to investigate white matter injuries in CP. The majority of the published studies involve the investigation of specific white matter structures in the brain, often correlating their findings with motor function[239-245]. Children with bilateral spastic cerebral palsy often present with reduced voluntary selective motor control and muscle spasticity due to damage to the corticospinal tract and the vestibulospinal and reticulospinal tracts of the upper motor neurons. The corticospinal tract plays an important role in spinal cord development and the development of motor control. As a result of the brain injury, intrinsic spinal cord networks may not mature and muscle development may be delayed[30]. Therefore, the

application of spinal cord DTI may reveal further abnormalities in the development of the central nervous system and may further explain a range of pathologies associated with cerebral palsy including reduced selective motor control and spasticity.

Histological studies have been performed comparing diffusion parameters with measured axon dimensions, density, area fraction, and average axon size in rats[246] and on excised human cervical spine[247]. These studies observed that ADC and FA were related to axon packing parameters. However, despite these results showing that a relationship exists between the DTI parameters and the underlying axon microstructure, it is important to note that a measured change in FA or ADC does not differentiate between changes in axon dimensions or packing parameters.

To date, the majority of DTI studies of the spinal cord have been animal studies. The results of these studies have demonstrated the application of DTI for spinal cord compressions[248], inflammatory diseases[249,250] and arteriovenous malformations[251]. Despite the use of MRI anatomical imaging, and recently DTI, in neurological imaging, no studies in the literature to date have investigated abnormalities in the spinal cord of patients with CP. However, DTI has not been widely used in the literature to investigate the spinal cord. Artefacts caused by the surrounding flowing cerebrospinal fluid and bone, respiratory and cardiac motion, and low signal-to-noise-ratio (SNR) due to its small size represents a challenge for sequence design. This is particularly true in the transverse plane as precise anatomical localisation, small in-plane voxel size, and insensitivity to motion and susceptibility artefact is required. These factors make spinal cord diffusion imaging a challenge for sequence design.

3.6.1 Spinal cord DTI techniques

DTI of the brain is usually performed using single-shot echo-planar imaging (SS-EPI) sequences. SS-EPI benefits from a high signal-to-noise ratio (SNR) and is relatively robust to movement ghosting artefacts[252]. However, these sequences are not directly transferable to the spinal cord due to susceptibility artefacts caused by the magnetic field inhomogeneities around the spinal column[253] and motion artefact from bulk motion of the spinal cord due to respiratory and cardiac motion, pulsating cerebrospinal fluid and swallowing. This bulk physiological motion causes non-linear phase errors

and shifts in k-space if the motion occurs during application of the diffusion encoding gradients[254].

The first diffusion weighted study of the human spinal cord *in vivo* was first published in 1999 by Clark *et al.*[255]. This study utilised a navigated, cardiac-gated pulsed-gradient spin echo diffusion imaging technique to produce ADC maps of the spinal cord in the sagittal plane[255]. The one-dimensional navigator echo was employed to correct the phase error accumulated in each line of k-space[256,254]. Single-shot techniques are sensitive to susceptibility artefact. This sensitivity can be reduced by employing a multi-shot EPI read out, which reduces the readout train length, and thus reducing the sensitivity to susceptibility artefacts[257]. This technique also enabled a greater spatial resolution through multiple shots[258]. This interleaved EPI technique results in superior image quality with reduced ghosting artefacts compared to fast spin echo techniques[259]. This motion artefact can be further reduced by employing a velocity-compensated diffusion gradients in tandem with a navigator echo[260].

Since the first diffusion weighted sequences for imaging the spinal cord were developed there has been a continual development of MRI machines, sequence design, and analysis techniques with the aim of generating increasingly robust and reliable DTI images for clinical applications.

As discussed above, DTI-EPI techniques in the brain are commonly performed using single shot spin-echo EPI sequences. Considering the strong susceptibility gradients around the spinal cord, alternative sequence designs have been produced using multiple spin-echo read out schemes. Spin echo read-out sequences have a major advantage compared to gradient echo read-out techniques as susceptibility artefacts caused by the bone are greatly reduced. However, spin echo techniques are susceptible to image artefacts caused by the diffusion gradients altering the spin phases during the echo train acquisition[258] and requires a longer read out time. Less common DTI techniques have also been used in the literature including a steady-state free procession sequence (SSFP)[261], and a radial k-space trajectory spin echo sequence with each line of acquired data passing through the k-space origin[262]. Single-shot techniques are advantageous due to dephasing caused by patient motion and increased scan time associated with multi-shot techniques. However, the relatively long readout time of a single-shot technique

results in increased T_2* decay resulting in sometimes significant blurring in the phase encoding direction. Therefore, current techniques attempt to reduce the magnetic susceptibility of these data sets by reducing the readout duration, which reduces the off-resonance related artefacts[263]. Of these techniques, reduced field-of-view single-shot EPI and ZOOM EPI have been shown to be feasible in a clinical population and will be discussed in detail below.

Reduced Field-of-view single shot EPI (reduced FOV SS-EPI)

Reduced FOV SS-EPI techniques have been recently been developed that reduce magnetic susceptibility artefacts of SS-EPI by implementing non co-planar SE selection[264-266], two-dimensional selective pulses[267,268], outer volume suppression[252] or a combination of these[269]. A reduced field of view reduces the number of k-space lines acquired, thus shortening the read out time and, therefore, reducing susceptibility artefacts. Saritas *et al*. presented a reduced FOV technique that utilised a two-dimensional spatially selective echo-planar RF excitation pulse followed by a 180° refocusing RF pulse to select a rectangular FOV[270]. This reduces the read-out duration in the phase encoding direction to enable a higher in-plane resolution to be acquired without increasing read-out time[270]. This technique also allows for contiguous multi-slice imaging without the need for inter-slice gaps[271]. Furthermore, the signal-to-noise ratio (SNR) is independent of the number of slices acquired[266]. An alternative approach is to use non co-planar SE selection to reduce the read-out duration in the phase encoding direction, however, this does not produce a rectangular field of view and aliasing from the outer volume is significant and alias reduction techniques, such as outer volume suppression (OVS)) are required. This is not true for the Saritas *et al* approach and represents an advantage over non-coplanar SE selection approaches. Wilm *et al* recently developed a reduced FOV technique with non-coplanar SE SS-EPI combined with OVS[272], as shown in Figure 3.4. The advantage of the Saritas *et al* technique compared to that proposed by Wilm *et al* is that OVS is not required.

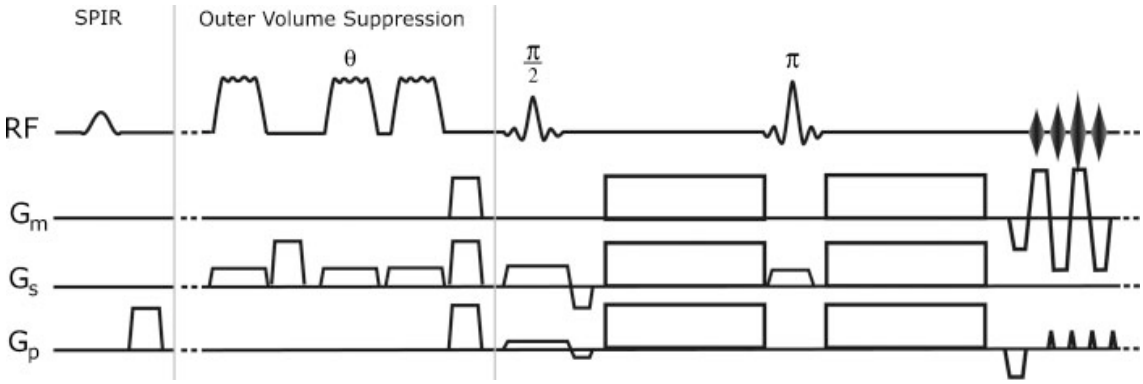

Figure 3.4 Schematic representation of the reduced field of view sequence (ZOOM). The SPIR fat saturation pulse precedes the outer volume suppression. Tilting of the π/2 pulse is achieved by an additional gradient in the phase-encoding direction during the π/2 slice selection[272]

Compared to traditional SS-EPI techniques reduced FOV SS EPI techniques do have a lower SNR. The SNR is reduced to only a square root of the signal to noise ratio of the full field of view due to the reduced number of k-space lines acquired. Despite this, a recent clinical study comparing reduced FOV SS-EPI with traditional SS-EPI showed improved image quality and other radiological metrics in a clinical population, and the reduced FOV SS-EPI images were rated as superior by a team of neuro-radiologists[273].

ZOOM-EPI

The higher resolution achieved with the reduced FOV SS-EPI approach, by reducing the k-space matrix size, results in potential aliasing from outside the FOV, particularly in the phase encoding direction. Zonally magnified oblique multi-slice echo planar imaging (ZOOM-EPI) was developed to correct this aliasing artefact for optic nerve imaging[265], and was subsequently successfully employed in the spinal cord[271]. ZOOM-EPI is a reduced FOV SE-EPI technique that uses a tilted 180° refocusing RF pulse to reduce the FOV. However, unlike the reduced FOV techniques discussed above, the read-out FOV can be freely chosen to obtain the desired resolution as aliasing artefacts are avoided by using standard receiver bandwidth limiting filters, enabling a zoomed image to be reconstructed[271]. This initial approach required a two-slice thick inter-slice gap, making contiguous slices unobtainable. However, ZOOM-EPI has since been further developed to enable the acquisition of contiguous slices. Contiguous slice ZOOM EPI (CO-ZOOM-EPI) selectively excites and refocuses only a narrow FOV while simultaneously suppressing the signal from regions outside the desired FOV through the application of a slice-selective 90° RF pulse followed by a dual spin echo refocusing RF pulse consisting of two 180° RF pulses that are slice selective in the

phase encoding direction[274]. This enables the excitation and refocusing of only a narrow cross-section of the image volume. Out-of-phase protons within the refocusing slice undergoing two 180° RF pulses resulting in the restoration of magnetisation and minimal saturation of protons[274].

3.7 Summary

The functional ability of individuals with cerebral palsy can be assessed clinically and reliably using the GMFM. However, clinical selective motor control and spasticity measures are not well developed in the literature. Spasticity in particular is difficult to assess and measure clinically and all currently available clinical tests have significant limitations. Although instrumented testing such as EMG and isokinetic testing could be used, the limited time scale available to assess selective motor control and spasticity measures in this study restricts their use. Due to their relatively wide use in the literature, SCALE and Modified Ashworth tests will be utilised to investigate selective motor control and joint stiffness respectively in this programme of work.

Dixon based imaging techniques are an important tool for assessing the distribution of fat in the body that can be implemented to assess intramuscular fat accumulation in cerebral palsy. However, to date, there are no studies in the literature evaluating the Dixon techniques for *in vivo* intramuscular fat quantification. Considering the increasing use of Dixon techniques for *in vivo* intramuscular fat quantification, an *in vivo* evaluation is required to investigate the accuracy of the technique for intramuscular fat quantification.

DTI MRI techniques provide a valuable tool for the characterisation of tissue microstructure *in vivo,* and are sensitive to the spinal cord microstructure, including axon dimensions, density, area fraction, and average axon size[246,247]. However, it is important to note that DTI parameters cannot differentiate between changes in axon dimensions, packing parameters, or myelination. Although DTI MRI has multiple technical limitations, the development of reduced field of view approaches that addresses some of the limitations enables the microstructure and pathology of the spinal cord to be investigated. In particular, reduced FOV SS-EPI has been shown to produce

improved image quality compared to traditional SS-EPI approaches in a clinical population and therefore is applicable for use in this programme of work. The approach developed by Wilm *et al*[252] is implemented for clinical use on the 3.0 T Phillips Achieva system (Philips Medical Systems, Best, The Netherlands) installed at the teaching hospital where all MRI scans in this programme of work will be performed. Therefore, the reduced FOV SS-EPI with outer volume suppression proposed by Wilm *et al* will be utilised for spinal cord DTI in this programme of work.

4. Programme of Work

As discussed in Chapters 1 and 2, individuals with cerebral palsy develop progressive musculoskeletal deformities secondary to an insult to the brain *in utero* or in early childhood that results in the development of a motor disorder[275]. These individuals also often suffer from a combination of altered sensation, cognition, communication, and perception and develop progressive musculoskeletal deformities[275]. Currently there is no cure for cerebral palsy and the primary aim of clinical interventions in children and adults are to improve a patient's functional capabilities. The primary interventions utilised to address these acquired musculoskeletal deformities are physiotherapy, botulinum toxin injections, soft tissue and bony orthopaedic surgery. The aim of the first four studies in this programme of work are to investigate the extent that lower limb abnormalities, including muscle size and composition, are altered in ambulant individuals with bilateral spastic cerebral palsy (BSCP). This is important as identifying the muscle groups most adversely affected in this population may enable improved targeted of interventions to enable to maximise an individual's functional ability with the aim of improving quality of life and reducing the decline in mobility[7] culminating in the early loss of mobility[7,8] in this group. Furthermore, altered intramuscular fat may have cardio-metabolic consequences[38,42,129,130] that may have important implications for an individual's general health, potentially contributing to the early mortality[8,10,11] in this patient group.

Periventricular leucomalacia (PVL) is the most common cause of BSCP, with lesions located in the posterior limb of the internal capsule bilaterally with damage to the corticospinal tract at this time. Many other areas of the brain may also be affected by the injury, either directly or by mal-development subsequent to the injury[3]. Although the extent of the damage and subsequent mal-development in the brain following PVL has been widely investigated in the literature, to date no studies have been published

investigating potential mal-development of the spinal cord following PVL. PVL occurs while the corticospinal system is developing. An injury to the developing corticospinal system may alter the refinement and elimination of afferent and efferent terminations in the spinal cord and the development of interneurons and intrinsic spinal cord networks. The aim of the fifth study in this programme of work is to investigate whether any potential disturbances to spinal cord development in PVL may explain alterations to functional ability, selective motor control, and muscle spasticity commonly observed in this patient group.

In this chapter, overviews of each of the five studies in this programme of work are outlined, including subject recruitment and ethical approval. The full details of each study are given in each of the result chapters (Chapters 5-9) that follow.

4.1 Subjects

All studies in this thesis, with the exception of study three, are case-control studies investigating aspects of bilateral spastic cerebral palsy and comparing to their typically developing peers. Local research ethics committees granted ethical approval for each study in thesis.

4.1.1 Case subjects

Individuals aged 10 – 24 years, with a diagnosis of bilateral spastic CP, Gross Motor Function Classification System (GMFCS) levels I-III, who met the safety requirements of MRI were included in this study. Patients who had undergone surgery, serial casting or botulinum toxin injections to the lower limbs within the previous year were excluded from the study. Case subjects were recruited as a convenience sample of individuals attending our hospital department, including physiotherapy, orthopaedic consultations and clinical gait analysis appointments. Consecutive patients that met the inclusion criteria invited to participate in the study. The inclusion criteria for case subjects in all studies were:

- Diagnosis of bilateral spastic cerebral palsy.
- No surgery, serial casting or botulinum toxin injections to the lower limbs within the previous year.

- All individuals must meet the safety requirements of MRI.
- Be able to understand what is being asked of them, and agree to take part in the study.

4.1.2 Control subjects

Controls subjects were recruited from students and staff at Guy's & St Thomas' NHS Foundation Trust and King's College London, and through individual's known to the local research team. The inclusion criteria for control subjects were:

- Have no diagnosis of any musculoskeletal or neurological conditions.
- Have never undergone surgery to their lower limbs.
- All individuals must meet the safety requirements of MRI.
- Be able to understand what is being asked of them, and agree to take part in the study.

4.2 Overview of studies

4.2.1 Study 1: Lower limb muscle volumes in bilateral spastic cerebral palsy

Muscle weakness is a feature of individuals with spastic cerebral palsy[53-55,96], however, in the literature there are few studies of muscle volume in this group. These limited studies have found reduced muscle volumes in individuals with cerebral palsy volume[53,56-61]. This study compares the volumes of nine major muscles in the lower limb in ambulant adolescents and young adults with BSCP with those of their typically developing peers. Nineteen independently ambulant subjects with bilateral spastic cerebral palsy (mean age 14.2 ± 2.7 years; 11 male; GMFCS levels I (n=5) and II (n=14)), and nineteen typically developing subjects (mean age 16.5 years (standard deviation 3.0), 11 male) took part in this study. This study is discussed in more detail in Chapter 5.

This study combines data from two studies examining muscles in cerebral palsy. All MRI data was collected on a 1.5 T Phillips Achieva system (Philips Medical Systems, Best, The Netherlands). I designed the MRI protocol used to collect data from twelve BSCP and ten TD subjects using a three point Dixon sequence (TE/TR = 4.6/13 ms,

echo time shift = 1.53 ms (120° echo phase shift), 20° flip angle, 0.9 x 0.9 mm in-plane voxel size, number of averages = 2, 5 mm slice thickness) with a quadrature body coil. Each scan took approximately 30 min. The MRI images of the lower legs of seven individuals with BSCP and nine TD subjects were collected as part of another PhD project (Nicola Fry, 2009). These subjects were scanned using a T1 weighted turbo spin echo sequence (TE/ TR = 18/1104.4 ms, number of averages = 2, echo train length = 3, 1.8 x 1.8 mm in-plane voxel size) with a quadrature body coil. Slices were collected contiguously with a slice thickness of 2 mm over the hip, knee and ankle joints and every 4 mm over the remainder of the lower limb. Image acquisition took approximately 20 min for each subject. Data processing was performed with another PhD student (Andrew Lewis, 2013). I performed the data analysis and manuscript preparation. This study is published in Brain & Development 36 (2014) 294-300. This paper is included in Chapter 5.

4.2.2 Study 2: Bone strength and muscle volume in bilateral spastic cerebral palsy

The Mechanostat Theory[86,87] states that bone remodelling, and therefore strength, is mediated by strain induced by muscle action, modulated by the hormonal system. Considering the prevalence of muscle weakness in cerebral palsy[53-55], the high fracture rate reported in this patient group[148-152] may be attributable to their reduced muscle strength. The objective of this study is to measure bony geometry, cortical bone cross-sectional area, and local muscle volume, and from these to estimate the relationship of bone bending and compressional strength to local muscle volume in individuals with bilateral spastic cerebral palsy.

Twenty-seven participants with BSCP (mean age: 14.6 ± 2.9 years; GMFCS levels I-III) and twenty-two typically developing peers (mean age: 16.7 ± 3.3 years) took part in this study. Periosteal and medullary diameter in the distal femur, cortical bone CSA in the femur and tibia along with nine lower limb muscle volumes were measured using MRI. The polar section modulus, cortical bone CSA and buckling ratio were calculated to estimate bone bending and compressional strength in the distal femur. This study is discussed in more detail in Chapter 6.

4.2.3 Study 3: *In vitro* and *in vivo* comparison of mDixon techniques

The objective of this study is to compare Dixon-based MRI techniques for fat quantification at 3T with magnetic resonance spectroscopy (MRS) *in vitro* and *in vivo*. *In vitro*, two- three- and four-point mDixon sequences, with 10°, 20° and 30° flip angles were acquired from seven test phantoms with sunflower oil-water percentages of 0-60% sunflower oil and calculated fat-water ratios compared with MRS. *In-vivo,* two- three- and four-point mDixon sequences with 10° flip angle were acquired and compared with MRS in the vastus medialis of nine typically developing subjects (aged 30.6 ± 5.3, BMI 22.2 ± 2.6). This study is published in The British Journal of Radiology, 87 (1036), 2014. This paper is included in Chapter 7.

4.2.4 Study 4: Intramuscular fat in ambulant young adults with bilateral spastic cerebral palsy

It is known that individuals with BSCP have small and weak muscles. However, no studies to date have investigated intramuscular fat infiltration in this group. The objective of this study is to determine whether adults with BSCP have greater inter- and intramuscular fat than their typically developing peers.

Ethical approval for this study was granted by Hampstead Research Ethics Committee London (09/H0720/120). The ethical approval letter and subject information sheets are given in Appendix B. 10 young adults with BSCP (7 male, mean age 22.5 years, GMFCS levels I-III), and 10 typically developing young adults (6 male, mean age 22.8 years) took part in this study. 11 cm sections of the left leg of all subjects were imaged using multi-echo gradient echo chemical shift imaging (mDixon). Percentage intermuscular fat, intramuscular fat, and a subcutaneous fat to muscle volume ratio (SF/M) were calculated. This study is discussed in more detail in Chapter 8.

4.2.5 Study 5: Spinal cord development in bilateral spastic cerebral palsy

The most common cause of BSCP, PVL, tends to occur between 24 and 33 PCW, before the transient spinal terminations of the corticospinal tract in the spinal cord grey matter have been eliminated and mature projections onto the cells of the spinal grey matter have formed. As a result of the injury, intrinsic cord networks may not mature and muscle development may be delayed[30]. Therefore, spinal cord and subsequent

muscle development is likely to be affected by the extent, severity and timing of the original brain injury. The objective of this study is to investigate the organisation of white matter in the spinal cord at the thoracic (T10-11) and cervical (C6-7) in individuals with BSCP using DTI MRI.

National Research Ethics committee West London (11/LO/1520) granted ethical approval for this study. The ethical approval letter and subject information sheets are given in Appendix C. 11 participants with BSCP were recruited to the study (mean age: 16.4 years ± 4.2; age range: 12.1 – 25.5 years; GMFCS level I: n=1, level II: n=4, level III n=5, level IV: n=1; 11 male) from clinics in our university hospital. Ten TD subjects were included in this study (mean age: 16.9 years ± 3.9; age range: 12.3 – 23.2 years, 12 male). The TD subjects had no previous surgery to their lower limbs and had no known neurological or musculoskeletal conditions. The T10/11 data from one TD subject was excluded from analysis due to significant subject movement during image acquisition. Diffusion measures of microstructure including fractional anisotropy and apparent diffusion coefficients will be compared between spinal levels and subject groups. Relationships between DTI measures and lower limb muscle volume and measures of selective motor control (SCALE) and functional ability (GMFM) in the case subjects will also be investigated. This study is discussed in more detail in Chapter 9.

5. Lower limb muscle volumes in bilateral spastic cerebral palsy

Abstract

Muscle weakness is a feature of individuals with bilateral spastic cerebral palsy (SCP) but there are few reports in the literature of muscle volume in this group. This study compares muscle volumes in adolescents and young adults with SCP with those of their typically developing (TD) peers. Measurements of the volumes of nine major lower limb muscles in 19 independently ambulant subjects with SCP (mean age 14.2 ± 2.7 years, 11 male, GMFCS I (n=5); GMFCS II (n=14)), 19 TD subjects (mean age 16.5 ± 3.0 years, 11 male) were made using magnetic resonance imaging. Muscle volumes were normalised to body mass to minimise the non-pathological variance in muscle size.

Lower limb muscles were smaller in the SCP group ($p \leq 0.023$ in all muscles) than the TD group with the exception of the vastii (lateralis + intermedius; $p=0.868$) and gluteus maximus ($p=0.056$). Average muscle volume deficit was 27.9%. Muscle volume deficits were significantly greater for distal muscles than proximal muscles ($p<0.001$). Reduced muscle size in adolescence and the natural history of sarcopenia in adulthood may contribute to the early loss of mobility of adults with SCP.

This chapter is the published manuscript in Brain & Development 36 (2014) 294-300. Additional information including tables of results and example images are given in Appendix D.

ELSEVIER

Brain & Development 36 (2014) 294–300

BRAIN & DEVELOPMENT
Official Journal of the Japanese Society of Child Neurology

www.elsevier.com/locate/braindev

Original article

Lower limb muscle volumes in bilateral spastic cerebral palsy

Jonathan J. Noble [a,*], Nicola R. Fry [b], Andrew P. Lewis [a], Stephen F. Keevil [c], Martin Gough [b], Adam P Shortland [b]

[a] *Division of Imaging Sciences and Biomedical Engineering, King's College London, The Rayne Institute, 4th Floor, Lambeth Wing, St. Thomas' Hospital, London SE1 7EH, United Kingdom*
[b] *One Small Step Gait Laboratory, Guy's and St. Thomas' NHS Foundation Trust, Guy's Hospital, London SE1 9RT, United Kingdom*
[c] *Department of Medical Physics, Guy's and St. Thomas' NHS Foundation Trust, The Rayne Institute, 4th Floor, Lambeth Wing, St. Thomas' Hospital, London SE1 7EH, United Kingdom*

Received 26 November 2012; received in revised form 15 April 2013; accepted 21 May 2013

Abstract

Aim: Muscle weakness is a feature of individuals with spastic cerebral palsy (SCP) but there are few reports in the literature of muscle volume in this group. This study compares muscle volumes in adolescents and young adults with SCP with those of their typically developing (TD) peers. *Design:* Measurements of the volumes of nine major lower limb muscles in 19 independently ambulant subjects with SCP (mean age 14.2 years (sd 2.7), 11 male, GMFCS I ($n = 5$); GMFCS II ($n = 14$)), 19 TD subjects (mean age 16.5 years (sd 3.0), 11 male) were made using magnetic resonance imaging. *Results:* Lower limb muscles were smaller in the SCP group ($p \leqslant 0.023$ in all muscles) than the TD group with the exception of the vastii (lateralis + intermedius; $p = 0.868$) and gluteus maximus ($p = 0.056$). Average muscle volume deficit was 27.9%. Muscle volume deficits were significantly greater for distal muscles than proximal muscles ($p < 0.001$). *Conclusions:* Reduced muscle size in adolescence and the natural history of sarcopenia in adulthood may contribute to the early loss of mobility of adults with SCP.

Keywords: Cerebral palsy; Independently ambulant; Lower limb; Muscle volume; Magnetic resonance imaging

Muscle weakness in individuals with spastic cerebral palsy (SCP) is well documented [1] and is in part attributable to reduced activation of the muscles in SCP [2–4] and to co-activation of agonists and antagonists [2,3]. Wiley and Damiano [1] demonstrated that during maximum voluntary contractions the muscle groups of children with SCP may produce only between 30% and 75% of the force of their typically-developing (TD) peers. Stackhouse et al. [2] compared forces from the quadriceps and plantarflexors during maximum voluntary contraction and augmented voluntary activation using electrical stimulation in groups of children with SCP and TD children. In both groups muscles could produce substantially greater forces when electrically stimulated. However, data from the subjects with SCP implied that lack of voluntary activation of the musculature alone could not explain muscle weakness. Elder et al. [4] attempted to quantify the agonist–antagonist co-activation and cross-sectional area of the triceps surae in children with SCP and found that both contributed significantly to weakness during voluntary activation. Their study investigated the triceps surae only and was limited to a small number of children.

Investigations of gross muscle morphology in SCP have largely been confined to the medial gastrocnemius. Volume deficits have been reported in children and young adults of between 22% and more than 50% [5–

* Corresponding author. Address: One Small Step Gait Laboratory, Guy's Hospital, Great Maze Pond, London SE1 9RT, United Kingdom. Fax: +44 (0) 20 7188 2477.
E-mail address: jonathan.noble@gstt.nhs.uk (J.J. Noble).

0387-7604/$ - see front matter © 2013 The Japanese Society of Child Neurology. Published by Elsevier B.V. All rights reserved.
http://dx.doi.org/10.1016/j.braindev.2013.05.008

7]. Fewer studies include measurements of muscle size for the whole lower limb. Lampe et al. [8] studied muscle volumes and lengths in a group of young adults with unilateral SCP using MRI. They found significant reductions in muscle volumes for nearly all the muscles in the lower limb when compared to the non-paretic limb and noted that the proximal musculature was less affected than the distal musculature. Riad et al. [9] also reported significantly reduced muscle volume for the majority of the muscles in the lower limb compared to the non-paretic limb in adolescents and young adults with unilateral SCP. However, these studies did not include TD adults as controls and was limited to unilateral subjects. Oberhofer et al. [10] published MRI data from a young group of six children with SCP (four bilaterally affected) and a matched group of TD children. They found significant differences in muscle volumes (normalised to body mass) for the quadriceps and the hamstrings in the children with CP, but not for the calf muscles. Their results are in contrast to Fry et al. [7] who found very large differences in muscle volume in the gastrocnemius muscles, and to Lampe et al. [8] who found the distal muscles to be more affected. A recent review of muscle morphology in SCP by Barret and Lichtwark [11] highlights the limited volume data studies published to date.

In this paper we measured the volume of nine major muscles of the lower limbs in adolescent and young adult subjects with bilateral SCP and in TD subjects. We hypothesised that we would find large reductions in muscle volumes in the individuals with SCP, and that the distal muscles would be more affected than the proximal ones due to increased distal motor impairment in this group [12].

1. Materials and methods

1.1. Participants

The local research ethics committee granted ethical approval for this study. SCP group inclusion criteria: age 10–24 years, diagnosis of bilateral SCP, Gross Motor Function Classification System (GMFCS) levels I–III and met the safety requirements of MRI. Patients were excluded from the study that had undergone surgery, serial casting or botulinum toxin injections to the lower limbs within the previous year. This is a convenience sample of individuals attending our hospital department, with consecutive patients that met the inclusion criteria were invited to participate in the study. Nineteen participants with bilateral SCP were recruited to the study (mean age: 14.4 years; age range: 10.2–19.7 years, GMFCS level I: $n = 5$, level II: $n = 14$, 11 male) from clinics in our university hospital. Nineteen TD subjects were included in this study (mean age: 16.5 years; age range: 10.6–22.3 years, 11 male, 8 female). The TD subjects had not had no previous surgery to their lower limbs and had no known neurological or musculoskeletal condition.

1.2. Data collection and analysis

Both lower limbs of all subjects were acquired with contiguous transverse slices from above the iliac crest to below the calcaneum. All subjects lay supine on the scanner bed and went feet first into the scanner with their feet resting against a wooden footplate giving an approximate plantarflexion angle of 25°.

All MRI data was collected on a 1.5 T Phillips Achieva system (Philips Medical Systems, Best, The Netherlands). Seven SCP and nine TD subjects were scanned using a T1 weighted turbo spin echo sequence (TE/TR = 18/1104.4 ms, number of averages = 2, echo train length = 3, 1.8 × 1.8 mm in-plane voxel size) with a quadrature body coil. Slices were collected contiguously with a slice thickness of 2 mm over the hip, knee and ankle joints and every 4 mm over the remainder of the lower limb. Image acquisition took approximately 20 min for each subject. Data was also collected from twelve SCP and ten TD subjects using a three point Dixon sequence (TE/TR = 4.6/13 ms, echo time shift = 1.53 ms (120° echo phase shift), 20° flip angle, 0.9 × 0.9 mm in-plane voxel size, number of averages = 2, 5 mm slice thickness) with a quadrature body coil. Each scan took approximately 30 min.

Volume measurements were performed using Osirix [13] (version 3.7.1). Visually, the proximal and distal endpoints of each muscle belly were identified and regions of interest were outlined on every image slice with the exception of T1 weighted scans with 2 mm slice thickness where regions were drawn on every other slice (effective slice thickness = 4 mm). The total volume was calculated within the software as the sum of the outlined cross sectional areas multiplied by slice thickness. The volumes of the medial gastrocnemius (MG), lateral gastrocnemius (LG), soleus (SOL), tibialis anterior (TA), rectus femoris (RF), vastus intermedius and lateralis composite (VI + VL), semimembranosus (SM), semtiendinosus (ST), and gluteus maximus (GMax) were measured. Sections of the boundary between VL and VI are difficult to identify in MRI. Therefore, to remove potential boundary inaccuracies, VL and VI were measured as a group VL + VI.

Individuals with SCP tend to be shorter and lighter than TD children of similar age [14]. To account for differences in body size across the age range and between groups, muscle volumes were normalised to body mass [6,7]. In general, the volumes of each muscle were averaged across legs of individual subjects prior to statistical analysis of normalised muscle volume between the two groups. When data was not available from a particular muscle due to image artefacts or subject compliance,

volume data for that muscle was taken from a single limb.

Shapiro–Wilks tests of normality found that the measured volume data was not normally distributed for all muscles ($p > 0.05$), and required non-parametric statistics. Therefore, independent sample median test were used to test for differences in normalised muscle volume between the two subject groups for each muscle investigated. Percentage muscle deficits (PMD) were calculated for the SCP group using Equation 1 and related samples Wilcoxon signed rank test was used to investigate whether the proximal (GMax, RF, VL + VI, SM, ST) or distal (MG, LG, SOL, TA) muscles were more affected. Since multiple statistical tests (10) were performed on the same subjects, the Benjamini [15] method to correct for false discovery rate was used. All statistical tests were performed using SPSS (Version 20.0; IBM SPSS, Chicago, USA).

$$\mathrm{PMD} = 100 \times \frac{(\mathrm{mean}_{\mathrm{control}} - \mathrm{value}_{\mathrm{case}})}{\mathrm{mean}_{\mathrm{control}}} \quad (1)$$

where PMD = percentage muscle deficit,
$\mathrm{mean}_{\mathrm{control}}$ = mean normalised value for TD subjects,
$\mathrm{value}_{\mathrm{case}}$ = normalised value for a subject with SCP.

2. Results

The physical characteristics of subjects in the SCP and TD groups are summarised in Table 1. There was no significant difference in age ($p = 0.052$), height ($p = 0.052$), or BMI ($p = 0.052$) between the groups: however, body mass ($p < 0.001$) was significantly smaller in the SCP group (Independent samples median test).

The subjects had undergone a range of previous interventions (see Table 2) but none within the previous year. Three of the subjects with SCP had previously had undergone femoral de-rotation osteotomies. These subjects had internal fixation devices on the lateral aspect of their proximal femurs that distorted the MRI images around this area preventing accurate assessment of RF, VI + VL, SM, ST and GMax. Persistent muscle activation or subject movement in 4 SCP subjects and 3 TD subjects prevented accurate delineation of various muscles for each of these subjects. One SCP subject became unwell during the MRI scan, which meant that images of the thigh region could not be collected. In the other eleven SCP and sixteen TD subjects all the muscles could be measured. The total number of muscles measured for each muscle is given in Fig. 1a.

Muscle volumes were normalised to body mass because of the strong and significant correlation between MG muscle volumes and body mass shown in our previous work [6]. Significant linear relationships were also found between muscle volume and body mass amongst the TD subjects for all muscles in this study with the exception of ST, as shown in Table 3. When normalised to body mass, muscle volumes did not vary significantly with either height or subject age.

Fig. 1a shows a histogram of normalised muscle volume for each muscle measured. A significant difference (Independent samples median tests with correction for multiple tests, Benjamini [13]) in normalised muscle volume was found between the SCP and TD subject groups for all muscles with the exception of the GMax and VI + VL composite (individual p-values are given in Fig. 1a. The mean PMD of all muscles combined was 27.9%, with the mean PMD ranging between 8.2% for VI + VL and 38.4% for MG (see Fig. 1b). In the individuals with SCP, distal muscles were more affected than proximal muscles and ($p < 0.001$, see Fig. 1b).

3. Discussion

Individuals with SCP have profound muscle weakness that compromises their physical performance [16–18]. However, the sizes of the muscles throughout the lower limb in this group have been elucidated in very few studies [8,10]. Here, we measured the volume of nine of the largest muscles in the lower limb and found them all (with the exception of VI + VL and GMax) to be significantly smaller in a group of ambulant adolescents and adults with SCP than in a group of TD young people of comparable age and sex, even when muscle volume was normalised to body mass (Fig. 1a). Average muscle volume deficits ranged from 8.2% for the VI + VL to 38.3% for MG. We found that distal muscles had greater deficits in volume than proximal muscles (Fig. 1b).

The deficits in muscle volume of the plantarflexors in this study were similar to those we have previously reported for the medial gastrocnemius in children with bilateral SCP awaiting surgery [7]. Overall, the reductions in muscle volume recorded throughout the limb were larger than those reported in a study of young adults with unilateral SCP [8]. These authors did not

Table 1
Physical characteristics (mean ± standard deviation) of SCP and control groups and number of SCP subjects in each GMFCS levels (I–II).

	SCP group	TD group
Number of subjects	19	19
Age (years)	14.4 ± 2.7	16.5 ± 2.0
Sex (m, f)	11, 8	11, 8
Body mass (kg) *	44.3 ± 11.5	67.2 ± 18.3
Height (m)	1.55 ± 0.13	1.72 ± 0.12
BMI (kg/m^2)	18.2 ± 2.8	22.5 ± 4.0
GMFCS level I	5	–
GMFCS level II	14	–

* Denotes significant difference between groups ($p = 0.001$).

Table 2
Previous interventions in the group of adolescents and adults with SCP.

Subject	Surgery	Botulinum toxin injection
1	Bilateral Achilles tendon lengthening (x3) Right hamstring lengthening	None
2	Bilateral gastrocnemius lengthening Left calcaneal osteotomy	None
3	None	None
4	Bilateral psoas release, medial hamstring lengthening and rectus femoris transfer	Bilateral gastrocnemius (x2) Bilateral to hamstrings (x1)
5	None	None
6	Bilateral psoas release and gastrocnemius lengthening, and femoral derotation	None
7	Right femoral derotation Bilateral hamstring and gastrocnemius lengthening	None
8	Left tibialis posterior recession and gastrocnemius lengthening	Left gastrocnemius (x1) Left tibialis posterior (x1)
9	Left hamstring lengthening	Left gastrocnemius (x2)
10	None	None
11	None	None
12	Right tibialis posterior, Achilles tendon, flexor digitorum longus, and flexor hallucis longus lengthening	Right gastrocnemius (x1)
13	Bilateral hamstring lengthening Right Achilles tendon, gastrocnemius and soleus lengthening	Right gastrocnemius (x1) Right hamstrings (x1)
14	Hamstring lengthening bilaterally Left Achilles tendon lengthening	Bilateral gastrocnemius (x4)
15	Left hamstring and gastrocnemius lengthening	None
16	Right femoral derotation osteotomy and gastrocnemius lengthening	None
17	Bilateral hamstring lengthening	None
18	None	None
19	None	None

have an independent control group but rather used the non-paretic limb as a control. In which case, they may have underestimated the deficits in muscle volume in the paretic limb. The statistically insignificant deficit of the quadriceps and gluteus maximus muscle volumes in our study suggests that these muscles may be utilised more than the other muscle groups in functional tasks and, therefore, a larger muscle volume is maintained.

Muscle weakness is not caused by reduced muscle size alone, but also by reduced muscle activation [2–4] and increased co-activation [2,3]. Stackhouse et al. [2] measured the torques produced by maximum voluntary contraction (MVC) and by MVCs augmented by electrical stimulation, from the plantarflexor and quadriceps muscle groups in ambulant children with bilateral SCP ($n = 12$, age range: 7–13 years) as well as TD subjects ($n = 10$, age range: 8–12 years). They found that the force (normalised to body mass) that could be generated by MVC alone was 56% lower for the quadriceps and 73% lower for the plantarflexors in those with bilateral SCP compared to control children. In addition, those with SCP were able to activate 33% and 49% less of the available mechanical potential of their quadriceps and plantarflexors respectively than control subjects. Barber et al. [19] found 33% lower active ankle plantarflexion torque across the available range of ankle joint motion in SCP compared to their TD peers. This reduced ankle platarflexion torque was partially explained by 37% smaller medial gastrocnemius muscle and 4% greater antagonistic co-contraction. The Achilles tendon slack length was also 10% longer in the SCP group. A relationship between reduced muscle activation and muscle volume is plausible: those with SCP may not develop sufficient tension frequently enough to encourage normal muscular growth [2,19].

3.1. Clinical implications

In previous studies, significant relationships have been found between muscle morphological parameters, strength and function in individuals with SCP. Ohata et al. [20] found a significant relationship between quadriceps muscle thickness and GMFCS level. Moreau et al. [21] demonstrated a strong relationship between VL thickness and knee extensor voluntary strength. We have previously shown that intense exercise may increase muscle volume in the plantarflexors of children with SCP [22], and two other studies have shown that neuromuscular electrical stimulation may also result in increases in muscle volume [23] and cross-sectional area [24]. It is possible that training exercises that produce increases in muscle volume may also increase muscle strength and improve function in this group, though perhaps, the more significant problem of reduced muscle growth, in these young people, is the effect on their long-term function. Their limited muscular reserve may expose them to the deleterious effects of aging on muscle earlier than their typically developing peers, and result

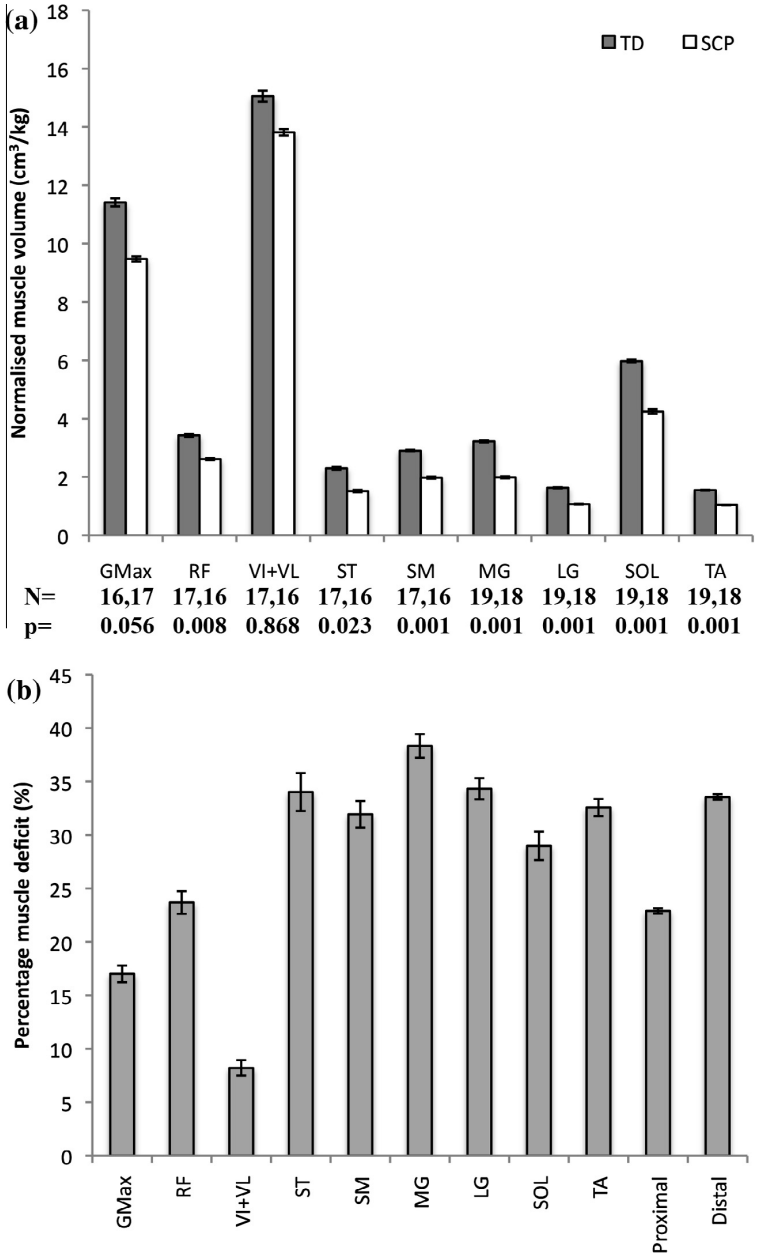

Fig. 1. (a). Normalised muscle volumes in the SCP group (white) and TD group (grey) for all muscles investigated. Where N = number of subjects (TD, SCP), p = p-value and *denotes a significant result (Benjamini corrected [13]). (b). Group averaged percentage muscle volume deficits for each muscle separately and for muscles grouped by anatomical location (distal, proximal) for the SCP group compared to the TD group mean. Error bars represent the standard error for each category.

in an early loss of mobility [25]. Preserving muscle volume may enhance long-term mobility in SCP.

There was much greater variation in normalised muscle volume for the young people with SCP than for their typically developing peers. Some of this variability in normalised muscle volume appears to be related to GMFCS level (see Fig. 2). However, the unequal group sizes (GMFCS level I [$n = 5$] and II $n = 14$]) limits power of this study to determine the contribution of GMFCS level on muscle volume. Volume imaging may have a role in tailoring individual treatment. For example, smaller muscles may benefit most from resis-

Table 3
Pearson correlation coefficients for muscle volume and body mass for the TD group.

Muscle	Pearson correlation	Significance (2-tailed)
MG	0.854*	0.002
LG	0.959*	<0.001
SOL	0.881*	0.001
TA	0.820*	0.004
VIVL	0.694*	0.026
RF	0.718*	0.019
SM	0.835*	0.003
ST	0.517	0.126
GMax	0.782*	0.008

* Denotes significant relationship ($p < 0.05$).

tance training, and knowledge of muscle size may be useful in dose optimisation for improving the efficacy of botulinum toxin injections.

3.2. Limitations

The number of subjects recruited may limit the scope and power of this study to investigate the relationship between muscle volumes and other variables such as gross motor function. Voluntary muscle strength depends on many factors, including age, sex and levels of voluntary muscle activation, as well as muscle size, architecture and composition. A future more sophisticated study is required to enable the muscular and neurological components of muscle weakness in SCP to be separated out. However, the differences in normalised muscle volume between the TD and SCP groups were large (see Fig. 1a) and we found the affected muscles to be significantly smaller for all muscles except VI + VL and GMax. Muscle volume deficits will contribute to the weakness observed in the lower limbs of individuals with CP [1], during voluntary activation as well as more automatic activities such as walking.

It is possible that the diverse histories of surgical intervention, serial casting, botulinum toxin injections and physiotherapy received by the individuals with SCP in this study may have influenced the development of particular muscles. Unfortunately, it is not possible to recruit a representative group of young adults and adolescents with SCP who have not had significant intervention during their lifetime. Longitudinal studies of the natural history of muscle impairments in SCP, as well as the effect of intervention, are required to improve the selection of treatments in this group and preserve muscle mass.

Acknowledgements

This research was supported by the National Institute for Health Research (NIHR) Biomedical Research Centre at Guy's and St Thomas' NHS Foundation Trust and King's College London. The views expressed are those of the author(s) and not necessarily those of the NHS, the NIHR or the Department of Health. Nicola Fry was funded on a fellowship from the National Coordinating Centre for Research Capacity Development (NCCRCD), Department of Health, UK.

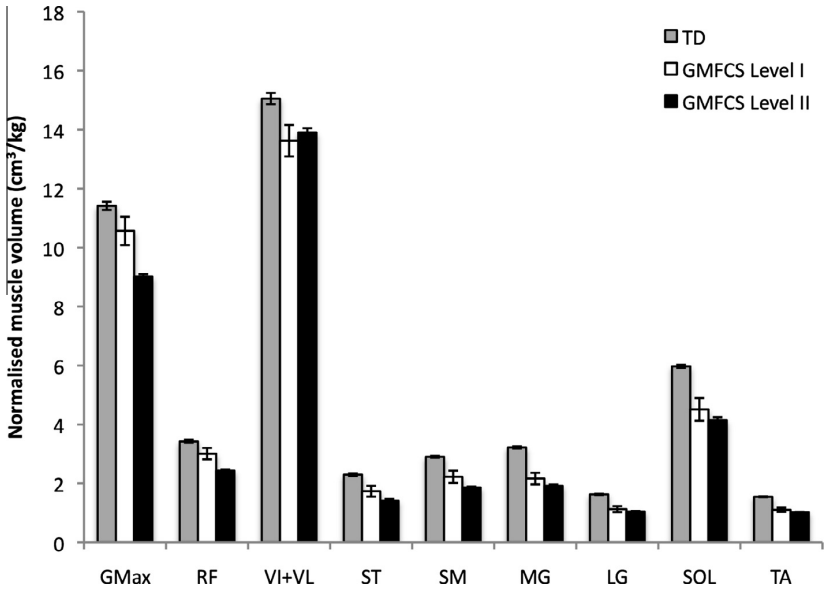

Fig. 2. Normalised muscle volumes in TD group (grey), SCP GMFCS level I (white), and SCP GMFCS level II (black) for all muscles investigated. Error bars represent the standard error of each group.

Andrew Lewis and Jonathan Noble were funded on PhD studentships from the Guy's and St. Thomas's Charity, London, UK.

References

[1] Wiley ME, Damiano DL. Lower-extremity strength profiles in spastic cerebral palsy. Dev Med Child Neurol 1998;40:100–7.

[2] Stackhouse SK, Binder-Macleod SA, Lee SC. Voluntary muscle activation, contractile properties, and fatigability in children with and without cerebral palsy. Muscle Nerve 2005;31:594–601.

[3] Rose J, McGill KC. Neuromuscular activation and motor-unit firing characteristics in cerebral palsy. Dev Med Child Neurol 2005;47:329–36.

[4] Elder GC, Kirk J, Stewart G, Cook K, Weir D, Marshall A, et al. Contributing factors to muscle weakness in children with cerebral palsy. Dev Med Child Neurol 2003;45:542–50.

[5] Barber L, Hastings-Ison T, Baker R, Barrett R, Lichtwark G. Medial gastrocnemius muscle volume and fascicle length in children aged 2 to 5 years with cerebral palsy. Dev Med Child Neurol 2011;53:543–8.

[6] Malaiya R, McNee AE, Fry NR, Eve LC, Gough M, Shortland AP. The morphology of the medial gastrocnemius in typically developing children and children with spastic hemiplegic cerebral palsy. J Electromyogr Kinesiol 2007;17:657–63.

[7] Fry NR, Gough M, McNee AE, Shortland AP. Changes in the volume and length of the medial gastrocnemius after surgical recession in children with spastic diplegic cerebral palsy. J Pediatr Orthop 2007;27:769–74.

[8] Lampe R, Grassl S, Mitternacht J, Gerdesmeyer L, Gradinger R. MRT-measurements of muscle volumes of the lower extremities of youths with spastic hemiplegia caused by cerebral palsy. Brain Dev 2006;28:500–6.

[9] Riad J, Modlesky CM, Gutierrez-Farewik EM, Brostrom E. Are muscle volume differences related to concentric muscle work during walking in spastic hemiplegic cerebral palsy? Clin Orthop Relat Res 2012;470:1278–85.

[10] Oberhofer K, Stott NS, Mithraratne K, Anderson IA. Subject-specific modelling of lower limb muscles in children with cerebral palsy. Clin Biomech 2010;25:88–94.

[11] Barrett RS, Lichtwark GA. Gross muscle morphology and structure in spastic cerebral palsy: a systematic review. Dev Med Child Neurol 2010;52:794–804.

[12] Fowler EG, Staudt LA, Greenberg MB. Lower-extremity selective voluntary motor control in patients with spastic cerebral palsy: increased distal motor impairment. Dev Med Child Neurol 2010;52:264–9.

[13] Rosset A, Spadola L, Ratib O. OsiriX: an open-source software for navigating in multidimensional DICOM images. J Digit Imaging 2004;17:205–16.

[14] Stevenson RD, Conaway M, Chumlea WC, Rosenbaum P, Fung EB, Henderson RC, et al. Growth and health in children with moderate-to-severe cerebral palsy. Pediatrics 2006;118:1010–8.

[15] Benjamini Y, Drai D, Elmer G, Kafkafi N, Golani I. Controlling the false discovery rate in behavior genetics research. Behav Brain Res 2001;125:279–84.

[16] Kramer JF, Ann MacPhail HE. Relationships among measures of walking efficiency, gross motor ability, and isokinetic strength in adolescents with cerebral palsy. Pediatr Phys Ther 1994;6:3–9.

[17] Damiano DL, Kelly LE, Vaughn CL. Effects of quadriceps femoris muscle strengthening on crouch gait in children with spastic diplegia. Phys Ther 1995;75:658–67 [discussion 68–71].

[18] Parker DF, Carriere L, Hebestreit H, Salsberg A, Bar-Or O. Muscle performance and gross motor function of children with spastic cerebral palsy. Dev Med Child Neurol 1993;35:17–23.

[19] Barber L, Barrett R, Lichtwark G. Medial gastrocnemius muscle fascicle active torque-length and Achilles tendon properties in young adults with spastic cerebral palsy. J Biomech 2012;45:2526–30.

[20] Ohata K, Tsuboyama T, Ichihashi N, Minami S. Measurement of muscle thickness as quantitative muscle evaluation for adults with severe cerebral palsy. Phys Ther 2006;86:1231–9.

[21] Moreau NG, Simpson KN, Teefey SA, Damiano DL. Muscle architecture predicts maximum strength and is related to activity levels in cerebral palsy. Phys Ther 2010;90:1619–30.

[22] McNee AE, Gough M, Morrissey MC, Shortland AP. Increases in muscle volume after plantarflexor strength training in children with spastic cerebral palsy. Dev Med Child Neurol 2009;51:429–35.

[23] Stackhouse SK, Binder-Macleod SA, Stackhouse CA, McCarthy JJ, Prosser LA, Lee SC. Neuromuscular electrical stimulation versus volitional isometric strength training in children with spastic diplegic cerebral palsy: a preliminary study. Neurorehabil Neural Repair 2007;21:475–85.

[24] Damiano DL, Prosser LA, Curatalo LA, Alter KE. Muscle plasticity and ankle control after repetitive use of a functional electrical stimulation device for foot drop in cerebral palsy. Neurorehabil Neural Repair 2013;27:200–7.

[25] Shortland A. Muscle deficits in cerebral palsy and early loss of mobility: can we learn something from our elders? Dev Med Child Neurol 2009;51(Suppl. 4):59–63.

6. Bone strength and muscle volume in bilateral spastic cerebral palsy

Abstract

There is a high prevalence of fractures in individuals with cerebral palsy[148-152], commonly occurring in the distal femur and proximal tibia[150]. The objective of this chapter is to investigate whether bone strength in the distal femur and proximal tibia is related to local muscle volume in ambulant individuals with bilateral spastic cerebral palsy (BSCP). Twenty-seven participants with CP (mean age: 14.6 ± 2.9 years; Gross Motor Function Classification System (GMFCS) levels I-III) and twenty-two typically developing (TD) peers (mean age: 16.7 ± 3.3 years) took part in this study. Periosteal and medullary diameter in the distal femur and cortical bone cross-sectional area (CSA) and thickness (CT) in the distal femur and proximal tibia were measured along with nine lower limb muscle volumes using MRI. Additionally, the polar section modulus (Zp) and buckling ratio (BR) were calculated to estimate bone bending strength and compressional bone stability respectively in the distal femur. The relationships of all measured parameters with muscle volume, height, age, body mass, gender, and subject group were investigated using a generalized linear model (GZLM).

In the distal femur, Zp was significantly positively related to thigh muscle volume ($p=0.007$), and height ($p=0.026$) but not significantly related to subject group ($p=0.076$) or body mass ($p=0.098$). BR was not significantly different between groups and was not related to any of the variables tested. Cortical bone CSA was significantly lower in the BSCP group at both the distal femur ($p=0.002$) and proximal tibia ($p=0.009$). It was

also positively associated with thigh muscle volume ($p<0.001$) at the distal femur, and with subject height ($p=0.005$) at the proximal tibia.

Conclusions: Bending and compressional strength of the femur, estimated from Zp and cortical bone CSA respectively, is associated with reduced thigh muscle volume. Increasing muscle volume by strength training may have a positive effect on bone mechanics in individuals with BSCP.

The work in this chapter has been published in Bone (Noble *et al*. Bone 2014 Sep; 66:251-5).

6.1 Introduction

There is a high prevalence of fractures in individuals with cerebral palsy[148-152], with lower limb fractures most prevalent[149,150], commonly occurring in the distal femur and proximal tibia[150]. In ambulant children with cerebral palsy, fractures are most commonly sustained through significant trauma. In typically developing children and adolescents, factors associated with bone fractures are bone mineral density (BMD), bone geometry, and bone size[153,276]. Poor nutrition, lack of weight-bearing physical activity, obesity and high exposure to trauma may also influence fracture risks in the general paediatric population[153].

Although Dual-energy X-ray Absorption (DXA) is the most common method for measuring BMD in cerebral palsy, the technique suffers from systematic errors that depend on skeletal site and body size[154]. Since individuals with cerebral palsy often have a smaller body size than their TD peers[155], an apparent low BMD score may be measured when assessed by DXA. Gold standard assessments using peripheral quantitative computed tomography, pQCT, suggest that children with cerebral palsy do not have a deficit in BMD, but in fact have reduced cortical bone thickness (CT)[147]. Bone geometry can also be assessed using MRI[277], which has shown reduced cortical bone thickness at the mid-femur of children with quadriplegic cerebral palsy[156].

Bone strength is related to BMD, however it is determined predominantly by bone geometry. The ability of a bone to resist bending and torsional forces (estimated using the polar section modulus, Zp) is inversely proportional to bone length to the third power and directly related to bone diameter to the third power[88]. The stability of a bone to compressional forces can be estimated by the buckling ratio (BR), which is a ratio of the bone radius to cortical bone thickness. In typically developing children, before and after puberty, bone strength and geometry is determined primarily by bone length and muscle CSA, modulated by physical activity and dietary calcium[91].

In adults, bone mass decreases with age: bending strength is maintained by a gradual increase in bone diameter by periosteal addition of bone, and endosteal resorption leading to a wider bone and a relatively thinner cortex. This maintains bending strength but reduces the ability of the bone to remain stable in the presence of larger compressive loads. In non-ambulant children with cerebral palsy, femoral bone bending and torsional strength, estimated from geometric measures, is lower than their typically developing peers[156]. Bone geometry in ambulant young adults with cerebral palsy has not been assessed.

Mechanical forces are a significant factor affecting bone strength and development. Longitudinal growth increases the length of lever arms and bending moments leading to greater forces experienced by the bone[80], with bending and torsional forces being the predominant loading factors in the long bone diaphysis[82,83]. Muscle weakness[55] and reduced muscle volumes[53,56-61,278] in individuals with cerebral palsy is well documented. Therefore, in individuals with cerebral palsy, the reduced bone strength and increased fracture rate may be due to the reduced mechanical loading applied to the bones by the local musculature. If there is relationship between bone strength and muscle size, this may provide an alternative treatment option to clinicians for reducing the fracture rate in this group.

In this study we investigate bone strength at the most common fracture sites in cerebral palsy: the distal femur and proximal tibia[150]. Cortical bone cross-sectional area (CSA) and cortical bone thickness (CT) in the distal femur and proximal tibia, femoral cross-sectional geometry, and the volume of nine major muscles of the lower limbs were measured in adolescent and young adults with bilateral spastic cerebral palsy (BSCP)

and their typically developing (TD) peers. Bone strength in the distal femur was estimated through calculation of Zp and BR. We hypothesised that cortical bone CSA, CT, BR and Zp are significantly related to the local muscle volume, independently of diagnosis and body mass.

6.2 Materials & Methods

6.2.1 Participants

The local research ethics committee granted ethical approval for this study. Individuals aged 10 – 24 years, with a diagnosis of bilateral spastic CP, Gross Motor Function Classification System (GMFCS) levels I-III, who met the safety requirements of MRI were included in this study. Patients who had undergone surgery, serial casting or botulinum toxin injections to the lower limbs within the previous year were excluded from the study. None of the subjects had had previous osteotomies of the long bones. This was a convenience sample of individuals attending our hospital department, with consecutive patients that met the inclusion criteria invited to participate in the study. 27 participants with bilateral spastic CP were recruited to the study (mean age: 14.6 years; age range: 10.2 – 23.1 years, GMFCS level I: n=5, level II: n=17, level III n =5, 19 male, 8 female) from clinics in our university hospital. 25 TD subjects were included in this study (mean age: 16.7 years; age range: 10.6 – 23.2 years, 17 male, 5 female). The TD subjects had no previous surgery to their lower limbs and had no known neurological or musculoskeletal condition. Z-scores for height-to-age and BMI-to-age were calculated based on the World Health Organization (WHO) growth reference data[279]. For individuals 20 years of age and older, the age-19 height and BMI *z*-score reference have been used in order to have a consistent metric of relative height and BMI for all subjects.

6.2.2 Data collection and analysis

MRI images of both lower limbs of all subjects were acquired with contiguous transverse slices from above the iliac crest to below the calcaneum. All subjects lay supine on the scanner bed with their feet resting against a wooden footplate giving an approximate plantarflexion angle of 25 degrees.

MRI data was collected on 1.5 T and 3.0 T Phillips Achieva systems (Philips Medical Systems, Best, The Netherlands). On the 1.5 T MRI system, seven BSCP and nine TD subjects were scanned using a T1-weighted turbo spin echo sequence (TE/TR=18/1104.4 ms, number of averages = 2, echo train length = 3, 1.8 x 1.8 mm in-plane voxel size) with a quadrature body coil. Slices were collected contiguously with a slice thickness of 2 mm over the hip, knee and ankle joints and every 4 mm over the remainder of the lower limb. Image acquisition took approximately 20 minutes for each subject. On the 3.0T system, 12 BSCP and 10 TD subjects using a three point Dixon sequence (TE/TR=4.6/13 ms, echo time shift = 1.53 ms (120 ^{o} echo phase shift), 20^{o} flip angle, 0.9 x 0.9 mm in-plane voxel size, number of averages = 2, 5 mm slice thickness) with a quadrature body coil. Each scan took approximately 30 minutes. On the 3.0T MRI system, data was collected from eight CP and six TD subjects using a three point Dixon sequence (TE/TR=2.11/5.2 ms, echo time shift = 0.76 ms (120 ^{o} echo phase shift), 10^{o} flip angle, 1.2 x 1.2 mm in-plane voxel size, number of averages = 2, 5 mm slice thickness) with a quadrature body coil. Image acquisition took approximately 15 minutes for each subject.

The proximal and distal endpoints of the femur and tibia were identified in the MRI images and the length of the bones calculated as the distance between the end points for each bone. The distal femur and proximal tibia were defined as 70% and 30% along the length of the bone from the proximal ends respectively. Cortical CSA was measured at the distal femur and proximal tibia by drawing regions of interest around the inner and outer cortical bone boundaries. Periosteal (T) and medullary diameter (M) were measured in the anterior-posterior direction at the distal femur and medio-laterally in the proximal tibia. CT was calculated using Equation 6.1. In the distal femur, assuming a cylindrical bone shape with circular cross-section, the polar moment of inertia (J) is calculated using Equation 6.2[89]. The polar section modulus (Zp), which is a measure of torsional and bending strength, is calculated using Equation 6.3[90]. Stability to compressional force was estimated by using the buckling ratio (BR), which is a ratio of the bone radius (r) to cortical bone thickness (CT) given by Equation 6.4.

The proximal and distal endpoints of each muscle belly were identified and regions of interest around the muscle cross-sections were manually outlined on every image slice with the exception of T1-weighted scans with 2 mm slice thickness where regions were

drawn on every other slice (effective slice thickness = 4 mm). The total volume was calculated within the software as the sum of the outlined cross sectional areas multiplied by slice thickness. The volumes of the medial gastrocnemius (MG), lateral gastrocnemius (LG), soleus (SOL), tibialis anterior (TA), rectus femoris (RF), vastus intermedius and lateralis composite (VI+VL), semimembranosus (SM), semtiendinosus (ST), and gluteus maximus (GMax) were measured. Sections of the boundary between VL and VI are difficult to identify in MRI. Therefore, to remove potential boundary inaccuracies, VL and VI were measured as a group VL+VI. The total thigh and shank muscle volumes were calculated from the addition of RF, VI+VL, SM, ST, GMax, and MG, LG, SOL, TA respectively. All MRI image measurements were performed manually using Osirix (version 3.7.1; Pixmeo, Geneva, Switzerland)[280].

$$Cortical\ thickness\,(CT) = \frac{(T - M)}{2} \qquad Equation\ 6.1$$

$$Polar\ moment\ of\ inertia\,(J) = \frac{\pi}{32}(T^4 - M^4) \qquad Equation\ 6.2$$

$$Polar\ section\ modulus\,(Zp) = \frac{J}{(T/2)} \qquad Equation\ 6.3$$

$$Buckling\ ratio\,(Br) = \frac{r}{CT} \qquad Equation\ 6.4$$

$$Where\ \ T = Periosteal\ diameter$$
$$M = Medullary\ diameter$$
$$r = Bone\ radius$$

Data from the left or right limb of each subject was selected at random. When data was not available from a particular limb due to image artefacts or lack of subject compliance, muscle volume and bone geometric data were taken from the other limb. Shapiro-Wilks tests of normality found that the measured cortical bone CSA and CT in the femur and tibia, and Zp and BR in the femur were normally distributed ($p>0.05$). A generalized linear model (GZLM) was employed to investigate relationships between cortical bone CSA, Zp, and BR with muscle volume. Subject group and gender were set as fixed factors, with shank and thigh muscle volume, height, age, and body mass as covariates. Multiple linear regression analysis was subsequently performed to assess linearity of the significant factors from the GZLM with each of the dependent variables

for cortical bone (CSA, CT, Zp, and BR). Co-linearity of the covariates was assessed by calculating the variance inflation factor (VIF) with the VIF co-linearity threshold set to 10[281]. All statistical tests were performed using SPSS (Version 20.0; IBM SPSS, Chicago, USA).

6.3 Results

The physical characteristics of the CP and TD subject groups are summarised in Table 6.1. The CP group was significantly younger ($p=0.02$), shorter ($p<0.001$) and lighter ($p<0.001$) than the TD group. There was no significant difference in BMI ($p=0.392$). Height-for-age and BMI-for-age Z-scores were significantly lower in the CP group ($p<0.001$ and $p=0.013$ respectively). VIF scores for co-linearity between the independent variables (age, height, body mass, and shank and thigh muscle volume) are summarised in Table 6.2. All VIF scores were less than 10, and therefore, all independent variables were included in the GZLM analysis. Example MRI images of the thigh and tibia of one CP subject and one TD subject along with the corresponding cortical bone CSA regions of interest are given in Figure 6.1. Group comparisons of thigh and shank muscle volume normalised to body weight are shown in Figure 6.2 and Table 6.3. Group comparisons of cortical bone CSA, CT, Zp, and BR are given in Figure 6.3 and Table 6.3.

	CP Group	TD Group
Number of subjects	27	25
Age (years)*	14.6 ± 2.9	16.7 ± 3.3
Gender (m,f)	19, 8	17, 8
Body mass (kg)*	48.2 ± 14.8	66.9 ± 17.0
Height (m)*	1.56 ± 0.13	1.72 ± 0.12
Height Z-score for age	-0.72 ± 0.87	0.70 ± 0.92
BMI (kg/m^2)	19.3 ± 3.9	22.3 ± 3.5
BMI Z-score for age	-0.29 ± 1.32	0.54 ± 0.95
GMFCS level I	5	-
GMFCS level II	17	-
GMFCS level III	5	-

Table 6.1 Physical characteristics (mean ± standard deviation) of CP and control groups and number of SCP subjects in each GMFCS levels (I-III). * Denotes significant difference between groups ($p<0.05$)

	Age	Body mass	Height	Shank muscle volume
Thigh muscle volume	2.07	4.001	5.361	
Age		4.349	4.961	7.513
Body Mass			4.152	6.29
Height				7.523

Table 6.2 Variance inflation factors of co-linearity between the co-variables

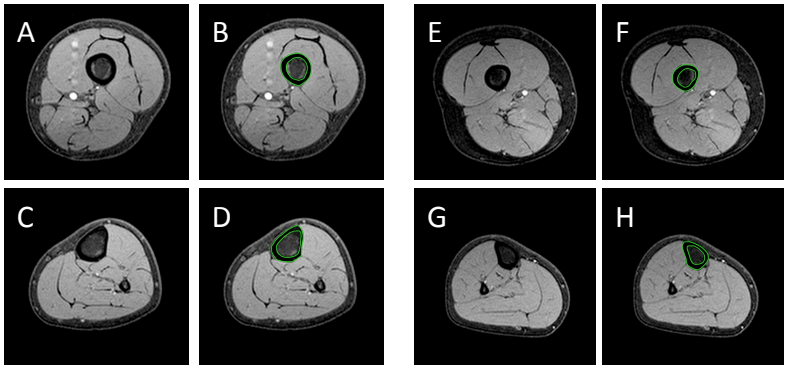

Figure 6.1 Example MRI images of the proximal femur (A-B,E-F) and tibia (C-D, G-H) for a age and sex matched TD subject (A-D) and CP subject (E-H). Regions of interest (green) are shown in B,D,F, and H identifying the inner and outer cortical bone boundaries for cortical bone CSA calculation.

Tibial cortical bone CSA was dependent on subject group, being lower in the BSCP group (p=0.009), and positively related to height (p=0.005), but was not related to shank muscle volume (p=0.166), body mass (p=0.492), gender (p=0.335), or age (p=0.151).. In the GZLM, a diagnosis of BSCP explained a reduction in tibial cortical bone CSA of 0.413 cm^2, accounting for 43.2% of the difference between the groups. Tibial cortical bone CSA increased by 0.024 cm^2 and 0.028 cm^2 per cm height in the BSCP and TD groups respectively. Within the multiple linear regression analysis, height explained 39.3% and 46.5% of the variance in tibial cortical bone CSA in the BSCP and TD subject groups respectively. A plot of proximal tibial cortical bone CSA versus the predicted tibial cortical bone CSA by subject height in each group is shown in Figure 6.4. CT in the proximal tibia is not significantly related to subject group (p=0.751), shank muscle volume (p=0.064), height (p=0.713), body mass (p=0.437), age (p=0.905), and gender (p=0.916).

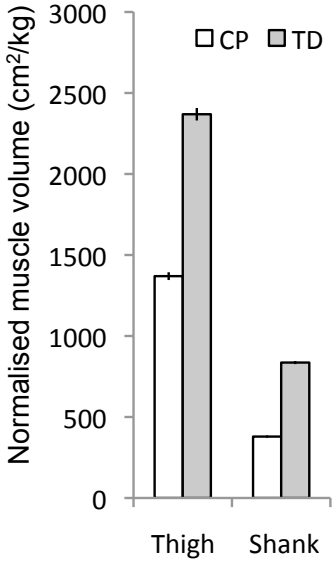

Figure 6.2 Thigh and shank muscle volume normalized to body mass in the CP group (white) and TD group (grey). Error bars represent the standard error in each group.

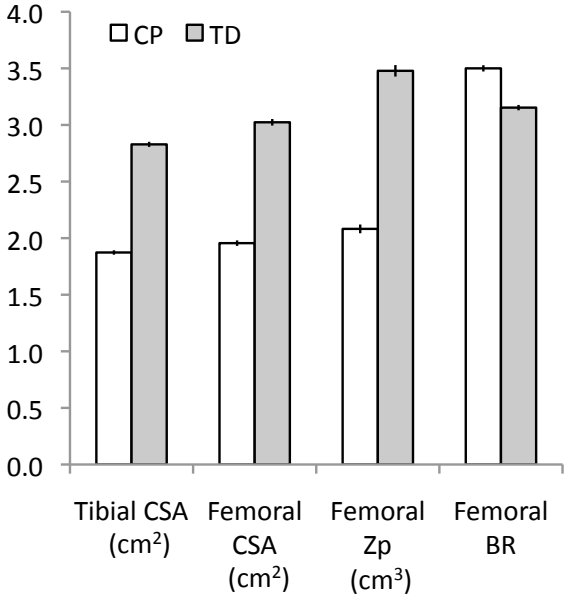

Figure 6.3 Cortical bone CSA in the proximal tibia and distal femur, and calculated Zp and BR in the femur for the CP group (white) and TD group (grey). Error bars represent the standard error in each group.

			95% Confidence Interval			
	Group	Mean	Lower Bound	Upper Bound	Standard deviation	Standard error
Body Mass (kg)	CP	49.60	42.22	56.98	16.22	3.54
	TD	66.51	59.40	73.62	16.04	3.42
Height (m)	CP	1.56	1.51	1.62	0.13	0.03
	TD	1.71	1.65	1.77	0.13	0.03
Shank normalised muscle volume (cm^3/kg)	CP	0.40	0.32	0.48	0.18	0.04
	TD	0.85	0.75	0.96	0.24	0.05
Thigh normalised muscle volume (cm^3/kg)	CP	1.40	1.17	1.62	0.50	0.11
	TD	2.37	2.01	2.73	0.81	0.17
Tibia CT (mm)	CP	2.40	2.18	2.61	0.47	0.10
	TD	2.94	2.72	3.17	0.51	0.11
Femur CT (mm)	CP	3.55	3.21	3.89	0.74	0.16
	TD	4.53	4.18	4.87	0.77	0.16
Tibia CSA (cm^2)	CP	1.88	1.65	2.11	0.51	0.11
	TD	2.81	2.59	3.03	0.50	0.11
Femur CSA (cm^2)	CP	1.99	1.77	2.22	0.49	0.11
	TD	3.02	2.75	3.29	0.61	0.13
BR (femur)	CP	3.47	3.21	3.74	0.58	0.13
	TD	3.15	2.93	3.37	0.50	0.11
Zp (femur) (cm^3)	CP	2.12	1.76	2.49	0.81	0.18
	TD	3.48	3.01	3.95	1.06	0.23

Table 6.3 Mean, 95% confidence interval of the mean, standard deviation and standard error for the CP and TD groups. CT = cortical bone thickness; CSA = cortical bone cross-sectional area; BR = buckling ratio; Zp = polar section modulus.

Distal femoral cortical bone CSA was significantly related to subject group (p=0.002) and thigh muscle volume (p<0.001), but was not significantly related to height (p=0.120), body mass (p=0.299), age (p=0.279), or gender (p=0.602). In the GZLM, BSCP explained an overall reduction in femoral cortical bone CSA of 0.412 cm^2, accounting for 38.6% of the difference between the groups. Femoral cortical bone CSA was increased by 0.871 cm^2 and 0.525 cm^2 per 1000 cm^3 of thigh muscle volume in the BSCP and TD groups respectively. Thigh muscle volume explained 74.7% and 48.4% of the variance in femoral cortical bone CSA in the BSCP and TD subject groups respectively. A plot of distal femoral cortical bone CSA versus the predicted femoral cortical bone CSA from thigh muscle volume in each group is shown in Figure 6.5. CT in the distal femur is significantly related to thigh muscle volume (p=0.01) and subject group (p=0.05), but is not related to height (p=0.559), body mass (p=0.408), age (p=0.117), and gender (p=0.129). In the GZLM, BSCP explained an overall reduction in femoral CT of 0.444 mm, accounting for 41.7% of the difference between groups. Femoral CT was increased by 0.571 mm and 0.758 mm per 1000 cm^3 of thigh muscle volume in the BSCP and TD groups respectively. A plot of distal femoral CT versus the predicted CT from thigh muscle volume in each group is shown in Figure 6.6.

The circularity assumption for Zp and BR is valid in the distal femur with the mean anterior-posterior and medial-lateral periosteal diameter ratio normally distributed about a mean of 0.98, standard deviation 0.09. In the GZLM, Zp is significantly related to thigh muscle volume (p=0.007) and height (p=0.026), but is not significantly related to subject group (p=0.117), body mass (p=0.145), age (p=0.407), or gender (p=0.427). Zp increased by 0.592 cm^3 per 1000 cm^3 of thigh muscle volume, and by 0.038 cm^3 per cm height. Thigh muscle volume and height explained 75.4% of the variance in Zp across all subjects. A plot of Zp versus the predicted Zp from thigh muscle volume and height is shown in Figure 6.7. BR was not significantly related to subject group (p=0.06), thigh muscle volume (p=0.446), height (p=0.671), body mass (p=0.670), age (p=0.197), or gender (p=0.095).

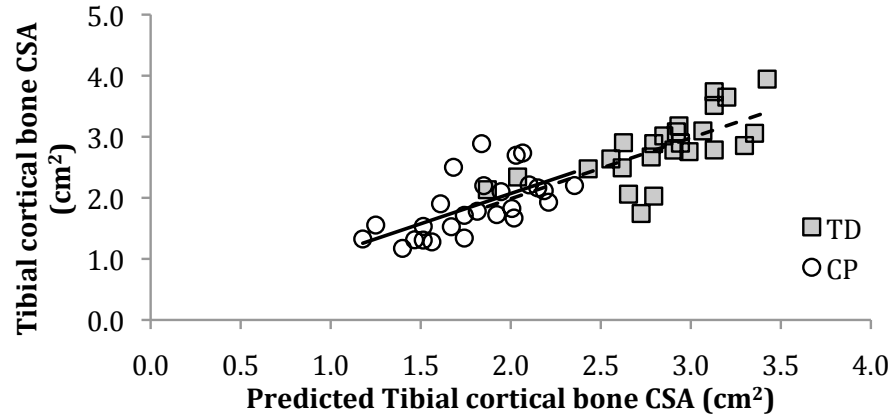

Figure 6.4 Height predicted cortical bone CSA in the proximal tibia versus measured cortical bone CSA for the CP group (white, solid line, $R^2 = 0.393$, y=0.9907x + 0.00891) and TD group (grey, dashed line, $R^2 = 0.465$, y=0.9962x – 0.007)

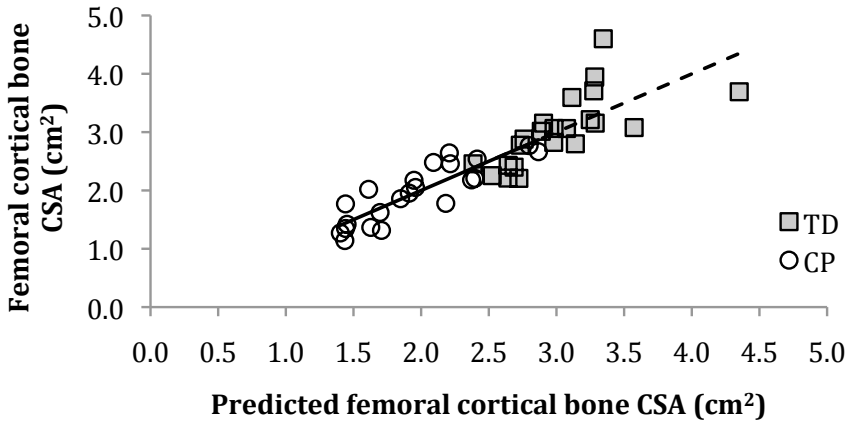

Figure 6.5 Thigh muscle volume predicted cortical bone CSA in the distal femur versus measured cortical bone CSA for the CP group (white, $R^2 = 0.747$, y=0.9997x + 0.0004) and TD group (grey $R^2 = 0.484$, y=0.9991x + 0.0016).

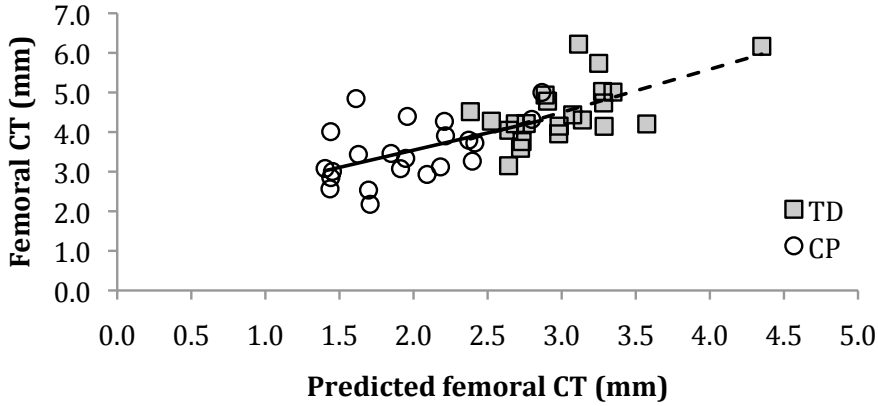

Figure 6.6 Thigh muscle volume predicted CT in the distal femur versus measured CT for the CP group (white, $R^2 = 0.259$, y=0.087x + 1.802) and TD group (grey $R^2 = 0.362$, y=0.109x + 1.235).

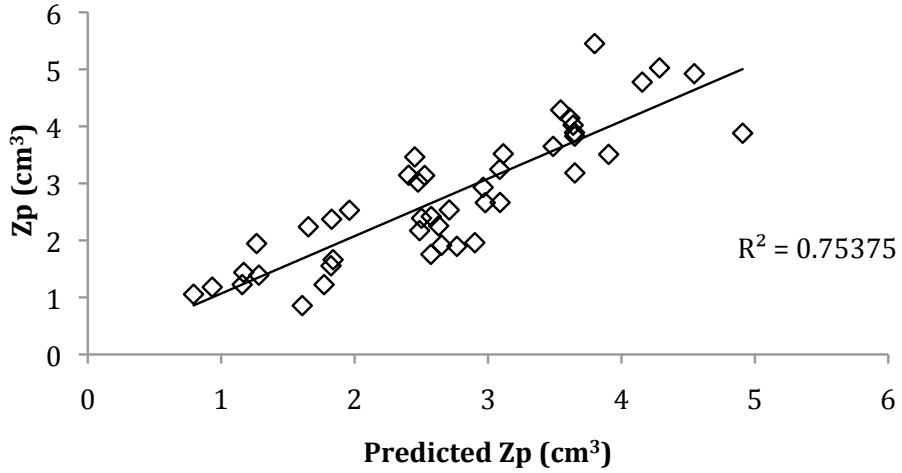

Figure 6.7 Thigh muscle volume and height predicted Zp in the distal femur versus measured Zp for both groups (R2 = 0.754).

6.4 Discussion

As hypothesised, this study has found that distal femoral cortical bone CSA, CT, and bone-bending strength (measured by Zp) is significantly related to the local muscle volume in ambulant individuals with BSCP. The significantly reduced lower limb muscle volume in this group[53,56-61,278] means that there is reduced mechanical loading experienced by the bones, therefore, stimulating bone growth less than in their TD peers. However, contrary to the hypothesis, tibial cortical bone CSA and CT were not significantly related to muscle volume.

Femoral bone-bending strength estimated from bony geometry (Zp) is related to thigh muscle volume and height, together accounting for 75.4% of the variation in Zp across groups. This result is consistent with the Mechanostat Theory[86,87]. In this theory, the muscle-bone relationship, expressed as the "muscle-bone unit," is modelled as a mechanical relationship in which bone remodelling is mediated by strain induced by muscle action and modulated by the hormonal system. Height is also an important factor influencing bending strength, with longer bones experiencing greater bending moments. Stability to buckling, (Buckling ratio BR) estimated as a ratio of the bone radius and CT, is not reduced in ambulant individuals with BSCP and is not related to gender, age, height, body mass, or muscle volume across the subject groups. The consistent BR (the ratio of bone radius to CT) across subject groups suggests that the overall radial geometry of the femoral diaphysis is maintained. Although BR is similar

between subject groups, the reduced cortical bone CSA in BSCP suggests that these individuals have reduced compressional bone strength.

This study found that proximal tibial cortical bone CSA is related to diagnosis and height but not to local muscle volume. The reduced tibial cortical bone CSA suggests that compressional bone strength may be reduced in BSCP. The lack of a relationship between cortical bone CSA and local muscle volume may also be due to the irregular cross-section of the proximal tibia and the uneven distribution of muscle around the tibia. Activity level, which was not measured in this study, may further explain the variability of tibial cortical bone CSA in both subject groups. Forces experienced in high impact activities such as running and jumping are not necessarily related to the size and strength of the surrounding muscle. The sedentary behaviour typically observed in CP[71,72] coupled with their reduced ability to run and jump may explain the diagnosis dependent reduced tibial cortical bone CSA in this study. This is an important finding that suggests that exercise interventions for bone strength development that utilise muscle-mediated loading of the long bones may have a greater impact on bone strength compared to traditional weight bearing therapies. However, a longitudinal study is required to investigate whether increasing muscle size leads to increased bone strength in this patient group.

6.4.1 Study limitations

The use of muscle volume as a surrogate of muscle strength is a limitation of this study However, measurements of muscle strength in CP are unreliable and may underestimate the maximum force generating capacity of muscle due to poor selective voluntary motor control and coactivation of antagonists[53,105,106]. However, muscle volume is reflective of the total number of sarcomeres and is linearly related to muscle power[118]. Therefore, it is reasonable to use muscle volume as a surrogate measure of maximal muscle force potential in CP.

The CP and TD groups were convenience samples, resulting in the CP group being younger ($p=0.02$), shorter ($p<0.001$) and lighter ($p<0.001$) than the TD group. Pubertal stage was not assessed in this study. To accommodate difference between the groups age, height and body mass were covariates in our statistical analysis.

Zp, Br, and cortical bone CSA are not direct measurements of bone strength. Zp and Br are parameters that are used in the field of civil engineering for geometrically uniform cylinders. The material properties of bone, including cortical bone density, have not been measured in this study and may be altered in individuals with CP.

MRI data was collected using three different MRI protocols on two scanners. The different protocols resulted in different images, particularly between the T1-weighted and Dixon sequences. This may have resulted in a systematic difference between the muscle and bony geometries measured between the different acquisition protocols, as an observer may indentify the boundaries between the tissues at slightly different locations depending on the image contrast. However, this systematic error is likely to be small due to the good image contrast between muscle, bone, and fat for all acquisition protocols enabling the bone and muscle boundaries to be easily identified. The repeatability of the image analysis technique employed was investigated for the measurement of muscle volume by a single rater and was found to be 'almost perfect' (Appendix D). However, this only reflects the reliability of the analysis technique employed. A second repeatability study is required that assesses the repeatability of the entire acquisition and analysis protocol, acquiring repeat images of a single subject using all image acquisition protocols and scanners.

6.4.2 Clinical implications

This study indicates that increased fracture risk in ambulant individuals with CP is related to reduced muscle volume and diagnosis, and is independent of body mass. Bones in adolescents and young adults with CP show the same adaptation to mechanical loading due to muscle contractions as their TD peers[282]. The results of the present study suggest that strength training to increase muscle size may increase bone strength and cortical bone CSA, decreasing the risk of fractures in this patient group.

6.5 Conclusion

Reduced bone bending and torsional strength and cortical bone CSA are related to thigh muscle volume in ambulant individuals with CP. Therefore, strength training exercises to increase muscle size and strength may improve bone strength and reduce the risk of bone fractures in CP.

7. *In vitro* and *in vivo* comparison of mDixon techniques

Abstract

The objective of this study is to compare Dixon-based MRI techniques for intramuscular fat quantification at 3T with MR spectroscopy (MRS) *in vitro* and in *vivo*. *In vitro*, two- three- and four-point mDixon sequences with 10°, 20° and 30° flip angles were acquired from seven test phantoms with sunflower oil–water percentages of 0–60% sunflower oil and calculated fat–water ratios compared with MRS. In vivo, two- three- and four-point mDixon sequences with 10° flip angle were acquired and compared with MRS in the vastus medialis of 9 healthy volunteers (aged 30.6±5.3 years; body mass index 22.2±2.6). Results: *In vitro*, all mDixon sequences correlated significantly with MRS ($r = 0.97$, $p < 0.002$) with the measured percentage fat dependent on flip angle ($p<0.001$) and mDixon sequence ($p = 0.005$). *In vivo*, a significant difference was observed between sequences ($p<0.001$), with all mDixon sequences overestimating the intramuscular fat content of the vastus medialis muscle compared with MRS. This study demonstrates that mDixon techniques have good linearity and low variability for use in intramuscular fat quantification. To avoid significant fat overestimation with short repetition time, a low flip angle should be used to reduce T1 effects.

This chapter is the published manuscript in The British Journal of Radiology 87:1036 (2014). A supplementary table of results is given in Appendix E.

BJR

Received: 21 November 2013 | Revised: 11 February 2014 | Accepted: 12 February 2014

doi: 10.1259/bjr.20130761

Cite this article as:
Noble JJ, Keevil SF, Totman J, Charles-Edwards GD. *In vitro* and *in vivo* comparison of two-, three- and four-point Dixon techniques for clinical intramuscular fat quantification at 3 T. Br J Radiol 2014;87:20130761.

FULL PAPER

In vitro and *in vivo* comparison of two-, three- and four-point Dixon techniques for clinical intramuscular fat quantification at 3 T

[1,2]J J NOBLE, MSc, [1,3]S F KEEVIL, PhD, [1]J TOTMAN, PhD and [1,3]G D CHARLES-EDWARDS, PhD

[1]Division of Imaging Sciences and Biomedical Engineering, King's College London, The Rayne Institute, St Thomas' Hospital, London, UK
[2]One Small Step Gait Laboratory, Guy's Hospital, London, UK
[3]Department of Medical Physics, Guy's and St Thomas' NHS Foundation Trust, The Rayne Institute, St Thomas' Hospital, London, UK

Address correspondence to: Mr Jonathan James Noble
E-mail: *jonathan.noble@gstt.nhs.uk*

Objective: To compare Dixon-based MRI techniques for intramuscular fat quantification at 3 T with MR spectroscopy (MRS) *in vitro* and *in vivo*.
Methods: *In vitro*, two- three- and four-point mDixon (Philips Medical Systems, Best, Netherlands) sequences with 10°, 20° and 30° flip angles were acquired from seven test phantoms with sunflower oil–water percentages of 0–60% sunflower oil and calculated fat–water ratios compared with MRS. *In vivo*, two- three- and four-point mDixon sequences with 10° flip angle were acquired and compared with MRS in the vastus medialis of nine healthy volunteers (aged 30.6 ± 5.3 years; body mass index 22.2 ± 2.6).
Results: *In vitro*, all mDixon sequences correlated significantly with MRS ($r > 0.97$, $p < 0.002$). The measured phantom percentage fat depended significantly on the flip angle ($p \leq 0.001$) and mDixon sequence ($p = 0.005$). Flip angle was the dominant factor influencing agreement with MRS. Increasing the flip angle significantly increased the overestimation of the mDixon sequences compared with MRS. *In vivo*, a significant difference was observed between sequences ($p < 0.001$), with all mDixon sequences overestimating the intramuscular fat content of the vastus medialis muscle compared with MRS. Two-point mDixon agreed best with MRS and had comparable variability with the other mDixon sequences.
Conclusion: This study demonstrates that mDixon techniques have good linearity and low variability for use in intramuscular fat quantification. To avoid significant fat overestimation with short repetition time, a low flip angle should be used to reduce T_1 effects.
Advances in knowledge: This is the first study investigating the optimal mDixon parameters for intramuscular fat quantification compared with MRS *in vivo* and *in vitro*.

Chronic diseases associated with obesity are strongly related to the amount of adipose tissue in and around skeletal muscle tissue.[1,2] Furthermore, many pathology exists, including cerebral palsy, where the patients exhibit reduced fat-free mass[3,4] but have increased fat infiltration into skeletal muscle.[5] Therefore, an effective method for quantification of intramuscular fat is required to determine which patients may develop obesity-related chronic diseases.

In the literature,[6–9] fat–water fraction measurements are predominantly obtained using localized proton (1-H) MR spectroscopy (MRS). However, MRS has a limited spatial resolution compared with imaging techniques. Consequently, MRI techniques for the measurement of fat–water ratios are desirable, particularly in spatially heterogeneous tissue. Chemical shift imaging methods established on the Dixon technique[10] that discriminate between fat and water spins based on their different resonance frequencies are now available on the majority of clinical MRI systems and are increasingly applied in clinical settings (mDixon, Philips Medical Systems, Best, Netherlands; Dixon, Siemens Healthcare, Erlangen, Germany; FatSep, Hitachi, Tokyo, Japan; and IDEAL, GE Healthcare, Waukesha, MI).

The original two-point Dixon (2PD) technique[10] acquired two images using a modified spin-echo pulse sequence. One image is a conventional spin-echo image with water and fat in phase, the second is acquired with the read out gradient shifted to produce an image with 180° water–fat phase difference. These images then undergo complex addition or subtraction to produce water only and fat only images, respectively, from which a fat–water ratio image can be calculated. Therefore, a fat–water fraction measurement can be made for a much larger region of interest and with much higher spatial resolution using Dixon techniques than MRS. The three-point Dixon (3PD)

technique[11] was developed to reduce sensitivity to magnetic field inhomogeneities and, therefore, phase errors associated with 2PD[12] by utilizing a combination of multipoint acquisition and image processing techniques. A four-point Dixon (4PD) technique has also been developed,[13] in which the extra acquisition enables a more accurate correction of the phase error. Recent advancements in image processing techniques, such as iterative decomposition of water and fat with echo asymmetry and least-squares approach (IDEAL)[14,15] have further helped to separate fat and water signals in inhomogeneous magnetic field regions.

Dixon imaging techniques have been widely used in the literature[16–23] for hepatic fat quantification hepatic steatosis (for a review see Reeder and Sirlin[16]) and are increasingly utilized for intramuscular fat quantification. However, limited validation studies comparing Dixon and MRS techniques for intramuscular fat quantification have been reported.[24] The purpose of this study was to perform such a validation at 3.0 T, as well as investigating optimal strategies by comparing two-, three- and four-point mDixon each with a range of flip angles.

METHODS AND MATERIALS

All MR data were acquired on a 3.0 T Achieva® system (Philips Medical Systems) running software v. 2.6.3, using an eight-channel receive-only phased array knee coil.

In vitro

Seven 50-ml test phantoms were produced consisting of 0%, 10%, 20%, 30%, 40%, 50% and 60%, respectively, sunflower oil mixed with water, to cover the range of intramuscular percentage fat observed *in vivo*.[19] These phantoms were made following a method described previously,[25] where 15 mmol of an anionic surfactant sodium dodecyl sulphate was added to 0.5 l of deionized water and 2.5 g of gelatine dissolved in the solution using a magnetic stirrer hotplate heated to 50 °C. The solution was poured into seven 50-ml plastic tubes along with the corresponding amount of sunflower oil, homogenized and placed on a roller overnight to set at room temperature (21 °C). All seven phantoms were placed within the knee coil to enable images of each phantom to be made within a single axial image acquisition. The scanner room temperature was set to 21 °C during image acquisition.

Figure 1. Examples of mDixon (a) water and (b) fat images of the phantoms acquired with two-point Dixon with 10° flip angle.

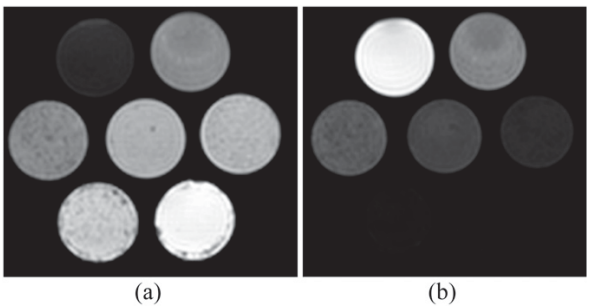

Figure 2. An example of *in vitro* MR spectroscopy spectrum of 40% sunflower oil phantom with water suppression. ppm, parts per million.

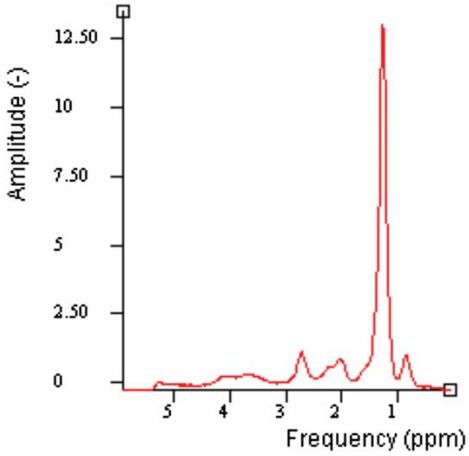

Localized MRS data were acquired of a voxel 40 × 40 × 5 mm at the centre of each phantom using a Point RESolved Spectroscopy (PRESS) sequence with echo time (TE)/repetition time (TR) = 35/5000 ms, 16 signals averaged (NSA), and with and without water suppression. Four axial gradient-echo mDixon imaging strategies were employed (see below) with three different flip angles (10°, 20° and 30°), slice thickness = 5 mm, 480 × 480 matrix size, 0.94 × 0.94 mm in plane resolution and 2 NSA.

1. two-point mDixon with water and fat signal phase sampling strategy (0, 180°); TE/TR = 2.3/5.0 ms, echo time shift (ΔTE) = 1.14 ms
2. three-point mDixon optimized for phase estimation ($3PD_P$) with (0, α, 2α) sampling strategy, where $\alpha = 120°$,[11] TE/TR = 2.11/5.2 and ΔTE = 0.76 ms
3. three-point mDixon optimized for magnitude estimation ($3PD_M$) with ($-\alpha$, 0, α) sampling strategy, where $\alpha = 180°$,[11,26,27] TE/TR = 2.3/5.4 ms and ΔTE = 0.76 ms

Figure 3. Average route mean square (RMS) difference between MR spectroscopy and mDixon measurements of phantom percentage fat. Error bars represent the standard error of the RMS difference. PD, point Dixon; PD_M, mDixon optimized for magnitude estimation; PD_P, mDixon optimized for phase estimation.

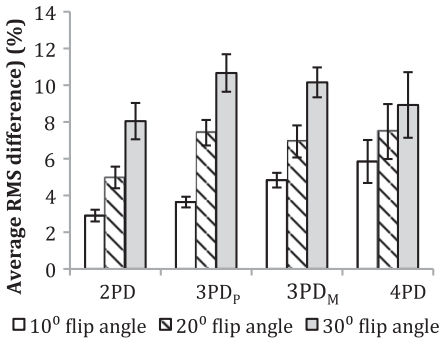

Figure 4. Bland–Altman plots of agreement between MR spectroscopy (MRS) and mDixon sequences with (a) 10° flip angle; (b) 20° flip angle; and (c) 30° flip angle. Mag, magnitude; PD, point Dixon.

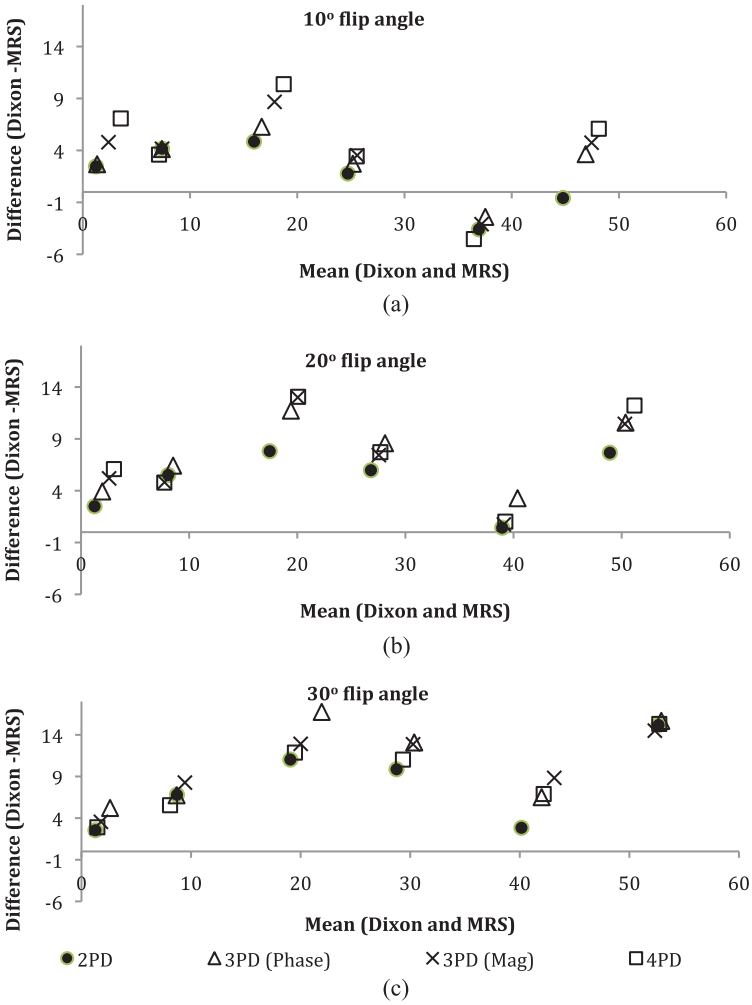

4. four-point mDixon with phase sampling strategy (0, α, 2α, 3α), where $\alpha = 90°$, TE/TR = 2.3/5.6 ms and $\Delta TE = 0.57$ ms.

Seven repeated acquisitions were acquired using each mDixon technique to assess reproducibility. Between each repeated scan, the phantoms were removed from the scanner and repositioned. To enable T_2 correction to be applied to the MRS data, the T_2 of the lipid and water in the 60% sunflower oil phantom was measured using stimulated echo acquisition mode MRS, TR = 10,000 ms, voxel size = 30 × 8 × 8 mm, NSA = 16 and TE = 40, 45, 50, 55, 60, 65, 70, 80, 90, 100 and 120 ms.

Data analysis

All MRS data were processed using the AMARES algorithm[28] in magnetic resonance user interface java version (jMRUI).[29] The percentage fat was measured according to Equation (1), with the lipid signal defined as the peak at 1.3 parts per million (ppm). The T_2 values of the 60% sunflower oil phantom were calculated by fitting an exponential to the water and lipid amplitudes over increasing TE. The fitted lipid and water peaks were T_2 corrected using T_2 values measured in the 60% sunflower oil phantom. All mDixon images were processed on the scanner using the manufacturers in-built mDixon algorithm that calculates four image series: water signal, fat signal, in-phase and out-of-phase images. Volumes of interest (VOIs) were drawn over the volume of the phantoms filled by the water–fat emulsions using OsiriX (Pixmeo, Geneva, Switzerland).[30] From these VOIs, the mean signal intensities from the fat and water images were measured to create a mDixon-based fat percentage [Equation (2)], and averaged across the seven repeated acquisitions. The mean percentage fat measured for each phantom using each technique was assessed for linearity using Pearson's correlations, and the route mean square (RMS) difference and Bland–Altman plots were calculated to assess the agreement with MRS. The RMS difference was not normally distributed (Kolmogorov–Smirnov test, $p = 0.023$), therefore, related-samples Friedman's two-way analysis of variance (ANOVA)

Figure 5. Reproducibility represented by percentage fat standard deviation over seven separate acquisitions averaged across phantoms. PD, point Dixon; PD_M, mDixon optimized for magnitude estimation; PD_P, mDixon optimized for phase estimation.

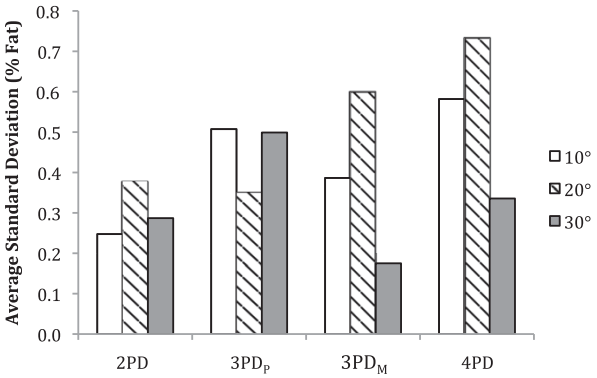

by ranks test was employed to test for significant differences in agreement with MRS between the four mDixon sequences tested and by flip angle. The reproducibility of the sequences was defined as the standard deviation of the measured percentage during each repeated acquisition averaged across all phantoms.

$$\%\mathrm{Fat(MRS)} = 100 \times \left(\frac{\mathrm{Fat}_{\text{signal amplitude}}}{\mathrm{Water}_{\text{signal amplitude}} + \mathrm{Fat}_{\text{signal amplitude}}} \right) \quad (1)$$

$$\%\mathrm{Fat(mDixon)} = 100 \times \left(\frac{\mathrm{Fat}_{\text{mean intensity}}}{\mathrm{Water}_{\text{mean intensity}} + \mathrm{Fat}_{\text{mean intensity}}} \right) \quad (2)$$

In vivo

Nine healthy adult volunteers (five males; mean age, 30.6 ± 5.3 years; body mass index, 22.2 ± 2.6 kg m^2) took part in the study. All volunteer scanning was approved by local research ethics committee (study number 01/11/12). Localized MRS data were acquired of the vastus medialis, PRESS, TE/TR = 35/2000 ms, 15 × 20 × 25 mm voxel and 32 NSA. mDixon images were also acquired with the same imaging parameters as *in vitro* with 10° flip angle and 10 NSA. Data acquisition times were 2:36, 4:03, 4:11 and 4:18 min for the 2PD, $3PD_P$, $3PD_M$ and 4PD sequences, respectively.

Figure 6. Examples of (a) water and (b) fat images of the same volunteer acquired with two-point Dixon (2PD) sequence. This subject had 3.15% fat measured by 2PD.

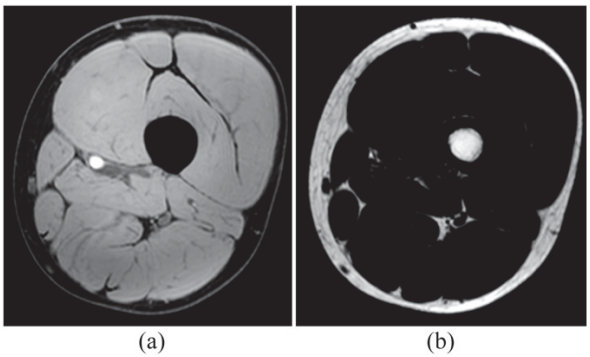

Figure 7. Example of (a) MR spectroscopy (MRS) spectrum of the vastus medialis from the same volunteer in Figure 5. This volunteer had 0.93% intramuscular fat measured by MRS. (b) Estimated intramyocellular (IMCL) and extramyocellular (EMCL) peaks. (c) Residual spectrum after fitting of IMCL and EMCL peaks. ppm, parts per million.

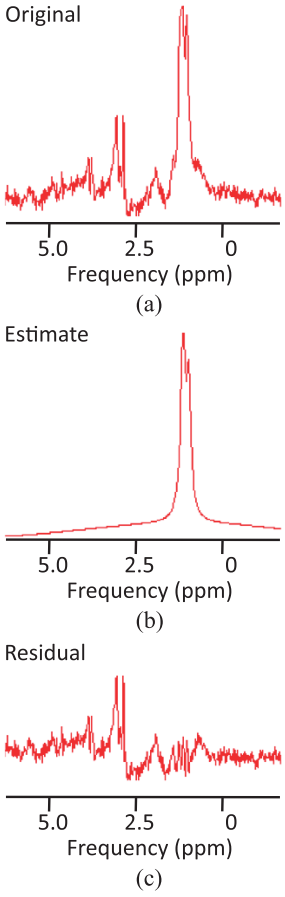

Data analysis

All MRS data were processed using the AMARES algorithm[28] in jMRUI.[29] Water, intramyocellular (IMCL) and extramyocellular (EMCL) lipid peaks were quantified (with prior knowledge of peaks at 1.3 and 1.2 ppm, after removal of the residual water) and percentage fat calculated using Equation (1). The measured water, EMCL and IMCL signals were T_2 corrected using T_2 values for water (31.3 ms), EMCL fat (77.6 ms) and IMCL fat (89.4 ms) previously measured at 3 T in muscle.[31]

Figure 8. Group mean intramuscular percentage fat in vastus medialis. Error bars represent the standard error of the group. MRS, MR spectroscopy; PD, point Dixon; PD_M, mDixon optimized for magnitude estimation; PD_P, mDixon optimized for phase estimation.

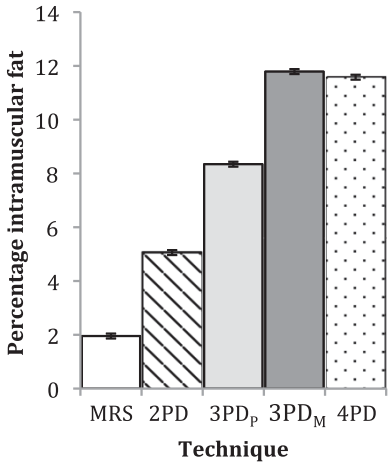

All mDixon images were analysed using OsiriX.[30] VOIs were drawn to match the corresponding MRS voxel locations for fat and water, with the fat voxel shifted in the x, y and z directions calculated using a 3.4 ppm chemical shift between water and lipid at 3.0 T. From these VOIs, the mean signal intensities from the fat and water images were measured to create an mDixon-based fat–water ratio [Equation (2)]. The percentage fat measured by MRS and mDixon were compared for agreement using Bland–Altman plots,[32] one-way ANOVA and Tukey *post hoc* test. All statistical analyses were performed using SPSS® v. 20.0 (SPSS, Chicago, IL).

RESULTS

In vitro

Figure 1a,b shows an example of water and fat images of the phantoms, respectively. An example *in vitro* spectrum with water suppression is shown in Figure 2. There were strong positive and significant correlations between MRS-derived and Dixon-based percentage fat measurement ratios for all Dixon sequences and flip angles ($r > 0.97$, $p < 0.002$). Figure 3 shows the average RMS difference between MRS and mDixon calculated phantom percentage fat by each technique and flip angle. A significant difference in the RMS difference was observed between flip angles ($p \leq 0.001$) and between mDixon sequences ($p = 0.005$). Compared with MRS, all four mDixon sequences exhibited greater average RMS difference with larger flip angles. Bland–Altman plots comparing Dixon- and MRS-based measures of percentage fat are shown in Figure 4. As the flip angle of the mDixon sequences is increased, mDixon increasingly overestimates the fat content of the phantoms for all sequences investigated. Figure 5 summarizes the mean, standard deviation and reproducibility (average standard deviation) for each phantom and mDixon technique investigated.

In vivo

Figure 6 shows example water and fat images of one volunteer. Figure 7 shows an example MRS spectrum of one volunteer and the fitted IMCL and EMCL peaks. Figure 8 shows a histogram of the group mean percentage intramuscular fat measured by all techniques investigated. A significant difference was observed between the measurement techniques (ANOVA, $p < 0.001$). The Tukey *post-hoc* tests found a significant difference between all measurements ($p \leq 0.001$) with the exception of 4PD and $3PD_M$ ($p = 0.998$). In the Bland–Altman plot in Figure 9, comparing each mDixon technique investigated with MRS, it can be seen that all mDixon techniques overestimated the percentage intramuscular fat in the vastus medialis compared with MRS. 2PD exhibited the closest agreement with MRS and 4PD the worst agreement with MRS.

DISCUSSION

In vitro, all mDixon techniques correlated very strongly with the MRS measured percentage fat ($r > 0.97$, $p < 0.002$). As shown in Figures 3 and 4, increasing the flip angle significantly overestimated the measured percentage fat using all mDixon techniques investigated compared with MRS, and this was found to have a much larger effect on the agreement between the Dixon and MRS than Dixon sequence type (2PD, $3PD_P$, $3PD_M$ or 4PD). This overestimation of the phantom fat content with increasing flip angle occurs owing to T_1 effects.[33] The T_1 of water is much longer than that of lipid; with the short TR and increasing flip angle, the water signal becomes increasingly more suppressed than the lipid signal, resulting in a higher measured percentage fat. This means that when the sequence TR is reduced to shorten scan time, the flip angle must also be reduced to prevent overestimation of the fat content due to T_1 weighting. The closest agreement between MRS and mDixon and a smaller average RMS difference than the other sequences investigated was observed for the 2PD sequence with a 10° flip angle. This is a surprising result. This may be owing to the recent development of the two-point mDixon algorithm to include the static magnetic field strength (B_0) inhomogeneity correction. Previously, two-point techniques have not included B_0 inhomogeneity correction[34] and, therefore, would

Figure 9. Bland–Altman plot showing the agreement between intramuscular percentage fat measured using MR spectroscopy (MRS) and the four mDixon sequences tested *in vivo*. Mag, magnitude; PD, point Dixon.

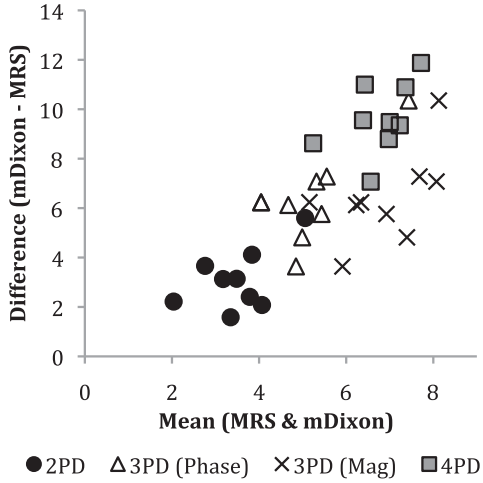

be likely to agree the least with MRS 2PD acquires only two signal acquisitions, one with the fat and water signals in phase and one out of phase. The better agreement of 2PD with MRS compared with the 3PD and 4PD sequences suggests that a different algorithm may be used by the mDixon implementation on the scanner when in 2PD. The 3PD (phase) exhibited a smaller average RMS difference than in the $3PD_M$ sequence and 4PD sequence. In the Bland–Atlman plots in Figure 4, there are no consistent differences between the two 3PD sequences and the 4PD sequence.

All mDixon results produced a similar behaviour when compared with MRS. Considering the sequences with 10° flip angles, all sequences exhibited the same pattern: increasing overestimation of the phantom fat content for the 0–20% sunflower oil phantoms and underestimation of the 40% sunflower oil phantom. Overestimation of the 0% sunflower oil phantom highlights a misregistration between water and fat. This may be caused by various factors, including spectral modelling simplification and magnetic field homogeneity. An example phantom spectrum given in Figure 1 shows that the phantom spectra are dominated by single lipid peak at 1.3 ppm. Combined with the overestimation of the 0% sunflower oil phantom, this suggests that spectrum simplification is unlikely to be the main cause of this overestimation of fat content and that magnetic field inhomogeneities may have a more significant affect.

The higher group average intramuscular fat measured using the magnitude optimized sequence ($3PD_M$) than in the phase estimation–optimized sequence ($3PD_P$) suggests that the phase errors caused by magnetic field inhomogeneities are one of the limiting factors of the mDixon sequences investigated. The large inhomogeneities *in vivo* would therefore significantly affect the accuracy of the mDixon sequences. Again, differences in spectral modelling may contribute to the difference in fat content measured between the two techniques. A two-lipid peak spectral model for MRS, corresponding to IMCL and EMCL, was employed in this study, as this is commonly performed in the literature, whereas more complex models have been described for Dixon.[34] However, the lipid peaks at 1.3 and 1.2 ppm dominate the muscle spectra, and any underestimation of the lipid content by utilizing a two-lipid peak model for the MRS is likely to be minimal. The use of T_2 values in the literature for T_2 correction may also contribute to the disagreement between the MRS and mDixon techniques, although measuring the T_2 values of the metabolites *in vivo* for each individual volunteer is time consuming and not representative of clinical practice.

In vivo, a significant difference was observed between all techniques with the exception of $3PD_P$ and 4PD, which were not significantly different from each other. However, these sequences also had the largest mean difference compared with MRS, with the 2PD sequence having the best agreement with MRS. The standard deviations of the subject group percentage intramuscular fat measurements were similar across the mDixon sequences, ranging from 1.25% (4PD) to 1.94% ($3PD_P$).

CONCLUSION

This study has compared two-point, three-point and four-point mDixon techniques with MRS in test phantoms over a range of physiologically expected fat–water ratios and *in vivo* for intramuscular fat quantification. *In vitro*, all sequences tested correlated strongly with MRS, with the 2PD in closest agreement. The flip angle was observed to have a more significant effect on agreement between mDixon and MRS than sequence type, with increasing flip angle resulting in an increasing overestimation of the fat content of the phantoms. *In vivo*, a significant difference was observed between MRS and all mDixon sequences investigated with the 2PD sequence in closest agreement with MRS and with comparable variability in the measured intramuscular fat across the subject group. The results of this study suggest that the two-point Dixon sequence provides the most accurate measurement of intramuscular fat and highlights the need for small flip angles to reduce fat overestimation due to T_1 effects when a short TR is utilized.

ACKNOWLEDGMENTS

The views expressed are those of the author(s) and not necessarily those of the National Health Service, the National Institute for Health Research or the Department of Health, UK.

FUNDING

Jonathan Noble was funded by a PhD studentship from the Guy's and St. Thomas's Charity, London, UK. This research was supported by the National Institute for Health Research Biomedical Research Centre at Guy's and St Thomas' NHS Foundation Trust and King's College London.

REFERENCES

1. Elder CP, Apple DF, Bickel CS, Meyer RA, Dudley GA. Intramuscular fat and glucose tolerance after spinal cord injury–a cross-sectional study. *Spinal Cord* 2004; **42**: 711–16. doi: 10.1038/sj.sc.3101652
2. Goodpaster BH, Thaete FL, Kelley DE. Thigh adipose tissue distribution is associated with insulin resistance in obesity and in type 2 diabetes mellitus. *Am J Clin Nutr* 2000; **71**: 885–92.
3. Azcue MP, Zello GA, Levy LD, Pencharz PB. Energy expenditure and body composition in children with spastic quadriplegic cerebral palsy. *J Pediatr* 1996; **129**: 870–6.
4. Bandini LG, Schoeller DA, Fukagawa NK, Wykes LJ, Dietz WH. Body composition and energy expenditure in adolescents with cerebral palsy or myelodysplasia. *Pediatr Res* 1991; **29**: 70–7. doi: 10.1203/00006450-199101000-00014
5. Johnson DL, Miller F, Subramanian P, Modlesky CM. Adipose tissue infiltration of skeletal muscle in children with cerebral palsy. *J Pediatr* 2009; **154**: 715–20. doi: 10.1016/j.jpeds.2008.10.046
6. Boesch C, Slotboom J, Hoppeler H, Kreis R. *In vivo* determination of intra-myocellular lipids in human muscle by means of localized ^{1}H-MR-spectroscopy. *Magn Reson Med* 1997; **37**: 484–93.

7. Pfirrmann CW, Schmid MR, Zanetti M, Jost B, Gerber C, Hodler J. Assessment of fat content in supraspinatus muscle with proton MR spectroscopy in asymptomatic volunteers and patients with supraspinatus tendon lesions. *Radiology* 2004; **232**: 709–15. doi: 10.1148/radiol.2323030442
8. Schick F, Machann J, Brechtel K, Strempfer A, Klumpp B, Stein DT, et al. MRI of muscular fat. *Magn Reson Med* 2002; **47**: 720–7.
9. Szczepaniak LS, Babcock EE, Schick F, Dobbins RL, Garg A, Burns DK, et al. Measurement of intracellular triglyceride stores by H spectroscopy: validation *in vivo*. *Am J Physiol* 1999; **276**: E977–89.
10. Dixon WT. Simple proton spectroscopic imaging. *Radiology* 1984; **153**: 189–94. doi: 10.1148/radiology.153.1.6089263
11. Glover GH. Multipoint Dixon technique for water and fat proton and susceptibility imaging. *J Magn Reson Imaging* 1991; **1**: 521–30.
12. Ma J. Dixon techniques for water and fat imaging. *J Magn Reson Imaging* 2008; **28**: 543–58. doi: 10.1002/jmri.21492
13. Reeder SB, Alley MT, Pelc NJ, editors. *Water and fat SSFP imaging with four-point Dixon techniques*. 10th Annual Meeting of ISMRM; 2002.
14. Reeder SB, Pineda AR, Wen Z, Shimakawa A, Yu H, Brittain JH, et al. Iterative decomposition of water and fat with echo asymmetry and least-squares estimation (IDEAL): application with fast spin-echo imaging. *Magn Reson Med* 2005; **54**: 636–44. doi: 10.1002/mrm.20624
15. Reeder SB, McKenzie CA, Pineda AR, Yu H, Shimakawa A, Brau AC, et al. Water–fat separation with IDEAL gradient-echo imaging. *J Magn Reson Imaging* 2007; **25**: 644–52. doi: 10.1002/jmri.20831
16. Reeder SB, Sirlin CB. Quantification of liver fat with magnetic resonance imaging. *Magn Reson Imaging Clin N Am* 2010; **18**: 337–57, ix. doi: 10.1016/j.mric.2010.08.013
17. Karampinos DC, Baum T, Nardo L, Alizai H, Yu H, Carballido-Gamio J, et al. Characterization of the regional distribution of skeletal muscle adipose tissue in type 2 diabetes using chemical shift-based water/fat separation. *J Magn Reson Imaging* 2012; **35**: 899–907. doi: 10.1002/jmri.23512
18. Kovanlikaya A, Mittelman SD, Ward A, Geffner ME, Dorey F, Gilsanz V. Obesity and fat quantification in lean tissues using three-point Dixon MR imaging. *Pediatr Radiol* 2005; **35**: 601–7. doi: 10.1007/s00247-005-1413-y
19. Wren TA, Bluml S, Tseng-Ong L, Gilsanz V. Three-point technique of fat quantification of muscle tissue as a marker of disease progression in Duchenne muscular dystrophy: preliminary study. *AJR Am J Roentgenol* 2008; **190**: W8–12. doi: 10.2214/AJR.07.2732
20. Fischmann A, Kaspar S, Reinhardt J, Gloor M, Stippich C, Fischer D. Exercise might bias skeletal-muscle fat fraction calculation from Dixon images. *Neuromuscular Disord* 2012; **22**(Suppl. 2): S107–10. doi: 10.1016/j.nmd.2012.05.014
21. Willis TA, Hollingsworth KG, Coombs A, Sveen ML, Andersen S, Stojkovic T, et al. Quantitative muscle MRI as an assessment tool for monitoring disease progression in LGMD2I: a multicentre longitudinal study. *PLoS One* 2013; **8**: e70993. doi: 10.1371/journal.pone.0070993
22. Wokke BH, Bos C, Reijnierse M, van Rijswijk CS, Eggers H, Webb A, et al. Comparison of dixon and T1-weighted MR methods to assess the degree of fat infiltration in duchenne muscular dystrophy patients. *J Magn Reson Imaging* 2013; **38**: 619–24. doi: 10.1002/jmri.23998
23. Fischmann A, Hafner P, Fasler S, Gloor M, Bieri O, Studler U, et al. Quantitative MRI can detect subclinical disease progression in muscular dystrophy. *J Neurol* 2012; **259**: 1648–54. doi: 10.1007/s00415-011-6393-2
24. Price DI, Patel D, Taylor SA, Halligan S, Lally P, Bainbridge A, et al. Pelvic floor atrophy assessment using a 2-point Dixon technique to measure muscle fat fraction. No. 633. Abstracts of the 30th Annual Scientific Meeting of the European Society for Magnetic Resonance in Medicine and Biology (ESMRMB); 3–5 October 2013; Toulouse, France. *MAGMA* 2013; **26**(Suppl. 1): 4–535.
25. Bernard CP, Liney GP, Manton DJ, Turnbull LW, Langton CM. Comparison of fat quantification methods: a phantom study at 3.0 T. *J Magn Reson Imaging* 2008; **27**: 192–7. doi: 10.1002/jmri.21201
26. Reeder SB, Wen Z, Yu H, Pineda AR, Gold GE, Markl M, et al. Multicoil Dixon chemical species separation with an iterative least-squares estimation method. *Magn Reson Med* 2004; **51**: 35–45. doi: 10.1002/mrm.10675
27. Xiang QS, An L. Water–fat imaging with direct phase encoding. *J Magn Reson Imaging* 1997; **7**: 1002–15.
28. Vanhamme L, van den Boogaart A, Van Huffel S. Improved method for accurate and efficient quantification of MRS data with use of prior knowledge. *J Magn Reson* 1997; **129**: 35–43.
29. Naressi A, Couturier C, Devos JM, Janssen M, Mangeat C, de Beer R, et al. Java-based graphical user interface for the MRUI quantitation package. *MAGMA* 2001; **12**: 141–52.
30. Rosset A, Spadola L, Ratib O. OsiriX: an open-source software for navigating in multidimensional DICOM images. *J Digit Imaging* 2004; **17**: 205–16. doi: 10.1007/s10278-004-1014-6
31. Krssak M, Mlynarik V, Meyerspeer M, Moser E, Roden M. ^{1}H NMR relaxation times of skeletal muscle metabolites at 3 T. *MAGMA* 2004; **16**: 155–9. doi: 10.1007/s10334-003-0029-1
32. Bland JM, Altman DG. Statistical methods for assessing agreement between two methods of clinical measurement. *Lancet* 1986; **1**: 307–10.
33. Liu CY, McKenzie CA, Yu H, Brittain JH, Reeder SB. Fat quantification with IDEAL gradient echo imaging: correction of bias from T(1) and noise. *Magn Reson Med* 2007; **58**: 354–64. doi: 10.1002/mrm.21301
34. Eggers H, Brendel B, Duijndam A, Herigault G. Dual-echo Dixon imaging with flexible choice of echo times. *Magn Reson Med* 2011; **65**: 96–107. doi: 10.1002/mrm.22578

8. Intramuscular fat in bilateral spastic cerebral palsy

Abstract

The objective of this study is to determine whether adults with bilateral spastic cerebral palsy (BSCP) have greater adiposity in and around their skeletal muscles than their typically developing (TD) peers as this may have significant functional and cardio-metabolic implications for this patient group. 10 young adults with BSCP (7 male, mean age 22.5 years, Gross Motor Function Classification System (GMFCS) levels I-III), and 10 TD young adults (6 male, mean age 22.8 years) took part in this study. 11 cm sections of the left leg of all subjects were imaged using multi-echo gradient echo chemical shift imaging (mDixon). Percentage intermuscular fat (IMAT), intramuscular fat (IntraMF) and a subcutaneous fat to muscle volume ratio (SF/M) were calculated. IntraMF was higher with BSCP for all muscles ($p=0.001$-0.013) and was significantly different between GMFCS levels ($p<0.001$), with GMFCS level III having the highest IntraMF content. IMAT was also higher with BSCP $p<0.001$). No significant difference was observed in SF/M between groups. Young adults with BSCP have increased intermuscular and intramuscular fat compared to their TD peers. The relationship between these findings and potential cardio-metabolic and functional sequelae are yet to be investigated.

The work in this chapter has been published in BMC Musculoskeletal Disorders (Noble *et al*. BMC Musculoskeletal Disorders 2014 15:236).

8.1 Background

The mechanical potential of muscle depends on gross morphology (cross sectional area, fibre length[118]), muscle fibre type, and muscle composition (fraction of intramuscular fat and connective tissue). Anatomical magnetic resonance imaging (MRI) and ultrasound imaging have demonstrated that the skeletal muscles of the lower limbs of individuals with bilateral spastic cerebral palsy (BSCP) are reduced in size by up to 50% compared to the muscles of their typically developing (TD) peers[56,57,278]. However, studies of microstructure and composition have been limited to a small number of biopsy studies[119,120]. In the lower limb, these have demonstrated increases in the connective tissue fraction, reduced muscle fibre diameter, and altered muscle fascicle stiffness[119,120].

Decreased physical activity is associated with increased intermuscular fat[63-66]. Due to the typically sedentary behaviour observed in this group[71,72], one aspect of muscle composition that may be altered in BSCP is the level of intra- and intermuscular fat. Fatty infiltration into muscle results in a reduced proportion of contractile tissue per unit muscle volume. Intramuscular fat also may secrete inflammatory cytokines that can reduce the myofibrillar force even in the absence of muscle atrophy[62]. If present in this group, raised intramuscular fat may have important consequences for physical performance, and implications for exercise regimes employed in their physical management[142].

Heightened levels of inter- and intra- muscular fat are associated with cardiovascular risk[44,121]. Adults with cerebral palsy may have a 2-3 times greater risk of dying from ischemic heart disease than their typically developing peers[13]. However, there are few studies in the literature that have attempted to document body or muscle composition in this group. Since individuals with cerebral palsy have reduced muscle mass, even those with body mass index (BMI) in the normal range may have relatively increased levels of adipose tissue. Previous studies in children with CP have suggested raised levels of fat[76,77]. In an MRI study of the lower limbs in children with quadriplegic cerebral palsy (Gross Motor Function Classification System (GMFCS) levels III-V), Johnson *et al*[76] found increased levels of intermuscular and subcutaneous fat[76]. To date, there have been no studies of intramuscular fat in adults or children with BSCP even though this

non-invasively quantified parameter appears to be one of those most associated with cardio-metabolic disease[122].

T_1-weighted image segmentation is primarily used to quantify IMAT, with IMAT defined as the MRI-visible fat within the muscles (intramuscular fat) and between the muscles beneath the fascia (intermuscular fat). Although this method is effective for assessing intermuscular and subcutaneous fat volumes, it is not an accurate method for measuring fat distribution within individual muscles. Chemical shift magnetic resonance imaging-based water/fat separation techniques based on that first proposed by Dixon[217] have been developed which utilise the chemical shift difference between fat and water to enable reconstruction of separate water and fat images. These techniques utilise the predictable difference in phase evolution between water and fat signals due to their chemical shift difference to enable the calculation of separate water and fat images, permitting the calculation of the fat fraction. The fat fraction is the signal intensity attributable to fat, normalised by the total signal from all mobile proton species. These techniques have been widely used in studies quantifying the degree of liver fat in hepatic steatosis (for review see Reeder[220]): although, to date, Dixon imaging has only been used in a small number of clinical intramuscular fat quantification studies[121,221,222].

The aim of this study was to investigate the intermuscular fat (IMAT), subcutaneous fat (SF) and intramuscular fat (IntraMF) content in five major muscles of the leg (medial and lateral gastrocnemius, soleus, tibialis posterior and tibialis anterior) in 10 subjects with BSCP and 10 TD subjects using multi-echo gradient echo chemical shift imaging (mDixon). We hypothesised that the subjects with BSCP would exhibit increased fat content compared to their TD peers.

8.2 Methods

Ethical approval for this study was granted by Hampstead Research Ethics Committee London (09/H0720/120). All subjects gave informed consent before they participated.

8.2.1 Subjects

Individuals aged 16 – 30 years, with a diagnosis of BSCP, Gross Motor Function Classification System (GMFCS) levels I-III, who met the safety requirements of MRI were included in this study. Patients who had undergone surgery, serial casting or botulinum toxin injections to the lower limbs within the previous year were excluded from the study. This was a convenience sample of individuals attending our hospital department, with consecutive patients that met the inclusion criteria invited to participate in the study.

10 adults with a diagnosis of BSCP (7 male, 3 female, mean age 22.5 years, range 18-27, GMFCS levels I-III from clinics in our university hospital and a convenience sample of 10 TD young adults (6 male, 4 female, mean age 22.8 years, range 18-27) recruited from individuals known to the research team participated in this study. None of the BSCP subjects had undergone surgery, serial casting or botulinum toxin injections to the lower limbs within the previous year. All TD subjects had no prior significant musculoskeletal trauma or disorders.

8.2.2 Data collection

MR data were acquired on a 3.0T Achieva system (Philips Healthcare, Best, The Netherlands) running software version 2.6.3, using an 8-channel receive-only phased array knee coil. One subject had a 30^{o} knee fixed flexion deformity; instead a 32-channel cardiac coil was used. An 11cm section of the left leg was scanned, centred at the largest circumference of the calf with the subject prone. Four point gradient echo mDixon images were acquired with TE/TR= 2.3/7.1ms, 35^{o} flip angle, 2.0 x 2.0 mm in-plane resolution, 4.0 mm slice thickness, echo-time shift = 1.0ms. Utilising the known chemical shift between water and fat signal constituents, separate water and fat images were calculated within the scanner software. Subject height and body mass were measured in standing before the MRI scan using a stadiometer and calibrated weighing scales. Patients at our centre are routine classified according the GMFCS in their medical record by their consulting physician or surgeon.

8.2.3 Data Processing

Regions of interest (ROIs) were manually drawn around the SF, muscle compartment (Figure 8.1B), and five individual muscles; the soleus, medial gastrocnemius, lateral gastrocnemius, tibialis anterior, and tibialis posterior (Figure 8.1C), on the mDixon water images using Osirix version 3.7.1[280]. SF volume was normalised to muscle volume (Equation 8.1), creating a SF to muscle volume ratio (SF/M). The ROIs around the entire musculature and individual muscles were eroded with a structuring element size of 2 pixels (4.0 mm) to remove any potential edge effects with surrounding subcutaneous fat (or intermuscular fat for IntraMF quantification). IMAT and IntraMF were calculated using a ratio of the water and fat signal intensities within the eroded ROIs (Equation 8.2). The reproducibility of the Dixon technique employed was measured using 5 acquisitions of one TD subject imaged over 3 visits, with the scan repeated twice during 2 of these visits. Reproducibility was defined as the average standard deviation of the measured percentage fat, i.e. the standard deviation averaged across all muscles investigated.

$$SF/M = \frac{SF\,volume}{Muscle\,volume} \qquad \textit{Equation 8.1}$$

$$Percentage\ fat = 100 \times \left(\frac{I_{Fat}}{I_{Fat} + I_{Water}} \right) \qquad \textit{Equation 8.2}$$

Where I = Signal intensity

Figure 8.1 (A) Example mDixon water image; (B) manually drawn region of interest (white) for the muscle compartment for IMAT segmentation; and (C) the 5 muscles analysed drawn around tibialis anterior (TA), tibialis posterior (TP), soleus (SOL), medial gastrocnemius (MG) and lateral gastrocnemius (LG) for IntraMF segmentation.

8.2.4 Data analysis

Following application of the Kolmogorov-Smirnov test for normality and Levene's test for equality of variance, independent samples t-tests were performed to investigate physical characteristic differences between the two subject groups for all measured parameters. Two-way ANOVA was performed on IntraMF with GMFCS level and muscle identity as fixed factors with a Tukey post-hoc test. Non-parametric independent samples median tests compared SF/M and IMAT between groups. The Kruskal-Wallis Test was used to investigate differences in SF/M and IMAT with GMFCS level. Pearson's correlations were used to investigate relationships between measured parameters. All statistical tests were performed using SPSS (Version 20.0; IBM SPSS) with significance set to $p \leq 0.05$.

8.3 Results

Physical characteristics of subjects in the BSCP and TD groups are summarised in Table 8.1. There were no group differences in age, body mass, height, or BMI ($p>0.05$). The GMFCS level of the BSCP subjects are also presented in Table 8.1. The BSCP subjects had undergone a range of previous interventions (see Table 8.2), although none of these were performed in the last year. The average standard deviation representing reproducibility of intramuscular fat averaged across all muscles was 0.33%. Example images for a case and age-matched control are given in Figure 8.4.

	BSCP group	**TD group**
Number of subjects	10	10
Age (years)	22.5 ± 2.9	22.8 ± 3.0
Sex (m,f)	7, 3	6, 4
Body mass (kg)	64.0 ± 11.5	71.2 ± 11.8
Height (m)	1.69 ± 0.08	1.76 ± 0.12
BMI (kg/m^2)	22.4 ± 3.6	22.9 ± 1.7
GMFCS level I	2	N/A
GMFCS level II	5	N/A
GMFCS level III	3	N/A

Table 8.1 Physical characteristics (mean ± standard deviation) of BSCP and TD groups and number of BSCP subjects in each GMFCS levels (I-III)

BSCP Subject	Intervention
1	None
2	Gastrocnemius lengthening
3	Gastrocnemius lengthening
4	None
5	Gastrocnemius lengthening
6	Gastrocnemius lengthening
7	Gastrocnemius lengthening
8	None
9	Gastrocnemius and Achilles tendon lengthening
10	None

Table 8.2 Previous left leg interventions in the group of adults with BSCP

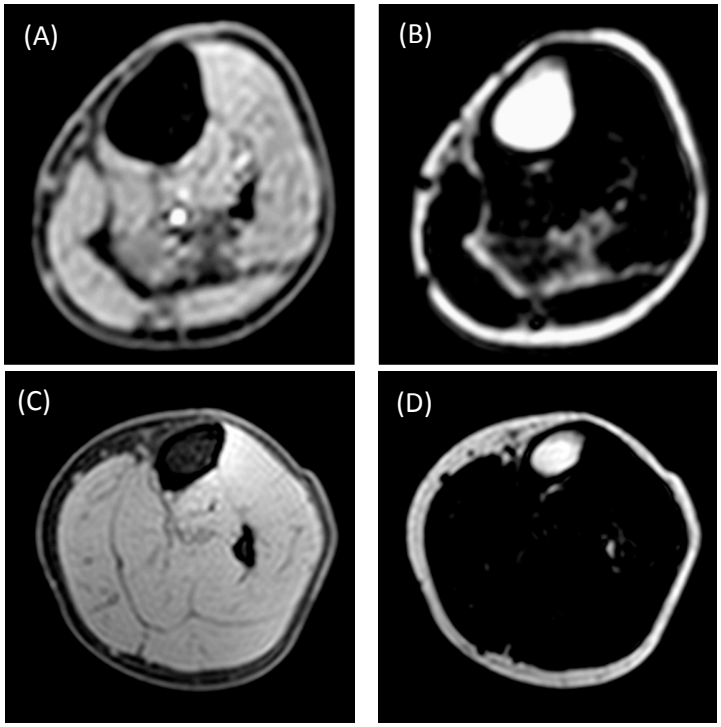

Figure 8.2 Example water (A and C) and fat (B and D) for one subject with BSCP (A and B), and an age matched TD subject (C and D).

Figure 8.3 shows a bar chart of group-averaged percentage IntraMF and IMAT. The BSCP group had a significantly higher average percentage IMAT ($p<0.001$) and IntraMF compared to the TD group for all muscles investigated ($p<0.001$), with the soleus having the largest percentage fat difference (12.9% greater in BSCP group). In the BSCP group, IntraMF was significantly correlated between all muscles measured

(r=0.697 to 0.947, p<0.001 to p=0.025) except for the soleus, which did not correlate with any other muscle (r= 0.437 to 0.587, p=0.074 to 0.206). Figure 8.4 shows a bar chart of group-averaged SF/M ratio. The mean SF/M ratio was 1.9 times greater in the BSCP group compared to the TD group; however, this difference was not statistically significant (p=0.179). Group means and 95% confidence intervals for intramuscular fat, IMAT, and SF/M are given in Table 8.3.

	Muscle	Group	Mean	95% Confidence Interval for Mean		Standard Deviation	Standard Error
				Lower Bound	Upper Bound		
Intra-muscular fat (%)	MG	CP	7.61	5.31	9.90	3.21	1.02
		TD	3.70	2.99	4.41	0.99	0.31
	LG	CP	7.75	4.64	10.86	4.35	1.38
		TD	3.24	2.85	3.64	0.55	0.17
	SOL	CP	16.56	9.42	23.69	9.97	3.15
		TD	3.66	3.15	4.16	0.71	0.22
	TA	CP	6.07	4.40	7.74	2.33	0.74
		TD	2.36	2.08	2.65	0.39	0.12
	TP	CP	5.48	3.15	7.81	3.26	1.03
		TD	2.30	1.89	2.70	0.56	0.18
IMAT (%)		CP	13.91	9.73	18.09	5.84	1.85
		TD	4.60	4.08	5.11	0.72	0.23
SF/M		CP	0.76	0.45	1.06	0.43	0.14
		TD	0.40	0.25	0.54	0.21	0.07

Table 8.3 Group mean, 95% confidence interval, standard deviation and standard error for the CP and TD groups. MG = medial gastrocnemius; LG = lateral gastrocnemius; SOL= soleus; TA = tibialis anterior; TP = tibialis posterior; IMAT = inter- + intramuscular fat; SF/M = subcutaneous fat to muscle volume ratio.

One-way ANOVA and post hoc analysis revealed significant differences in IntraMF levels by GMFCS level (p<0.001), with GMFCS level III significantly higher compared to GMFCS levels I and II (p<0.001 and p=0.001 respectively). No significant difference was observed in IMAT or SF/M with GMFCS level (p=0.131). In the TD group, SF/M was correlated with IMAT (r=0.81, p=0.005) but not with IntraMF (r=0.182, p=0.206), and no correlation was observed between IMAT and IntraMF (r=0.251, p=0.079). In the BSCP group, no correlations were observed between SF/M and IMAT (r=0.392, p=0.262) or IntraMF (r=0.134, p=0.353); IMAT and IntraMF were significantly correlated (r=0.529, p<0.001).

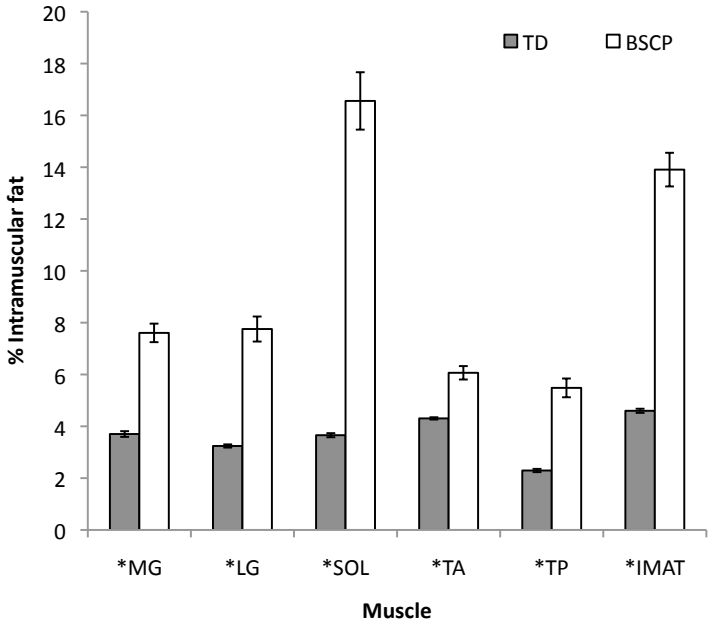

Figure 8.3 Percentage IntraMF and IMAT in the medial gastrocnemius (MG), lateral gastrocnemius (LG), soleus (SOL), tibialis anterior (TA), tibialis posterior (TP) and in the BSCP group (white) and TD group (grey). IMAT and IntraMF in all muscles were significantly different between groups ($p < 0.05$). Error bars represent the standard error of each group.

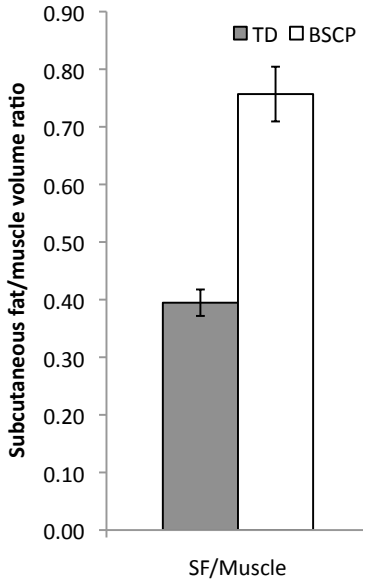

Figure 8.4 Subcutaneous fat to muscle volume ratio in the BSCP group (white) and TD group (grey). Error bars represent the standard error of each group.

8.4 Discussion

We conducted MRI measurements of IMAT, SF/M ratio, and IntraMF on 10 young adults with BSCP and 10 of their TD peers. This is the first study to show that ambulant adults with BSCP have raised levels of IntraMF, ranging from 2.3 to 34.4%. Percentage IntraMF was also found to be significantly different between GMFCS levels, with those at GMFCS III having greater fatty infiltration. These differences in IntraMF by GMFCS level suggest IntraMF may be related to the degree of mobility impairment. This may be due to decreased physical activity with increasing mobility impairments.

The 1.9 fold greater SF/M ratio in the BSCP group is comparable to the results of Johnson *et al*[76], who reported 2 fold greater SF/M ratio in the mid thigh of children with quadriplegic cerebral palsy GMFCS levels III-V[76]. This is surprising due to the higher functional ability of the subjects in this study (GMFCS levels I-III). IMAT values cannot be compared between these studies due to the separation by Johnson *et al* of IMAT into intermuscular and sub-fascial fat and the different imaging and analysis techniques employed.

8.4.1 Clinical Implications

Children and young adults with cerebral palsy have been shown to have reduced muscle volumes in their lower limbs[53,56-61,278] and increased IMAT[76]. This study demonstrates that these muscles also have greater levels of intramuscular fat that is independent of subcutaneous fat levels. This combination of morphological and compositional changes may have implications both for the mechanical performance of these skeletal muscles and also for the predisposition of the adult with BSCP to cardio-metabolic disease[122].

Muscle weakness is a prevalent feature of individuals with cerebral palsy[53-55]. Muscle weakness, in this group, is in part caused by an inability to fully activate available muscular resources[75], increased co-activation[105] and by reduced muscle volume[53,56-61,278]. For a given muscle volume, a higher intramuscular fat content will correspond to reduced contractile tissue content, resulting in a weaker muscle than predicted from muscle mass alone. Furthermore, inflammatory cytokines produced by intramuscular fat may interfere with the action of myofibrillar proteins reducing specific force production[62]. These secondary pathologies may contribute to a deficit in the "functional reserve" of adults with BSCP, and may expose these individuals to a heightened risk of immobility with increasing age[60].

Greater intramuscular fat content in BSCP may expose these individuals to a greater risk of developing cardio-metabolic disease[122]. There is a strong relationship between intramuscular fat content, insulin resistance and type-II diabetes[44-46]. Within skeletal muscle, fat is stored in two separate compartments: Intramyocellular lipid (IMCL) and extramyocellular lipid (EMCL). EMCL is found within adipose cells adjacent to the muscle fibres, and IMCL is located along with enzymes involved in fatty acid esterification, hydrolysis, and transport into the mitochondria[47]. Enhanced storage of IMCL occurs due to the combined effects of high concentration of serum insulin and free fatty acids[48]. In particular, greater IMCL in the soleus correlates with glucose-insulin-lipid metabolism and insulin sensitivity[49-52], with soleus IMCL content being the only differentiating feature in a study of lean insulin-resistant subjects and their TD peers matched for BMI, body fat distribution, percentage body fat and physical fitness[52]. However, IntraMF quantification using Dixon imaging techniques measure IMCL and EMCL as a composite. IMCL has been shown to be unrelated to measures of

adiposity[283,49]. In this study IntraMF did not correlate with SF/M. This suggests that the raised IntraMF measured in BSCP may be due to greater IMCL content. However, although the mDixon scans showed raised IntraMF with BSCP, whether this is due to raised IMCL, EMCL, or both is not yet known. Therefore, further investigations are required using magnetic resonance spectroscopy to determine to contributions of IMCL and EMCL to the raised IntraMF.

Greater intramuscular fat may also be a marker of impaired mitochondrial content and/or function[41]. The increased intramuscular fat content observed in this study, particularly in the soleus, indicates that patients with cerebral palsy may have a greater risk of developing obesity related diseases, particularly type-II diabetes. Since IntraMF was observed to be greater with increasing GMFCS level, this risk of obesity-related disease may increase with decreasing functional ability. However, intramuscular fat is only one factor associated with the risk of developing obesity related diseases. Future studies of activity levels, fat levels, and glucose tolerance, are required to investigate the risk developing cardio-metabolic diseases in this patient group.

Greater intramuscular fat can be caused by a chronic mismatch between energy intake and expenditure[53,284]. Such a mismatch would also result in greater subcutaneous fat levels. In this study, however, despite SF/M being greater in the BSCP group, this was not statistically significant. This suggests that other factors as well as any potential energy mismatch are adversely affecting the intramuscular fat content in BSCP.

IntraMF has been correlated with deficits in central muscle activation[67], increased risk of future mobility loss[68,69], and insulin resistance[70] in the elderly population. Preliminary studies have also shown that particular exercise regimes in older adults may prevent and decrease intramuscular fat[66]. Since skeletal muscle in cerebral palsy has similarities with muscles in the elderly, including reduced muscle volume[73], increased stiffness[74] and reduced voluntary muscle activation[75], these exercise studies could have important implications for the physical management of this group as suggested by Peterson *et al*[142].

8.4.2 Limitations

The number of subjects recruited may limit the scope and power of this study. However, the differences in intramuscular fat between the TD and BSCP groups were large and statistically significant. The group differences were also were much larger than the reproducibility of the mDixon technique used in this study, defined as the average standard deviation of measured percentage fat across all muscles (0.33%).

Despite having good accuracy and reproducibility, fat-fractions measured using multi-echo techniques are not standardised and platform-independent. The precision of the quantified fat fraction depends on five confounding factors; T1 bias, T2* decay, spectral complexity of fat, noise bias, and eddy currents[220]. The T1 bias and the assumption that fat has a single frequency peak, results in an inadvertent misidentification of some signal from fat as arising from water, and hence to quantification errors[285]. The T1 bias is due to the T1 weighting of the mDixon sequence, in order to reduce scan time. When there is partial-volume mixing of fat and muscle tissue within pixels, signal from fat, which has a shorter T1 than water, is overestimated. Therefore, despite being suitable for comparisons within single site studies, comparison of absolute values of intramuscular fat quantified in this study across sites where different techniques and sequence designs have been employed will be more difficult.

Six of the ten BSCP subjects had undertaken gastrocnemius recessions to the left leg; with one of these six subjects also having had Achilles tendon lengthening. Since muscle injury can lead to fatty degradation of muscle tissue[286-289], it is possible that the histories of surgical intervention received by the individuals with BSCP in this study may have influenced the development of particular muscles. A bar chart comparing the percentage intramuscular fat between the TD group, BSCP subjects with no intervention, and BSCP subjects who have previously received gastrocnemius lengthening is given in Figure 8.5. Percentage intramuscular fat was significantly dependent on intervention and muscle ($p=0.048$ and $p=0.009$ respectively). Despite not being operated on directly, the soleus had significantly higher intramuscular fat content compared to MG and LG ($p=0.006$ and $p=0.007$ respectively). This data suggests that gastrocnemius lengthening may result in damage to the soleus causing fatty accumulation. It has previously been shown that following tendo-Achilles lengthening

and gastrocnemius recession surgeries in a rabbit model, the gastroc-soleus undergoes atrophy and fat infiltration with immobilisation not contributing to either of these processes[290]. However, longitudinal studies are required to determine whether surgery results in greater accumulation of intramuscular fat, or conversely whether those with heightened levels of intramuscular fat are more likely to have surgery in this patient group.

The subjects groups were not age, BMI, and sex matched: however, the physical characteristic differences between the two groups were minimal with no significant difference in age, body mass, height, or BMI observed between the groups. It is possible that the large differences in fat levels in BSCP are due to large differences in life style, including activity levels and diet. Alternatively, the greater fat levels observed in this study may be due to an inherent predisposition with BSCP. To assess the contribution of the factors, further research is required to identify the cause of the increased intramuscular fat in BSCP.

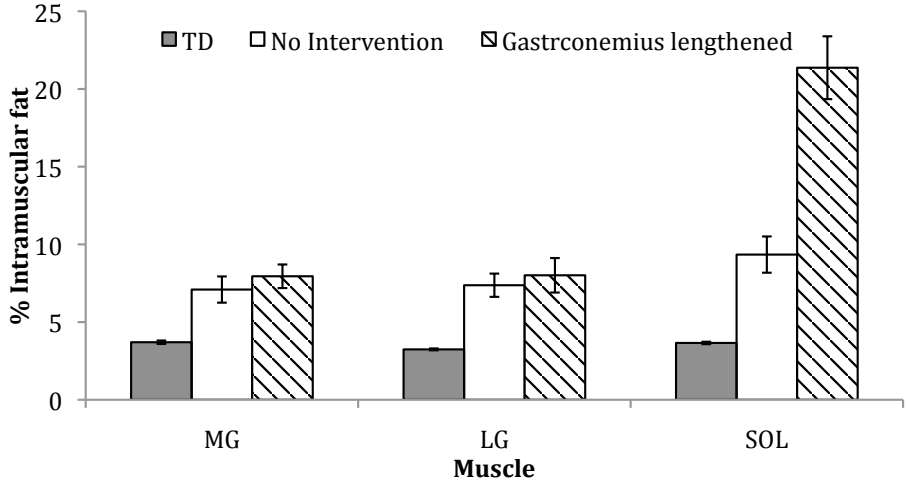

Figure 8.5 Percentage intramuscular fat in the medial gastrocnemius (MG), lateral gastrocnemius (LG) and soleus (SOL) for the TD group (grey), the no intervention BSCP subjects (white) and the gastrocnemius recession BSCP subjects (striped).

8.5 Conclusion

Greater intramuscular fat and IMAT is found in BSCP compared to their TD peers; with the amount of intramuscular fat related to GMFCS level. Despite normal BMIs, the patients in this group may have an increased risk of developing obesity-related diseases,

with risk increasing with decreasing functional ability. Furthermore, the increasing intramuscular fat content may help to explain deficits in muscle performance in this group.

9. Spinal cord white matter organisation in bilateral spastic cerebral palsy

The aim of this chapter is to investigate white matter organisation in the spinal cord at the C6/7 and T10/11 spinal levels in individuals with bilateral spastic cerebral palsy (BSCP) and their typically developing (TD) peers. 11 individuals with bilateral spastic cerebral palsy (BSCP) (mean age: 16.4 years ± 4.2; GMFCS level I: n=1, level II: n=4, level III n=5, level IV: n=1) and 10 of their TD peers (mean age: 16.9 years ± 3.9) took part in this study. T2-weighted and reduced field of view DTI data was acquired at the T10/11 and C6/C7 spinal levels and the mean ADC and FA values of the total white matter and left and right lateral spinal cord white matter were measured in each subject. The functional ability (GMFM-66), selective motor control (SCALE) and spasticity (Modified Ashworth) were assessed by a physiotherapist and relationships between these clinical measures and white matter ADC and FA values investigated.

Spinal cord white matter cross-sectional area was significantly smaller in the BSCP group compared to their TD peers at both C6/7 (p=0.047) and T10/11 (p=0.027) spinal levels. No significant difference was observed in grey matter cross-sectional area at C6/7 and T10/11 spinal levels. A significant lower ADC (p=0.012) was observed at C6/7 in the BSCP group, no difference in FA value was observed at this level. No significant difference was observed in ADC or FA between subject groups at T10/11. No relationships were observed with the clinical measures (GMFM-66, SCALE, and Modified Ashworth). These results suggest that there is no difference in spinal cord white matter microstructure in individuals with BSCP compared to their TD peers. However, the sensitivity of these results to alterations in white matter microstructure,

particularly at the T10/11 level, is limited by image quality at data acquisition and low subject numbers.

9.1 Introduction

Periventricular leucomalacia (PVL) is the most common brain injury in bilateral spastic cerebral palsy (BSCP) and is caused by a primary arterial ischemic injury to the white matter, including damage to the corticospinal tract. The corticospinal system has multiple functions including inhibition and excitation of motor neurones, and the control of spinal reflexes. The corticospinal tract conducts impulses from the brain, originating at the primary motor cortex, the supplementary motor area, and the pre-motor cortex to the spinal cord grey matter via axonal projections of the neurons in the motor cortex. These axonal projections form the corticospinal tract that descends the spinal cord.

As the corticospinal tract develops, a course network of connections between the corticospinal tract and spinal motor neurons are initially formed which are then refined by neuronal activity causing the elimination of transient corticospinal connections, and by the growth of axon terminal branches and synaptic boutons[21,22]. There is also evidence that there are interactions between the developing corticospinal and afferent muscle systems[23]. The elimination of transient corticospinal terminals may leave more space in the spinal grey matter reducing the competition and thereby reducing the pruning of muscle afferent fibre branches[24]. This refined connectivity ultimately determines the specific functional network required to perform precise voluntary movements[14].

PVL tends to occur between 24 and 33 PCW, before the transient spinal terminations of the corticospinal tract in the spinal cord grey matter have been eliminated and mature projections onto the cells of the spinal grey matter have formed. As a result of this injury, intrinsic cord networks may not mature and muscle development may be delayed[30]. An injury to the developing corticospinal tract results in the loss of fine selective voluntary muscle control in distal limb muscles. Spinal cord and subsequent muscle development is likely to be affected by the extent, severity and timing of the original brain injury.

As well as damaging the corticospinal tract, PVL can also damage the reticulospinal and vestibulospinal tracts that facilitate the control of muscle tone. The vestibulospinal tracts originate from the vestibulospinal nuclei and are involved in balance and support with the vestibulospinal tracts exciting the motor neurons in the spinal cord causing contractions of the extensor muscles in the lower limbs. The reticulospinal tracts originate from the reticular nuclei and form the medial and lateral reticulospinal tracts. The medial reticulospinal tract stimulates the extensor muscles and inhibiting the flexor muscles of the proximal limb musculature and the lateral reticulospinal tract has the complementary effect, having an inhibitory effect on the extensors muscle and an excitatory effect on the flexor muscles of proximal limb musculature. Therefore, altered muscle tone may be caused by damage to the reticulospinal and vestibulospinal systems. PVL is an upper motor neuron lesion and as a result can have both negative and positive effects. The negative effects include loss of power, decrease in fine motor control. The positive effects include spasticity, involuntary movements, and co-contractions. It is possible that damage to the reticulospinal and vestibulospinal tracts in PVL may alter the structure or organisation of these tracts in the spinal cord white matter.

In the literature, DTI has been used successfully in the brain to investigate white matter injuries in individuals with cerebral palsy, often correlating their findings with motor function[239-245]. Spinal cord DTI techniques have only recently started to be applied to the spinal cord, with recently published studies investigating a range of pathology including spinal cord compressions[248], inflammatory diseases[249] and arteriovenous malformations[251]. Diffusion parameters, the Apparent Diffusion Coefficient (ADC), a measure of the magnitude of diffusion, and Fractional Anisotropy (FA), a measure of the degree of isotropy in diffusion, have been shown in histological studies to be sensitive to the underlying axon microstructure[246,247]. However, it is important to note that a measured change in FA or ADC does not differentiate between specific changes in axon dimensions or packing parameters. Therefore, DTI parameters can only detect a change in an underlying microstructure but cannot identify how this microstructure has changed.

The aim of this study is to investigate white matter organisation in the spinal cord at the C6/7 and T10/11 spinal levels in individuals with BSCP and their typically developing (TD) peers using DTI. Spinal cord grey and white matter areas are also measured. We

hypothesise that at the T10/11 spinal level, compared to their TD peers, individuals with BSCP will have decreased FA and increased ADC values associated with increased transient connections between the grey and white matter in the spinal cord. These FA and ADC values will be correlated to their functional ability. At the C6/7 spinal level, we hypothesise that, considering the lesser involvement of the upper limbs in BSCP, no significant difference will be observed in FA or ADC values in the spinal cord white matter between subject groups. Considering the reduced cerebral white matter volume following PVL[291,292], we hypothesise that the damage to the white matter tracks in the PLIC will result in reduced white matter volume in the spinal cord and that this will be related to their functional level (GMFM-66).

9.2 Methods

9.2.1 Participants

West London National Research Ethics committee granted ethical approval for this study. Individuals aged 12 – 25 years, with a diagnosis of BSCP, Gross Motor Function Classification System (GMFCS) levels I-III, who met the safety requirements of MRI were included in this study. Patients who had undergone surgery, serial casting or botulinum toxin injections to the lower limbs within the previous year were excluded from the study. This was a convenience sample of individuals attending our hospital department, with consecutive patients that met the inclusion criteria invited to participate in the study. 11 participants with BSCP were recruited to the study (mean age: 16.4 years ± 4.2; age range: 12.1 – 25.5 years; GMFCS level I: n=1, level II: n=4, level III n=5, level IV: n=1; 11 male) and ten TD subjects were included in this study (mean age: 16.9 years ± 3.9; age range: 12.3 – 23.2 years, 12 male). The TD subjects had no previous surgery to their lower limbs and had no known neurological or musculoskeletal conditions.

9.2.2 Data collection

All MR data were acquired on a 3.0T Achieva system (Philips Medical Systems. Best, Netherlands) using a 16-channel neurovascular coil for C6/7 and a 16-channel posterior cardiac coil for T10/11. *Imaging protocol*: At each spinal level, anatomical images of the spinal cord were acquired with an accumulated T2*-weighted gradient echo

sequence with TR= 1000 ms, TE= 6.5, 15.2, 23.8, 32.4, and 41.0 ms, flip angle=28^{o}, 0.5 x 0.5 mm in plane voxel size, 5.0 mm slice thickness, 4 signal averages, 224 x 203 matrix size. The accumulated T2*-weighted gradient echo sequence improves the image contrast between grey and white matter in the spinal cord compared to images acquired with a single TE. Cardiac gated reduced field of view EPI DTI images were acquired of the cervical and thoracic spinal cord with b=0 and 750 s/mm2, 6 directions, 5.0 mm slice thickness, TE = 55 ms, TR ≃ 2000 ms (dependent on subject heart rate), 90° flip angle, 0.5 x 0.5 mm in plane voxel size, 64 x 64 acquisition matrix, 40 x 40 x 30 mm FOV, acquisition time ≃ 8 minutes (depending on the subject's heart rate), small FOV option - slab thickness 120 mm, 3 NSA. ADC and FA maps were calculated on the scanner.

Functional ability (Gross Motor Function Measure 66 (GMFM-66)[184]), selective voluntary motor control (*Selective* Control Assessment of the Lower Extremity (SCALE)[188]), and spasticity (modified Ashworth[293]) of the lower limbs of the subjects with BSCP was assessed by a physiotherapist on the same day as the MRI scan.

9.2.3 Data analysis

The ADC and FA maps were calculated from the acquired DTI data on the Philips Achieva scanner after each scan and exported to Matlab (R2013b, Natwick, USA). The FA and ADC maps from the DTI data sets were registered to the T2-weighted image series and the spinal cord white matter manually segmented on the T2-weighted images and the grey and white matter areas calculated (Figure 9.1b). Regions of interest were manually drawn around the lateral spinal cords defined by a line from the postero-lateral sulcus to the junction of the anterior and posterior horn and on to the antero-lateral sulcus (Figure 9.1c). This enabled the spinal cord white matter to be segmented into left and right lateral spinal cord regions as shown in Figure 9.1d. The mean and standard deviations of the FA and ADC maps were then calculated for the total spinal cord white matter and separately for the left and right lateral spinal cord segments. The mean FA and ADC values were compared between subject groups and between spinal cord levels within each group using independent samples t-tests. The relationships of FA and ADC values with functional clinical tests (GMFM-66, SCALE, and modified Ashworth) were investigated using Pearson's correlation tests. To assess the test-retest repeatability of

the grey and white matter segmentation method in 18 subjects at the T10 spinal level was examined using a one-way intra-class correlation coefficient (ICC) reporting single measure reliability. The benchmarks for ICC proposed by Landis and Koch (1977)[294]: 0-0.2 'poor'; 0.21-0.40 'fair'; 0.41-0.60 'moderate'; 0.61-0.80 'substantial'; and 0.81-1.00 'almost perfect'. The standard error of measurement (SEM) was calculated using Equation 9.1. The smallest detectable difference (SDD) with 95% confidence interval was calculated using Equation 9.2 to estimate the minimal difference between muscles to exceed measurement error. All statistical tests were performed using SPSS (Version 22.0; IBM SPSS, Chicago, USA).

$$SEM = SD_{diff} * \sqrt{(1 - ICC)} \qquad \text{Equation 9.1}$$

Where SD_{diff} is the standard deviation of the differences between the repeated measures.

$$SDD = 1.96 * \sqrt{2} * SEM \qquad \text{Equation 9.2}$$

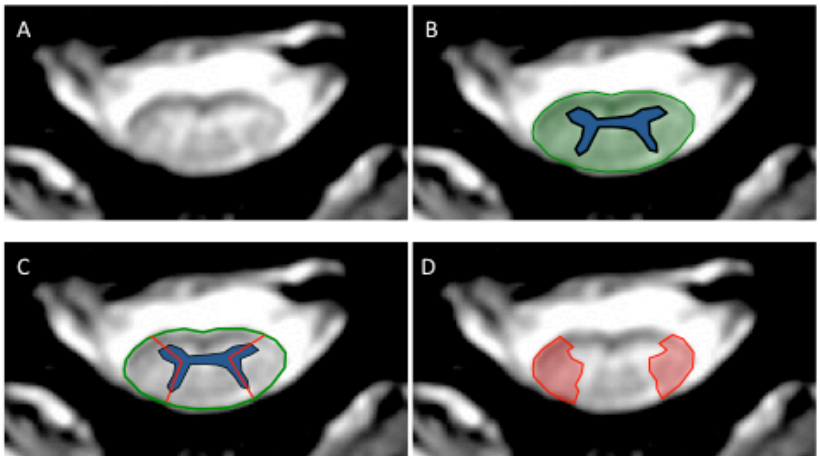

Figure 9.1(A) Cervical spinal cord at C6/7 of one volunteer; (B) Segmented white matter (green) and grey matter (blue; (C) Lateral spinal cord white matter defined by lines from the postero-lateral sulcus to the junction of the anterior and posterior horn and on to the antero-lateral sulcus (red); (D) Lateral spinal cord regions (red).

9.3 Results

Table 9.1 summarises the physical characteristics of each group. No significant difference was observed in age ($p = 0.787$), subject height ($p = 0.218$), body mass ($p = 0.378$) or body mass index (BMI) ($p = 0.888$) between the two subject groups. The

T10/11 data from one TD subject was excluded from analysis due to significant subject movement during image acquisition. The repeatability of the grey and white matter segmentation technique is summarised in Table 9.2. 'Almost perfect' ICC was observed for the grey and white matter segmentation technique.

	CP group	TD Group
Age (years)	16.4 ± 4.2	16.9 ± 3.9
Height (m)	1.64 ± 0.13	1.73 ± 0.13
Body mass (kg)	59.7 ± 17.1	65.5 ± 11.2
BMI (kg/m^2)	21.6 ± 4.6	21.8 ± 1.7
GMFCS level I	N = 1	N/A
GMFCS level II	N = 4	N/A
GMFCS level III	N = 5	N/A
GMFCS level IV	N = 1	N/A

Table 9.1 Subject group physical characteristics

	Mean Difference (standard deviation)	ICC	95% ICC Confidence Interval		SEM	SDD
			Lower bound	Upper bound		
Grey Matter	33.5 (29.9)	0.819	0.454	0.941	12.74	35.31
White Matter	-63.9 (53.2)	0.845	0.533	0.95	20.93	58.02

Table 9.2 Mean difference in initial and repeated measure of white matter and grey matter area at the T10/11 spinal level with the corresponding intraclass correlation coefficient (ICC) values. The standard error of measurement (SEM) and smallest detectable difference (SDD) and the paired-test p-value for bias are also given. Significance was set at $p \leq 0.05$.

Group mean ADC and FA values, and grey and white matter areas are given in Tables 9.3 and 9.4 for C6/7 and T10/11 spinal levels respectively. Example ADC and FA maps from one CP subject at the cervical and thoracic spinal levels are shown in Figures 9.2. Figures 9.3 and 9.4 show bar charts of ADC and FA values for each group at the C6/7 and T10/11 spinal levels respectively. No significant difference was observed between the TD and BSCP groups at T10/11 spinal level white matter mean group ADC values (all white matter p=0.581; left lateral cord p = 0.418; right lateral cord p = 0.564) or FA values (all white matter p=0.597; left lateral cord p = 0.990; right lateral cord p = 0.485). A significant difference was observed between TD and BSCP groups at C6/7 spinal level white matter ADC values (all white matter p = 0.012; left lateral cord p =

0.011; right lateral cord p = 0.04). No significant difference was observed in FA at C6/7 between groups (all white matter p=0.495; left lateral cord p = 0.634; right lateral cord p = 0.127). No significant relationships were observed between any of the measured ADC (r^2<0.19, p>0.05) or FA (r^2<0.25, p>0.05) parameters with GMFM-66, SCALE, or modified Ashworth tests. Figure 9.5 shows a bar chart of the grey and white matter areas at each spinal level investigated for the BSCP and TD groups. The white matter area was significantly lower in the BSCP group for both the C6/7 (p=0.047) and T10/11 (p=0.027) spinal levels. However, white matter area did not correlate with GMFM-66, SCALE, or Modified Ashworth scale at either C6/7 or T10/11 spinal levels (r^2=0.01-0.16). No significant difference was observed in the grey matter areas between the two groups at the C6/7 (p=0.223) and T10/11 (p=0.537) and grey matter area did not correlate with GMFM-66, SCALE, or Modified Ashworth scale at either C6/7 or T10/11 spinal levels (r^2=0.04-0.33).

C6/7	Group	Mean	95% Confidence Interval for Mean		Standard Deviation	Standard error
			Lower Bound	Upper Bound		
Grey matter area (mm^2)	CP	301	260	343	62	19
	TD	333	295	372	50	17
White matter area (mm^2)	CP	1125	1023	1228	153	46
	TD	1297	1137	1456	207	69
White matter ADC (mm^2/s)	CP	437	358	517	119	36
	TD	562	509	616	69	23
White matter FA	CP	0.817	0.801	0.834	0.024	0.007
	TD	0.827	0.793	0.86	0.044	0.015
Left lateral WM ADC (mm^2/s)	CP	432	349	516	124	38
	TD	570	507	633	82	27
Left lateral WM FA	CP	0.822	0.801	0.843	0.031	0.009
	TD	0.812	0.774	0.851	0.05	0.017
Right lateral WM ADC (mm^2/s)	CP	432	356	508	113	34
	TD	530	472	587	74	25
Right lateral WM FA	CP	0.811	0.784	0.838	0.04	0.012
	TD	0.842	0.807	0.878	0.046	0.015

Table 9.3 Mean, 95% confidence interval of the mean, standard deviation and standard error for the CP and TD groups at the C6/7 spinal level. ADC = apparent diffusion coefficient; FA = fractional anisotropy; WM = white matter; GM = grey matter.

T10/11	Group	Mean	95% Confidence Interval for Mean		Standard Deviation	Standard error
			Lower Bound	Upper Bound		
Grey matter area (mm^2)	CP	237	204	269	48	14
	TD	269	224	315	59	20
White matter area (mm^2)	CP	744	696	792	71	21
	TD	833	761	904	93	31
White matter ADC (mm^2/s)	CP	510	345	676	246	74
	TD	490	349	631	183	61
White matter FA	CP	0.813	0.761	0.866	0.078	0.024
	TD	0.805	0.77	0.84	0.046	0.015
Left lateral WM ADC (mm^2/s)	CP	534	356	713	265	80
	TD	491	352	629	180	60
Left lateral WM FA	CP	0.779	0.726	0.832	0.079	0.024
	TD	0.77	0.723	0.817	0.061	0.02
Right lateral WM ADC (mm^2/s)	CP	449	302	597	220	66
	TD	434	299	569	176	59
Right lateral WM FA	CP	0.805	0.759	0.851	0.069	0.021
	TD	0.797	0.756	0.839	0.054	0.018

Table 9.4 Mean, 95% confidence interval of the mean, standard deviation and standard error for the CP and TD groups at the T10/11 spinal level. ADC = apparent diffusion coefficient; FA = fractional anisotropy; WM = white matter; GM = grey matter.

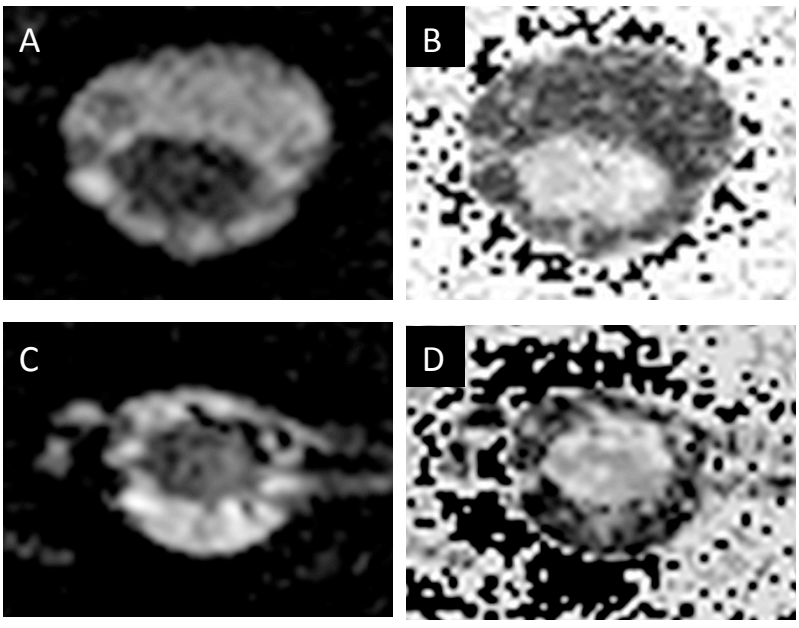

Figure 9.2 Example ADC (A and C) and FA maps (B and C) at the C6/7 (A-B) and T10/11 (C and D) spinal levels from one CP subject

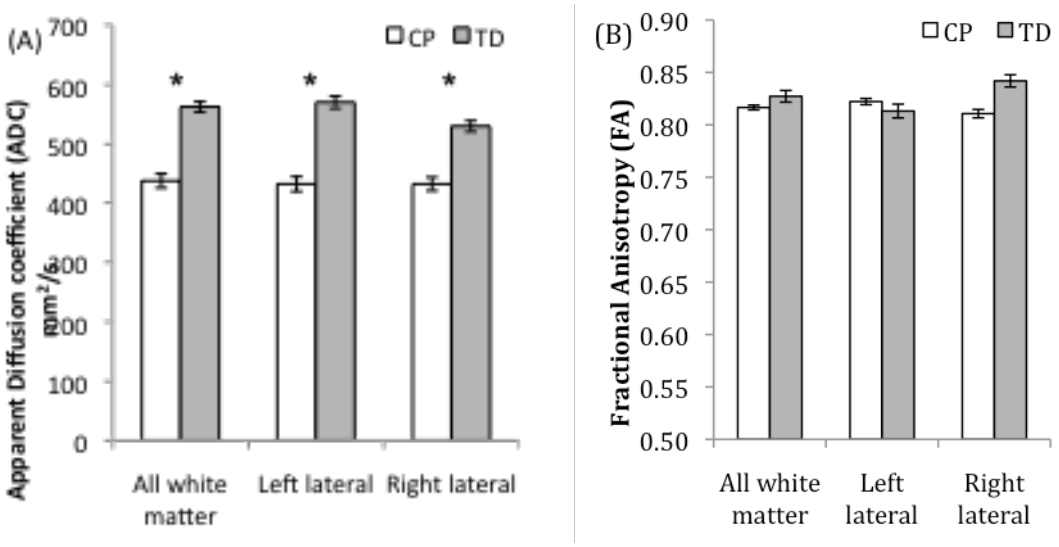

Figure 9.3 Mean (A) ADC and (B) FA values for the CP (white) and TD (grey) subject groups at the C6/7 spinal level. Error bars represent ± one standard error for each group. * Denotes a significant difference between subjects groups ($p \leq 0.05$).

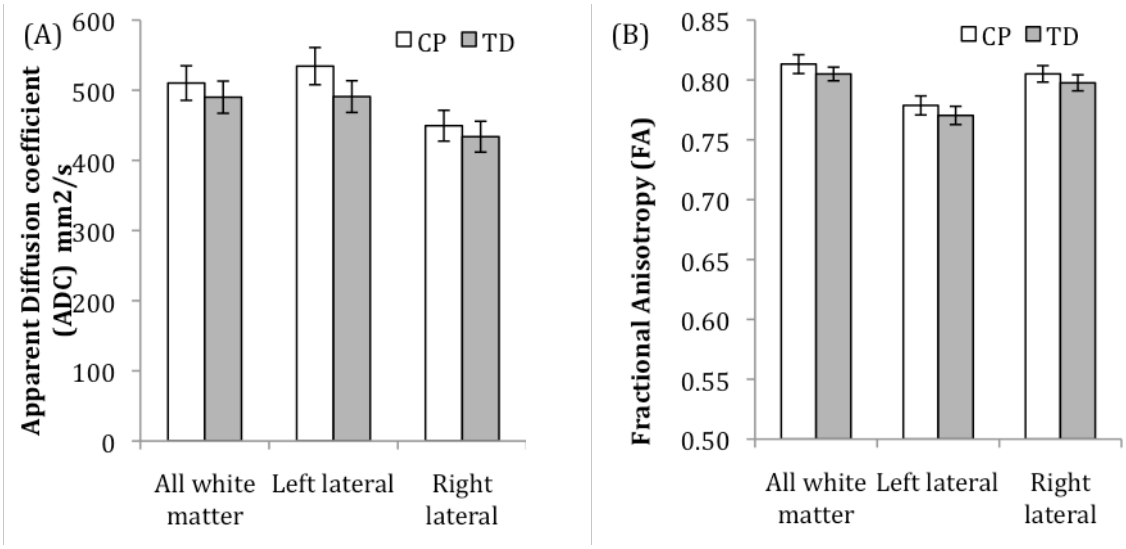

Figure 9.4 Mean (A) ADC and (B) FA values for the CP (white) and TD (grey) subject groups at the T10/11 spinal level. Error bars represent ± one standard error for each group.

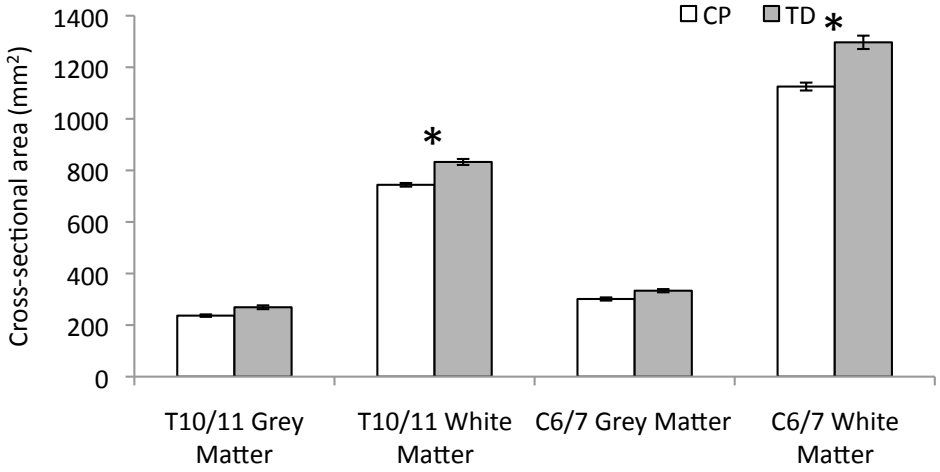

Figure 9.5 (A) Grey and white matter spinal cord areas at the C6/7 and T10/11 spinal levels in the CP (white) and TD (grey) groups. B) The ratio of grey and white matter cross-sectional areas in the CP (white) and TD (grey) groups. Error bars represent ± one standard error for each group. * Denotes a significant difference between subjects groups ($p \leq 0.05$).

9.4 Discussion

This study has found a reduced white matter cross-sectional area at both T10/11 and C6/7 spinal levels in individuals with BSCP compared to their TD peers. As there was no significant difference in body size (height or body mass) between the two subject groups, this suggests that body size does not account for the differences in white matter area between the two groups. This suggests that there may be reduced numbers of axons descending the spinal cord, reduced axon diameter, increased axon density, reduced myelination, or a combination of these factors in subjects with BSCP. The reduced spinal white matter area in BSCP observed in this study matches the reduced cerebral white matter volumes reported in individuals with PVL[291,292]. This suggests that PVL may adversely affect the development of white matter in the spinal cord, however the white matter area did not correlate with any of the outcome measures investigated.

Despite the difference in white matter cross-sectional area between the groups, no significant differences in ADC and FA values in the spinal cord white matter were observed in individuals with BSCP compared to their TD peers at the T10/11 spinal level. This is in disagreement with the original hypothesis. Due to the timing and location of the injury to the posterior limb of the internal capsule in PVL, and the clinical presentation of individuals with PVL (increased muscle tone, reduced voluntary

selective motor control, and reduced function ability) we hypothesised that the corticospinal tract will abnormally develop resulting in altered microstructure in the spinal cord. However, reduced ADC values were measured at C6/7 spinal levels. This suggests that there is restricted diffusion in the cervical cord white matter. This may be related to alternations in white matter organisation including axon number and axon diameter[246]. However, no significant differences in FA values were observed between the subject groups.

Although a reduced ADC was observed in the cervical spinal cord, the insignificant finding for FA at this level and for both ADC and FA in the thoracic spinal cord suggests that spinal cord microstructure may not be significantly altered in BSCP. However, the difference between the two groups may be masked by two limiting factors: the contrast and resolution of the T2-weighted anatomical image series and the image quality of the DTI protocol. The image contrast and in-plane resolution of the T2-weighted scans enables the cross section of the spinal cord to be coarsely segmented into grey and white matter. The individual tracts of the spinal cord cannot be distinguished. It is possible that the local microstructure of the corticospinal tract may be altered in subjects with PVL; however, the regions of interest in this study are much larger than the size of the tracts. The inclusion of the different tracts of the spinal cord may limit the sensitivity of the technique to detect a change in structure that is restricted to the local region of the corticospinal tract. The limited resolution of the regions of interest employed in this study may also explain the insignificant relationships found between the ADC and FA parameters and the functional measures GMFM-66, SCALE, and modified Ashworth, as only particular regions of the spinal cord, such as the regions of the vestibulospinal and reticulospinal tracts in the white matter may correlate with one of the measures. The ‘noise’ acquired by including other white matter regions not related to muscle inhibition or excitation may limit the sensitivity of this study to detect subtle changes in microstructure of the individual white matter tracts, resulting in an insignificant result. The resolution and image contrast also limits the accuracy with which grey and white matter can be segmented. This may inadvertently result in the inclusion of cerebrospinal fluid or grey matter in the white matter regions of interest. This would artificially increase the variability in the measured parameters due to the significantly different structure and therefore ADC and FA of the cerebrospinal fluid and grey matter compared to the white matter.

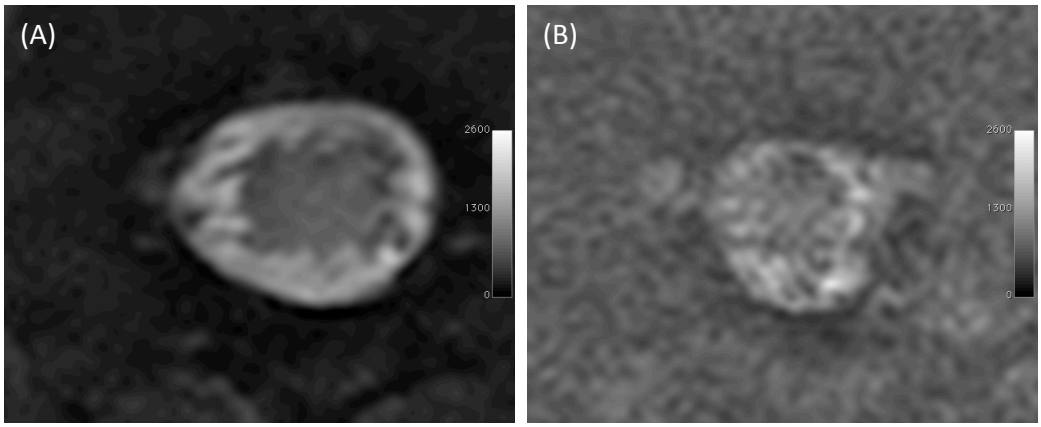

Figure 9.6 Example axial b0 images of the spinal cord at the T10/11 spinal level of two volunteers with (A) high SNR, and (B) low SNR

The DTI acquisition protocol may be a serious limitation to the sensitivity of the study to detect any potential difference in white matter organisation compared to their TD peers. Image quality, including distortion and SNR of the T10/11 DTI datasets are variable between individuals in this study. Example variation in SNR between two subjects is shown in Figure 9.5. If the variability of the DTI parameters is less than the variability due to noise in the DTI dataset, no difference between the subject groups will be detected. FA is SNR dependent: low SNR regions results in a higher FA being measured[295-297]. When the SNR is high, FA is stable since the small difference in FA due to SNR variation is low. If the SNR varies significantly between subjects, the difference in FA due to the change in SNR will be dominant compared to the small difference in FA due to the underlying tissue microstructure. The SNR of the acquired DTI datasets cannot be calculated; however, the coefficient of variation (CoV) of the cerebral spinal fluid signal intensity in the b=0 images of each dataset can provide an indication of the image quality. The CoV of the C6/7 datasets were significantly higher ($p<0.001$) than the T10/11 datasets (Figure 9.6). No significant difference in CoV was observed between subject groups at the T10/11 ($p=0.351$) or C6/7 ($p=0.873$) spinal levels. The low image quality of the T10/11 datasets limits the sensitivity of the sequence to detect small differences in underlying tissue microstructure. Therefore, it is possible that this study has a false negative result.

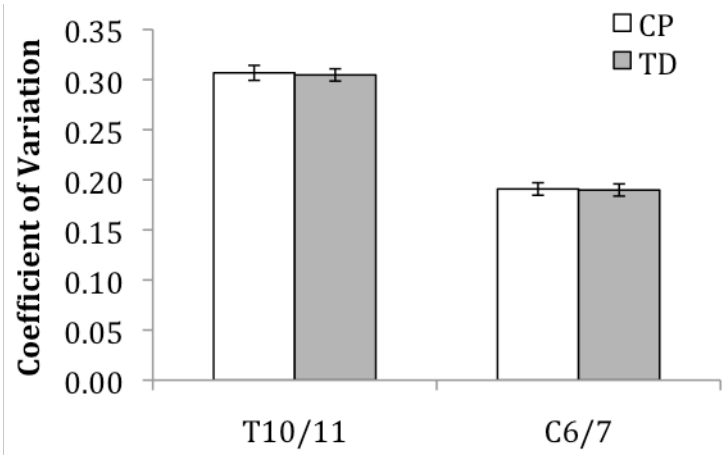

Figure 9.7 Coefficient of variation of the cerebrospinal fluid in the b=0 images at C6/7 and T10/11 spinal levels in the CP (white) and TD (grey) subject groups. Error bars represent the standard error of the coefficient of variation of signal intensity

The ADC and FA values of white matter in the cervical spinal cord have previously been published in TD subjects by Wilm *et al*[272] using reduced-field-of-view DTI on a Philips Achieva 3T system. Wilm *et al*[272] reported an average FA values of 0.75 ± 0.07 and ADC values of 910 ± 100 mm^2/sec from four TD subjects. This FA value is lower compared to the mean FA of the TD subjects in this study (FA = 0.83 ± 0.04), and the ADC is higher than those measured in the cervical spinal cord of TD subjects in this study (ADC = 562 ± 70 mm^2/sec). This difference in ADC is much larger compared to the reproducibility of brain ADC measured across centres[298] and is indicative of motion during data collection. This further suggests that the DTI results in this study are compromised by low SNR, which results in artefactually low ADC values and high FA values.

One factor that may be contributing to the low image quality is the shimming of the magnetic field in the region of interest, resulting in image distortion. Qualitatively, the SNR also appears to vary between subjects at the T10/11 spinal level. The influence of noise on the DTI results could be improved by increasing the number of diffusion directions and removing cardiac gating to enable a greater number of gradient directions to be acquired for the same scan time. Further investigation of the apparent subject dependency of the SNR is required.

Limiting this study to the analysis of spinal cord white matter microstructure may also be a limiting factor. It is possible that the microstructure of the spinal cord grey matter

is altered in BSCP, potentially to a greater extent than the white matter tracts. During corticospinal tract development, the elimination of transient corticospinal terminals in the spinal cord grey matter may result in greater changes to the grey matter microstructure than the white matter. As a result, an injury to the developing corticospinal tract would result in greater abnormalities in the grey matter compared to the white matter. Therefore, the spinal cord grey matter may be a more sensitive target to altered spinal cord development than imaging the corticospinal tract itself. However, in this study the grey matter cannot be reliably and accurately identified in the acquired data sets due to the resolution of the acquisition protocol. In a future study this could be addressed by acquiring images with a higher resolution and increased SNR by increasing the TR and increasing the number of diffusion gradient directions acquired.

9.5 Conclusion

This study has found that individuals with BSCP have a reduced white matter cross-sectional area compared to their TD peers. However, except for a significantly reduced ADC of the cervical cord white matter, no significant difference in diffusion parameters were observed, suggesting that the white matter microstructure is not significantly different in individuals with BSCP compared to their TD peers. Small subject groups and poor image quality of the DTI protocol, particularly at the T10/11 spinal level, may limit the sensitivity of this study to detect any potential alterations in white matter microstructure. A future study with increased SNR, reduced distortion, and increased in plane resolution is required to establish the validity of the results of this study. This would also enable the spinal cord grey matter microstructure to also be investigated simultaneously with the white matter analysis.

10. Summary

10.1 Review of aims

This programme of work set out the following set of aims:

1. To compare lower limb muscle volumes of subjects with bilateral spastic cerebral palsy (BSCP) to their typically developing (TD) peers using MRI.
2. To investigate if there is a relationship between muscle volume and bone strength in the lower limb.
3. To compare muscle adiposity in subjects with BSCP and compare with their TD peers.
4. To investigate white matter organisation in the cervical and thoracic spines of adolescents and young adults with BSCP and compare with their TD peers using diffusion tensor imaging (DTI) MRI.
5. To investigate any relationships between white matter organisation in the thoracic spine and gross motor function, selective motor control.

The major findings of this programme of work are:

10.1.1 Lower limb muscle volume

Seven of the nine lower limb muscles investigated in this study (medial gastrocnemius (MG), lateral gastrocnemius (LG), soleus (SOL), tibialis anterior (TA), rectus femoris (RF), semimembranosus (SM), semtiendinosus (ST)) were smaller in subjects with BSCP compared to their TD peers. Gluteus maximus (GMax) and the vastus intermedius and lateralis composite (VI+VL) were also reduced in the BSCP group: however, this was not statistically significantly. The average muscle volume deficit in

the BSCP group compared to the TD group mean muscle volume was 27.9%. Muscle volume deficits were significantly greater for distal muscles than proximal muscles ($p<0.001$).

Reduced lower limb muscle volume in BSCP is an important finding. Although lower limb muscle volumes have previously been investigated in cerebral palsy[53,56-60], few studies include measurements of muscle size for the whole lower limb[116,299,57], and are limited to studies of hemiplegic subjects[116,299], or do not compare muscle volumes to TD subjects[116,299]. This is the first study investigating muscle volumes with all subjects diagnosed with BSCP, with the muscle volumes compared to their TD peers. This study also has greater subject numbers (19 subjects in each group) than currently published in the literature. Although only nine of the major lower limb muscles have been measured in this study, the greater muscle volume deficits of the distal muscles provides a general guide for strength training interventions in ambulant individuals with BSCP.

10.1.2 Bone strength and muscle volume in ambulant individuals with BSCP

In the distal femur, the polar section modulus **(**Zp), a measure of bone bending and torsional strength, was significantly positively related to thigh muscle volume and height, independent of body mass and diagnosis. The buckling ratio (BR), a measure of bone buckling stability was not significantly different between groups and was not related to any of the variables tested. Cortical bone CSA, related to bone compressional strength, was significantly dependent on diagnosis and positively associated with thigh muscle volume in the distal femur, and to diagnosis and subject height in the proximal tibia.

Tibial cortical bone cross-sectional area, an indicator of compressional bone strength was observed to be dependent on diagnosis and independent on muscle volume. This is a surprising result that may be explained by the irregular cross-section of the proximal tibia and uneven distribution of muscle around it. The uneven distribution of muscle around the tibia results in an uneven distribution of load applied to the tibia by the surrounding musculature. Therefore, any adaptations to muscle induced stress and strain may be location dependent. Therefore, the relationship between the muscle volume and

cortical thickness needs to be investigated considering the loading direction of the muscle groups.

This is the first study investigating the relationship between bone geometry and strength with muscle volume in individuals with cerebral palsy. These results suggest that bone growth in BSCP show the same adaptation to mechanical loading as their TD peers, a process known as Wolf's law, a finding supported by a recently published study showing bone adaptation following low-magnitude vibration training[282], with the stress and strain mediated by muscle action having significant influence over bone remodelling and, therefore, bone strength Although predominantly prescribed for non-ambulant individuals with cerebral palsy, weight-bearing exercises and drug therapies are often utilised to improve bone strength. However, the associations between femoral bone strength and thigh muscle volume in this study suggest that weak bones may not be a direct consequence of having cerebral palsy, but may be related to muscle size. This suggests that strength training to increase muscle size, that in turn exposes the bones to greater stress and strain, may increase bone strength and cortical bone CSA, decreasing the risk of fractures in this patient group. Future work is required to determine whether the relationship between bone strength and muscle volume is also present in non-ambulant individuals with cerebral palsy and whether bone strength can be increased through muscle strength training. Directly loading the bones may also produce a similar remodelling affect to those mediated by muscle action, which may provide an alternative treatment on the bones

Study limitations

Muscle volume has been used as a surrogate of muscle strength in this study. In typically developing individuals directly measuring muscle strength may improve the relationship between muscle and bone. However, measurement of muscle strength in cerebral palsy is unreliable and may underestimate the maximum force generating capacity of muscle due to poor selective voluntary motor control and co-activation of antagonist muscle groups[53,105,106]. However, muscle volume is reflective of the total number of sarcomeres and is linearly related to muscle power[118]. Therefore, it is reasonable to use muscle volume as a surrogate measure of maximal muscle force potential in BSCP. Similarly, Zp, Br, and cortical bone CSA are not direct

measurements of bone strength and assume uniform material properties of bone, including cortical bone density, across all subjects in this study.

The MRI data was collected using three MRI protocols on two different MRI scanners. Although the bone and muscle geometries for each individual were measured from a single scan, the use of two different scanners may result in a systematic error in the measured muscle and bone geometries between the subjects. This systematic error is likely to be small due to required geometric reproducibility of clinical imaging across different MRI machines. However, the reproducibility of the geometric measures across scanners should be investigated to ensure that any potential systematic error is small compared to the differences in muscle and bone geometries between the subject groups.

10.1.3 Muscle adiposity in BSCP

Intramuscular fat was higher in subjects with BSCP for all muscles tested (MG, LG, SOL, TA) compared to their TD peers. Intramuscular fat was significantly related to GMFCS level ($p<0.001$). Intermuscular fat (IMAT) was also higher in subjects with BSCP $p<0.001$). No significant difference was observed in subcutaneous fat normalised to muscle volume (SF/M) between groups.

The number of subjects recruited may limit the scope and power of this study. However, the differences in intramuscular fat between the TD and BSCP groups were large and statistically significant. The group differences were also were much larger than the reproducibility of the mDixon technique used in this study, defined as the average standard deviation of measured percentage fat across all muscles (0.33%).

Surgical intervention may also have an effect on the results of this study. Six of the ten BSCP subjects had undertaken gastrocnemius recessions to the left leg; with one of these six subjects also having had Achilles tendon lengthening. It is possible that the histories of surgical intervention received by the individuals with BSCP in this study may have influenced the development of particular muscles, with percentage intramuscular fat significantly dependent on intervention and muscle ($p=0.048$ and $p=0.009$ respectively). Despite not being operated on directly, the soleus had significantly higher intramuscular fat content compared to MG and LG ($p=0.006$ and

p=0.007 respectively). This data suggests that gastrocnemius lengthening may result in damage to the soleus causing fatty accumulation. This is an interesting finding as the lengthening intervention is performed on the gastrocnemius muscles, not the soleus. This suggests that gastrocnemius lengthening may expose the soleus to much greater forces in the post-operative period, resulting in muscle damage. The degree of soleus injury may be related to the size and strength of the soleus pre-operatively, with larger muscles more likely to be able to withstand greater forces without suffering a muscle injury leading to fatty degradation. Alternatively, the muscle injury caused by the surgery may lead to fatty degradation of the muscle tissue. There are currently no studies investigating the effect of surgical intramuscular lengthening on intramuscular fat. However, a rabbit model of gastrocnemius lengthening and Achilles tendon lengthening surgeries found increased intramuscular fat and reduced volume after surgery[290]. Longitudinal studies are required to determine whether surgery influences intramuscular fat, or whether those individuals with heightened levels of intramuscular fat are more likely to have surgery.

Increased adiposity in BSCP may help to explain deficits in muscle performance in this group: however, increased adiposity may also have further physiological implications. This study suggests that despite having a body mass index (BMI) within the healthy range (18-25), the patients in this group may have an increased risk of developing obesity-related diseases, with risk increasing with decreasing functional ability. However, to date there are no reports of glucose intolerance or diabetes in adolescents and young adults with cerebral palsy. It is possible that the prevalence of metabolic conditions in cerebral palsy have not been investigated. Alternatively, increased adiposity in this population may have a different aetiology or implication or metabolic function. Future studies are required to investigate the physiological implications of raised intramuscular fat in BSCP.

10.1.4 Spinal cord white matter imaging in BSCP

No significant difference was observed in grey matter cross-sectional area at C6/7 and T10/11 spinal levels. No significant difference was observed in ADC or FA between subject groups. No relationships were observed for ADC or FA of spinal cord white matter with the clinical measures (GMFM-66, SCALE, and Modified Ashworth) at both T10/11 and C6/7 spinal levels. Spinal cord white matter cross-sectional area was

significantly smaller in the BSCP group compared to their TD peers at both C6/7 (p=0.047) and T10/11 (p=0.027) spinal levels.

These results suggest that despite the presence of a reduced white matter cross-sectional area, there is no difference in spinal cord white matter microstructure in individuals with BSCP compared to their TD peers. However, this study is limited by image quality in the DTI datasets. The sensitivity of these results to alterations in white matter microstructure, particularly at the T10/11 level, appears to be limited by poor image quality at data acquisition. Image quality, including distortion and the signal-to-noise ratio (SNR) of the T10/11 DTI datasets are variable between individuals of both groups in this study. ADC and FA are SNR dependent: low SNR results in a higher FA and lower ADC values. When the SNR is high, FA is stable since the small difference in FA due to SNR variation is low[295-297]. When the SNR is low and variable between subjects, the difference in FA due to the change in SNR will mask a small difference in FA due to the underlying tissue microstructure. Compared to previously published ADC and FA values acquired with a similar acquisition protocol in TD subjects[272], this study measured lower ADC and higher FA values, further suggesting that the DTI results in this study are compromised by low SNR.

Preliminary tests have established that image distortion is related to subject dependency of the magnetic field shimming, resulting in image translation or wrap artefacts in the image. Increasing the shim region and changing from a pencil beam to a volume-based approach has reduced the prevalence of the wrap artefact. The low and variable SNR has also been investigated, however, this has not been resolved. In the acquired datasets the SNR has only been a limiting factor in the reduced-field-of-view DTI datasets. This has been investigated through increasing the number of diffusion directions, using a 15-channel spine coil, and by removing cardiac gating to remove the heart rate dependency of the repetition time (TR). Despite these modifications, the SNR remains subject dependant and, therefore, this study has been suspended until the issue has been resolved with the assistance of the manufacturer. A future study is required to confirm the results of this study once the study limitations have been addressed.

10.2 Clinical implications

The results of the musculoskeletal imaging sections of this programme of work have important clinical implications. This programme of work has found that adolescents and young adults with BSCP have reduced lower limb muscle volumes compared to their typically developing peers, with the distal muscle more greatly reduced. Muscle volume together with selective motor control is a strong predictor of functional ability, with lower limb muscle volume and Selective Control Assessment of the Lower Extremity (SCALE) explaining 90.3% of the variation in Gross Motor Function Measure (GMFM-66) (Appendix F). Since selective motor control in individuals with BSCP is static, with limited changes to muscle activation patterns in gait following surgery[300,301], maximising muscle volume through strength training may be an important factor for an individual to maximise their functional ability. The relatively greater reduction in distal muscle volume suggests that strength-training exercises should include, and perhaps focus on, the distal muscles in these individuals, as these muscles are comparatively more affected than the proximal musculature. However, exercise prescription should still be patient specific, taking into account the degree of involvement of specific muscles, the patient's functional ability, and goals.

As well as having reduced muscle size, these muscles also have greater intramuscular fat than their typically developing peers. Reduced muscle volumes and increased adiposity may further explain the reduced muscle strength and functional ability in this patient group. The increased intra- and intermuscular fat in cerebral palsy observed in this programme of work may have important implications for the metabolic health of these patients. Raised intramuscular fat levels are strongly associated with insulin resistance and type-II diabetes[44-46]. These morphological and compositional changes may have implications both for the mechanical performance of these skeletal muscles and also for the predisposition of the adult with cerebral palsy to cardio-metabolic disease[122]. This data suggests that individuals with cerebral palsy may benefit from an exercise intervention targeting both the strength and metabolic function of their lower limb muscles through strength and cardio-vascular training with the aim to both decrease their intramuscular far content and their muscle size and strength. However, the cause and implications of increased intramuscular fat requires investigation to fully in form the clinical management of this patient population.

This programme of work has also observed that muscle volume has an important role in bone strength in ambulant individuals with BSCP. Muscle volume and height are significantly related to femoral bone strength estimated from bony geometry, independent of diagnosis and body mass. This may have important implications for the clinical management of fracture risk in this population and in non-ambulatory individuals with cerebral palsy. Traditionally these individuals receive weight bearing therapies, medication to increase bone mass, or a combination of these. The insignificant relationship between body mass and bone strength in the ambulant individuals with cerebral palsy suggests that weight bearing therapies are unlikely to improve bone strength. Therapies where the direction of loading is not aligned with the long axis of the bone imparts greater bending forces, and therefore, may cause greater bone remodelling to occur. These forces can be mediated by muscle action, however, the bones may also remodel in response to passive loading, which may be more applicable therapy for a non-ambulant population. However, this is a cross-sectional study and longitudinal studies are required to determine whether the long bones of individuals with cerebral palsy increase in strength following a loading mediated by muscle action or by passive loading.

10.3 Methodological findings

In this programme of work, MRI has been used successfully to image the lower limbs of individuals with BSCP, facilitating the measurement of muscle and bone morphology, and intramuscular fat quantification. Two main methodological findings have been made during this programme of work that can be applied to both future studies of cerebral palsy, and other conditions.

10.3.1 Intramuscular fat quantification

In the literature, T_1-weighted image segmentation is primarily used to quantify IMAT, with IMAT defined as the MRI-visible fat within the muscles (intramuscular fat) and between the muscles beneath the fascia (intermuscular fat). Although this method is effective for assessing intermuscular and subcutaneous fat volumes, it is not an accurate method for measuring fat distribution within individual muscles.

Multi-echo imaging techniques for fat quantification have been evaluated against

magnetic resonance spectroscopy (MRS) *in vitro* with fat-water phantoms and *in vivo* in vastus medialis of TD subjects. Although multi-echo techniques have been widely used and evaluated for hepatic fat quantification, this is the first study published study investigating Dixon imaging, specifically mDixon imaging, for *in vivo* intramuscular fat quantification. This study investigated the dependence of the mDixon technique on the flip angle of the excitation radio-frequency pulse, and on the selection of the number of data points acquired and their timing, informing sequence design for future intramuscular fat quantification studies. However, it is important to note that fat quantification measured using multi-echo techniques are not standardised and platform-independent. The precision of the quantified fat fraction depends on five confounding factors; T1 bias, T2* decay, spectral complexity of fat, noise bias, and eddy currents[220]. This work is discussed in detail in Chapter 7 and has been published in the British Journal of Radiology[302].

10.3.2 Drawing regions of interest

This programme of work has involved the manual identification of muscle boundaries throughout the lower limbs of over 50 individuals. Although automatic segmentation algorithms can successfully segment MRI images by tissue type based on pixel intensity, pixel intensity based segmentation techniques are currently not successful at indentifying complex boundaries between neighbouring muscles. Therefore, all muscle regions of interest in this programme of work were performed manually. In order to minimise the processing time of these images, a novel method was employed where the input of an iPad was used to facilitate the direct tracing of muscle boundaries on MRI images using a touch screen pen.

10.4 Future work

10.4.1 Do patients with bilateral spastic cerebral palsy have an increased risk of developing obesity-related diseases?

Adults with cerebral palsy may have a 2-3 times greater risk of dying from ischemic heart disease than their typically developing peers[13]. Chronic sedentary behaviour, which is often prevalent in cerebral palsy, is generally accepted as the predominant cause of cardio-metabolic decline and sarcopenia in the general population[303], with

sedentary behaviour strongly associated with disease, disability and shortened lifespan among all adults[304].

An atherogenic lipid profile has been widely reported in persons with chronic spinal cord injuries (SCI)[305-309]. Subjects with a SCI have similar functional difficulties and sedentary behaviour patients with BSCP. Both patient groups exhibit reduced muscle size, reduced muscle activation, and reduced activity levels. In SCI, the most consistent lipid profile alteration is a depressed blood plasma concentration of high-density lipoprotein cholesterol (HDL-C)[305,306,310-312]. HDL-C has a range of functions including protection against the development of vascular disease[313]. Altered lipid profiles, including low HDL-C, have also been linked with insulin resistance in non-disabled clinical populations[314,315]. Due to the strong relationship of cardiovascular disease with altered blood lipid profiles and similar activity levels with SCI patients, measuring the lipid profiles of BSCP subjects is an important step in assessing their risk of developing cardiovascular diseases.

The increased inter and intramuscular fat in BSCP observed in this programme of work (Chapter 8) may expose patients with cerebral palsy to a greater risk of developing cardiovascular[44,121] and cardio-metabolic disease[122]. However, the cardio-metabolic implications of this are unknown. There is a strong relationship between intramuscular fat content, insulin resistance and type-II diabetes[44,46,45]. In particular, increased intramyocellular lipid in the soleus correlates with glucose-insulin-lipid metabolism and insulin sensitivity[49-52,41]. Since individuals with BSCP have reduced muscle mass, even individuals with body mass index in the normal range may have relatively increased levels of adipose tissue compared to their typically developing peers. As discussed in Chapter 8, young adults with BSCP have significantly higher intramuscular fat content compared to their typically developing peers, with the soleus the most adversely affected. The level of intramuscular fat also appears to be dependent on the degree of their mobility impairment (GMFCS level). Previous studies in children with CP have also suggested raised levels of fat[76,77]. Therefore, investigating the risk factors including blood lipid profiles, glucose tolerance, and adiposity is important to assess the risk of adults with BSCP to developing cardio-metabolic disease.

10.4.2 The relationship between surgical intervention and muscle quality

Surgical muscle lengthening is a common intervention performed on individuals with cerebral palsy with the aim to correct the joint range of movement following the development of muscle contractures. In Chapter 8, the intramuscular fat content of the plantarflexor muscle group in individuals with BSCP was found to be significantly dependent on whether an individual had received a surgical gastrocnemius lengthening, with the soleus having higher intramuscular fat content compared to the medial and lateral gastrocnemius muscles. As this study was cross-sectional, the relationship between surgical intervention and intramuscular fat accumulation cannot be elucidated:

1. Surgical intramuscular lengthening may lead to intramuscular fat accumulation through the same mechanism of fatty degradation following muscle injuries[286-289].
2. Heightened intramuscular fat levels may be associated with the development of muscle contracture, with the raised intramuscular fat levels measured in Chapter 8 being present prior to surgery. If the intramuscular fat is present prior to the intervention, the degree of fatty infiltration into the muscles may be related to surgical outcome.

A longitudinal study, with intramuscular far measurements performed pre- and post-intervention, to determine whether surgery results in greater accumulation of intramuscular fat, whether individuals with heightened levels of intramuscular fat are more likely to have surgery, and whether intramuscular fat content prior to surgery predicts surgical outcome.

10.4.3 Measurement of bony morphology using MRI

Bony morphology is often investigated using computed tomography (CT). Although CT produces high quality images of the skeletal system, it is associated with a high dose of ionising radiation (X-rays). MRI does not use involve ionising radiation and has been increasingly used in the literature for measurements of bony geometry. Despite having lower water content and very short relaxation times, cortical bone can be identified on MRI images due to the very low MR signal acquired compared to the surround fat and muscular tissue.

Femoral anteversion is the inclination of the axis of the femoral neck with respect to the knee joint axis in the transverse plane. The angle at which the femoral neck is inclined is the anteversion angle. At birth a child has approximately 30-50° of femoral anteversion[316]. As the child matures and develops they progress through several key motor milestones including crawling, standing and walking. These activities induce stress on the proximal end of the femur. In response to the applied stress, the proximal end of the femur remodels with femoral anteversion decreasing rapidly in the first three to four years of life to approximately 15° at skeletal maturity[316,317]. The delay of motor milestone acquisitions which often occurs with cerebral palsy results in the degree of anteversion remodelling in early life being reduced[316], with increased femoral anteversion persisting into adulthood[318,319]. The number of years spent walking independently may be a significant factor influencing the remodelling of femoral anteversion in ambulant individuals with BSCP (Appendix G).

Internal foot progression is a common gait abnormality in ambulant children with cerebral palsy[320]. Internal foot progression can be caused by deformity of femur, tibia, and/or foot in the transverse plane, with internal hip rotation commonly related to excessive femoral anteversion angle[321]. The primary treatment for excessive femoral anteversion is a femoral derotation osteotomy (FDRO). During an FDRO, the femur is cut and the distal segment of the femur is externally rotated and then fixed to the proximal segment. However, excessive femoral anteversion is not the only cause of internal hip rotation[321] and FDRO does not consistently correct internal hip rotation in gait[322,323], with one study reporting that internal hip rotation persisted in 33.3% of cases at a mean post FDRO follow-up of 22 months with a reoccurrence of internal hip rotation at 53 months post surgery in 9.5% of the individuals that reported with corrected internal hip rotation at 22 months[323]. Three dimensional gait analysis and clinical examination of femoral anteversion improve the surgical outcomes of FDRO[322,324,325]; however, the clinical test of femoral anteversion, the greater trochanter prominence test (GTPT), is problematic.

The GTPT is performed with the patient in prone with the hip in a neutral coronal position and knee flexed to 90°, the hip was rotated internally and externally while palpating the most prominent part of the greater trochanter. Femoral anteversion is the

angle of the tibia to vertical when the greater trochanter is at its most prominent lateral position. However, in a study comparing the GTPT with MRI, there was only moderate agreement, with the true femoral anteversion value being within 11.8° of GTPT (95% confidence limit)[326].

Seventeen of the individuals with BSCP volunteering for studies in this programme of work also attended the One Small Step Gait Laboratory at Guy's Hospital for clinical 3D gait analysis within four months of their MRI scan, during which their femoral anteversion is measured using the GTPT and mean internal hip rotation in gait is measured. A weak but significant positive linear relationship ($r=0.379$, $p=0.030$) was observed between the femoral anteversion angle measured using the GTPT and from MRI using the Murphy method[327], with the GTPT underestimating the femoral anteversion angle by 20°($p \leq 0.001$). However, the passive internal hip rotation range of the lower limb also limits the applicability of the GTPT. When the maximum passive internal hip rotation is less than the femoral anteversion angle, it is not possible to measure the femoral anteversion angle by the GTPT, instead an erroneous measure is made on the palpation of a false lateral prominence of the greater trochanter. In this subject group, 24% (8 lower limbs) exhibited femoral anteversion angles measured by MRI outside the maximum internal range of movement of the hip.

Setting the upper limit of the normal range to the 95% confidence limit (mean plus two standard deviations of the TD subjects) for femoral anteversion (31.3°) and mean internal hip rotation in gait (10.6°) enables the interaction between femoral anteversion and internal hip rotation to be investigated. Of the lower limbs of the BSCP subjects that volunteered for studies in this programme of work, 33.3% exhibited excessive femoral anteversion and excessive internal hip rotation compared to the normal range, 48.5% had excessive femoral anteversion without excessive internal hip rotation in gait, 18.2% had both femoral anteversion and internal hip rotation within the normal range, and 3% had excessive internal hip rotation without excessive femoral anteversion. These results demonstrate that the cause of internal hip rotation in gait is multi-factorial and improving selection of patients who may benefit from a FDRO by measuring femoral geometry from MRI may improve surgical outcome.

A weak but significant relationship was observed between femoral anteversion angle and mean internal hip rotation during gait for both the GTPT (r=0.415, p=0.026) and MRI method (r=0.545, p=0.001). However, when only the lower limbs that presented with both excessive femoral anteversion and excessive mean internal hip rotation (Figure 10.1), a strong positive correlation is observed between MRI measured femoral anteversion and mean internal hip rotation (r=0.650), but no correlation is observed between the GTPT and mean internal hip rotation (r=0.127). This means that 65% of the variability in internal hip rotation in individuals with excessive femoral anteversion and mean internal hip rotation can be explained by their femoral anteversion angle when measured by MRI. These results suggest that measuring femoral anteversion by MRI instead of the GTPT when indentifying individuals who may suitable for a FDRO may improve surgical outcome. Therefore, a future study is required to investigate whether MRI based femoral anteversion measures improve patient outcome (correction of internal hip rotation in gait) following FDRO.

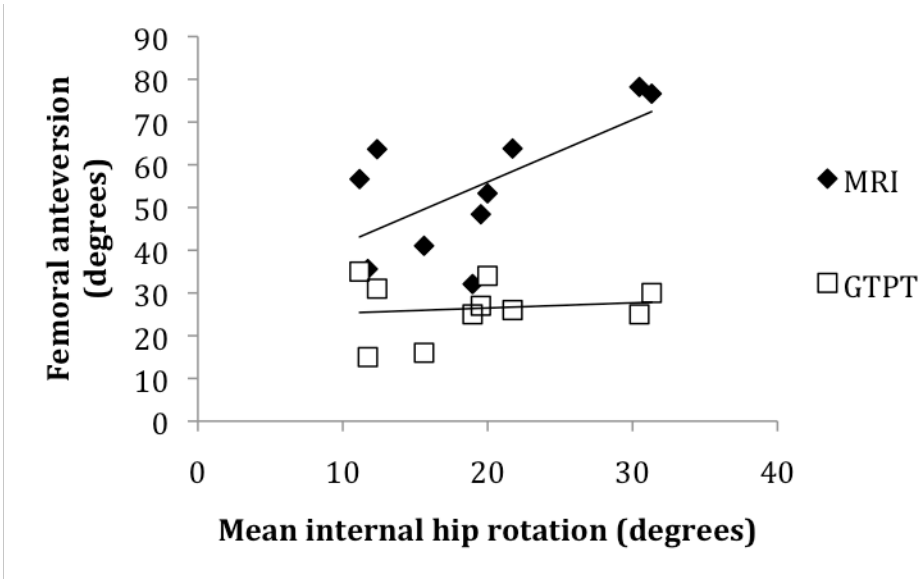

Figure 10.1 Scatter plot of femoral anteversion angle measured by MRI (black) (r=0.650) and GTPT (white) (r=0.127) versus mean internal hip rotation in gait for lower limbs exhibiting both excessive femoral anteversion and excessive internal hip rotation.

10.4.4 The effect of strength training on the muscle bone unit

The relationships observed between bone strength and muscle volume, independent of body mass, in Chapter 6 have important implications for the physical management of the cerebral palsy patient group. This suggests that muscle weakness, which is prevalent

in cerebral palsy[55], may be a significant factor in bone growth and development in this group. Low functioning individuals with cerebral palsy are often prescribed weight-bearing activities to improve bone strength and reduce their risk of fractures. The results of the study in Chapter 6 suggests that strength training to increase muscle size and strength may be more likely to result in increased bone strength compared to traditional weight bearing therapies. Although it should be noted that the relationship between bone strength and muscle volume was not observed in the tibia, possibly due to the irregular shape of the tibia and distribution of musculature around it. Lower limb muscle strength training may enable individuals to maximise the mechanical forces experienced by the bones and thereby maximise the potential for bone development.

It is known that muscle strength in cerebral palsy can be improved through strength training[328-330], resulting in an improved functional ability[328-330]. Bones in adolescents and young adults with cerebral palsy also show the same adaptation to mechanical loading due to muscle contractions as their TD peers[282]. Therefore, the effect of muscle strength training on bone strength requires further investigation. This could be achieved by a 12-week strength training interventional study in which subjects have their lower limb muscle strength measured and undergo an MRI scan of their lower limbs at the start of the strength training programme (0 weeks), 6 weeks, at completion of the strength training programme (12 weeks), and 3 months after completing the programme.

10.4.5 Spinal cord DTI

Significantly reduced spinal cord white matter cross sectional area was observed in individuals with BSCP compared to their TD peers in Chapter 9. This is comparable to the reduced cerebral white matter volume reported in studies of PVL[291,292]. However, as discussed in section 9.1.4, the study failed to determine whether there is altered white matter microstructure organisation in BSCP due to poor image quality of the DTI datasets. Therefore, the potential difference in white matter organisation suggested by the reduced white matter cross-sectional area observed in this study, requires further investigation. The inclusion of spinal cord grey matter DTI in a future study is also advisable as this may prove to be a more sensitive region to altered corticospinal tract development than the white matter as damage to the developing corticospinal tract may affect the elimination of transient spinal terminations of the corticospinal tract in the spinal cord grey matter and the development mature projections onto the cells of the

spinal grey matter. The image quality can be improved in future studies by dedicating more acquisition time to the DTI acquisition protocol, with a greater number of diffusion directs acquired at a higher resolution. The effect of cardiac gating on image quality could be investigated. The removal of cardiac gating would enable a standardised TR to be used across patients to reduce the T1 weighting and SNR variability between patients,

10.5 Conclusion

This programme of work has found that the lower limb muscles of adolescents and young adults with bilateral spastic cerebral palsy have reduced have reduced volume and increased intramuscular fat compared to their typically developing peers. These reduced muscle volumes are related to altered bony geometry and reduced strength of the distal femur and proximal tibia. These findings suggest that individuals with cerebral palsy may benefit from strength training programmes to improve their muscle and bone strength, and that they may be exposed to greater cardio-metabolic risk due to increased intramuscular fat content, particularly in the soleus.

This programme of work has also observed reduced white matter volume in the thoracic and cervical spinal cord of individuals with cerebral palsy compared to their typically developing peers. This result indicates that spinal cord as well as cerebral development may be affected in these individuals. Future work is required to elucidate any micro-structural changes in the spinal cord that make relate to the severity of the condition.

References

1. Surman G, Bonellie S, Chalmers J, Colver A, Dolk H, Hemming K, King A, Kurinczuk JJ, Parkes J, Platt MJ. UKCP: a collaborative network of cerebral palsy registers in the United Kingdom. J Public Health (Oxf) 2006;28(2):148-156.
2. Rosenbaum P, Paneth N, Leviton A, Goldstein M, Bax M, Damiano D, Dan B, Jacobsson B. A report: the definition and classification of cerebral palsy April 2006. Dev Med Child Neurol Suppl 2007;109:8-14.
3. Volpe JJ. Brain injury in premature infants: a complex amalgam of destructive and developmental disturbances. Lancet Neurol 2009;8(1):110-124.
4. Palisano R, Rosenbaum P, Walter S, Russell D, Wood E, Galuppi B. Development and reliability of a system to classify gross motor function in children with cerebral palsy. Dev Med Child Neurol 1997;39(4):214-223.
5. Russell DJ, Rosenbaum PL, Cadman DT, Gowland C, Hardy S, Jarvis S. The gross motor function measure: a means to evaluate the effects of physical therapy. Dev Med Child Neurol 1989;31(3):341-352.
6. Hanna SE, Rosenbaum PL, Bartlett DJ, Palisano RJ, Walter SD, Avery L, Russell DJ. Stability and decline in gross motor function among children and youth with cerebral palsy aged 2 to 21 years. Dev Med Child Neurol 2009;51(4):295-302.
7. Day SM, Wu YW, Strauss DJ, Shavelle RM, Reynolds RJ. Change in ambulatory ability of adolescents and young adults with cerebral palsy. Dev Med Child Neurol 2007;49(9):647-653.
8. Strauss D, Ojdana K, Shavelle R, Rosenbloom L. Decline in function and life expectancy of older persons with cerebral palsy. NeuroRehabilitation 2004;19(1):69-78.
9. Jahnsen R, Villien L, Egeland T, Stanghelle JK, Holm I. Locomotion skills in adults with cerebral palsy. Clin Rehabil 2004;18(3):309-316.
10. Strauss D, Shavelle R, Reynolds R, Rosenbloom L, Day S. Survival in cerebral palsy in the last 20 years: signs of improvement? Dev Med Child Neurol 2007;49(2):86-92.
11. Hemming K, Hutton JL, Pharoah PO. Long-term survival for a cohort of adults with cerebral palsy. Dev Med Child Neurol 2006;48(2):90-95.
12. Reid SM, Carlin JB, Reddihough DS. Survival of individuals with cerebral palsy born in Victoria, Australia, between 1970 and 2004. Dev Med Child Neurol 2012;54(4):353-360.
13. Strauss D, Cable W, Shavelle R. Causes of excess mortality in cerebral palsy. Dev Med Child Neurol 1999;41(9):580-585.
14. Martin JH. The corticospinal system: from development to motor control. Neuroscientist 2005;11(2):161-173.
15. Williams PL, Bannister LH, Gray HAd, surgical. Gray's anatomy : the anatomical basis of medicine and surgery. New York ; Edinburgh: Churchill Livingstone; 1995.

16. KIM RC. Development of the Human Spinal Cord: An Interpretation Based on Experimental Studies in Animals. Journal of Neuropathology & Experimental Neurology 2002;61(2):212.
17. Joosten EA, Gribnau AA, Dederen PJ. An anterograde tracer study of the developing corticospinal tract in the rat: three components. Brain Res 1987;433(1):121-130.
18. Joosten EA, Gribnau AA, Dederen PJ. Postnatal development of the corticospinal tract in the rat. An ultrastructural anterograde HRP study. Anatomy and embryology 1989;179(5):449-456.
19. Tessier-Lavigne M, Goodman CS. The molecular biology of axon guidance. Science 1996;274(5290):1123-1133.
20. Mueller BK. Growth cone guidance: first steps towards a deeper understanding. Annual review of neuroscience 1999;22:351-388.
21. Li Q, Martin JH. Postnatal development of corticospinal axon terminal morphology in the cat. The Journal of comparative neurology 2001;435(2):127-141.
22. Li Q, Martin JH. Postnatal development of connectional specificity of corticospinal terminals in the cat. The Journal of comparative neurology 2002;447(1):57-71.
23. Gibson CL, Arnott GA, Clowry GJ. Plasticity in the rat spinal cord seen in response to lesions to the motor cortex during development but not to lesions in maturity. Experimental neurology 2000;166(2):422-434.
24. Gibson CL, Clowry GJ. Retraction of muscle afferents from the rat ventral horn during development. Neuroreport 1999;10(2):231-235.
25. Meng Z, Martin JH. Postnatal development of corticospinal postsynaptic action. J Neurophysiol 2003;90(2):683-692.
26. Lemon RN, Griffiths J. Comparing the function of the corticospinal system in different species: organizational differences for motor specialization? Muscle Nerve 2005;32(3):261-279.
27. Banker BQ, Larroche JC. Periventricular leukomalacia of infancy. A form of neonatal anoxic encephalopathy. Arch Neurol 1962;7:386-410.
28. Miller SP, Ramaswamy V, Michelson D, Barkovich AJ, Holshouser B, Wycliffe N, Glidden DV, Deming D, Partridge JC, Wu YW, Ashwal S, Ferriero DM. Patterns of brain injury in term neonatal encephalopathy. J Pediatr 2005;146(4):453-460.
29. Surveillance of cerebral palsy in Europe: a collaboration of cerebral palsy surveys and registers. Surveillance of Cerebral Palsy in Europe (SCPE). Dev Med Child Neurol 2000;42(12):816-824.
30. Clowry GJ. The dependence of spinal cord development on corticospinal input and its significance in understanding and treating spastic cerebral palsy. Neurosci Biobehav Rev 2007;31(8):1114-1124.
31. Lance JW. pathophysiology of spasticity and clinical experience with baclofen. Feldman RG, Young RR, Koella WP, editors. Miama, Fla: Symposia Specialists; 1980.
32. Pandyan AD, Gregoric M, Barnes MP, Wood D, Van Wijck F, Burridge J, Hermens H, Johnson GR. Spasticity: clinical perceptions, neurological realities and meaningful measurement. Disabil Rehabil 2005;27(1-2):2-6.

33. Lieber RL. Skeletal muscle structure, function, and plasticity : the physiological basis of rehabilitation. Baltimore, MD: Wolters Kluwer/Lippincott Williams & Wilkins; 2010. viii, 304 p. p.
34. Tortora GJ, Grabowski SR. Introduction to the human body : the essentials of anatomy and physiology. New York, N.Y. ; [Chichester]: Wiley; 2007. 1 v. (various pagings) p.
35. Astrand PO. Diet and athletic performance. Fed Proc 1967;26(6):1772-1777.
36. Zurlo F, Larson K, Bogardus C, Ravussin E. Skeletal muscle metabolism is a major determinant of resting energy expenditure. J Clin Invest 1990;86(5):1423-1427.
37. DeFronzo RA, Gunnarsson R, Bjorkman O, Olsson M, Wahren J. Effects of insulin on peripheral and splanchnic glucose metabolism in noninsulin-dependent (type II) diabetes mellitus. J Clin Invest 1985;76(1):149-155.
38. Baron AD, Brechtel G, Wallace P, Edelman SV. Rates and tissue sites of non-insulin- and insulin-mediated glucose uptake in humans. Am J Physiol 1988;255(6 Pt 1):E769-774.
39. Kelley DE. Skeletal muscle fat oxidation: timing and flexibility are everything. J Clin Invest 2005;115(7):1699-1702.
40. Storlien L, Oakes ND, Kelley DE. Metabolic flexibility. Proc Nutr Soc 2004;63(2):363-368.
41. Stump CS, Henriksen EJ, Wei Y, Sowers JR. The metabolic syndrome: role of skeletal muscle metabolism. Ann Med 2006;38(6):389-402.
42. Kelley DE, Goodpaster B, Wing RR, Simoneau JA. Skeletal muscle fatty acid metabolism in association with insulin resistance, obesity, and weight loss. Am J Physiol 1999;277(6 Pt 1):E1130-1141.
43. Kiens B. Skeletal muscle lipid metabolism in exercise and insulin resistance. Physiol Rev 2006;86(1):205-243.
44. Elder CP, Apple DF, Bickel CS, Meyer RA, Dudley GA. Intramuscular fat and glucose tolerance after spinal cord injury--a cross-sectional study. Spinal Cord 2004;42(12):711-716.
45. Kewalramani G, Bilan PJ, Klip A. Muscle insulin resistance: assault by lipids, cytokines and local macrophages. Curr Opin Clin Nutr Metab Care 2010;13(4):382-390.
46. Lara-Castro C, Garvey WT. Intracellular lipid accumulation in liver and muscle and the insulin resistance syndrome. Endocrinol Metab Clin North Am 2008;37(4):841-856.
47. Schick F, Eismann B, Jung WI, Bongers H, Bunse M, Lutz O. Comparison of localized proton NMR signals of skeletal muscle and fat tissue in vivo: two lipid compartments in muscle tissue. Magn Reson Med 1993;29(2):158-167.
48. Brechtel K, Dahl DB, Machann J, Bachmann OP, Wenzel I, Maier T, Claussen CD, Haring HU, Jacob S, Schick F. Fast elevation of the intramyocellular lipid content in the presence of circulating free fatty acids and hyperinsulinemia: a dynamic 1H-MRS study. Magn Reson Med 2001;45(2):179-183.
49. Krssak M, Falk Petersen K, Dresner A, DiPietro L, Vogel SM, Rothman DL, Roden M, Shulman GI. Intramyocellular lipid concentrations are correlated with insulin sensitivity in humans: a 1H NMR spectroscopy study. Diabetologia 1999;42(1):113-116.

50. Petersen KF, Hendler R, Price T, Perseghin G, Rothman DL, Held N, Amatruda JM, Shulman GI. 13C/31P NMR studies on the mechanism of insulin resistance in obesity. Diabetes 1998;47(3):381-386.
51. Misra A, Sinha S, Kumar M, Jagannathan NR, Pandey RM. Proton magnetic resonance spectroscopy study of soleus muscle in non-obese healthy and Type 2 diabetic Asian Northern Indian males: high intramyocellular lipid content correlates with excess body fat and abdominal obesity. Diabet Med 2003;20(5):361-367.
52. Jacob S, Machann J, Rett K, Brechtel K, Volk A, Renn W, Maerker E, Matthaei S, Schick F, Claussen CD, Haring HU. Association of increased intramyocellular lipid content with insulin resistance in lean nondiabetic offspring of type 2 diabetic subjects. Diabetes 1999;48(5):1113-1119.
53. Elder GC, Kirk J, Stewart G, Cook K, Weir D, Marshall A, Leahey L. Contributing factors to muscle weakness in children with cerebral palsy. Dev Med Child Neurol 2003;45(8):542-550.
54. Poon DM, Hui-Chan CW. Hyperactive stretch reflexes, co-contraction, and muscle weakness in children with cerebral palsy. Dev Med Child Neurol 2009;51(2):128-135.
55. Wiley ME, Damiano DL. Lower-extremity strength profiles in spastic cerebral palsy. Dev Med Child Neurol 1998;40(2):100-107.
56. Fry NR, Gough M, McNee AE, Shortland AP. Changes in the volume and length of the medial gastrocnemius after surgical recession in children with spastic diplegic cerebral palsy. J Pediatr Orthop 2007;27(7):769-774.
57. Oberhofer K, Stott NS, Mithraratne K, Anderson IA. Subject-specific modelling of lower limb muscles in children with cerebral palsy. Clin Biomech (Bristol, Avon) 2010;25(1):88-94.
58. Barber L, Hastings-Ison T, Baker R, Barrett R, Lichtwark G. Medial gastrocnemius muscle volume and fascicle length in children aged 2 to 5 years with cerebral palsy. Dev Med Child Neurol 2011;53(6):543-548.
59. Malaiya R, McNee AE, Fry NR, Eve LC, Gough M, Shortland AP. The morphology of the medial gastrocnemius in typically developing children and children with spastic hemiplegic cerebral palsy. J Electromyogr Kinesiol 2007;17(6):657-663.
60. Shortland A. Muscle deficits in cerebral palsy and early loss of mobility: can we learn something from our elders? Dev Med Child Neurol 2009;51 Suppl 4:59-63.
61. Barrett RS, Lichtwark GA. Gross muscle morphology and structure in spastic cerebral palsy: a systematic review. Dev Med Child Neurol 2010;52(9):794-804.
62. Hardin BJ, Campbell KS, Smith JD, Arbogast S, Smith J, Moylan JS, Reid MB. TNF-alpha acts via TNFR1 and muscle-derived oxidants to depress myofibrillar force in murine skeletal muscle. J Appl Physiol 2008;104(3):694-699.
63. Manini TM, Clark BC, Nalls MA, Goodpaster BH, Ploutz-Snyder LL, Harris TB. Reduced physical activity increases intermuscular adipose tissue in healthy young adults. Am J Clin Nutr 2007;85(2):377-384.
64. Tuttle LJ, Sinacore DR, Cade WT, Mueller MJ. Lower physical activity is associated with higher intermuscular adipose tissue in people with type 2 diabetes and peripheral neuropathy. Phys Ther 2011;91(6):923-930.

65. Leskinen T, Sipila S, Alen M, Cheng S, Pietilainen KH, Usenius JP, Suominen H, Kovanen V, Kainulainen H, Kaprio J, Kujala UM. Leisure-time physical activity and high-risk fat: a longitudinal population-based twin study. International journal of obesity 2009;33(11):1211-1218.
66. Goodpaster BH, Chomentowski P, Ward BK, Rossi A, Glynn NW, Delmonico MJ, Kritchevsky SB, Pahor M, Newman AB. Effects of physical activity on strength and skeletal muscle fat infiltration in older adults: a randomized controlled trial. J Appl Physiol 2008;105(5):1498-1503.
67. Yoshida Y, Marcus RL, Lastayo PC. Intramuscular adipose tissue and central activation in older adults. Muscle Nerve 2012;46(5):813-816.
68. Visser M, Kritchevsky SB, Goodpaster BH, Newman AB, Nevitt M, Stamm E, Harris TB. Leg muscle mass and composition in relation to lower extremity performance in men and women aged 70 to 79: the health, aging and body composition study. J Am Geriatr Soc 2002;50(5):897-904.
69. Marcus RL, Addison O, Dibble LE, Foreman KB, Morrell G, Lastayo P. Intramuscular adipose tissue, sarcopenia, and mobility function in older individuals. J Aging Res 2012;2012:629637.
70. Petersen KF, Befroy D, Dufour S, Dziura J, Ariyan C, Rothman DL, DiPietro L, Cline GW, Shulman GI. Mitochondrial dysfunction in the elderly: possible role in insulin resistance. Science 2003;300(5622):1140-1142.
71. Gaskin CJ, Morris T. Physical activity, health-related quality of life, and psychosocial functioning of adults with cerebral palsy. J Phys Act Health 2008;5(1):146-157.
72. van Eck M, Dallmeijer AJ, Beckerman H, van den Hoven PA, Voorman JM, Becher JG. Physical activity level and related factors in adolescents with cerebral palsy. Pediatr Exerc Sci 2008;20(1):95-106.
73. Faulkner JA, Larkin LM, Claflin DR, Brooks SV. Age-related changes in the structure and function of skeletal muscles. Clin Exp Pharmacol Physiol 2007;34(11):1091-1096.
74. Alnaqeeb MA, Al Zaid NS, Goldspink G. Connective tissue changes and physical properties of developing and ageing skeletal muscle. J Anat 1984;139 (Pt 4):677-689.
75. Stackhouse SK, Stevens JE, Lee SC, Pearce KM, Snyder-Mackler L, Binder-Macleod SA. Maximum voluntary activation in nonfatigued and fatigued muscle of young and elderly individuals. Phys Ther 2001;81(5):1102-1109.
76. Johnson DL, Miller F, Subramanian P, Modlesky CM. Adipose tissue infiltration of skeletal muscle in children with cerebral palsy. J Pediatr 2009;154(5):715-720.
77. Bandini LG, Schoeller DA, Fukagawa NK, Wykes LJ, Dietz WH. Body composition and energy expenditure in adolescents with cerebral palsy or myelodysplasia. Pediatr Res 1991;29(1):70-77.
78. Gilbert SF. Developmental biology. Sunderland, Mass.: Sinauer Associates ; Basingstoke : Macmillan; 2000.
79. Parfitt AM. The actions of parathyroid hormone on bone: relation to bone remodeling and turnover, calcium homeostasis, and metabolic bone disease. Part III of IV parts; PTH and osteoblasts, the relationship between bone turnover and bone loss, and the state of the bones in primary hyperparathyroidism. Metabolism 1976;25(9):1033-1069.

80. van der Meulen MC, Ashford MW, Jr., Kiratli BJ, Bachrach LK, Carter DR. Determinants of femoral geometry and structure during adolescent growth. J Orthop Res 1996;14(1):22-29.
81. Rauch F, Schoenau E. The developing bone: slave or master of its cells and molecules? Pediatr Res 2001;50(3):309-314.
82. Rubin CT, Lanyon LE. Limb mechanics as a function of speed and gait: a study of functional strains in the radius and tibia of horse and dog. The Journal of experimental biology 1982;101:187-211.
83. Aamodt A, Lund-Larsen J, Eine J, Andersen E, Benum P, Husby OS. In vivo measurements show tensile axial strain in the proximal lateral aspect of the human femur. J Orthop Res 1997;15(6):927-931.
84. Parfitt AM. The two faces of growth: benefits and risks to bone integrity. Osteoporos Int 1994;4(6):382-398.
85. Seeman E, Hopper JL, Young NR, Formica C, Goss P, Tsalamandris C. Do genetic factors explain associations between muscle strength, lean mass, and bone density? A twin study. Am J Physiol 1996;270(2 Pt 1):E320-327.
86. Frost HM. Bone "mass" and the "mechanostat": a proposal. Anat Rec 1987;219(1):1-9.
87. Frost HM. Muscle, bone, and the Utah paradigm: a 1999 overview. Med Sci Sports Exerc 2000;32(5):911-917.
88. Rauch F. Bone growth in length and width: the Yin and Yang of bone stability. J Musculoskelet Neuronal Interact 2005;5(3):194-201.
89. Timoshenko S, Gere JM. Mechanics of materials. New York ; London: Van Nostrand Reinhold; 1972.
90. Ruff C. Growth in bone strength, body size, and muscle size in a juvenile longitudinal sample. Bone 2003;33(3):317-329.
91. Macdonald H, Kontulainen S, Petit M, Janssen P, McKay H. Bone strength and its determinants in pre- and early pubertal boys and girls. Bone 2006;39(3):598-608.
92. Smith EL, Gilligan C. Physical activity effects on bone metabolism. Calcif Tissue Int 1991;49 Suppl:S50-54.
93. Carter DR. The relationship between in vivo strains and cortical bone remodeling. Critical reviews in biomedical engineering 1982;8(1):1-28.
94. Jones HH, Priest JD, Hayes WC, Tichenor CC, Nagel DA. Humeral hypertrophy in response to exercise. J Bone Joint Surg Am 1977;59(2):204-208.
95. Haapasalo H, Kannus P, Sievanen H, Pasanen M, Uusi-Rasi K, Heinonen A, Oja P, Vuori I. Effect of long-term unilateral activity on bone mineral density of female junior tennis players. Journal of bone and mineral research : the official journal of the American Society for Bone and Mineral Research 1998;13(2):310-319.
96. Brown JK, Rodda J, Walsh EG, Wright GW. Neurophysiology of lower-limb function in hemiplegic children. Dev Med Child Neurol 1991;33(12):1037-1047.
97. Foran JR, Steinman S, Barash I, Chambers HG, Lieber RL. Structural and mechanical alterations in spastic skeletal muscle. Dev Med Child Neurol 2005;47(10):713-717.
98. Lieber RL, Steinman S, Barash IA, Chambers H. Structural and functional changes in spastic skeletal muscle. Muscle Nerve 2004;29(5):615-627.

99. Castle ME, Reyman TA, Schneider M. Pathology of spastic muscle in cerebral palsy. Clin Orthop Relat Res 1979(142):223-232.
100. Tedroff K, Knutson LM, Soderberg GL. Synergistic muscle activation during maximum voluntary contractions in children with and without spastic cerebral palsy. Dev Med Child Neurol 2006;48(10):789-796.
101. Perry J. Determinants of muscle function in the spastic lower extremity. Clin Orthop Relat Res 1993(288):10-26.
102. Rose J, Martin JG, Torburn L, Rinsky LA, Gamble JG. Electromyographic differentiation of diplegic cerebral palsy from idiopathic toe walking: involuntary coactivation of the quadriceps and gastrocnemius. J Pediatr Orthop 1999;19(5):677-682.
103. Davids JR, Holland WC, Sutherland DH. Significance of the confusion test in cerebral palsy. J Pediatr Orthop 1993;13(6):717-721.
104. Berger W, Quintern J, Dietz V. Pathophysiology of gait in children with cerebral palsy. Electroencephalogr Clin Neurophysiol 1982;53(5):538-548.
105. Stackhouse SK, Binder-Macleod SA, Lee SC. Voluntary muscle activation, contractile properties, and fatigability in children with and without cerebral palsy. Muscle Nerve 2005;31(5):594-601.
106. Rose J, McGill KC. Neuromuscular activation and motor-unit firing characteristics in cerebral palsy. Dev Med Child Neurol 2005;47(5):329-336.
107. Gormley ME, Jr. Treatment of neuromuscular and musculoskeletal problems in cerebral palsy. Pediatr Rehabil 2001;4(1):5-16.
108. Murphy KP, Molnar GE, Lankasky K. Medical and functional status of adults with cerebral palsy. Dev Med Child Neurol 1995;37(12):1075-1084.
109. Friden J, Lieber RL. Spastic muscle cells are shorter and stiffer than normal cells. Muscle Nerve 2003;27(2):157-164.
110. O'Dwyer NJ, Neilson PD, Nash J. Mechanisms of muscle growth related to muscle contracture in cerebral palsy. Dev Med Child Neurol 1989;31(4):543-547.
111. Mohagheghi AA, Khan T, Meadows TH, Giannikas K, Baltzopoulos V, Maganaris CN. In vivo gastrocnemius muscle fascicle length in children with and without diplegic cerebral palsy. Dev Med Child Neurol 2008;50(1):44-50.
112. Mohagheghi AA, Khan T, Meadows TH, Giannikas K, Baltzopoulos V, Maganaris CN. Differences in gastrocnemius muscle architecture between the paretic and non-paretic legs in children with hemiplegic cerebral palsy. Clin Biomech (Bristol, Avon) 2007;22(6):718-724.
113. Shortland AP, Harris CA, Gough M, Robinson RO. Architecture of the medial gastrocnemius in children with spastic diplegia. Dev Med Child Neurol 2002;44(3):158-163.
114. Riad J, Haglund-Akerlind Y, Miller F. Power generation in children with spastic hemiplegic cerebral palsy. Gait Posture 2008;27(4):641-647.
115. Ross SA, Engsberg JR. Relationships between spasticity, strength, gait, and the GMFM-66 in persons with spastic diplegia cerebral palsy. Arch Phys Med Rehabil 2007;88(9):1114-1120.
116. Lampe R, Grassl S, Mitternacht J, Gerdesmeyer L, Gradinger R. MRT-measurements of muscle volumes of the lower extremities of youths with

spastic hemiplegia caused by cerebral palsy. Brain Dev 2006;28(8):500-506.
117. Shortland AP. Muscle volume and motor development in spastic cerebral palsy. Dev Med Child Neurol 2011;53(6):486.
118. Lieber RL, Friden J. Functional and clinical significance of skeletal muscle architecture. Muscle Nerve 2000;23(11):1647-1666.
119. Booth CM, Cortina-Borja MJ, Theologis TN. Collagen accumulation in muscles of children with cerebral palsy and correlation with severity of spasticity. Dev Med Child Neurol 2001;43(5):314-320.
120. Lieber RL, Runesson E, Einarsson F, Friden J. Inferior mechanical properties of spastic muscle bundles due to hypertrophic but compromised extracellular matrix material. Muscle Nerve 2003;28(4):464-471.
121. Kovanlikaya A, Mittelman SD, Ward A, Geffner ME, Dorey F, Gilsanz V. Obesity and fat quantification in lean tissues using three-point Dixon MR imaging. Pediatr Radiol 2005;35(6):601-607.
122. Bauman WA. The potential metabolic consequences of cerebral palsy: inferences from the general population and persons with spinal cord injury. Dev Med Child Neurol 2009;51 Suppl 4:64-78.
123. Morino K, Petersen KF, Dufour S, Befroy D, Frattini J, Shatzkes N, Neschen S, White MF, Bilz S, Sono S, Pypaert M, Shulman GI. Reduced mitochondrial density and increased IRS-1 serine phosphorylation in muscle of insulin-resistant offspring of type 2 diabetic parents. J Clin Invest 2005;115(12):3587-3593.
124. Houmard JA, Tanner CJ, Yu C, Cunningham PG, Pories WJ, MacDonald KG, Shulman GI. Effect of weight loss on insulin sensitivity and intramuscular long-chain fatty acyl-CoAs in morbidly obese subjects. Diabetes 2002;51(10):2959-2963.
125. Cree MG, Newcomer BR, Katsanos CS, Sheffield-Moore M, Chinkes D, Aarsland A, Urban R, Wolfe RR. Intramuscular and liver triglycerides are increased in the elderly. J Clin Endocrinol Metab 2004;89(8):3864-3871.
126. Goodpaster BH, Krishnaswami S, Harris TB, Katsiaras A, Kritchevsky SB, Simonsick EM, Nevitt M, Holvoet P, Newman AB. Obesity, regional body fat distribution, and the metabolic syndrome in older men and women. Arch Intern Med 2005;165(7):777-783.
127. Kuhlmann J, Neumann-Haefelin C, Belz U, Kalisch J, Juretschke HP, Stein M, Kleinschmidt E, Kramer W, Herling AW. Intramyocellular lipid and insulin resistance: a longitudinal in vivo 1H-spectroscopic study in Zucker diabetic fatty rats. Diabetes 2003;52(1):138-144.
128. Perseghin G, Scifo P, De Cobelli F, Pagliato E, Battezzati A, Arcelloni C, Vanzulli A, Testolin G, Pozza G, Del Maschio A, Luzi L. Intramyocellular triglyceride content is a determinant of in vivo insulin resistance in humans: a 1H-13C nuclear magnetic resonance spectroscopy assessment in offspring of type 2 diabetic parents. Diabetes 1999;48(8):1600-1606.
129. Dube J, Goodpaster BH. Assessment of intramuscular triglycerides: contribution to metabolic abnormalities. Curr Opin Clin Nutr Metab Care 2006;9(5):553-559.
130. Schrauwen P, Hesselink MK. Oxidative capacity, lipotoxicity, and mitochondrial damage in type 2 diabetes. Diabetes 2004;53(6):1412-1417.

131. Zoico E, Rossi A, Di Francesco V, Sepe A, Olioso D, Pizzini F, Fantin F, Bosello O, Cominacini L, Harris TB, Zamboni M. Adipose tissue infiltration in skeletal muscle of healthy elderly men: relationships with body composition, insulin resistance, and inflammation at the systemic and tissue level. J Gerontol A Biol Sci Med Sci 2010;65(3):295-299.
132. Roden M, Price TB, Perseghin G, Petersen KF, Rothman DL, Cline GW, Shulman GI. Mechanism of free fatty acid-induced insulin resistance in humans. J Clin Invest 1996;97(12):2859-2865.
133. Yu C, Chen Y, Cline GW, Zhang D, Zong H, Wang Y, Bergeron R, Kim JK, Cushman SW, Cooney GJ, Atcheson B, White MF, Kraegen EW, Shulman GI. Mechanism by which fatty acids inhibit insulin activation of insulin receptor substrate-1 (IRS-1)-associated phosphatidylinositol 3-kinase activity in muscle. J Biol Chem 2002;277(52):50230-50236.
134. Lowell BB, Shulman GI. Mitochondrial dysfunction and type 2 diabetes. Science 2005;307(5708):384-387.
135. Schrauwen-Hinderling VB, Kooi ME, Hesselink MK, Jeneson JA, Backes WH, van Echteld CJ, van Engelshoven JM, Mensink M, Schrauwen P. Impaired in vivo mitochondrial function but similar intramyocellular lipid content in patients with type 2 diabetes mellitus and BMI-matched control subjects. Diabetologia 2007;50(1):113-120.
136. Phielix E, Schrauwen-Hinderling VB, Mensink M, Lenaers E, Meex R, Hoeks J, Kooi ME, Moonen-Kornips E, Sels JP, Hesselink MK, Schrauwen P. Lower intrinsic ADP-stimulated mitochondrial respiration underlies in vivo mitochondrial dysfunction in muscle of male type 2 diabetic patients. Diabetes 2008;57(11):2943-2949.
137. Petersen KF, Dufour S, Befroy D, Garcia R, Shulman GI. Impaired mitochondrial activity in the insulin-resistant offspring of patients with type 2 diabetes. N Engl J Med 2004;350(7):664-671.
138. Goodpaster BH, He J, Watkins S, Kelley DE. Skeletal muscle lipid content and insulin resistance: evidence for a paradox in endurance-trained athletes. J Clin Endocrinol Metab 2001;86(12):5755-5761.
139. Tarnopolsky MA, Rennie CD, Robertshaw HA, Fedak-Tarnopolsky SN, Devries MC, Hamadeh MJ. Influence of endurance exercise training and sex on intramyocellular lipid and mitochondrial ultrastructure, substrate use, and mitochondrial enzyme activity. Am J Physiol Regul Integr Comp Physiol 2007;292(3):R1271-1278.
140. Chomentowski P, Coen PM, Radikova Z, Goodpaster BH, Toledo FG. Skeletal muscle mitochondria in insulin resistance: differences in intermyofibrillar versus subsarcolemmal subpopulations and relationship to metabolic flexibility. J Clin Endocrinol Metab 2011;96(2):494-503.
141. Crane JD, Devries MC, Safdar A, Hamadeh MJ, Tarnopolsky MA. The effect of aging on human skeletal muscle mitochondrial and intramyocellular lipid ultrastructure. J Gerontol A Biol Sci Med Sci 2010;65(2):119-128.
142. Peterson MD, Gordon PM, Hurvitz EA. Chronic disease risk among adults with cerebral palsy: the role of premature sarcopoenia, obesity and sedentary behaviour. Obes Rev 2012.
143. Ward KA, Roberts SA, Adams JE, Mughal MZ. Bone geometry and density in the skeleton of pre-pubertal gymnasts and school children. Bone 2005;36(6):1012-1018.

144. Schoenau E, Neu MC, Manz F. Muscle mass during childhood--relationship to skeletal development. J Musculoskelet Neuronal Interact 2004;4(1):105-108.
145. Heinonen A, McKay HA, Whittall KP, Forster BB, Khan KM. Muscle cross-sectional area is associated with specific site of bone in prepubertal girls: a quantitative magnetic resonance imaging study. Bone 2001;29(4):388-392.
146. McKay HA, Petit MA, Khan KM, Schutz RW. Lifestyle determinants of bone mineral: A comparison between prepubertal Asian- and Caucasian-Canadian boys and girls. Calcified Tissue Int 2000;66(5):320-324.
147. Binkley T, Johnson J, Vogel L, Kecskemethy H, Henderson R, Specker B. Bone measurements by peripheral quantitative computed tomography (pQCT) in children with cerebral palsy. J Pediatr 2005;147(6):791-796.
148. Lee JJ, Lyne ED. Pathologic fractures in severely handicapped children and young adults. J Pediatr Orthop 1990;10(4):497-500.
149. McIvor WC, Samilson RL. Fractures in patients with cerebral palsy. J Bone Joint Surg Am 1966;48(5):858-866.
150. Presedo A, Dabney KW, Miller F. Fractures in patients with cerebral palsy. J Pediatr Orthop 2007;27(2):147-153.
151. Leet AI, Mesfin A, Pichard C, Launay F, Brintzenhofeszoc K, Levey EB, P DS. Fractures in children with cerebral palsy. J Pediatr Orthop 2006;26(5):624-627.
152. Stevenson RD, Conaway M, Barrington JW, Cuthill SL, Worley G, Henderson RC. Fracture rate in children with cerebral palsy. Pediatr Rehabil 2006;9(4):396-403.
153. Goulding A. Risk factors for fractures in normally active children and adolescents. Medicine and sport science 2007;51:102-120.
154. Prentice A, Parsons TJ, Cole TJ. Uncritical use of bone mineral density in absorptiometry may lead to size-related artifacts in the identification of bone mineral determinants. Am J Clin Nutr 1994;60(6):837-842.
155. Stallings VA, Charney EB, Davies JC, Cronk CE. Nutritional status and growth of children with diplegic or hemiplegic cerebral palsy. Dev Med Child Neurol 1993;35(11):997-1006.
156. Modlesky CM, Kanoff SA, Johnson DL, Subramanian P, Miller F. Evaluation of the femoral midshaft in children with cerebral palsy using magnetic resonance imaging. Osteoporos Int 2009;20(4):609-615.
157. Ahnert-Hilger G, Bigalke H. Molecular aspects of tetanus and botulinum neurotoxin poisoning. Prog Neurobiol 1995;46(1):83-96.
158. Blasi J, Chapman ER, Link E, Binz T, Yamasaki S, De Camilli P, Sudhof TC, Niemann H, Jahn R. Botulinum neurotoxin A selectively cleaves the synaptic protein SNAP-25. Nature 1993;365(6442):160-163.
159. Borodic GE, Ferrante R, Pearce LB, Smith K. Histologic assessment of dose-related diffusion and muscle fiber response after therapeutic botulinum A toxin injections. Mov Disord 1994;9(1):31-39.
160. Boyce WF, Gowland C, Hardy S, Rosenbaum PL, Lane M, Plews N, Goldsmith C, Russell DJ. Development of a quality-of-movement measure for children with cerebral palsy. Phys Ther 1991;71(11):820-828; discussion 828-832.
161. Novacheck TF, Stout JL, Tervo R. Reliability and validity of the Gillette Functional Assessment Questionnaire as an outcome measure in children with walking disabilities. J Pediatr Orthop 2000;20(1):75-81.

162. Podsiadlo D, Richardson S. The timed "Up & Go": a test of basic functional mobility for frail elderly persons. J Am Geriatr Soc 1991;39(2):142-148.
163. Palisano RJ, Rosenbaum P, Bartlett D, Livingston MH. Content validity of the expanded and revised Gross Motor Function Classification System. Dev Med Child Neurol 2008;50(10):744-750.
164. Wood E, Rosenbaum P. The gross motor function classification system for cerebral palsy: a study of reliability and stability over time. Dev Med Child Neurol 2000;42(5):292-296.
165. Rosenbaum PL, Walter SD, Hanna SE, Palisano RJ, Russell DJ, Raina P, Wood E, Bartlett DJ, Galuppi BE. Prognosis for gross motor function in cerebral palsy: creation of motor development curves. JAMA 2002;288(11):1357-1363.
166. Oeffinger D, Gorton G, Bagley A, Nicholson D, Barnes D, Calmes J, Abel M, Damiano D, Kryscio R, Rogers S, Tylkowski C. Outcome assessments in children with cerebral palsy, part I: descriptive characteristics of GMFCS Levels I to III. Dev Med Child Neurol 2007;49(3):172-180.
167. Russell DR, PL. Gowland, C. Manual Gross Motor Function; A measure of Gross Motor Function in Cerebral Palsy. Hamilton, Ontario Canada: Chedoke-McMaster Hospitals; 1990.
168. Bjornson K, Graubert C, McLaughlin J. Test-retest reliability of the gross motor function measure in children with cerebral palsy. Pediatr Phys Ther 2000;12(4):200-202.
169. Wong EC, Man DW. Gross motor function measure for children with cerebral palsy. Int J Rehabil Res 2005;28(4):355-359.
170. McLaughlin JF, Bjornson KF, Astley SJ, Graubert C, Hays RM, Roberts TS, Price R, Temkin N. Selective dorsal rhizotomy: efficacy and safety in an investigator-masked randomized clinical trial. Dev Med Child Neurol 1998;40(4):220-232.
171. Steinbok P, Reiner AM, Beauchamp R, Armstrong RW, Cochrane DD, Kestle J. A randomized clinical trial to compare selective posterior rhizotomy plus physiotherapy with physiotherapy alone in children with spastic diplegic cerebral palsy. Dev Med Child Neurol 1997;39(3):178-184.
172. Wright FV, Sheil EM, Drake JM, Wedge JH, Naumann S. Evaluation of selective dorsal rhizotomy for the reduction of spasticity in cerebral palsy: a randomized controlled tria. Dev Med Child Neurol 1998;40(4):239-247.
173. Tedroff K, Lowing K, Jacobson DN, Astrom E. Does loss of spasticity matter? A 10-year follow-up after selective dorsal rhizotomy in cerebral palsy. Dev Med Child Neurol 2011.
174. Nordmark E, Jarnlo GB, Hagglund G. Comparison of the Gross Motor Function Measure and Paediatric Evaluation of Disability Inventory in assessing motor function in children undergoing selective dorsal rhizotomy. Dev Med Child Neurol 2000;42(4):245-252.
175. Nordmark E, Josenby AL, Lagergren J, Andersson G, Stromblad LG, Westbom L. Long-term outcomes five years after selective dorsal rhizotomy. BMC Pediatr 2008;8:54.
176. Lundkvist Josenby A, Jarnlo GB, Gummesson C, Nordmark E. Longitudinal construct validity of the GMFM-88 total score and goal total score and the GMFM-66 score in a 5-year follow-up study. Phys Ther 2009;89(4):342-350.

177. Farmer JP, Sabbagh AJ. Selective dorsal rhizotomies in the treatment of spasticity related to cerebral palsy. Childs Nerv Syst 2007;23(9):991-1002.
178. Reynolds MR, Ray WZ, Strom RG, Blackburn SL, Lee A, Park TS. Clinical outcomes after selective dorsal rhizotomy in an adult population. World Neurosurg 2011;75(1):138-144.
179. Steinbok P, McLeod K. Comparison of motor outcomes after selective dorsal rhizotomy with and without preoperative intensified physiotherapy in children with spastic diplegic cerebral palsy. Pediatr Neurosurg 2002;36(3):142-147.
180. Almeida GL, Campbell SK, Girolami GL, Penn RD, Corcos DM. Multidimensional assessment of motor function in a child with cerebral palsy following intrathecal administration of baclofen. Phys Ther 1997;77(7):751-764.
181. Bower E, McLellan DL, Arney J, Campbell MJ. A randomised controlled trial of different intensities of physiotherapy and different goal-setting procedures in 44 children with cerebral palsy. Dev Med Child Neurol 1996;38(3):226-237.
182. MacPhail HE, Kramer JF. Effect of isokinetic strength-training on functional ability and walking efficiency in adolescents with cerebral palsy. Dev Med Child Neurol 1995;37(9):763-775.
183. Abel MF, Damiano DL, McLaughlin JF, Song KM, Graubert CS, Bjornson KF. Comparison of functional outcomes from orthopedic and neurosurgical interventions in spastic diplegia. Neurosurg Focus 1998;4(1):e2.
184. Russell DJ, Avery LM, Rosenbaum PL, Raina PS, Walter SD, Palisano RJ. Improved scaling of the gross motor function measure for children with cerebral palsy: evidence of reliability and validity. Phys Ther 2000;80(9):873-885.
185. McLaughlin J, Bjornson K, Temkin N, Steinbok P, Wright V, Reiner A, Roberts T, Drake J, O'Donnell M, Rosenbaum P, Barber J, Ferrel A. Selective dorsal rhizotomy: meta-analysis of three randomized controlled trials. Dev Med Child Neurol 2002;44(1):17-25.
186. Steinbok P, Reiner A, Kestle JR. Therapeutic electrical stimulation following selective posterior rhizotomy in children with spastic diplegic cerebral palsy: a randomized clinical trial. Dev Med Child Neurol 1997;39(8):515-520.
187. Sanger TD, Chen D, Delgado MR, Gaebler-Spira D, Hallett M, Mink JW, Taskforce on Childhood Motor D. Definition and classification of negative motor signs in childhood. Pediatrics 2006;118(5):2159-2167.
188. Fowler EG, Staudt LA, Greenberg MB, Oppenheim WL. Selective Control Assessment of the Lower Extremity (SCALE): development, validation, and interrater reliability of a clinical tool for patients with cerebral palsy. Dev Med Child Neurol 2009;51(8):607-614.
189. Evarts EV. Relation of pyramidal tract activity to force exerted during voluntary movement. J Neurophysiol 1968;31(1):14-27.
190. Staudt M, Pavlova M, Bohm S, Grodd W, Krageloh-Mann I. Pyramidal tract damage correlates with motor dysfunction in bilateral periventricular leukomalacia (PVL). Neuropediatrics 2003;34(4):182-188.

191. Lindberg PG, Feydy A, Maier MA. White matter organization in cervical spinal cord relates differently to age and control of grip force in healthy subjects. J Neurosci 2010;30(11):4102-4109.
192. Voorman JM, Dallmeijer AJ, Knol DL, Lankhorst GJ, Becher JG. Prospective longitudinal study of gross motor function in children with cerebral palsy. Arch Phys Med Rehabil 2007;88(7):871-876.
193. Boyd RN, Graham HK. Objective measurement of clinical findings in the use of botulinum toxin type A for the management of children with cerebral palsy. European Journal of Neurology 1999;6:s23-s35.
194. Fowler EG, Knutson LM, DeMuth SK, Sugi M, Siebert K, Simms V, Azen SP, Winstein CJ. Pediatric endurance and limb strengthening for children with cerebral palsy (PEDALS)--a randomized controlled trial protocol for a stationary cycling intervention. BMC Pediatr 2007;7:14.
195. Fowler EG, Staudt LA, Greenberg MB. Lower-extremity selective voluntary motor control in patients with spastic cerebral palsy: increased distal motor impairment. Dev Med Child Neurol 2010;52(3):264-269.
196. Fowler EG, Goldberg EJ. The effect of lower extremity selective voluntary motor control on interjoint coordination during gait in children with spastic diplegic cerebral palsy. Gait Posture 2009;29(1):102-107.
197. Lindberg P, Ody C, Feydy A, Maier MA. Precision in isometric precision grip force is reduced in middle-aged adults. Exp Brain Res 2009;193(2):213-224.
198. Scholtes VA, Becher JG, Beelen A, Lankhorst GJ. Clinical assessment of spasticity in children with cerebral palsy: a critical review of available instruments. Dev Med Child Neurol 2006;48(1):64-73.
199. Ashworth B. Preliminary Trial of Carisoprodol in Multiple Sclerosis. Practitioner 1964;192:540-542.
200. Tardieu G, Shentoub S, Delarue R. [Research on a technic for measurement of spasticity]. Rev Neurol (Paris) 1954;91(2):143-144.
201. Held J-P. Reeducation Motrice des Affections Neurologiques. Paris: Bailliere; 1969.
202. Little JW, Halar EM. H-reflex changes following spinal cord injury. Arch Phys Med Rehabil 1985;66(1):19-22.
203. Crone C, Johnsen LL, Biering-Sorensen F, Nielsen JB. Appearance of reciprocal facilitation of ankle extensors from ankle flexors in patients with stroke or spinal cord injury. Brain 2003;126(Pt 2):495-507.
204. Levin MF, Hui-Chan C. Are H and stretch reflexes in hemiparesis reproducible and correlated with spasticity? J Neurol 1993;240(2):63-71.
205. Bakheit AM, Maynard VA, Curnow J, Hudson N, Kodapala S. The relation between Ashworth scale scores and the excitability of the alpha motor neurones in patients with post-stroke muscle spasticity. J Neurol Neurosurg Psychiatry 2003;74(5):646-648.
206. Pisano F, Miscio G, Del Conte C, Pianca D, Candeloro E, Colombo R. Quantitative measures of spasticity in post-stroke patients. Clin Neurophysiol 2000;111(6):1015-1022.
207. Pandyan AD, Price CI, Rodgers H, Barnes MP, Johnson GR. Biomechanical examination of a commonly used measure of spasticity. Clin Biomech (Bristol, Avon) 2001;16(10):859-865.

208. Pandyan AD, Price CI, Barnes MP, Johnson GR. A biomechanical investigation into the validity of the modified Ashworth Scale as a measure of elbow spasticity. Clin Rehabil 2003;17(3):290-293.
209. Chen JJ, Wu YN, Huang SC, Lee HM, Wang YL. The use of a portable muscle tone measurement device to measure the effects of botulinum toxin type a on elbow flexor spasticity. Arch Phys Med Rehabil 2005;86(8):1655-1660.
210. Biering-Sorensen F, Nielsen JB, Klinge K. Spasticity-assessment: a review. Spinal Cord 2006;44(12):708-722.
211. Khoury V, Cardinal E, Brassard P. Atrophy and fatty infiltration of the supraspinatus muscle: sonography versus MRI. AJR Am J Roentgenol 2008;190(4):1105-1111.
212. Goutallier D, Postel JM, Bernageau J, Lavau L, Voisin MC. Fatty muscle degeneration in cuff ruptures. Pre- and postoperative evaluation by CT scan. Clin Orthop Relat Res 1994(304):78-83.
213. Pfirrmann CW, Schmid MR, Zanetti M, Jost B, Gerber C, Hodler J. Assessment of fat content in supraspinatus muscle with proton MR spectroscopy in asymptomatic volunteers and patients with supraspinatus tendon lesions. Radiology 2004;232(3):709-715.
214. Boesch C, Slotboom J, Hoppeler H, Kreis R. In vivo determination of intra-myocellular lipids in human muscle by means of localized 1H-MR-spectroscopy. Magn Reson Med 1997;37(4):484-493.
215. Schick F, Machann J, Brechtel K, Strempfer A, Klumpp B, Stein DT, Jacob S. MRI of muscular fat. Magn Reson Med 2002;47(4):720-727.
216. Szczepaniak LS, Babcock EE, Schick F, Dobbins RL, Garg A, Burns DK, McGarry JD, Stein DT. Measurement of intracellular triglyceride stores by H spectroscopy: validation in vivo. Am J Physiol 1999;276(5 Pt 1):E977-989.
217. Dixon WT. Simple proton spectroscopic imaging. Radiology 1984;153(1):189-194.
218. Reeder SB, Pineda AR, Wen Z, Shimakawa A, Yu H, Brittain JH, Gold GE, Beaulieu CH, Pelc NJ. Iterative decomposition of water and fat with echo asymmetry and least-squares estimation (IDEAL): application with fast spin-echo imaging. Magn Reson Med 2005;54(3):636-644.
219. Reeder SB, McKenzie CA, Pineda AR, Yu H, Shimakawa A, Brau AC, Hargreaves BA, Gold GE, Brittain JH. Water-fat separation with IDEAL gradient-echo imaging. J Magn Reson Imaging 2007;25(3):644-652.
220. Reeder SB, Sirlin CB. Quantification of liver fat with magnetic resonance imaging. Magn Reson Imaging Clin N Am 2010;18(3):337-357, ix.
221. Karampinos DC, Baum T, Nardo L, Alizai H, Yu H, Carballido-Gamio J, Yap SP, Shimakawa A, Link TM, Majumdar S. Characterization of the regional distribution of skeletal muscle adipose tissue in type 2 diabetes using chemical shift-based water/fat separation. J Magn Reson Imaging 2012;35(4):899-907.
222. Wren TA, Bluml S, Tseng-Ong L, Gilsanz V. Three-point technique of fat quantification of muscle tissue as a marker of disease progression in Duchenne muscular dystrophy: preliminary study. AJR Am J Roentgenol 2008;190(1):W8-12.
223. Wokke BH, Bos C, Reijnierse M, van Rijswijk CS, Eggers H, Webb A, Verschuuren JJ, Kan HE. Comparison of dixon and T1-weighted MR methods

to assess the degree of fat infiltration in duchenne muscular dystrophy patients. J Magn Reson Imaging 2013;38(3):619-624.
224. Glover GH. Multipoint Dixon technique for water and fat proton and susceptibility imaging. J Magn Reson Imaging 1991;1(5):521-530.
225. Ma J. Dixon techniques for water and fat imaging. J Magn Reson Imaging 2008;28(3):543-558.
226. S B Reeder MTA, N J Pelc. Water and Fat SSFP Imaging with Four-Point Dixon Techniques. 2002
227. Muller K, Homberg V. Development of speed of repetitive movements in children is determined by structural changes in corticospinal efferents. Neuroscience letters 1992;144(1-2):57-60.
228. Nezu A, Kimura S, Uehara S, Kobayashi T, Tanaka M, Saito K. Magnetic stimulation of motor cortex in children: maturity of corticospinal pathway and problem of clinical application. Brain Dev 1997;19(3):176-180.
229. Carr LJ, Harrison LM, Evans AL, Stephens JA. Patterns of central motor reorganization in hemiplegic cerebral palsy. Brain 1993;116 (Pt 5):1223-1247.
230. Eyre JA, Taylor JP, Villagra F, Smith M, Miller S. Evidence of activity-dependent withdrawal of corticospinal projections during human development. Neurology 2001;57(9):1543-1554.
231. Staudt M, Grodd W, Gerloff C, Erb M, Stitz J, Krageloh-Mann I. Two types of ipsilateral reorganization in congenital hemiparesis: a TMS and fMRI study. Brain 2002;125(Pt 10):2222-2237.
232. Maegaki Y, Maeoka Y, Ishii S, Eda I, Ohtagaki A, Kitahara T, Suzuki N, Yoshino K, Ieshima A, Koeda T, Takeshita K. Central motor reorganization in cerebral palsy patients with bilateral cerebral lesions. Pediatr Res 1999;45(4 Pt 1):559-567.
233. Meyer BU, Roricht S, Grafin von Einsiedel H, Kruggel F, Weindl A. Inhibitory and excitatory interhemispheric transfers between motor cortical areas in normal humans and patients with abnormalities of the corpus callosum. Brain 1995;118 (Pt 2):429-440.
234. Heinen F, Kirschner J, Fietzek U, Glocker FX, Mall V, Korinthenberg R. Absence of transcallosal inhibition in adolescents with diplegic cerebral palsy. Muscle Nerve 1999;22(2):255-257.
235. Arzoumanian Y, Mirmiran M, Barnes PD, Woolley K, Ariagno RL, Moseley ME, Fleisher BE, Atlas SW. Diffusion tensor brain imaging findings at term-equivalent age may predict neurologic abnormalities in low birth weight preterm infants. AJNR Am J Neuroradiol 2003;24(8):1646-1653.
236. Woodward LJ, Anderson PJ, Austin NC, Howard K, Inder TE. Neonatal MRI to predict neurodevelopmental outcomes in preterm infants. N Engl J Med 2006;355(7):685-694.
237. Nanba Y, Matsui K, Aida N, Sato Y, Toyoshima K, Kawataki M, Hoshino R, Ohyama M, Itani Y, Goto A, Oka A. Magnetic resonance imaging regional T1 abnormalities at term accurately predict motor outcome in preterm infants. Pediatrics 2007;120(1):e10-19.
238. Bax M, Tydeman C, Flodmark O. Clinical and MRI correlates of cerebral palsy: the European Cerebral Palsy Study. JAMA 2006;296(13):1602-1608.

239. Fan GG, Yu B, Quan SM, Sun BH, Guo QY. Potential of diffusion tensor MRI in the assessment of periventricular leukomalacia. Clinical radiology 2006;61(4):358-364.
240. Hoon AH, Jr., Stashinko EE, Nagae LM, Lin DD, Keller J, Bastian A, Campbell ML, Levey E, Mori S, Johnston MV. Sensory and motor deficits in children with cerebral palsy born preterm correlate with diffusion tensor imaging abnormalities in thalamocortical pathways. Dev Med Child Neurol 2009;51(9):697-704.
241. Nagae LM, Hoon AH, Jr., Stashinko E, Lin D, Zhang W, Levey E, Wakana S, Jiang H, Leite CC, Lucato LT, van Zijl PC, Johnston MV, Mori S. Diffusion tensor imaging in children with periventricular leukomalacia: variability of injuries to white matter tracts. AJNR Am J Neuroradiol 2007;28(7):1213-1222.
242. Panigrahy A, Barnes PD, Robertson RL, Sleeper LA, Sayre JW. Quantitative analysis of the corpus callosum in children with cerebral palsy and developmental delay: correlation with cerebral white matter volume. Pediatr Radiol 2005;35(12):1199-1207.
243. Son SM, Ahn YH, Sakong J, Moon HK, Ahn SH, Lee H, Yu IK, Shin YJ, Jang SH. Diffusion tensor imaging demonstrates focal lesions of the corticospinal tract in hemiparetic patients with cerebral palsy. Neuroscience letters 2007;420(1):34-38.
244. Thomas B, Eyssen M, Peeters R, Molenaers G, Van Hecke P, De Cock P, Sunaert S. Quantitative diffusion tensor imaging in cerebral palsy due to periventricular white matter injury. Brain 2005;128(Pt 11):2562-2577.
245. Yoshida S, Hayakawa K, Yamamoto A, Okano S, Kanda T, Yamori Y, Yoshida N, Hirota H. Quantitative diffusion tensor tractography of the motor and sensory tract in children with cerebral palsy. Dev Med Child Neurol 2010;52(10):935-940.
246. Schwartz ED, Cooper ET, Fan Y, Jawad AF, Chin CL, Nissanov J, Hackney DB. MRI diffusion coefficients in spinal cord correlate with axon morphometry. Neuroreport 2005;16(1):73-76.
247. Golabchi FN, Brooks DH, Hoge WS, De Girolami U, Maier SE. Pixel-based comparison of spinal cord MR diffusion anisotropy with axon packing parameters. Magn Reson Med 2010;63(6):1510-1519.
248. Facon D, Ozanne A, Fillard P, Lepeintre JF, Tournoux-Facon C, Ducreux D. MR diffusion tensor imaging and fiber tracking in spinal cord compression. AJNR Am J Neuroradiol 2005;26(6):1587-1594.
249. Renoux J, Facon D, Fillard P, Huynh I, Lasjaunias P, Ducreux D. MR diffusion tensor imaging and fiber tracking in inflammatory diseases of the spinal cord. AJNR Am J Neuroradiol 2006;27(9):1947-1951.
250. Clark CA, Werring DJ, Miller DH. Diffusion imaging of the spinal cord in vivo: estimation of the principal diffusivities and application to multiple sclerosis. Magn Reson Med 2000;43(1):133-138.
251. Ozanne A, Krings T, Facon D, Fillard P, Dumas JL, Alvarez H, Ducreux D, Lasjaunias P. MR diffusion tensor imaging and fiber tracking in spinal cord arteriovenous malformations: a preliminary study. AJNR Am J Neuroradiol 2007;28(7):1271-1279.

252. Wilm BJ, Svensson J, Henning A, Pruessmann KP, Boesiger P, Kollias SS. Reduced field-of-view MRI using outer volume suppression for spinal cord diffusion imaging. Magn Reson Med 2007;57(3):625-630.
253. Bammer R, Fazekas F. Diffusion imaging of the human spinal cord and the vertebral column. Topics in magnetic resonance imaging : TMRI 2003;14(6):461-476.
254. Anderson AW, Gore JC. Analysis and correction of motion artifacts in diffusion weighted imaging. Magn Reson Med 1994;32(3):379-387.
255. Clark CA, Barker GJ, Tofts PS. Magnetic resonance diffusion imaging of the human cervical spinal cord in vivo. Magn Reson Med 1999;41(6):1269-1273.
256. Ordidge RJ, Helpern JA, Qing ZX, Knight RA, Nagesh V. Correction of motional artifacts in diffusion-weighted MR images using navigator echoes. Magn Reson Imaging 1994;12(3):455-460.
257. Butts K, de Crespigny A, Pauly JM, Moseley M. Diffusion-weighted interleaved echo-planar imaging with a pair of orthogonal navigator echoes. Magn Reson Med 1996;35(5):763-770.
258. Clark CA, Werring DJ. Diffusion tensor imaging in spinal cord: methods and applications - a review. NMR Biomed 2002;15(7-8):578-586.
259. Bammer R, Augustin M, Prokesch RW, Stollberger R, Fazekas F. Diffusion-weighted imaging of the spinal cord: interleaved echo-planar imaging is superior to fast spin-echo. J Magn Reson Imaging 2002;15(4):364-373.
260. Clark CA, Barker GJ, Tofts PS. Improved reduction of motion artifacts in diffusion imaging using navigator echoes and velocity compensation. J Magn Reson 2000;142(2):358-363.
261. Baur A, Stabler A, Bruning R, Bartl R, Krodel A, Reiser M, Deimling M. Diffusion-weighted MR imaging of bone marrow: differentiation of benign versus pathologic compression fractures. Radiology 1998;207(2):349-356.
262. Dietrich O, Herlihy A, Dannels WR, Fiebach J, Heiland S, Hajnal JV, Sartor K. Diffusion-weighted imaging of the spine using radial k-space trajectories. Magnetic Resonance Materials in Biology, Physics, and Medicine 2001;12(1):23-31.
263. Andre JB, Bammer R. Advanced diffusion-weighted magnetic resonance imaging techniques of the human spinal cord. Topics in magnetic resonance imaging : TMRI 2010;21(6):367-378.
264. Feinberg DA, Hoenninger JC, Crooks LE, Kaufman L, Watts JC, Arakawa M. Inner volume MR imaging: technical concepts and their application. Radiology 1985;156(3):743-747.
265. Wheeler-Kingshott CA, Parker GJ, Symms MR, Hickman SJ, Tofts PS, Miller DH, Barker GJ. ADC mapping of the human optic nerve: increased resolution, coverage, and reliability with CSF-suppressed ZOOM-EPI. Magn Reson Med 2002;47(1):24-31.
266. Jeong EK, Kim SE, Guo J, Kholmovski EG, Parker DL. High-resolution DTI with 2D interleaved multislice reduced FOV single-shot diffusion-weighted EPI (2D ss-rFOV-DWEPI). Magn Reson Med 2005;54(6):1575-1579.
267. Mansfield P, et al. Zonally magnified EPI in real time by NMR. Journal of Physics E: Scientific Instruments 1988;21(3):275.

268. Rieseberg S, Frahm J, Finsterbusch J. Two-dimensional spatially-selective RF excitation pulses in echo-planar imaging. Magn Reson Med 2002;47(6):1186-1193.
269. Wheeler-Kingshott CA, Trip SA, Symms MR, Parker GJ, Barker GJ, Miller DH. In vivo diffusion tensor imaging of the human optic nerve: pilot study in normal controls. Magn Reson Med 2006;56(2):446-451.
270. Saritas EU, Cunningham CH, Lee JH, Han ET, Nishimura DG. DWI of the spinal cord with reduced FOV single-shot EPI. Magn Reson Med 2008;60(2):468-473.
271. Wheeler-Kingshott CA, Hickman SJ, Parker GJ, Ciccarelli O, Symms MR, Miller DH, Barker GJ. Investigating cervical spinal cord structure using axial diffusion tensor imaging. NeuroImage 2002;16(1):93-102.
272. Wilm BJ, Gamper U, Henning A, Pruessmann KP, Kollias SS, Boesiger P. Diffusion-weighted imaging of the entire spinal cord. NMR Biomed 2009;22(2):174-181.
273. Zaharchuk G, Saritas EU, Andre JB, Chin CT, Rosenberg J, Brosnan TJ, Shankaranarayan A, Nishimura DG, Fischbein NJ. Reduced field-of-view diffusion imaging of the human spinal cord: comparison with conventional single-shot echo-planar imaging. AJNR Am J Neuroradiol 2011;32(5):813-820.
274. Dowell NG, Jenkins TM, Ciccarelli O, Miller DH, Wheeler-Kingshott CA. Contiguous-slice zonally oblique multislice (CO-ZOOM) diffusion tensor imaging: examples of in vivo spinal cord and optic nerve applications. J Magn Reson Imaging 2009;29(2):454-460.
275. Bax MC, Flodmark O, Tydeman C. Definition and classification of cerebral palsy. From syndrome toward disease. Dev Med Child Neurol Suppl 2007;109:39-41.
276. Clark EM, Ness AR, Bishop NJ, Tobias JH. Association between bone mass and fractures in children: A prospective cohort study. Journal of Bone and Mineral Research 2006;21(9):1489-1495.
277. Hogler W, Blimkie CJR, Cowell CT, Kemp AF, Briody J, Wiebe P, Farpour-Lambert N, Duncan CS, Woodhead H. A comparison of bone geometry and cortical density at the mid-femur between prepuberty and young adulthood using magnetic resonance imaging. Bone 2003;33(5):771-778.
278. Noble JJ, Fry NR, Lewis AP, Keevil SF, Gough M, Shortland AP. Lower limb muscle volumes in bilateral spastic cerebral palsy. Brain Dev 2013.
279. The WHO Growth reference data for 5-19 years.
280. Rosset A, Spadola L, Ratib O. OsiriX: an open-source software for navigating in multidimensional DICOM images. J Digit Imaging 2004;17(3):205-216.
281. Kutner M. Applied linear regression models. Boston ; London: McGraw-Hill Education; 2004.
282. Wren TAL, Lee DC, Hara R, Rethlefsen SA, Kay RM, Dorey FJ, Gilsanz V. Effect of High-frequency, Low-magnitude Vibration on Bone and Muscle in Children With Cerebral Palsy. J Pediatr Orthoped 2010;30(7):732-738.
283. Pan DA, Lillioja S, Kriketos AD, Milner MR, Baur LA, Bogardus C, Jenkins AB, Storlien LH. Skeletal muscle triglyceride levels are inversely related to insulin action. Diabetes 1997;46(6):983-988.

284. Ryan AS, Dobrovolny CL, Smith GV, Silver KH, Macko RF. Hemiparetic muscle atrophy and increased intramuscular fat in stroke patients. Arch Phys Med Rehabil 2002;83(12):1703-1707.
285. Yokoo T, Bydder M, Hamilton G, Middleton MS, Gamst AC, Wolfson T, Hassanein T, Patton HM, Lavine JE, Schwimmer JB, Sirlin CB. Nonalcoholic fatty liver disease: diagnostic and fat-grading accuracy of low-flip-angle multiecho gradient-recalled-echo MR imaging at 1.5 T. Radiology 2009;251(1):67-76.
286. Gerber C, Fuchs B, Hodler J. The results of repair of massive tears of the rotator cuff. J Bone Joint Surg Am 2000;82(4):505-515.
287. Liu W, Liu Y, Lai X, Kuang S. Intramuscular adipose is derived from a non-Pax3 lineage and required for efficient regeneration of skeletal muscles. Dev Biol 2012;361(1):27-38.
288. Contreras-Shannon V, Ochoa O, Reyes-Reyna SM, Sun D, Michalek JE, Kuziel WA, McManus LM, Shireman PK. Fat accumulation with altered inflammation and regeneration in skeletal muscle of CCR2-/- mice following ischemic injury. Am J Physiol Cell Physiol 2007;292(2):C953-967.
289. Gumucio JP, Davis ME, Bradley JR, Stafford PL, Schiffman CJ, Lynch EB, Claflin DR, Bedi A, Mendias CL. Rotator cuff tear reduces muscle fiber specific force production and induces macrophage accumulation and autophagy. J Orthop Res 2012;30(12):1963-1970.
290. Booth BA, Mistovich RJ, Janout M, Stills HF, Laughlin RT. Fatty infiltration of the gastrocsoleus after tendo-achilles lengthening and gastrocnemius recession in a rabbit model. Foot & ankle international 2009;30(8):778-782.
291. Inder TE, Huppi PS, Warfield S, Kikinis R, Zientara GP, Barnes PD, Jolesz F, Volpe JJ. Periventricular white matter injury in the premature infant is followed by reduced cerebral cortical gray matter volume at term. Annals of Neurology 1999;46(5):755-760.
292. Skranes JS, Martinussen M, Smevik O, Myhr G, Indredavik M, Vik T, Brubakk AM. Cerebral MRI findings in very-low-birth-weight and small-for-gestational-age children at 15 years of age. Pediatr Radiol 2005;35(8):758-765.
293. Bohannon RW, Smith MB. Interrater reliability of a modified Ashworth scale of muscle spasticity. Phys Ther 1987;67(2):206-207.
294. Landis JR, Koch GG. The measurement of observer agreement for categorical data. Biometrics 1977;33(1):159-174.
295. Landman BA, Farrell JAD, Huang H, Prince JL, Mori S. Diffusion tensor imaging at low SNR: nonmonotonic behaviors of tensor contrasts. Magnetic Resonance Imaging 2008;26(6):790-800.
296. Bastin ME, Armitage PA, Marshall I. A theoretical study of the effect of experimental noise on the measurement of anisotropy in diffusion imaging. Magnetic Resonance Imaging 1998;16(7):773-785.
297. Anderson AW. Theoretical analysis of the effects of noise on diffusion tensor imaging. Magnet Reson Med 2001;46(6):1174-1188.
298. Grech-Sollars M HP, Miyazaki K, Raschke F, Rodriguez D, Wilson M, Gill SK, Banks T, Saunders DE, Clayden JD, Gwilliam M, Barrick TR, Morgan PS, Davies NP, Rossiter J, Auer DP, Grundy R, Leach MO, Howe FA, Peet AC, Clark CA. Multi-centre reproducibility of diffusion MRI parameters for

clinical sequences in the brain. 2014; Proc Intl Soc Mag Reson Med. Milan, Italy.
299. Riad J, Modlesky CM, Gutierrez-Farewik EM, Brostrom E. Are muscle volume differences related to concentric muscle work during walking in spastic hemiplegic cerebral palsy? Clin Orthop Relat Res 2012;470(5):1278-1285.
300. Patikas D, Wolf SI, Schuster W, Armbrust P, Dreher T, Doderlein L. Electromyographic patterns in children with cerebral palsy: do they change after surgery? Gait Posture 2007;26(3):362-371.
301. Dreher T, Brunner R, Vegvari D, Heitzmann D, Gantz S, Maier MW, Braatz F, Wolf SI. The effects of muscle-tendon surgery on dynamic electromyographic patterns and muscle tone in children with cerebral palsy. Gait Posture 2013;38(2):215-220.
302. Noble JJ, Keevil SF, Totman J, Charles-Edwards GD. In vitro and in vivo comparison of two-, three- and four-point Dixon techniques for clinical intramuscular fat quantification at 3 T. The British journal of radiology 2014;87(1036):20130761.
303. Fielding RA, Vellas B, Evans WJ, Bhasin S, Morley JE, Newman AB, Abellan van Kan G, Andrieu S, Bauer J, Breuille D, Cederholm T, Chandler J, De Meynard C, Donini L, Harris T, Kannt A, Keime Guibert F, Onder G, Papanicolaou D, Rolland Y, Rooks D, Sieber C, Souhami E, Verlaan S, Zamboni M. Sarcopenia: an undiagnosed condition in older adults. Current consensus definition: prevalence, etiology, and consequences. International working group on sarcopenia. J Am Med Dir Assoc 2011;12(4):249-256.
304. Balboa-Castillo T, Guallar-Castillon P, Leon-Munoz LM, Graciani A, Lopez-Garcia E, Rodriguez-Artalejo F. Physical activity and mortality related to obesity and functional status in older adults in Spain. Am J Prev Med 2011;40(1):39-46.
305. Bauman WA, Spungen AM, Adkins RH, Kemp BJ. Metabolic and endocrine changes in persons aging with spinal cord injury. Assist Technol 1999;11(2):88-96.
306. Zlotolow SP, Levy E, Bauman WA. The serum lipoprotein profile in veterans with paraplegia: the relationship to nutritional factors and body mass index. J Am Paraplegia Soc 1992;15(3):158-162.
307. Bauman WA, Adkins RH, Spungen AM, Herbert R, Schechter C, Smith D, Kemp BJ, Gambino R, Maloney P, Waters RL. Is immobilization associated with an abnormal lipoprotein profile? Observations from a diverse cohort. Spinal Cord 1999;37(7):485-493.
308. Karlsson AK, Attvall S, Jansson PA, Sullivan L, Lonnroth P. Influence of the sympathetic nervous system on insulin sensitivity and adipose tissue metabolism: a study in spinal cord-injured subjects. Metabolism 1995;44(1):52-58.
309. Maki KC, Briones ER, Langbein WE, Inman-Felton A, Nemchausky B, Welch M, Burton J. Associations between serum lipids and indicators of adiposity in men with spinal cord injury. Paraplegia 1995;33(2):102-109.
310. Bauman WA, Spungen AM. Disorders of carbohydrate and lipid metabolism in veterans with paraplegia or quadriplegia: a model of premature aging. Metabolism 1994;43(6):749-756.

311. Washburn RA, Figoni SF. High density lipoprotein cholesterol in individuals with spinal cord injury: the potential role of physical activity. Spinal Cord 1999;37(10):685-695.
312. Zhong YG, Levy E, Bauman WA. The relationships among serum uric acid, plasma insulin, and serum lipoprotein levels in subjects with spinal cord injury. Horm Metab Res 1995;27(6):283-286.
313. Grundy SM. Atherogenic dyslipidemia: lipoprotein abnormalities and implications for therapy. Am J Cardiol 1995;75(6):45B-52B.
314. Cominacini L, Zocca I, Garbin U, Davoli A, Micciolo R, De Bastiani P, Bosello O. High-density lipoprotein composition in obesity: interrelationships with plasma insulin levels and body weight. Int J Obes 1988;12(4):343-352.
315. Hashimoto R, Adachi H, Tsuruta M, Tashiro H, Toshima H. Association of hyperinsulinemia and serum free fatty acids with serum high density lipoprotein-cholesterol. J Atheroscler Thromb 1995;2(1):53-59.
316. Fabry G, MacEwen GD, Shands AR, Jr. Torsion of the femur. A follow-up study in normal and abnormal conditions. J Bone Joint Surg Am 1973;55(8):1726-1738.
317. Lincoln TL, Suen PW. Common rotational variations in children. The Journal of the American Academy of Orthopaedic Surgeons 2003;11(5):312-320.
318. Laplaza FJ, Root L, Tassanawipas A, Glasser DB. Femoral torsion and neck-shaft angles in cerebral palsy. J Pediatr Orthop 1993;13(2):192-199.
319. Bobroff ED, Chambers HG, Sartoris DJ, Wyatt MP, Sutherland DH. Femoral anteversion and neck-shaft angle in children with cerebral palsy. Clin Orthop Relat Res 1999(364):194-204.
320. Wren TA, Rethlefsen S, Kay RM. Prevalence of specific gait abnormalities in children with cerebral palsy: influence of cerebral palsy subtype, age, and previous surgery. J Pediatr Orthop 2005;25(1):79-83.
321. O'Sullivan R, Walsh M, Hewart P, Jenkinson A, Ross LA, O'Brien T. Factors associated with internal hip rotation gait in patients with cerebral palsy. J Pediatr Orthop 2006;26(4):537-541.
322. Dreher T, Wolf S, Braatz F, Patikas D, Doderlein L. Internal rotation gait in spastic diplegia--critical considerations for the femoral derotation osteotomy. Gait Posture 2007;26(1):25-31.
323. de Morais Filho MC, Kawamura CM, dos Santos CA, Mattar R, Jr. Outcomes of correction of internal hip rotation in patients with spastic cerebral palsy using proximal femoral osteotomy. Gait Posture 2012;36(2):201-204.
324. Dreher T, Wolf SI, Heitzmann D, Swartman B, Schuster W, Gantz S, Hagmann S, Doderlein L, Braatz F. Long-term outcome of femoral derotation osteotomy in children with spastic diplegia. Gait Posture 2012;36(3):467-470.
325. Wren TA, Lening C, Rethlefsen SA, Kay RM. Impact of gait analysis on correction of excessive hip internal rotation in ambulatory children with cerebral palsy: a randomized controlled trial. Dev Med Child Neurol 2013;55(10):919-925.
326. Souza RB, Powers CM. Concurrent criterion-related validity and reliability of a clinical test to measure femoral anteversion. J Orthop Sports Phys Ther 2009;39(8):586-592.
327. Murphy SB, Simon SR, Kijewski PK, Wilkinson RH, Griscom NT. Femoral anteversion. J Bone Joint Surg Am 1987;69(8):1169-1176.

328. McNee AE, Gough M, Morrissey MC, Shortland AP. Increases in muscle volume after plantarflexor strength training in children with spastic cerebral palsy. Dev Med Child Neurol 2009;51(6):429-435.
329. Eek MN, Tranberg R, Zugner R, Alkema K, Beckung E. Muscle strength training to improve gait function in children with cerebral palsy. Dev Med Child Neurol 2008;50(10):759-764.
330. Damiano DL, Abel MF. Functional outcomes of strength training in spastic cerebral palsy. Arch Phys Med Rehabil 1998;79(2):119-125.
331. McRobbie DW. MRI from picture to proton. Cambridge: Cambridge University Press; 2007. xii, 394 p. p.
332. Galban CJ, Maderwald S, Stock F, Ladd ME. Age-related changes in skeletal muscle as detected by diffusion tensor magnetic resonance imaging. J Gerontol A Biol Sci Med Sci 2007;62(4):453-458.

Chapter 5 References

[1] Wiley ME, Damiano DL. Lower-extremity strength profiles in spastic cerebral palsy. Dev Med Child Neurol. 1998;40:100-7.
[2] Stackhouse SK, Binder-Macleod SA, Lee SC. Voluntary muscle activation, contractile properties, and fatigability in children with and without cerebral palsy. Muscle Nerve. 2005;31:594-601.
[3] Rose J, McGill KC. Neuromuscular activation and motor-unit firing characteristics in cerebral palsy. Dev Med Child Neurol. 2005;47:329-36.
[4] Elder GC, Kirk J, Stewart G, Cook K, Weir D, Marshall A, et al. Contributing factors to muscle weakness in children with cerebral palsy. Dev Med Child Neurol. 2003;45:542-50.
[5] Barber L, Hastings-Ison T, Baker R, Barrett R, Lichtwark G. Medial gastrocnemius muscle volume and fascicle length in children aged 2 to 5 years with cerebral palsy. Dev Med Child Neurol. 2011;53:543-8.
[6] Malaiya R, McNee AE, Fry NR, Eve LC, Gough M, Shortland AP. The morphology of the medial gastrocnemius in typically developing children and children with spastic hemiplegic cerebral palsy. J Electromyogr Kinesiol. 2007;17:657-63.
[7] Fry NR, Gough M, McNee AE, Shortland AP. Changes in the volume and length of the medial gastrocnemius after surgical recession in children with spastic diplegic cerebral palsy. J Pediatr Orthop. 2007;27:769-74.
[8] Lampe R, Grassl S, Mitternacht J, Gerdesmeyer L, Gradinger R. MRT-measurements of muscle volumes of the lower extremities of youths with spastic hemiplegia caused by cerebral palsy. Brain Dev. 2006;28:500-6.
[9] Riad J, Modlesky CM, Gutierrez-Farewik EM, Brostrom E. Are muscle volume differences related to concentric muscle work during walking in spastic hemiplegic cerebral palsy? Clin Orthop Relat Res. 2012;470:1278-85.
[10] Oberhofer K, Stott NS, Mithraratne K, Anderson IA. Subject-specific modelling of lower limb muscles in children with cerebral palsy. Clin Biomech. 2010;25:88-94.
[11] Barrett RS, Lichtwark GA. Gross muscle morphology and structure in spastic cerebral palsy: a systematic review. Dev Med Child Neurol. 2010;52:794-804.

[12] Fowler EG, Staudt LA, Greenberg MB. Lower-extremity selective voluntary motor control in patients with spastic cerebral palsy: increased distal motor impairment. Dev Med Child Neurol. 2010;52:264-9.
[13] Rosset A, Spadola L, Ratib O. OsiriX: an open-source software for navigating in multidimensional DICOM images. J Digit Imaging. 2004;17:205-16.
[14] Stevenson RD, Conaway M, Chumlea WC, Rosenbaum P, Fung EB, Henderson RC, et al. Growth and health in children with moderate-to-severe cerebral palsy. Pediatrics. 2006;118:1010-8.
[15] Benjamini Y, Drai D, Elmer G, Kafkafi N, Golani I. Controlling the false discovery rate in behavior genetics research. Behav Brain Res. 2001;125:279-84.
[16] Kramer JF, Ann MacPhail HE. Relationships Among Measures of Walking Efficiency, Gross Motor Ability, and Isokinetic Strength In Adolescents With Cerebral Palsy. Pediatric Physical Therapy. 1994;6:3-9.
[17] Damiano DL, Kelly LE, Vaughn CL. Effects of quadriceps femoris muscle strengthening on crouch gait in children with spastic diplegia. Phys Ther. 1995;75:658-67; discussion 68-71.
[18] Parker DF, Carriere L, Hebestreit H, Salsberg A, Bar-Or O. Muscle performance and gross motor function of children with spastic cerebral palsy. Dev Med Child Neurol. 1993;35:17-23.
[19] Barber L, Barrett R, Lichtwark G. Medial gastrocnemius muscle fascicle active torque-length and Achilles tendon properties in young adults with spastic cerebral palsy. J Biomech. 2012;45:2526-30.
[20] Ohata K, Tsuboyama T, Ichihashi N, Minami S. Measurement of muscle thickness as quantitative muscle evaluation for adults with severe cerebral palsy. Phys Ther. 2006;86:1231-9.
[21] Moreau NG, Simpson KN, Teefey SA, Damiano DL. Muscle architecture predicts maximum strength and is related to activity levels in cerebral palsy. Phys Ther. 2010;90:1619-30.
[22] McNee AE, Gough M, Morrissey MC, Shortland AP. Increases in muscle volume after plantarflexor strength training in children with spastic cerebral palsy. Dev Med Child Neurol. 2009;51:429-35.
[23] Stackhouse SK, Binder-Macleod SA, Stackhouse CA, McCarthy JJ, Prosser LA, Lee SC. Neuromuscular electrical stimulation versus volitional isometric strength training in children with spastic diplegic cerebral palsy: a preliminary study. Neurorehabil Neural Repair. 2007;21:475-85.
[24] Damiano DL, Prosser LA, Curatalo LA, Alter KE. Muscle Plasticity and Ankle Control After Repetitive Use of a Functional Electrical Stimulation Device for Foot Drop in Cerebral Palsy. Neurorehabil Neural Repair. 2013;27:200-7.
[25] Shortland A. Muscle deficits in cerebral palsy and early loss of mobility: can we learn something from our elders? Dev Med Child Neurol. 2009;51 Suppl 4:59-63.

Chapter 7 References

1. Elder CP, Apple DF, Bickel CS, Meyer RA, Dudley GA. Intramuscular fat and glucose tolerance after spinal cord injury--a cross-sectional study. Spinal Cord 2004;42(12):711-716.

2. Goodpaster BH, Thaete FL, Kelley DE. Thigh adipose tissue distribution is associated with insulin resistance in obesity and in type 2 diabetes mellitus. Am J Clin Nutr 2000;71(4):885-892.
3. Azcue MP, Zello GA, Levy LD, Pencharz PB. Energy expenditure and body composition in children with spastic quadriplegic cerebral palsy. J Pediatr 1996;129(6):870-876.
4. Bandini LG, Schoeller DA, Fukagawa NK, Wykes LJ, Dietz WH. Body composition and energy expenditure in adolescents with cerebral palsy or myelodysplasia. Pediatr Res 1991;29(1):70-77.
5. Johnson DL, Miller F, Subramanian P, Modlesky CM. Adipose tissue infiltration of skeletal muscle in children with cerebral palsy. J Pediatr 2009;154(5):715-720.
6. Boesch C, Slotboom J, Hoppeler H, Kreis R. In vivo determination of intra-myocellular lipids in human muscle by means of localized 1H-MR-spectroscopy. Magn Reson Med 1997;37(4):484-493.
7. Pfirrmann CW, Schmid MR, Zanetti M, Jost B, Gerber C, Hodler J. Assessment of fat content in supraspinatus muscle with proton MR spectroscopy in asymptomatic volunteers and patients with supraspinatus tendon lesions. Radiology 2004;232(3):709-715.
8. Schick F, Machann J, Brechtel K, Strempfer A, Klumpp B, Stein DT, Jacob S. MRI of muscular fat. Magn Reson Med 2002;47(4):720-727.
9. Szczepaniak LS, Babcock EE, Schick F, Dobbins RL, Garg A, Burns DK, McGarry JD, Stein DT. Measurement of intracellular triglyceride stores by H spectroscopy: validation in vivo. Am J Physiol 1999;276(5 Pt 1):E977-989.
10. Dixon WT. Simple proton spectroscopic imaging. Radiology 1984;153(1):189-194.
11. Glover GH. Multipoint Dixon technique for water and fat proton and susceptibility imaging. J Magn Reson Imaging 1991;1(5):521-530.
12. Ma J. Dixon techniques for water and fat imaging. J Magn Reson Imaging 2008;28(3):543-558.
13. S B Reeder MTA, N J Pelc. Water and Fat SSFP Imaging with Four-Point Dixon Techniques. 2002
14. Reeder SB, Pineda AR, Wen Z, Shimakawa A, Yu H, Brittain JH, Gold GE, Beaulieu CH, Pelc NJ. Iterative decomposition of water and fat with echo asymmetry and least-squares estimation (IDEAL): application with fast spin-echo imaging. Magn Reson Med 2005;54(3):636-644.
15. Reeder SB, McKenzie CA, Pineda AR, Yu H, Shimakawa A, Brau AC, Hargreaves BA, Gold GE, Brittain JH. Water-fat separation with IDEAL gradient-echo imaging. J Magn Reson Imaging 2007;25(3):644-652.
16. Reeder SB, Sirlin CB. Quantification of liver fat with magnetic resonance imaging. Magn Reson Imaging Clin N Am 2010;18(3):337-357, ix.
17. Karampinos DC, Baum T, Nardo L, Alizai H, Yu H, Carballido-Gamio J, Yap SP, Shimakawa A, Link TM, Majumdar S. Characterization of the regional distribution of skeletal muscle adipose tissue in type 2 diabetes using chemical shift-based water/fat separation. J Magn Reson Imaging 2012;35(4):899-907.
18. Kovanlikaya A, Mittelman SD, Ward A, Geffner ME, Dorey F, Gilsanz V. Obesity and fat quantification in lean tissues using three-point Dixon MR imaging. Pediatr Radiol 2005;35(6):601-607.

19. Wren TA, Bluml S, Tseng-Ong L, Gilsanz V. Three-point technique of fat quantification of muscle tissue as a marker of disease progression in Duchenne muscular dystrophy: preliminary study. AJR Am J Roentgenol 2008;190(1):W8-12.
20. Fischmann A, Kaspar S, Reinhardt J, Gloor M, Stippich C, Fischer D. Exercise might bias skeletal-muscle fat fraction calculation from Dixon images. Neuromuscular disorders : NMD 2012;22 Suppl 2:S107-110.
21. Willis TA, Hollingsworth KG, Coombs A, Sveen ML, Andersen S, Stojkovic T, Eagle M, Mayhew A, de Sousa PL, Dewar L, Morrow JM, Sinclair CD, Thornton JS, Bushby K, Lochmuller H, Hanna MG, Hogrel JY, Carlier PG, Vissing J, Straub V. Quantitative muscle MRI as an assessment tool for monitoring disease progression in LGMD2I: a multicentre longitudinal study. PLoS One 2013;8(8):e70993.
22. Wokke BH, Bos C, Reijnierse M, van Rijswijk CS, Eggers H, Webb A, Verschuuren JJ, Kan HE. Comparison of dixon and T1-weighted MR methods to assess the degree of fat infiltration in duchenne muscular dystrophy patients. J Magn Reson Imaging 2013;38(3):619-624.
23. Fischmann A, Hafner P, Fasler S, Gloor M, Bieri O, Studler U, Fischer D. Quantitative MRI can detect subclinical disease progression in muscular dystrophy. J Neurol 2012;259(8):1648-1654.
24. Price D, I., Patel D, Taylor S, A., Halligan S, Lally P, Bainbridge A, Cady E, B., Emmanuel A. 'Pelvic floor atrophy assessment using a 2-point Dixon technique to measure muscle fat fraction'. no. 633. Abstracts of the 30th Annual Scientific Meeting of the European Society for Magnetic Resonance in Medicine and Biology (ESMRMB). Toulouse, France. October 3-5, 2013. MAGMA 2013;26 Suppl 1:4-535.
25. Bernard CP, Liney GP, Manton DJ, Turnbull LW, Langton CM. Comparison of fat quantification methods: a phantom study at 3.0T. J Magn Reson Imaging 2008;27(1):192-197.
26. Reeder SB, Wen Z, Yu H, Pineda AR, Gold GE, Markl M, Pelc NJ. Multicoil Dixon chemical species separation with an iterative least-squares estimation method. Magn Reson Med 2004;51(1):35-45.
27. Xiang QS, An L. Water-fat imaging with direct phase encoding. J Magn Reson Imaging 1997;7(6):1002-1015.
28. Vanhamme L, van den Boogaart A, Van Huffel S. Improved method for accurate and efficient quantification of MRS data with use of prior knowledge. J Magn Reson 1997;129(1):35-43.
29. Naressi A, Couturier C, Devos JM, Janssen M, Mangeat C, de Beer R, Graveron-Demilly D. Java-based graphical user interface for the MRUI quantitation package. Magn Reson Mater Phy 2001;12(2-3):141-152.
30. Rosset A, Spadola L, Ratib O. OsiriX: an open-source software for navigating in multidimensional DICOM images. J Digit Imaging 2004;17(3):205-216.
31. Krssak M, Mlynarik V, Meyerspeer M, Moser E, Roden M. 1H NMR relaxation times of skeletal muscle metabolites at 3 T. MAGMA 2004;16(4):155-159.
32. Bland JM, Altman DG. Statistical methods for assessing agreement between two methods of clinical measurement. Lancet 1986;1(8476):307-310.
33. Liu CY, McKenzie CA, Yu H, Brittain JH, Reeder SB. Fat quantification with IDEAL gradient echo imaging: correction of bias from T(1) and noise. Magn Reson Med 2007;58(2):354-364.

34. Eggers H, Brendel B, Duijndam A, Herigault G. Dual-echo Dixon imaging with flexible choice of echo times. Magn Reson Med 2011;65(1):96-107.

Appendices

A. Magnetic resonance imaging

MRI relies on the interactions of nuclei with an external applied magnetic field to produce images. The nuclei predominantly used are those of hydrogen, where each nucleus consists of a single proton. Hydrogen is abundant within the body within all water and fat molecules. A fundamental property of a proton is spin. Protons can have a spin of $\pm {}^{1}/_{2}$. Particles with a net spin can absorb and are, therefore, excited by radiowaves at a frequency ω_0 whilst in an applied magnetic field B. This frequency, the Larmor frequency, is dependent on the gyro-magnetic ratio, γ of the particle and the external field strength (B) (Equation A.1).

$$\omega_0 = \gamma B \qquad \textit{Equation A.1}$$

The spin of the proton gives it two properties: angular momentum (J) and a magnetic moment (μ_s). The angular momentum is due to the net spin and odd mass number, which together with the electrical charge of the proton produce the magnetic moment. The interactions of spin with a magnetic field can be considered from both a classical and quantum mechanical approach. Classically, the angular momentum of a proton is given in Equation A.2. In an applied magnetic field, the magnetic moment of the proton changes the angular momentum since γ where I is the moment of inertia and $\hbar$ is the reduced Planck's constant. This causes the magnetic moment to precess around the direction of the applied magnetic field. This precession frequency is the Larmor frequency. Quantum mechanically, in an applied magnetic field a proton has energy given by Equation A.3.

$$\bar{J} = \bar{I}\hbar \qquad \textit{Equation A.2}$$

$$E = -\mu_s.B \qquad \textit{Equation A.3}$$

Since a proton can have a spin of +/- ½, the protons can occupy two distinct energy states:

$$E = +\mu_s B \quad \text{or} \quad E = -\mu_s B \qquad \textit{Equation A.4}$$

If energy is supplied equal to the gap between the two energy states, proton transition will take place between the two states. This can be achieved by applying a Radio Frequency pulse at the Larmor frequency. Therefore, a proton in an applied magnetic field can have a magnetic moment in one of these two states, aligned parallel or anti-parallel to the applied field. These are described as 'spin up' and 'spin down' respectively. There is a small difference in the spin populations of these two states; this causes a net magnetisation vector (M) parallel to the applied magnetic field.

A.1 Excitation

At equilibrium, the net magnetisation vector lies along the direction of the applied magnetic field B_o and is called the equilibrium magnetisation M_o. Therefore, the Z component of magnetisation M_Z, the longitudinal magnetisation, is equal to M_o. Since M_Z is equal to M_o there is no transverse magnetisation. Excitation of the spins is caused by the application of a radiofrequency (RF) pulse at the Larmor frequency of the proton. Quantum mechanically, the effect of the RF pulse is to alter the relative populations of the two spin states changing the direction of the net magnetisation vector. Classically, the magnetic field of the RF field interacts with the net magnetisation vector, causing the net magnetisation vector to nutate from the z-axis towards the transverse plane. Equation A.5 gives the 'flip angle' of the net magnetisation vector from the longitudinal axis, where t is the length of time the RF field is applied. For example, a 90^o pulse will flip the net magnetisation vector from the Z direction into the transverse xy-plane. Any flip angle is possible, although the most common used are 90^o and 180^o.

$$\theta = \gamma B_1 t \qquad \textit{Equation A.5}$$

A.2 Relaxation

Relaxation is the return of the net magnetization vector to its equilibrium state following a perturbation event by an applied RF field. There are two types of relaxation: spin-lattice and spin-spin. Spin- lattice relaxation is the longitudinal relaxation caused by spins losing energy to the bulk structure and realigning back along the longitudinal axis with $M_{Z,}$ returning to M_0 exponentially with a time constant T_1. Spin- Spin relaxation is transverse relaxation of M_{XY} to zero. Spin-spin relaxation is due to exchanges of energy between adjacent spins. M_{XY} decays exponentially, with a time constant T_2. T_2 is always less than or equal to T_1. Transverse and longitudinal relaxations occur simultaneously after the application of an excitation RF pulse.

$$M_z = M_0\left(1 - e^{-\frac{t}{T_1}}\right) \qquad \text{Equation A.6}$$

$$M_{xy} = M_0\left(e^{-\frac{t}{T_2}}\right) \qquad \text{Equation A.7}$$

Since the signal acquired is due to oscillations in the transverse magnetic field, i.e. when the net magnetisation vector is in the transverse plane, the decay of the signal measured, known as the Free Induction Decay (FID), is characterised by T_2. However, in practice the actual decay constant of the FID is characterised by T_2*, which takes into account the additional dephasing caused by microscopic inhomogeneities in B_0.

$$\frac{1}{T_2^*} = \frac{1}{T_2} + \frac{1}{2}\gamma\Delta B_0 \qquad \text{Equation A.8}$$

A.3 Image contrast

The basic MR image signal strength depends on the proton density and mobility. Therefore, for example, air and bone appear inherently dark due to their negligible hydrogen content. Proton mobility also affects the image contrast; immobile protons, such as those contained in large molecules, produce a small signal with free water producing the highest signal. This will, therefore, cause Cerebral Spinal Fluid (CSF)

and urine to appear bright. This inherent contrast is called proton-density weighted, as it fundamentally depends on the number of protons in a given region. Proton density, however, is not the only source of image contrast. Relaxation times of protons strongly depend on their physicochemical environment. Therefore, different tissues have different relaxation parameters T_1 and T_2 introduced in Section A.2 This means that the amount of signal received from prospective tissue types can be manipulated to alter image contrast and obtain various degrees of T_1 or T_2 weighting. Table A.1 shows example T_1 and T_2 values for some tissue types at 1.5T.

Tissue	T_1	T_2
White matter	560	82
Grey matter	1100	92
CSF	2060	160
Muscle	1075	33

Table A.1 Summary of approximate relaxation times for the three main tissue types[331]

The relative T_1 and T_2 weighting of the resultant image is dependent on the relative timings of the acquisition sequence; the repetition time of the excitation pulses (TR) and the echo time between excitation and the middle of signal acquisition (TE). Generally, the shorter the TR the stronger the T_1 weighting: the longer the TE, the stronger the T_2 weighting. For example in a T_2 weighted, to maximise the contrast between two tissues the TE is chosen when there is the largest difference in their relative signal intensities. Another method for controlling image contrast other than TR and TE manipulation is by varying the flip angle of the excitation pulse. A flip angle of less than 90^o only transfers part of the net magnetisation vector into the transverse plane, leaving part in the longitudinal plane. This means that T_1 recovery is much quicker so that a shorter TR can be used without any T_1 weighting.

A.4 Spatial localisation

As explained in above, the Larmor frequency of spin depends on the strength of the external magnetic field. Applying a magnetic field gradient will cause the magnetic field and Larmor frequency to vary with respect to position. MRI utilises linear magnetic gradients to achieve this. One-dimensional gradients vary along only one direction, e.g. the x direction. Therefore, in order to accurately locate the origin point of

a signal in space the magnetic field needs to be varied along three orthogonal axes. The gradients along the x,y and z directions (G_x G_y G_z) are switched on and off to achieve signal localization in the following ways:

A.4.1 Slice selection

Slice selection is achieved by applying a linear magnetic field gradient during the period that the RF pulse is applied. This gradient is known as the slice-select gradient G_s or G_z (if the slice select gradient is applied in the z-direction, e.g. for axial or transverse slices). This causes the Larmor frequency of spins within the object to vary along z through the object (Equation A.1). A 90^o pulse is applied in conjunction with a magnetic field gradient to rotate spins into the transverse plane that are located in a particular slice. The applied 90^o pulse contains a band of frequencies equal to the frequency band of the slice of interest through the object as determined by the slice select gradient. Therefore, only the spins in the slice of interest will be excited by the pulse and rotated 90^o into the transverse plane. A schematic diagram showing slice selection is shown in Figure A.1.

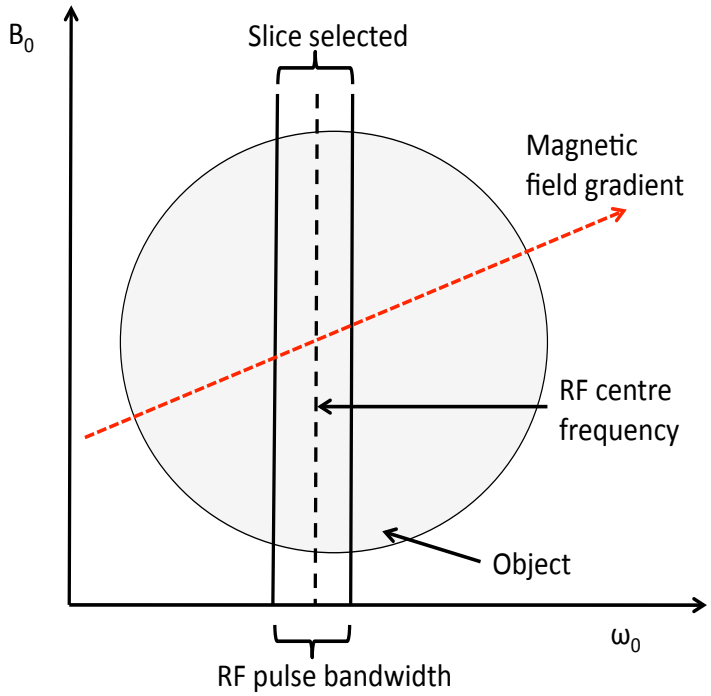

Figure A. 1 Slice select schematic diagram through application of a linear magnetic field gradient and an excitatory RF pulse of centre frequency and bandwidth to define slice position and slice thickness respectively through the object to be imaged

A.4.2 Phase encoding

Phase encoding utilises the application of a second gradient orthogonal to the slice select gradient, known as the phase encoding gradient G_p. This gradient enables the signal to be located in the y direction. The phase encoding gradient is applied between the excitation pulse and signal acquisition (read-out) and changes the phase of the spins according to their y position.

A.4.3 Frequency encoding

Frequency encoding involves the application of a gradient orthogonal to the slice select and phase encoding gradients during signal acquisition, known as the read-out gradient G_r. This allows the signal to be located in the x direction within the slice defined by the slice select gradient. The application of the gradient changes the Larmor frequency for each x co-ordinate allowing the total signal to be decomposed from each location using Fourier analysis. Applying these three localisation methods in a pulse sequence enable the signal to be located within 3D voxels within the subject. Once the signal has been acquired the whole process is repeated but with a different phase encoding gradient to enable the whole signal for the area of interest to be acquired. This is best-understood using k-space.

A.4.4 K-space

The simplest description of K-space is that it is a 'raw data' matrix that stores the encoded MR signal. K-space contains the frequency rather than spatial information of the image from which the image can be obtained by applying a Fourier Transform. The frequency and phase encoding matrix, i.e. how many steps of phase and frequency for which the signal is read, controls the size of both K-space and the final image in terms of the number of data points. For example, if a 256-matrix size is chosen for phase encoding, the signal needs to be acquired 256 times to fill k-space, filling 256 columns. However, it is important to note that each voxel in k-space does not correspond to the respective voxel in the final image due to the Fourier Transform process used. The middle of k-space contains the low frequency and, therefore, the contrast information of the image. The outer edges contain the high frequency information, which includes the image resolution data such as edges. There is, therefore, a relationship between the field of view (FOV) in k-space and image space. Gradients applied during a sequence control

the location in k-space at which the signal is acquired. The phase encoding gradient controls the position in $k_{PE,}$ and the read out gradient controls the location along k_{FE} with the initial excitation pulse enters k-space at its centre (0,0). Sequences are, therefore, designed to traverse k-space in different ways, the most common of which are explained in the next section.

A.5 Basic sequences

It is important to note that the raw FID is not acquired; this would require the readout gradient to be switched on instantaneously following the excitation pulse, which would not enable 3D signal location techniques to be employed. Therefore, all sequences actually acquire an echo of the raw FID utilising either spin or gradient echo techniques.

A.5.1 Gradient Echo

Gradient Echo (GE) sequences use a read gradient to rephase spins into a FID echo. A GE sequence is shown in Figure A.2. GE sequences can be used to produce T_1, T_2* or proton density weighted images. The negative portion of the read gradient is used to control the position in k-space from which the signal will start to be acquired. The positive gradient then enables the MR signal to be sampled across the frequency encoding direction in k-space. It is important to note that the production of a signal echo using a gradient rephases the dephasing caused by the first gradient but does not correct for the dephasing caused by inhomogeneities in B_0. Consequently, the images can only be T_2* or T_1 weighted. It is also important to note that the negative 'blip' of the read gradient also repositions the observer in k-space to the far left of k_{FE}. The readout gradient then moves the observer across the width of k space acquiring the signal at various points defined by the readout matrix. As explained in Section A.1.4, the phase encoding gradient is then altered between each acquisition to obtain data in the consecutive lines of k-space.

A.5.2 Spin Echo

Spin Echo (SE) sequences are very similar to GE sequences but have a 180^o RF pulse to refocus the spins instead of the application of a negative read gradient (see Figure A.3). This RF pulse flips the spins in the transverse plane. Therefore, any dephasing occurring due to magnetic field inhomogeneities now cause rephasing to produce an

echo of the FID, with the signal only having decayed by T_2 processes. SE sequences can be used to produce T_1, T_2 or proton density weighted images.

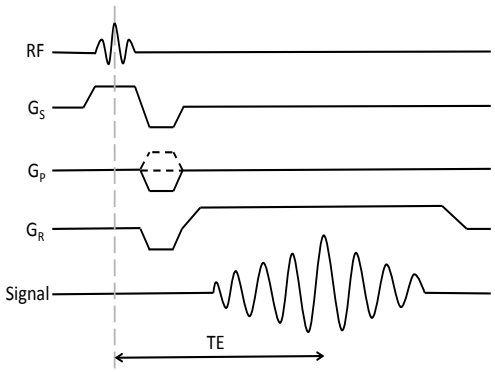

Figure A. 2 Gradient Echo sequence diagram

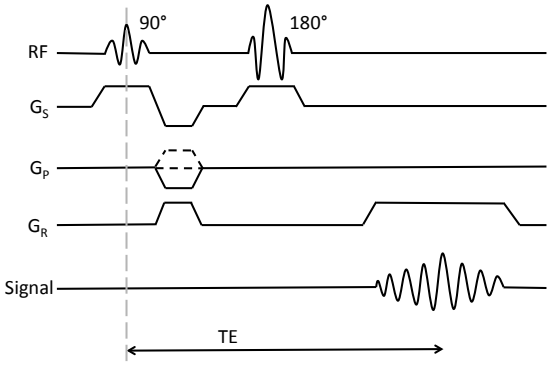

Figure A. 3 Spin Echo sequence diagram

A.6 Fast imaging sequences and techniques

Various techniques have been developed to speed up the imaging process to reduce patient time within the scanner. This also reduces the chance of patient movement during sequential image slice acquisitions and to permit the imaging of moving body parts such as the heart. The most common techniques are presented in this section. These techniques can also be used together to further decrease the scan duration.

A.6.1 Fast/Turbo Spin Echo (FSE/TSE)

Fast spin echo (FSE) is a SE technique that utilises a chain of multiple 180^o RF pulses to form an echo train. These echoes are used to acquire multiple lines of k-space following a single excitation pulse. Therefore, each refocusing pulse has a different phase encoding gradient. The 180^o pulses are equally spaced in time. The number of 180^o pulses and, therefore, acquired echoes, is known at the echo train length (ETL).

A.6.2 Echo Planar Imaging (EPI)

Echo Planar Imaging (EPI) is a readout technique that acquires an entire slice per excitation pulse. EPI can be single shot or multi-shot, SE or GE. In 'blipped' EPI readout, k-space is traversed through the application of a chain of frequency encoding gradients of opposite sign, between which small phase encoding gradients are applied to change between different lines of k-space. A GE EPI sequence is shown in Figure A.4. 'Blipped' EPI produces regular paths through k-space as shown in Figure A.5. This also

speeds up image reconstruction. Large readout gradient amplitudes are required to enable the fast sampling of the points in k_{FE} and the whole k_{PE} following a single excitation pulse. Due to the FID, EPI is limited to acquisition times of approximately 100 ms after which the FID has become too small to acquire. EPI readout is very useful when rapid imaging is critically important, for example in diffusion tensor imaging (DTI).

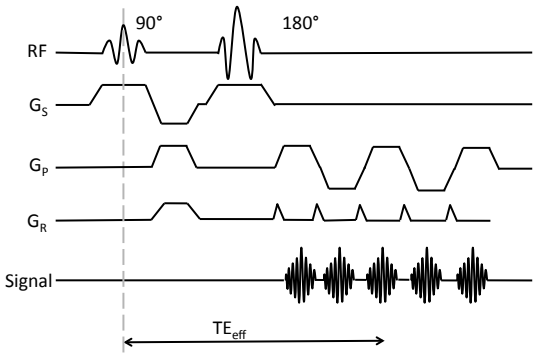

Figure A. 4 Spin echo sequence with EPI readout

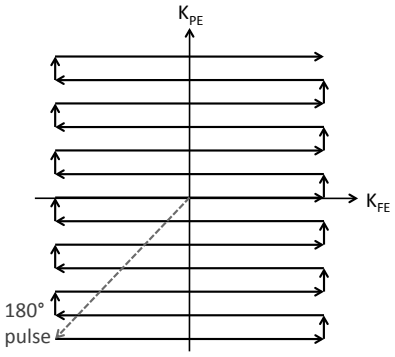

Figure A. 5 EPI movement through k-space

A.6.3 Half Fourier

In Half Fourier acquisitions just over half of k-space is acquired. The half that is not acquired is estimated from the other half using complex conjugate synthesis. This reduces scan time by nearly 50% without significant drop in spatial resolution, but it does reduce SNR by approximately 30% since the noise is effectively copied to the non acquired half of k-space resulting in the noise no longer being uncorrelated [331].

A.6.4 Multi-slice imaging

In single slice imaging, a single slice is excited and one line of k-space is read, then after a time (TR) the slice is excited again to read another line of k-space. This clearly results in a lot of time within each repetition for which the scanner is idle waiting to commence the next repetition unless a sequence with a short TR is used. For example, for a TE/TR of 20/600 ms, it takes approximately 30 ms to excite and acquire the data leaving 570 ms in which the scanner is idle. Multi-slice imaging takes advantages of the idle time by acquiring lines of k-space within other slices during the TR. Therefore; within a single TR the scanner excites and collects data from multiple slices within the object. The excitation of other slices during the TR does not interfere with the relaxation

processes occurring in that slice due small gaps between imaging slice through the object, which ensure no cross-excitation between the slices occurs.

A.6.5 Parallel imaging

Parallel imaging techniques, such as Sensitivity Encoding (SENSE), are methods of combining simultaneous images from multiple coils (phased array coils) around an object. SENSE utilises knowledge of the sensitivity of each coil element, to calculate the aliased signal component at each point. This technique can be used to improve SNR, improve spatial resolution or to reduce overall scan time. SNR increases because the signal between each element is correlated and, therefore, will combine to increase the resultant image signal, whereas the noise is uncorrelated and will combine destructively. The number of individual coil elements in the phase encoding direction determines the maximum time reduction factor. Time reduction is possible by under sampling k-space and recording images simultaneously from multiple imaging coils (phased array coils). Under sampling reduces the acquisition time and the use of multiple RF coils eliminates the wrap artefact, where part of the imaged anatomy located outside of the field of view appears inside of the field of view, caused by the under sampling.

SENSE reconstruction is a post Fourier Transform process applied to the images from each coil of the phased array. In SENSE, reduced k-space is acquired by acquiring fewer points in the phase encoding direction of k-space. If, for example, an image is acquired in a conventional acquisition process with half the number of phase encoding steps, the scan time would be halved but the resultant image would be aliased due to the under sampling. However, the position of the aliased information in the resultant image can be predicted through knowledge of the field of view [331]. SENSE utilises knowledge of the sensitivity of each coil element, to calculate the aliased signal component at each point. Therefore, each acquisition with SENSE requires a short, low resolution, calibration scan from which sensitivity maps are calculated. Figure A.6 shows how under sampling k-space affects the resultant image and how parallel imaging enables under sampling of k-space without seriously affecting the image. Figure A.6 (B) shows that by reducing the matrix size by half in the phase encoding direction by sampling on the centre of k-space the resolution of the image is reduced since the high frequency data is around the edges of k-space. However, the matrix size can be reduced but maintaining resolution by reducing the number of lines in k-space but still acquiring

over the same range. This however, results in aliasing of the image since field of view (FOV) is dependent on the sample spacing in k-space. Parallel imaging corrects for this aliased signal by using knowledge of the element sensitivities to interpolate between the acquired lines of k-space.

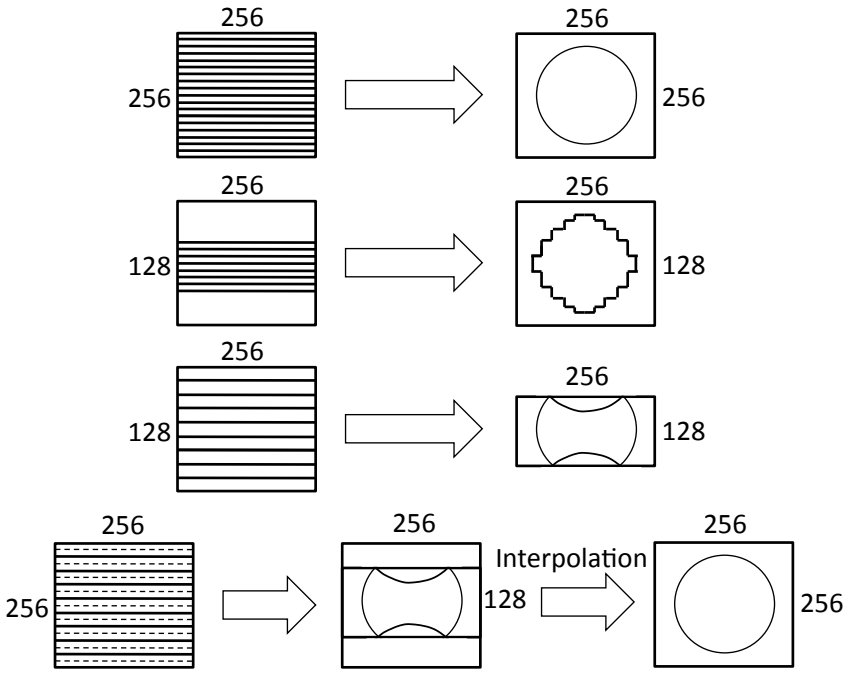

Figure A. 6 K-space and image matrix behaviour and parallel imaging. (A) 256x256 matrix (B) 256x128 matrix resulting in low image resolution (C) 256x128 matrix resulting in aliased signal wrapping back onto image (D) Parallel imaging corrects for aliasing for the matrix used in (C)

A.7 Diffusion tensor imaging (DTI)

Diffusion Weighted (DW) images are sensitive to small microscopic movements of Hydrogen nuclei within the body, such that regions with free water diffusion are dark and areas of restricted diffusion are bright. This is achieved by applying two symmetrical gradients either side of an 180^{o} pulse as shown in Figure A.7. The first gradient gives a phase to the spins dependant on their position within the slice. If the spins are in the same position after the 180^{o} pulse the identical gradient will now produce the opposite phase change since the spins have been flipped in the transverse plane between the applications of the two gradients by the 180^{o} pulse. This causes the spins to be rephased, resulting in a strong signal. For spins that have moved between the applications of the two gradients, different and unique phase changes will be

experienced, causing the spins to be out of phase reducing the net transverse magnetisation, resulting in a smaller signal. The degree of dephasing and signal intensity of the spins will be dependent on the difference between the two phase changes experienced and, therefore, dependant on the motion of the spins.

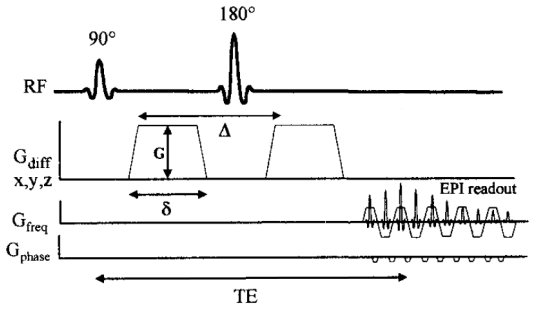

Figure A. 7 Basic Pulsed Gradient Spin Echo (PGSE) sequence with EPI read-out

The b-value is defined for the PGSE sequence shown in Figure A.8 in Equation A.9, where G is the gradient amplitude δ is the gradient duration, and Δ is the separation of the two gradients. The b-value determines the amount of diffusion weighting in the resultant image. Increasing the b-value increases the diffusion weighting; this results in a higher sensitivity to diffusion but with an increase in overall signal loss and, therefore, reduction in SNR.

$$b = \gamma^2 G^2 \delta^2 \left(\Delta - \frac{\delta}{3} \right) \qquad \textit{Equation A.9}$$

The ADC calculation removes influences on signal from image weighting and other sources including bulk flow and bulk motion. The ADC can be calculated from two or more images with different *b*-values enabling the image to be displayed as ADC map. The calculation of the ADC map is shown in Equation A.10, where the TE is equal in both the DW and T_2 weighted images.

$$ADC\ map = -\frac{1}{b} \ln \left(\frac{DW\ image}{T2W\ image} \right) \qquad \textit{Equation A.10}$$

The b-value in Equation A.10 is a user-prescribed DTI parameter dependant on the amplitude, duration, and timing of the diffusion-sensitising gradient-pulse waveform

and is a primary determinant of the molecular water diffusion sensitivity. As the b-value is increased, the amount of diffusion weighting in the acquisition increases.

The diffusion weighting can only be applied in one direction at a time. In order to model diffusion as a tensor, a minimum of six diffusion directions are required, this technique is known as diffusion tensor imaging (DTI). Each voxel in DTI is a measure of the diffusion magnitude and direction at that location. Diffusion can be visualised as ellipsoids, with the eigenvectors of the Diffusion tensor representing the three orthogonal axes. For example, in skeletal muscle, it has been shown that the principal eigenvalue (λ_1) corresponds to diffusion directed along the fibre's length, with the other two eigenvalues (λ_2 and λ_3) in the cross-sectional plane [332]. Notably, DTI permits the calculation of Fractional Anisotropy (FA). FA is a scalar whose value, between 0 and 1, describes the degree of anisotropy of diffusion, where FA=0 describes isotropic diffusion. FA is calculated using Equation A.11, where D is the mean of the trace diffusion constant in three dimensions (Equation A.12).

$$FA = \frac{\sqrt{3((\lambda_1 - D^2)^2 + (\lambda_2 - D^2)^2 + (\lambda_3 - D^2)^2)}}{\sqrt{2(\lambda_1^2 + \lambda_2^2 + \lambda_3^2)}} \qquad \textit{Equation A.11}$$

$$D = \frac{(\lambda_1 + \lambda_2 + \lambda_3)}{3} \qquad \textit{Equation A.12}$$

B. Study 4 Ethics

B.1 Ethical approval letter

National Research Ethics Service
Royal Free Hospital & Medical School
Research Ethics Committee
Royal Free Hospital NHS Trust
Royal Free Hospital
South House, Block A
Pond Street
London
NW3 2QG

07 January 2010

Mr Jonathan Noble
MEP, Faraday building
King's College Hosital,Denmark Hill
Camberwell
SE5 9RS

Dear Mr Noble

Study Title: **Muscular assessment by magnetic resonance imaging and ultrasound of young people with cerebral palsy**
REC reference number: **09/H0720/120**

Thank you for your letter of 4th December, responding to the Committee's request for further information on the above research and submitting revised documentation.

The further information has been considered on behalf of the Committee by the Chair.

Confirmation of ethical opinion

On behalf of the Committee, I am pleased to confirm a favourable ethical opinion for the above research on the basis described in the application form, protocol and supporting documentation as revised, subject to the conditions specified below.

Ethical review of research sites

The favourable opinion applies to all NHS sites taking part in the study, subject to management permission being obtained from the NHS/HSC R&D office prior to the start of the study (see "Conditions of the favourable opinion" below).

The Committee has not yet been notified of the outcome of any site-specific assessment (SSA) for the non-NHS research site(s) taking part in this study. The favourable opinion does not therefore apply to any non-NHS site at present. I will write to you again as soon as one Research Ethics Committee has notified the outcome of a SSA. In the meantime no study procedures should be initiated at non-NHS sites.

Conditions of the favourable opinion

The favourable opinion is subject to the following conditions being met prior to the start of the study.

Management permission or approval must be obtained from each host organisation prior to the start of the study at the site concerned.

For NHS research sites only, management permission for research ("R&D approval") should be obtained from the relevant care organisation(s) in accordance with NHS research governance arrangements. Guidance on applying for NHS permission for research is available in the Integrated Research Application System or at http://www.rdforum.nhs.uk. *Where the only involvement of the NHS organisation is as a Participant Identification Centre, management permission for research is not required but the R&D office should be notified of the study. Guidance should be sought from the R&D office where necessary.*

Sponsors are not required to notify the Committee of approvals from host organisations.

It is the responsibility of the sponsor to ensure that all the conditions are complied with before the start of the study or its initiation at a particular site (as applicable).

Approved documents

The final list of documents reviewed and approved by the Committee is as follows:

Document	*Version*	*Date*
REC application		
Protocol	1	02 October 2009
Investigator CV		
Participant Consent Form: Cases	1	02 October 2009
Participant Consent Form: Control	1	02 October 2009
Referees or other scientific critique report		02 October 2009
Advertisement		
Participant Information Sheet: Patients	3	04 December 2009
Participant Information Sheet: Controls	2	04 December 2009
Response to Request for Further Information		

Statement of compliance

The Committee is constituted in accordance with the Governance Arrangements for Research Ethics Committees (July 2001) and complies fully with the Standard Operating Procedures for Research Ethics Committees in the UK.

After ethical review

Now that you have completed the application process please visit the National Research Ethics Service website > After Review

You are invited to give your view of the service that you have received from the National Research Ethics Service and the application procedure. If you wish to make your views known please use the feedback form available on the website.

The attached document *"After ethical review – guidance for researchers"* gives detailed guidance on reporting requirements for studies with a favourable opinion, including:

- Notifying substantial amendments
- Adding new sites and investigators
- Progress and safety reports
- Notifying the end of the study

The NRES website also provides guidance on these topics, which is updated in the light of changes in reporting requirements or procedures.

We would also like to inform you that we consult regularly with stakeholders to improve our service. If you would like to join our Reference Group please email referencegroup@nres.npsa.nhs.uk.

09/H0720/120	**Please quote this number on all correspondence**

Yours sincerely

Dr Michael Pegg
Chair
Email: Thomas.mcquillan@royalfree.nhs.uk

Enclosures: "After ethical review – guidance for researchers" *[SL-AR1 for CTIMPs, SL- AR2 for other studies]*

Copy to: *Karen Ignatian, Guy's & St Thomas'Foundation NHS Trust*
Dr Adam Shortland, Guy's & St Thomas' NHS Foundation Trust

B.2 Subject information sheet

Guy's and St Thomas' NHS
NHS Foundation Trust
St Thomas' Hospital
Westminster Bridge Road
London SE1 7EH

Hospital No: 020 7188 7188
Direct Line: 020 7188 2476
Fax: 020 7188 2477
E-mail: adam.shortland@gstt.nhs.uk

YOUR INFORMATION SHEET (PATIENTS)

STUDY TITLE

Muscular assessment by MRI and Ultrasound of young people with cerebral palsy

INTRODUCTION

You are invited to take part in a research study. Before you decide whether you want to take part, it is important for you to understand why the research is being done and what it will involve. Please take time to read the following information carefully and discuss it with friends, relatives and your GP if you wish. Ask us if there is anything that is not clear or if you would like more information. Take time to decide whether or not you and your child wish to take part.

WHAT IS THE PURPOSE OF THIS STUDY?

In this study, we hope to learn about the differences in calf muscles of typically developing young adults and young adults with cerebral palsy. We think that individuals with cerebral palsy suffer from changes, primarily fat and connective tissue, of the muscle that causes their muscles to be weaker than their typically developing peers.

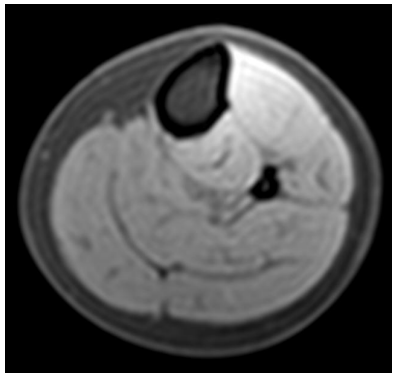

Figure 1: A typical MRI image we will be acquiring through the calf muscles.

We will compare the fat and connective tissue content of the calf muscles and their microstructure using ultrasound imaging and magnetic resonance imaging (MRI). A typical image we will obtain using MRI is shown in figure 1. We will use the same sort of ultrasound technology that is used to scan pregnant women to look at their unborn child. The MRI will involve lying in an MRI scanner for up to 1 hour. By comparing the MRI data and the ultrasound data of the two groups we will understand more about how muscles are affected for individuals with cerebral palsy.

WHY HAVE YOU BEEN CHOSEN?

You have cerebral palsy. We are asking 10 individuals who have cerebral palsy to participate. We hope to learn more about how the muscles of individuals with cerebral palsy differ from their typically developing peers by comparing the data from typically developing young adults and young adults with cerebral palsy.

WHO DECIDES IF I WILL TAKE PART?

Any typically young adult aged between 16 and 35 years of age diagnosed with cerebral palsy may be asked to take part. It is important that they have not received any orthopaedic surgery or treatment on their lower limbs in the last 12 months. The decision to take part is up to you. If you decide to take part, you will be asked to sign a consent form.

WHAT IS BEING ASKED OF YOU?

If you agree to take part in the study, you will need to attend St Thomas' hospital. We will make some measurements of height and weight. We will then place an ultrasound probe (like those use to scan pregnant mothers) on the skin of your calf to obtain images of the calf muscles. You will then be accompanied by a member of staff to the MRI unit. You will be asked to lie in an MRI scanner for up to 1 hour. The position you will be asked to lie in is shown in figure 2 and 3 below. During the MRI scan you can listen to the radio or you can bring along a CD to listen to. The whole process should take less than one and a half hours.

Figure 2: The position you will be required to lie in during the scan

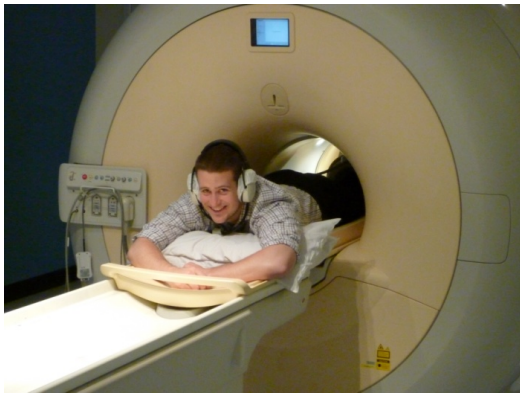

Figure 3: A member of the research team in the MRI scanner

WHAT ARE THE POSSIBLE RISKS/BENEFITS?

Ultrasound is considered a safe imaging technique. MRI is also considered safe and does not involve the use of ionising radiation. However, there are certain indirect hazards, primarily the presence of a strong magnetic field that will exert a force on magnetic materials near the scanner. Rigorous safety policies are in place to minimise these risks that meet the national and

international safety guidelines for MRI. MRI has been carried out on tens of thousands of patients and volunteers at Guy's and St Thomas' over more than 20 years without a serious adverse incident.

There are no benefits from taking part in this study.

WHAT IF YOU CHANGE YOUR MIND?

If you wish to withdraw from the study, you can do so at any time and without giving any reason.

WHAT ABOUT CONFIDENTIALITY?

All information collected during the course of this study will be kept strictly confidential. Any information leaving the hospital will have your personal details removed so that you cannot be recognised from it.

ARE THERE ANY COSTS?

Yes. You may incur some travelling expenses for which you will be reimbursed.

WHAT WILL HAPPEN TO THE RESULTS OF THIS STUDY?

We expect that the results of this study will be published in medical journals and presented at national and international meetings to other medical professionals.

WHO HAS REVIEWED THIS STUDY?

The research ethics committee at the Royal Free Hospital and Medical School has reviewed this study.

WHAT SHOULD BE DONE WITH THIS INFORMATION SHEET?

Please take your time to read this information carefully. Keep it for reference if you and your child decide to take part.

WHEN YOU HAVE MADE A DECISION

If you decide to participate, please contact Adam Shortland (telephone: 0208 7188 2476) and he will organise an appointment for you to come in to the gait laboratory. You will need to bring the consent form with you (at the back of this information pack). You should sign the consent form at the appointment.

A copy of the consent form will provided to you for your records.

ANY QUESTIONS?

If you would like any more information about the study or have any concerns please contact:

Adam Shortland, Clinical Scientist on 020 7188 2476
Geoff Charles-Edwards, MRI Clinical scientist on 020 7188 0133

Muscular fat infiltration of young people with Cerebral Palsy (PATIENTS)
Version 3 04/12/2009

4

C. Study 5 Ethics

C.1 Ethical approval letter

NHS
Health Research Authority
NRES Committee London - West London
Room 4W/12, 4th Floor
Charing Cross Hospital
Fulham Palace Road
London
W6 8RF
Telephone: 020 3311 7258
Facsimile: 020 3311 7280

Dr Adam Shortland
Consultant Clinical Scientist and Manager
Guy's & St Thomas' NHS Foundation Trust
One Small Step Gait Laboratory
Guy's Hospital, St Thomas' Street
London SE1 9RT

13 December 2011

Dear Dr Shortland

Study title: **Are MRI diffusion parameters in the corticospinal tract related to abnormalities of motor control and muscle growth in bilateral spastic cerebral palsy?**
REC reference: **11/LO/1520**

Thank you for your letter of 28 October 2011, responding to the Committee's request for further information on the above research and submitting revised documentation.

The further information has been considered on behalf of the Committee by the Chair.

Confirmation of ethical opinion

On behalf of the Committee, I am pleased to confirm a favourable ethical opinion for the above research on the basis described in the application form, protocol and supporting documentation as revised, subject to the conditions specified below.

Ethical review of research sites

NHS sites

The favourable opinion applies to all NHS sites taking part in the study, subject to management permission being obtained from the NHS/HSC R&D office prior to the start of the study (see "Conditions of the favourable opinion" below).

Non-NHS sites

The Committee has not yet been notified of the outcome of any site-specific assessment (SSA) for the non-NHS research site(s) taking part in this study. The favourable opinion does not therefore apply to any non-NHS site at present. We will write to you again as soon as one Research Ethics Committee has notified the outcome of a SSA. In the meantime no study procedures should be initiated at non-NHS sites.

Conditions of the favourable opinion

The favourable opinion is subject to the following conditions being met prior to the start of the study.

Management permission or approval must be obtained from each host organisation prior to

the start of the study at the site concerned.

Management permission ("R&D approval") should be sought from all NHS organisations involved in the study in accordance with NHS research governance arrangements.

Guidance on applying for NHS permission for research is available in the Integrated Research Application System or at http://www.rdforum.nhs.uk.

Where a NHS organisation's role in the study is limited to identifying and referring potential participants to research sites ("participant identification centre"), guidance should be sought from the R&D office on the information it requires to give permission for this activity.

For non-NHS sites, site management permission should be obtained in accordance with the procedures of the relevant host organisation.

Sponsors are not required to notify the Committee of approvals from host organisations

It is the responsibility of the sponsor to ensure that all the conditions are complied with before the start of the study or its initiation at a particular site (as applicable).

Approved documents

The final list of documents reviewed and approved by the Committee is as follows:

Document	*Version*	*Date*
Investigator CV	Adam Shortland	02 September 2011
Letter of invitation to participant	Adult v1	31 August 2011
Other: Letter of invitation to participant	Parent/Guardian v1	31 August 2011
Other: Advert: Adults Under 25	2	28 October 2011
Other: Advert: Parents/Guardians Of Children Over 12	2	28 October 2011
Other: GSFM Score Sheet	1.0	
Other: LIFE-H	3.0	
Participant Information Sheet: Adult (Cases)	1	31 August 2011
Participant Information Sheet: Parent/Guardian (Controls)	2	28 October 2011
Participant Information Sheet: Parent/Guardian (Cases)	2	28 October 2011
Participant Information Sheet: Child (Controls)	2	28 October 2011
Participant Information Sheet: Child (Cases)	2	28 October 2011
Participant Information Sheet: Adult (Controls)	2	28 October 2011
Protocol	1	26 July 2011
REC application		02 September 2011
Referees or other scientific critique report	Action Medical Research	
Response to Request for Further Information		

Statement of compliance

The Committee is constituted in accordance with the Governance Arrangements for Research Ethics Committees (July 2001) and complies fully with the Standard Operating Procedures for Research Ethics Committees in the UK.

A Research Ethics Committee established by the Health Research Authority

After ethical review

Reporting requirements

The attached document *"After ethical review – guidance for researchers"* gives detailed guidance on reporting requirements for studies with a favourable opinion, including:

- Notifying substantial amendments
- Adding new sites and investigators
- Notification of serious breaches of the protocol
- Progress and safety reports
- Notifying the end of the study

The NRES website also provides guidance on these topics, which is updated in the light of changes in reporting requirements or procedures.

Feedback

You are invited to give your view of the service that you have received from the National Research Ethics Service and the application procedure. If you wish to make your views known please use the feedback form available on the website.

Further information is available at National Research Ethics Service website > After Review

11/LO/1520	**Please quote this number on all correspondence**

With the Committee's best wishes for the success of this project

Yours sincerely

Dr Catherine Urch
Chair

Email: clive.collett@imperial.nhs.uk

Enclosures: "After ethical review – guidance for researchers"

Copy to: *Ms Karen Ignatian, Guy's and St Thomas' NHS Foundation Trust*

A Research Ethics Committee established by the Health Research Authority

C.2 Adult case subject information sheet

One Small Step Gait Laboratory
Guy's Hospital
London
SE1 9RT

Guy's and St Thomas' NHS
NHS Foundation Trust
Hospital No: 020 7188 7188
Gait Lab No: 020 7188 2476
Gait Lab Fax: 020 7188 2477
E-mail: adam.shortland@gstt.nhs.uk

ADULT INFORMATION SHEET

STUDY TITLE
Are MRI diffusion parameters in the corticospinal tract related to abnormalities of motor control and muscle growth in bilateral spastic cerebral palsy?

INTRODUCTION
You are invited to take part in a research study. Before you decide whether or not you would like to take part, it is important for you to understand why the research is being done and what it will involve. Please take time to read the following information carefully and discuss it with friends, relatives and your GP if you wish. Ask us if there is anything that is not clear or if you would like more information. Take time to decide whether or not you wish to take part.

WHAT IS THE PURPOSE OF THIS STUDY?
The central nervous system is organised into two parts: grey matter (where all the main bodies of the neurones are located) and white matter (consisting of long thin extensions of neurones that allow communication between the cells of the central nervous system). Many people with cerebral palsy have injuries that affect the development of the white matter and muscles.

In this study we wish to investigate the organisation of the white matter in the spinal cord, and measure the volumes of the muscles of the leg. We hope to learn about whether there are differences in white matter organisation in people with cerebral palsy compared with their typically developing peers. We think that individuals with cerebral palsy suffer from decreased white matter organisation that would cause a reduction in selective motor control ability. We will also investigate how lower limb muscle volumes relate to white matter organisation in the spine. Changes in muscle volumes in cerebral palsy can cause their muscles to be weaker than their typically developing peers.

We will take measurements of your spine, brain, and lower limb muscles using magnetic resonance imaging (MRI). We will also assess your ability to perform particular controlled movements and your overall functional ability through a clinical examination and questionnaire. We want to see if the altered development of the white matter is

associated with deficits in motor control and functional ability in a group of individuals with cerebral palsy.

WHY HAVE YOU BEEN CHOSEN?
You have cerebral palsy. We are asking 20 individuals who have cerebral palsy to participate. We hope to learn more about how the spinal cord and muscles of individuals with cerebral palsy differ from their typically developing peers by comparing the data from typically developing subjects and subjects with cerebral palsy.

WHO DECIDES IF I WILL TAKE PART?
Adults and children, aged between 12 and 25 years of age, with cerebral palsy may be asked to take part. It is important that you have not received any orthopaedic surgery on their your limbs in the last 12 months. The decision to take part is up to you. If you decide to you would like to take part then you will be asked to sign a consent form.

WHAT IS BEING ASKED OF YOU?
If you agree to take part in the study, you will need to attend St Thomas' hospital. Once at the hospital we will check that you are still happy to take part in the study and if so ask you to sign the consent form. For the MRI scan you will need to remove any metal objects that you are wearing, which will be stored in a secure area, and you will be asked to ***lie in an MRI scanner for up to 1 hour***. The inside of the scanner is shown in figure 1. For approximately 10 minutes of the scan you will be required to lie with your head inside of a special coil, which will give us better pictures of your brain as shown in figure 2. After scanning your brain, we will reposition you in the scanner without the plastic helmet and we will take imaged of your spinal cord and lower limb muscles.


Figure 1: Inside the scanner


Figure 2: Plastic helmet for part of the scan

The scanner can be quite noisy and so we will give you ear-defenders to wear. These also contain speakers so you can still talk to the research team and listen to the radio or you can bring along a CD to listen to. The whole process should take less than one and three quarter hours. You are welcome to visit the MRI scanner in a separate visit to see what it will be like during the scan.

After your MRI scan, a physiotherapist or a clinical scientist will perform a brief examination of the range of motion of your ankles knees and hips, and assess your

ability to control your lower limbs. They will also ask you to perform particular functional tasks (sitting kneeling etc.). These tests will require you to change into either shorts and a t-shirt, or swimwear, and will take about one hour and thirty minutes.

This means that in total you will be with us for about 3 hours.

WHAT ARE THE POSSIBLE RISKS/BENEFITS?
MRI is considered safe and does not involve the use of ionising radiation. However, there are certain indirect hazards, primarily the presence of a strong magnetic field that will exert a force on magnetic materials near the scanner. Rigorous safety policies are in place to minimise these risks that meet the national and international safety guidelines for MRI. MRI has been carried out on tens of thousands of patients and volunteers at Guy's and St Thomas' Hospitals over more than 20 years without a serious adverse incident.

There are no benefits from taking part in this study.

WHAT IF YOU CHANGE YOUR MIND?
If you wish, you can withdraw from the study at any time and without giving any reason.

WHAT ABOUT CONFIDENTIALITY?
All information collected during the course of this study will be kept confidential. Any information leaving the hospital will have your personal details removed.

ARE THERE ANY COSTS?
No, you will be reimbursed for travelling expenses.

WHAT WILL HAPPEN TO THE RESULTS OF THIS STUDY?
We expect that the results of this study will be published in medical journals and presented at national and international meetings to other medical professionals. Participants will not be given any of their individual MRI results.

We may use your anonymised study data in future research. If you are happy for us to use your data in another study please sign the relevant section of the consent form.

WHO HAS REVIEWED THIS STUDY?
This study has been reviewed by the West London Research Ethics Committee.

WHAT SHOULD BE DONE WITH THIS INFORMATION SHEET?
Please take your time to read this information carefully and keep it for reference if you decide to take part in this study.

WHEN YOU HAVE MADE A DECISION

If you decide that you would like to participate in this study then please contact Adam Shortland (see below) and he will organise an appointment for you to come to St Thomas' Hospital. You will need to bring the consent form with you, which is located at the back of this information pack. You should sign the consent form at the appointment and you will receive a copy for your records.

ANY QUESTIONS?

If you would like any more information about the study or have any concerns please contact: Adam Shortland, Clinical Scientist on 020 7188 2476.

C.3 Consent form

One Small Step Gait Laboratory
Guy's Hospital
London
SE1 9RT

Guy's and St Thomas' NHS
NHS Foundation Trust
Hospital No: 020 7188 7188
Gait Lab No: 020 7188 2476
Gait Lab Fax: 020 7188 2477
E-mail: adam.shortland@gstt.nhs.uk

ADULT CONSENT FORM

Study Number: 11/L0/1520

Study Title: Corticospinal tract organisation, muscle growth & motor control in BCP
Researchers: Adam Shortland, Geoff Charles-Edwards, Jonathan Noble

Please initial box

1. I confirm that I have read and understand the patient information sheet dated 28/10/11 (v.2) for the above study and have had the opportunity to ask questions. ☐
2. I understand that participation is voluntary and that I am free to withdraw at any time, without giving any reason, without my medical care or legal rights being affected. ☐
3. I understand that sections of any of my medical notes may be looked at by medical staff or from regulatory authorities where it is relevant to my taking part in research. I give permission for these individuals to have access to my records. ☐
4. I agree to take part in the above study. ☐
5. I am happy for my anonymised data to be used for future research studies. ☐

_____	_____	_____
Name of Patient	Date	Signature
_____	_____	_____
Name of Person taking consent (if different from researcher)	Date	Signature
_____	_____	_____
Researcher	Date	Signature

(1 for patient; 1 for researcher; 1 to be kept with hospital notes)

D. Supplementary information for Chapter 5.

D.1 Repeatability of muscle volume measurement

The accurate measurement of muscle volume in this study is dependent on the manual delineation of muscles within the MRI images. This is a subjective process and the measured muscle volume is inter-observer and intra-observer dependent. A single person, the primary assessor, drew the majority of the muscle volume regions of interest drawn in this study. A second assessor drew the regions of muscle around the quadriceps and hamstring muscles of ten BSCP and ten TD subjects. To minimise the inter-observer error, the regions of interest drawn by the second assessor were checked and corrected if required by the primary assessor.

To assess the test-retest repeatability of the muscle volume measurement of the primary assessor, muscle volume measurements were repeated 18 months apart on five muscles (MG, SOL, ST, RF, and GMax) of five subjects (three BSCP and two TD subjects) on the same data sets with the assessor blinded to the results. Inter-observer reliability was examined using a one-way intra-class correlation coefficient (ICC) reporting single measure reliability in SPSS ((Version 20.0; IBM SPSS, Chicago, USA). The ICC is a score from 0 to 1, The benchmarks for ICC proposed by Landis and Koch (1977)[294]: 0-0.2 ‘poor’; 0.21-0.40 ‘fair’; 0.41-0.60 ‘moderate’; 0.61-0.80 ‘substantial’; and 0.81-1.00 ‘almost perfect’. The standard error of measurement (SEM) was calculated using Equation D.1. The smallest detectable difference (SDD) with 95% confidence interval was calculated using Equation D.2 to estimate the minimal difference between muscles to exceed measurement error.

$$SEM = SD_{diff} * \sqrt{(1 - ICC)} \qquad \text{Equation D.1}$$

Where SD_{diff} is the standard deviation of the differences between the repeated measures.

$$SDD = 1.96 * \sqrt{2} * SEM \qquad \text{Equation D.2}$$

Table D.1 summarises the results of the test—re-test consistency of measuring muscle volume. 'Almost perfect' ICC coefficients were observed for all muscles investigated. The smallest detectable difference for each muscle is much lower than the difference between the muscle volumes of the two subject groups in this study.

Muscle	Mean Difference (standard deviation)	ICC	95% ICC Confidence Interval		SEM	SDD
			Lower bound	Upper bound		
Gmax	-7.2 (9.3)	0.999	0.991	1	0.29	0.82
RF	-2.4 (6.4)	0.997	0.972	1	0.35	0.97
ST	-0.8 (4.7)	0.999	0.99	1	0.15	0.41
SOL	-2.6 (7.7)	0.998	0.98	1	0.34	0.95
MG	2.8 (10.9)	0.988	0.883	0.999	1.19	3.31

Table D.1 Mean difference in initial and repeated measure of muscle volume with the corresponding intraclass correlation coefficient (ICC) values for each muscle tested. The standard error of measurement (SEM) and smallest detectable difference (SDD) and the paired-test p-value for bias are also given. Significance was set at $p \leq 0.05$. GMax = Gluteus maximus; RF = Rectus Femoris; ST = Semtiendinosus; SOL = Soleus; MG = Medial Gastrocnemius).

Although a very good agreement was observed between the repeated measurements, this repeatability only examines the repeatability of the measurement of the muscle volumes and does not include the repeatability of the acquisition of the MRI scan. The MRI data was collected using two different image acquisition protocols: T1-weighted and mDixon. This results in different image contrasts in the acquired data sets affecting the detection of muscle boundaries. This may result in a systematic error in the muscle volume measured between the two imaging techniques. This systematic error is likely to be comparable in size to the repeatability of the manual muscle volume measurement discussed above. However, a comparison of muscle volume measurements for the same subject acquired using both imaging protocols is required to investigate the validity of

the grouping of the two data sets in this study. However, it is likely that any systematic error between volume measurements for the two imaging protocols is much smaller than the large difference in muscle volume between the two subject groups and therefore should not significantly affect the results of this study.

D.2 Example images

Figure D.1 shows example transverse MRI images of the thigh (a and c) and shank (b and d) muscles of a CP and an age and sex matched TD subject respectively.

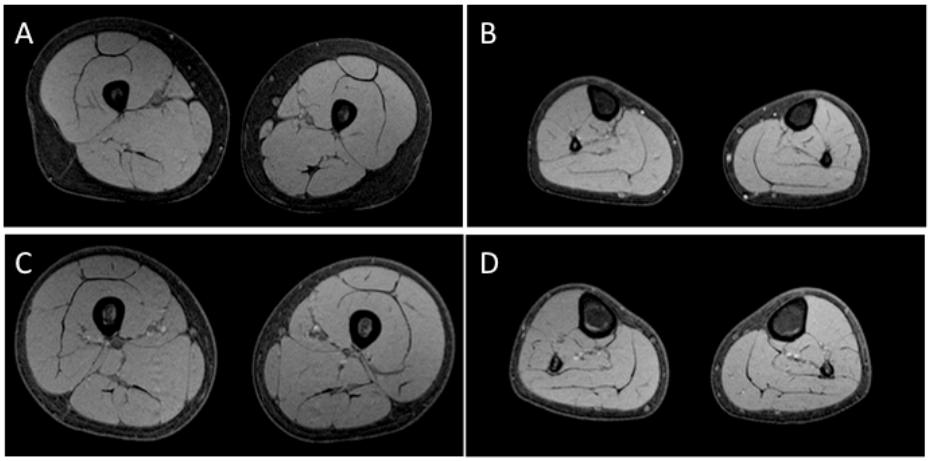

Figure D.1 Example MRI traverse images of the thigh (a and c) and shank (b and d) muscles of a CP and an age and sex matched TD subject respectively

D.3 Rationale for normalisation of muscle volume to body mass

The strong linear relationship between muscle volume and body mass in the typically developing subjects in this study (r= 0.694-0.959, see Chapter 5 Table 3) and in our previous work[59] demonstrates the body mass is a significant non-pathological factor influencing lower limb muscle volume. Therefore, in order to identify any pathological difference in muscle volume in cerebral palsy the significant non-pathological differences in muscle volume due to body size should be accounted for. Therefore, the lower limb muscle volumes of the subjects in this study were normalised to body mass to minimise the non-clinical variation between the subjects in this study

D.4 Tables of results

Muscle	Group	Normalised muscle volume (cm^3/kg)		
			95% Confidence Interval for Median	
		Median	Lower Bound	Upper Bound
GMax	CP	9.1	8.24	10.27
	TD	11.835	9.21	12.98
RF	CP	2.53	2.17	2.81
	TD	3.34	2.78	3.79
VI&VL	CP	13.92	12.74	15.09
	TD	13.92	12.57	17.13
ST	CP	1.5	0.99	2.01
	TD	2.07	1.74	2.88
SM	CP	1.88	1.66	2.28
	TD	2.82	2.44	3.15
MG	CP	1.985	1.51	2.37
	TD	3.11	2.77	3.58
LG	CP	1.015	0.93	1.24
	TD	1.65	1.45	1.82
SOL	CP	4.085	3.28	4.95
	TD	5.87	5.42	6.41
TA	CP	1.005	0.87	1.2
	TD	1.57	1.35	1.72

Table D.2 Median and 95% confidence intervals of the median of the normalised muscle volumes for the CP and TD groups for each muscle investigated.

Muscle	Percentage muscle volume deficits (%)		
	95% Confidence Interval for Median		
	Median	Lower Bound	Upper Bound
GMax	20.30	10.0	27.8
RF	26.25	17.9	33.6
VI&VL	11.40	4.0	20.0
ST	35.00	12.4	56.9
SM	35.20	29.5	49.3
MG	39.20	26.5	53.0
LG	37.85	23.9	43.2
SOL	35.80	18.7	52.9
TA	35.05	22.3	43.7
Proximal	26.75	20.0	30.0
Distal	36.80	33.1	41.7

Table D.3 Median and 95% confidence intervals of the median of the percentage muscle volume deficit for each muscle investigated and when grouped by location in the lower limb (proximal and distal) in the CP group compared to the TD group.

E. Supplementary information for Chapter 7.

	Mean	95% Confidence Interval for Mean		Standard Deviation	Standard error
		Lower Bound	Upper Bound		
MRS	1.95	1.39	2.51	0.73	0.24
$3PD_p$	8.34	6.96	9.73	1.80	0.60
$3PD_m$	11.79	10.29	13.28	1.94	0.65
2PD	5.06	4.06	6.05	1.29	0.43
4PD	11.58	10.62	12.54	1.25	0.42

Table E.1 Median and 95% confidence intervals of the median of the percentage intramuscular fat measured by each method investigated.

F. SCALE and muscle volume predicts gross motor function

AACPDM 2014 Free Papers

Title: Selective motor control and muscle volume predicts gross motor function in bilateral spastic cerebral palsy

Background/Objectives: Gross motor function in cerebral palsy is often considered to be dependent on spasticity, muscle size/strength, and selective motor control. However, limited studies have been performed investigating the contribution of these factors to gross motor function. In this study we investigate the predictive nature of these factors on gross motor function measure (GMFM-66) in bilateral spastic cerebral palsy (BSCP).

Design: Cohort study

Study participants & Setting: 10 adolescents and young adults with BSCP (10 male, 15.7±3.7 years, Gross Motor Function Classification System levels I [n=1], II [n=4], III [n=4], and IV[n=1]).

Materials and Methods: Magnetic resonance images were acquired on a 3.0T Achieva system (Philips Healthcare), with a quadrature body coil. Three point Dixon sequence (TE/TR=2.11/5.2 ms, echo time shift = 0.76 ms (120 ^{o} echo phase shift), 10^{o} flip angle, 1.2 x 1.2 mm in-plane voxel size, number of averages = 2, 5 mm slice thickness) were acquired of both lower limbs. Muscle volumes were manually segmented in Osirix (version 5.8.2) for 18 muscles in both legs (medial gastrocnemius, lateral gastrocnemius, soleus, tibialis anterior, tibialis posterior, vastus medialis, rectus femoris, vastus intermedius and lateralis composite, semimembranosus, semtiendinosus, gracilis, sartorious, biceps femoris long and short head, adductors composite, gluteus maximus, gluteus medius, and gluteus minimus). Muscle volumes were normalised to body mass and averaged between legs for each individual. Gross motor function (GMFM), lower limb selective motor control (SCALE), and spasticity (Modified Ashworth) were assessed. Pearson's correlations were used to investigate relationships between the measured parameters, and forward stepwise multiple linear regression analysis used to identify which clinically significant factors (SCALE, modified Ashworth, and normalised lower limb muscle volume) predicted gross motor function. All statistical tests were performed using SPSS (version 20.0; IBM SPSS) with significance set to $p \leq 0.05$.

Results: GMFM-66 is significantly positively correlated to SCALE ($r=0.915$, $p \leq 0.001$) and total lower limb muscle volume ($r=0.749$, $p=0.013$). GMFM-66 was not related to modified Ashworth score. Forward stepwise multiple linear regression analysis showed that SCALE and lower limb muscle volume explained 90.3% of the variation in GMFM-66 ($p \leq 0.001$).

Conclusions/Significance: Selective motor control and muscle volume, rather than spasticity, are the significant factors limiting gross motor function in ambulant individuals with bilateral spastic cerebral palsy.

G. Femoral anteversion remodelling

CMAS 2010 Clinical Movement Analysis Society — the Discovery of Hidden Aspects of Motion Analysis

On the remodelling of femoral anteversion in cerebral palsy

Noble. J.J. [1*], Shortland. A.P.[2*]

[1*] King's College Hospital NHS Foundation Trust, UK, Jonathan.Noble@kcl.ac.uk
[2*] Guy's & St Thomas' NHS Foundation Trust, UK, Adam.Shortland@gstt.nhs.uk

Introduction

At birth a child has approximately 30-50° of femoral anteversion (FA)[1,2]. As the child matures and develops they progress through several key motor milestones including crawling, standing and walking. These activities induce stress on the proximal end of the femur[1]. In response to the applied stress, the proximal end of the femur remodels with FA decreasing rapidly in the first three to four years of life[1]. The delay of motor milestone acquisitions which often occurs with cerebral palsy (CP) results in the degree of FA remodelling in early life being reduced[2].

This is a retrospective study analysing the degree of FA in patients with CP, who attended the One Small Step Gait Laboratory at Guy's Hospital between 2007 and 2009, to determine if there is a relationship between their age of first independent walking and the number of years spent walking independently, and the degree of FA.

Materials and methods

128 bilateral (aged 5-25; 81 male) and 51 unilateral CP patients (aged 4-24; 31 male) who walked independently and had not had a femoral de-rotation were reviewed. Patients were categorised by condition (bilateral or unilateral) and into 8 age categories according to when they first walked independently (6 month intervals except for the first (6-18 months) and last (60+ months) intervals; parent reported). FA was measured with the patient in prone with the hip in a neutral coronal position and knee flexed to 90°, the hip was rotated internally and externally until the most prominent part of the greater trochanter was palpated (the trochanteric prominence test). The angle between the shank and the vertical was taken as the angle of FA. Data was analysed using univariate analysis of variance (ANCOVA) methods using patients grouped by age of first independent walk as the main factor and the number of years spent walking independently as the covariate. For each of the bilateral patients, FA was averaged between legs. For unilateral patients, only the measurements of the affected limb were considered. Significance was defined as $p \leq 0.05$.

Results and discussion

FA was found to exhibit a significant relationship only with number of years spent walking independently ($p = 0.038$) for the bilateral patient group. Age of first independent walk was not significantly related to degree of FA. There was no significant relationship between FA and either of the independent factors for the unilateral group (Table 1). There was no significant difference in FA between bilateral and unilateral groups ($p = 0.428$).

Patient category	Factor/Covariate	P-value
Bilateral	Age of first independent walk	0.281
	Time walking independently	0.038
Unilateral	Age of first independent walk	0.293
	Time walking independently	0.297

Table 1: Summary of statistical analysis results

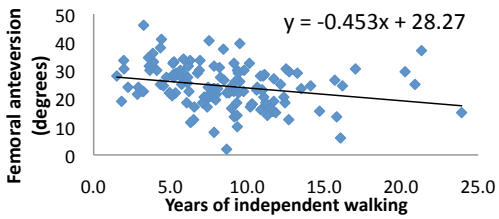

Figure 1: Femoral anteversion relationship with years of independent walking for bilateral patients

These results suggest that FA is negatively correlated with the number of years spent walking independently in the case of bilaterally-affected patients. However, there was no such relationship for unilateral CP. Figure 1 suggests that FA decreases by 0.5° per year for bilateral CP patients on average. While this rate of remodelling may be considered clinically insignificant, it may be possible that a subgroup of subjects remodel at a greater rate. Further investigations on a larger sample may be required to distinguish these sub-groups (e.g. GMFCS, gait pattern). Identifying individuals that remodel FA rapidly may help inform treatment decision making. Off-loading of the affected limb in unilateral CP may explain the lack of relationship between the number of years spent walking independently and the degree of FA.

Conclusion

This study has found that the femur remodels significantly with the number of years spent walking independently for bilateral CP patients and is not dependent on age of acquisition of independent walking. Remodelling of the femur does not appear to be dependent on years spent walking independently or timing of acquisition of motor skills for unilaterally-affected patients with CP.

References

[1] Gage J. *et al* 2009 21-30 ISBN 978-I-898683-65-O
[2] Fabry G. *et al* J Bone Joint Surg Am 1973 55:1726-1738